Understanding the Role of RNA-binding Proteins in Regulating Autophagy During Nutrient Limitation

by

Shree Padma Metur

A dissertation submitted in partial fulfillment
of the requirements for the degree of
Doctor of Philosophy
(Molecular, Cellular and Developmental Biology)
in the University of Michigan
2024

Doctoral Committee:

Professor Daniel J Klionsky, Chair
Associate Professor Kristin Koutmou
Professor Anuj Kumar
Associate Professor Ming Li
Professor Nils Walter

“The idea was fantastically, wildly improbable. But like most fantastically, wildly improbable ideas it was at least as worthy of consideration as a more mundane one to which the facts had been strenuously bent to fit”

Douglas Adams

Shree Padma Metur

spadma@umich.edu

ORCID iD: 0000-0003-4782-6611

Dedication

To my parents, Raju Metur and Geethamani PN

Acknowledgements

Embarking on a PhD journey was like being told you are going on a luxurious cruise, only to find out your ship is piloted by a dolphin who only communicates in interpretive dance. Every "Eureka" moment you anticipated transformed into a bewildering "What does it mean?"- This led to six years spent deciphering the mixed signals from a model organism that behaves like a diva on most days, all the while hoping that "so long, thanks for all the fish" is not the feedback you will receive on your dissertation. As I complete this dissertation, I find myself less certain than when I started about what I know regarding mRNA dynamics during starvation. However, one thing I am certain of is that the secret to unlocking the mysteries of the universe really lies in a well-organized notebook and always expecting the Spanish Inquisition.

While a PhD is a solo quest, it is impossible to complete without a community of supportive mentors, colleagues, and friends who provide guidance, encouragement, and inspiration throughout the journey. First, I would like to thank my PhD mentor, Prof Daniel Klionsky for providing me the opportunity to work in his lab. In dealing with the unexpected, especially the numerous times an experiment can fail, he always offered a simple piece of advice with his ever-present calm disposition: “There is always a second time to do it properly.” That quiet encouragement instilled in me a fearlessness to pursue scientific questions without hesitation. I thank him for always having my back, for believing in me in moments of self-doubt, and for his optimism regarding my work. As much as I have learned from him about the importance of integrity, enthusiasm and a sense of humor in science, I will also carry with me the lessons he

taught about treating people with kindness, even in moments of intense scientific debates. Second, I would like to thank my committee members Prof Anuj Kumar, Prof Ming Li, Prof Kristin Koutmou and Prof Nils Walter for their helpful critiques, invaluable suggestions and unwavering support throughout the years.

I find myself lucky to have found amazing friends in my labmates especially Tony Yu, Dr. Wayne Hawkins and Dr. Dimitra Dialynaki who always make time to trouble-shoot experiments, collectively rant about the difficulties of science or just enjoy a good Tuesday evening playing some bad pool. I would also like to thank the present and the past members of the Klionsky lab, especially Dr. Dibyendu Bhattacharyya, Dr. Hana Popelka, Dr. Damian Gatica Mizala, Dr. Aileen Ariosa and Dr. Vikramjit Lahiri for their guidance and collaboration. Of course, I cannot end this section without mentioning my "Army of Undergrads", Faris Jafri, Megan Moore, Nathan Shatz, Sophie Mehta and Shunsuke Imasaka who taught me the joys and challenges of mentoring. Special thanks to Yash Chouhan for turning the quiet lab days into lively and fun discussions.

I would like to thank my best friend and partner, Ashwin Bhat, for supporting me in all my endeavors and failures, and for powering my goofball island. Finally, I would like to thank my parents, for their encouragement, support and the sacrifices, even the ones I am unaware of. Without their support, this dissertation would not be possible.

Table of Contents

Dedication ii

Acknowledgements iii

List of Tables ix

List of Figures x

Abstract xii

Chapter 1 Introduction 1

1.1 Overview of Autophagy 3

1.1.1 Autophagy in *Saccharomyces cerevisiae* 3

1.1.2 Autophagy in mammalian cells 5

1.2 Induction of Autophagy by the External Nutrient Environment 10

1.2.1 Autophagy induction by nitrogen and amino acid starvation 10

1.2.2 Autophagy induction by carbon starvation 17

1.3 Regulation of *ATG* gene expression 25

1.3.1 RNA-binding protein: primary drivers of mRNA life cycle 25

1.4 Post-transcriptional regulation of autophagy in yeast 31

1.5 Post-transcriptional regulation of autophagy in mammals 32

1.6 Outlook 34

1.7 References 37

Chapter 2 : Identification of Translational Regulators of Autophagy 52

2.1 Introduction 53

2.2 Results 55

2.2.1 An in vitro interactome capture reveals several new binding partners of *ATG1* mRNA 55

2.2.2 Npl3 is a novel regulator of Atg1 protein expression and autophagy 56

2.2.3 Npl3 regulates *ATG1* expression and autophagy in an RRM-dependent manner. .. 63

2.2.4 Pub1 promotes the translation of *ATG1* mRNA and autophagy. 71

2.2.5 TIA1 promotes *ULK1* expression and autophagy 78

2.2.6 Npl3 coordinates with Pub1 to export *ATG1* mRNA and recruit polysomes for translation 80

2.3 Discussion 89

2.3.1 *ATG1* mRNA-protein interaction landscape 89

2.3.2 The Npl3-Pub1 axis facilitates *ATG1* mRNA export and translation 91

2.3.3 Possible dual role of Pub1 in response to nutrient stress 92

2.3.4 Modularity of *ATG* regulation 95

2.4 Materials and Methods 99

2.4.1 Yeast Methods 99

2.4.2 RNA methods 99

2.4.3 Protein methods 103

2.4.4 Mammalian methods 104

2.4.5 Statistical methods 104

2.5 Tables 105

2.6 References 107

Chapter 3 : Translational Regulation of Macroautophagy During Distinct Nutrient Stress 111

3.1 Introduction 112

3.2 Results 114

3.2.1 Differential autophagy flux during distinct nutrient stresses is not determined by ATG transcription 114

3.2.2 Post-transcriptional activation of *ATG* gene expression is a critical node determining autophagy during nitrogen starvation 124

3.2.3 Post-transcriptional regulation of *ATG1* expression by Rad53 facilitates nitrogen starvation-induced autophagy 134

3.2.4 Ded1 binds *ATG1* mRNA to promote Atg1 expression 148

3.2.5 DDX3 regulates *ULK1* expression and autophagy in mammalian cells 162

3.3 Discussion 170

3.4 Materials and Methods 174

3.4.1 Yeast growth and starvation media 174

3.4.2 Protein sample preparation and Immunoblotting 175

3.4.3 RNA isolation, RNA-Sequencing, and qRT-PCR 176

3.4.4 SILAC sample preparation and LC-MS/MS analysis 178

3.4.5 Ultrastructural analysis 180

3.4.6 Auxin-inducible degradation 181

3.4.7 RNA Immunoprecipitation 182

3.4.8 In vitro RNA interactome capture screen/mRNA IP 183

3.4.9 Mammalian cell culture, transfection, and infection 184

3.4.10 Quantification and statistical analyses 185

3.5 Acknowledgements 185

3.6 Tables 185

3.7 References 191

Chapter 4 Summary and Future Directions 201

4.1 Systematic workflow to identify RNA-binding proteins that regulate autophagy 201

4.2 Differential translational regulation of *ATG1* dependent on external nutrient availability 203

4.3 Stress granule formation and function 204
4.4 RNA-binding proteins as therapeutic targets to modulate autophagy 205
4.5 References 207

List of Tables

Table 1. Significantly enriched RBPs on the *ATG1* 5' UTR. 105

Table 2. Strains used in this study. 106

Table 3. Yeast strains used in this study. 185

Table 4. Primers for yeast genetics. 187

Table 5. Primers for qRT-PCR. 190

Table 6 Primers for shRNA-mediated knockdown. 190

.

List of Figures

Figure 1: Overview of autophagy in mammalian cells. 9

Figure 2: Exploring *ATG1*-RBP interactions reveals Npl3 as a novel regulator of autophagy. .. 59

Figure 3: An *ATG1* 5' UTR in vitro mRNA interactome capture identifies previously known interactions. 62

Figure 4: Npl3 promotes *ATG1* translation and autophagy through an RRM-motif dependent mechanism. 67

Figure 5: Npl3 mutants do not affect global translation during nitrogen starvation. 70

Figure 6: Nuclear localization of Npl3 is necessary for *ATG1* mRNA interaction and Atg1 protein expression. 74

Figure 7: Loss of Pub1 does not affect global translation during nitrogen starvation. 77

Figure 8: TIA1 promotes ULK1 protein expression and autophagy during nutrient starvation.. 80

Figure 9: Pub1 links *ATG1* mRNA export and translation. 85

Figure 10: Nuclear localization of Npl3 is required to upregulate Atg1 protein expression. 88

Figure 11: Pub1 interactors bind to the *ATG1* 5' UTR. 98

Figure 12: Differential autophagy flux during distinct nutrient stresses is not determined by ATG transcription. 119

Figure 13: Differential autophagy flux during distinct nutrient stresses is not determined by ATG transcription. 122

Figure 14: Post-transcriptional activation of *ATG* gene expression is a critical node determining autophagy during nitrogen starvation. 128

Figure 15: Post-transcriptional activation of *ATG* gene expression is a critical node determining autophagy during nitrogen starvation. 132

Figure 16: Post-transcriptional regulation of *ATG1* expression by Rad53 facilitates nitrogen starvation-induced autophagy. 139

Figure 17: Post-transcriptional regulation of *ATG1* expression by Rad53 facilitates nitrogen starvation-induced autophagy. 143

Figure 18: Mec1 and Cdc28 are not involved in Rad53 activation during nitrogen starvation-induced autophagy. 146

Figure 19: Ded1 binds *ATG1* mRNA to promote Atg1 expression. 153

Figure 20: Ded1 regulates autophagy in yeast. 157

Figure 21: Ded1 regulates Atg1 expression and autophagy in yeast. (A) The loss of Ded1 activity impairs Atg1 expression during nitrogen starvation. 160

Figure 22: DDX3 regulates autophagy in mammalian cells. 165

Figure 23: DDX3 regulates autophagy in mammalian cells. 168

Abstract

Macroautophagy/autophagy is a conserved, eukaryotic, highly regulated cellular degradative process that removes superfluous cytoplasmic components and damaged organelles in either non-selective or selective manner. Autophagy occurs at the basal level in almost all cells to ensure homeostatic removal of cytoplasmic components, however, it is significantly upregulated in response to stressful conditions such as nutrient starvation. For the appropriate induction and execution of the process, the coordinated function of several autophagy proteins is required. However, during nutrient starvation, global translation is downregulated to conserve essential metabolic reserves such as nucleotides and amino acids. Therefore, an important question arises, how does the cell selectively upregulate the translation of autophagy related (*ATG*) genes in response to nutrient starvation?

Protein synthesis is controlled by post-transcriptional mechanisms influenced by RNA-binding proteins. The localization, stability and translational efficiency is controlled by RNA-binding proteins that target specific mRNAs. In order the understand the mechanisms of post-transcriptional control of autophagy, in this dissertation, I focus on *ATG1* mRNA that encodes for an important kinase required for autophagy induction, Atg1. I ask if there are specific protein marks that prime *ATG1* transcript for translation during nitrogen starvation.

Towards this, in Chapter 2, I develop an in vitro assay using labeled mRNA to specifically identify RNA-binding proteins that bind to *ATG1* 5' and 3' untranslated regions (UTRs). Through this method, I identify Npl3 and Pub1 as positive regulators of autophagy that

targets 5' and 3' UTR of *ATG1* respectively. Further analyses into the role of Npl3 and Pub1 revealed that Npl3 "imprints" *ATG1* transcript with Pub1 in the nucleus. Pub1, subsequently, facilitates export of *ATG1* transcript to the cytoplasm and recruits translational factors and ribosome components to enhance translation of Atg1. Intriguingly, in non-small cell lung cancer cells, the mammalian homolog pf Pub1, TIA1, regulates the expression of ULK1, the mammalian counterpart of Atg1, at the post-transcriptional level, thereby positively upregulating autophagy.

In Chapter 3, I explore the differential regulation of autophagy in yeast in response to two different nutrient states: nitrogen starvation and amino acid starvation. I discover that the differential regulation occurs at the level of post-transcriptional regulation of the *ATG1* transcript. Utilizing the approach developed in Chapter 2, I discovered that Ded1 is a nutrient responsive regulator of *ATG1* regulation. Further investigation revealed that its upstream kinase Rad53 selectively enhances *ATG1* and Ded1 interaction to facilitate the translational upregulation of Atg1. Additionally, I demonstrate that ULK1 undergoes similar post-transcriptional regulation by DDX3, the mammalian homolog of Ded1, highlighting the conservation of this regulatory mechanism.

In summary, this dissertation, uncovers novel post-transcriptional regulatory mechanisms of autophagy. I develop a high-throughput methodology to identify RNA-binding proteins that specifically bind to a transcript, especially *ATG1*. I identify novel and conserved regulators of autophagy, Npl3 and Pub1. Finally, this dissertation expands the repertoire of autophagy regulators with potential clinical benefit.

Chapter 1 Introduction

The ability to sense external nutrient pools and coordinate nutrient availability with growth and development is an inherent feature ubiquitous across all living organisms (Dibble & Manning, 2013). This fundamental process of detecting external and internal nutrient pools, including amino acids, sugars, and lipids, and integration with growth factors and stress-responsive pathways is critical in cellular decision-making (Efeyan et al., 2015). For instance, nutrients such as amino acids and glucose can act as determinants of cell fate by influencing global transcription, protein translation, and organelle biogenesis to enhance cell growth and proliferation (Zhu & Thompson, 2019). Conversely, the absence of amino acids and glucose can result in a global downregulation of protein translation, restructuring of cellular contents, and sometimes even cell death. Therefore, nutrient molecules can orchestrate intricate gene expression programs and regulate metabolic fluxes via signaling pathways, ultimately modulating cellular physiology (Metur et al., 2023).

In an ever-changing landscape, eukaryotic cells have developed elegant strategies to survive. One such process is macroautophagy (hereafter, autophagy). Autophagy is a conserved, catabolic process that maintains cellular homeostasis in response to environmental cues and nutrient availability. Autophagy removes superfluous cellular components via lysosomal/vacuolar degradation and releases essential macromolecules such as amino acids and nucleic acids, providing cells with the necessary building blocks to sustain essential functions. While autophagy occurs at a basal level in normal conditions, it is significantly upregulated Metur, S. P., & Klionsky, D. J. (2021), Metur, S. P., Lei, Y., Zhang, Z., & Klionsky, D. J. (2023), Metur, S. P., & Klionsky, D. J. (2024).

under nutrient-starvation conditions, therefore playing an important role in facilitating survival and adapting to the dynamic extracellular environment (Metur et al., 2023).

The latter, the changing environment, offers a range of stressors, wherein some biomolecules are abundant while others are scarce. Cells rely on nutrient sensing and signaling pathways that precisely transduce nutrient status to the cell and appropriately induce autophagy to maintain metabolic homeostasis. This regulatory system maintains a delicate balance between excessive degradation of essential cellular components and insufficient recycling, ensuring cellular homeostasis (Lei et al., 2022; Russell et al., 2014).

Autophagy is a highly regulated cellular process of degradation and recycling observed across various eukaryotes, from yeast to more complex organisms (Metur et al., 2023). This coordinated process requires the functioning of several Atg proteins that work together to initiate and complete the process resulting in the degradation of unwanted cytoplasmic material. Due to its degradative nature, it is crucial that the strength of autophagy induction is appropriately regulated in response to environmental stress to prevent the degradation of essential cellular components. Dysregulation of autophagy is implicated in the manifestation of several diseases, including cancer, neurodegeneration and metabolic disorders. Therefore, modulation of autophagy, genetically or pharmacologically, has been used as a therapeutic strategy. However, complete block in autophagy can be detrimental to cell survival and therefore, a nuanced approach to subtly change autophagic processes provides a more optimal approach to preventing cell death. To this end, identifying regulators that modulate the strength of autophagic induction is crucial to devise novel therapeutic strategies.

In this chapter I discuss the following: 1. The overview of the autophagic process in *Saccharomyces cerevisiae* and mammalian cells; 2. signaling pathways that induce autophagy; 3. RNA-binding proteins; and 4. post-transcriptional regulation of autophagy.

1.1 Overview of Autophagy

1.1.1 Autophagy in Saccharomyces cerevisiae

Autophagy is crucial in breaking down and recycling long-lived proteins, large protein complexes, and organelles, unlike the proteasome, which degrades short-lived individual proteins. Autophagy is responsible for the delivery of cytoplasmic cargo to the vacuole where it is ultimately degraded. This process encompasses three primary types of autophagy: microautophagy, macroautophagy, and chaperone-mediated autophagy/CMA, with chaperone-mediated autophagy not present in fungi (Yang & Klionsky, 2009; Parzych & Klionsky, 2014). Among these types, macroautophagy has been extensively studied and will be referred to as autophagy throughout this chapter (Parzych & Klionsky, 2014). A defining feature of autophagy is the formation of autophagosomes (Nakatogawa, 2020). Once formed, the outer membrane of the autophagosome fuses with the lysosome/vacuole, initiating hydrolysis of the inner membrane and cargo within the degradative organelle's lumen, ultimately releasing breakdown products into the cytosol (Yim & Mizushima, 2020).

Autophagy has been extensively studied and is categorized into distinct stages, including induction and nucleation of the phagophore, subsequent expansion and maturation of the phagophore into a fully closed, double-membraned autophagosome, tethering and fusion of the autophagosome with the vacuole, and, ultimately, degradation and release of the breakdown products (Ariosa et al., 2021; Delorme-Axford & Klionsky, 2018; Wen & Klionsky, 2016) .

Initially identified in yeast, more than 40 genes associated with the process of autophagy are grouped under the autophagy related (ATG) classification (Ohsumi, 2014). While numerous papers have provided comprehensive insights into this subject, this chapter will concisely outline the autophagy process in yeast (Figure 1) (Gatica et al., 2022; Metur et al., 2023; Parzych & Klionsky, 2014; Wen & Klionsky, 2016).

The process of autophagy initiation commences at a distinct location, known as the phagophore assembly site (PAS), located proximal to the vacuole. This step is tightly regulated by the Atg1 protein complex, consisting of the Atg1 kinase, Atg13, and the ternary subcomplex Atg17-Atg31-Atg29 (Mizushima, 2010; Suzuki et al., 2001). During the nucleation phase, the Atg14-containing class III phosphatidylinositol 3-kinase complex I, comprised of Vps34, Vps30, Vps15, Atg14, and Atg38, is recruited to the PAS. Subsequently, the phagophore undergoes expansion and closure, ultimately forming the autophagosome. Central components involved at this stage are two ubiquitin-like (Ubl) conjugation systems responsible for conjugating Ubl proteins Atg12 and Atg8 (Geng & Klionsky, 2008). Atg12 is activated by Atg7 (an E1-like enzyme) and subsequently conjugated to Atg5 through Atg10 (an E2-like enzyme), and the Atg12–Atg5 conjugate associates non-covalently with Atg16 (Yin et al., 2020). This system facilitates membrane recruitment during phagophore expansion.

The second Ubl protein, Atg8, is conjugated to the lipid phosphatidylethanolamine (PE), allowing for its association with the membrane. Atg8 initially contains a C-terminal extension, which the Atg4 cysteine protease cleaves to expose a C-terminal Gly (Yin et al., 2020). The modified Atg8 is then activated by Atg7 and transferred to an E2 enzyme, called Atg3. This process attaches the C terminal Gly to phosphatidylethanolamine (PE) to generate Atg8–PE. Atg8–PE is present on both sides of the phagophore and initially the autophagosome; the portion

on the autophagosome's outer membrane is deconjugated (removed from PE) by a second Atg4-dependent cleavage upon autophagosome formation completion. The transmembrane protein Atg9 may undergo cycling between the PAS and peripheral sites, potentially facilitating membrane delivery during the expansion phase. Once matured, the intact autophagosome fully encloses the cargo and fuses with the vacuolar membrane to deliver the cargo to the vacuole. Various hydrolases degrade the cargo within the vacuole, and the breakdown products are released back into the cytoplasm through permeases in the vacuolar membrane (Reggiori et al., 2004).

1.1.2 Autophagy in mammalian cells

Autophagy in mammalian cells follows a similar pathway as in yeast, including the four stages of autophagy: induction and nucleation of phagophore, expansion and closure of autophagosome, fusion with the vacuole and finally, degradation and efflux of nutrients. While most of the autophagy components discovered in yeast are homologous in mammalian cells, a few proteins found in the core autophagy machinery in yeast are not present in mammals (Figure 1).

The initiation of the double-membrane phagophore begins with the phosphorylation of various components of the PIK3C3/VPS34 kinase complex (comprised of BECN1, PIK3C3/VPS34, PIK3R4/VPS15, ATG14, NRBF2 and AMBRA1) (Yu et al., 2015) by the ULK kinase complex comprised of ULK1/ULK2, RB1CC1/FIP200, ATG13 and ATG101 (Figure 1). This results in the activation of the lipid kinase PIK3C3/VPS34 and the production of local pools of phosphatidylinositol-3-phosphate (PtdIns3P) needed for the nucleation of the phagophore (Hurley & Young, 2017). The ATG9 trafficking system, composed of ATG2, WDR45/WIPI4 and

the transmembrane protein ATG9A in conjunction with lipid channeling from the ER, supplies membrane precursors to meet the high demands of membranes required for autophagosome biogenesis (Chowdhury et al., 2018; Mari et al., 2010; Nishimura & Tooze, 2020; Valverde et al., 2019). Following phagophore nucleation, two ubiquitin-like conjugation systems are essential for membrane expansion and fusion. The two systems function to covalently conjugate the Atg8-family proteins (i.e., the MAP1LC3/LC3 and GABARAP subfamilies) to the expanding phagophore. First, the E1 like enzyme ATG7 and the E2 like enzyme ATG10 conjugate the ubiquitin-like protein ATG12 to ATG5. This complex subsequently binds to ATG16L1 and acts as an E3 enzyme for the conjugation of Atg8-family proteins to the membrane resident lipid phosphatidylethanolamine, with the help of E1 enzyme ATG7 and E2 enzyme ATG3. Lipidation of the Atg8-family proteins drives phagophore expansion and facilitates the recognition of specific cargo via interaction with receptors (Yu et al., 2018; Martens & Fracchiolla, 2020). Through completion of phagophore expansion and closure, the resulting double-membraned autophagosome topologically separates the autophagic cargo from the cytoplasm (Figure 1). Following the dissociation of the autophagic machinery from its surface, the outer membrane of the autophagosome fuses with the lysosome to form an autolysosome. Subsequently, the inner membrane and its enclosed contents are exposed to the lysosomal resident hydrolases and are degraded to generate simple metabolites, which are released into the cytoplasm via transporters and subsequently reused.

Autophagy is induced constitutively at a basal level for homeostatic maintenance of cellular function. However, when cells are subject to stress conditions, specifically nutrient starvation, autophagy is upregulated to meet the demands of the situation and promote the turnover of superfluous or damaged organelles to restore homeostasis. This tunable, rheostatic control of

autophagy, thus ensures that autophagic induction and execution is aligned with the stress observed.

In the following sections, I will discuss the various factors that induce autophagy, including sensors and regulators that coordinate to influence autophagy by integrating external signaling cues and internal metabolic homeostasis.

Figure 1

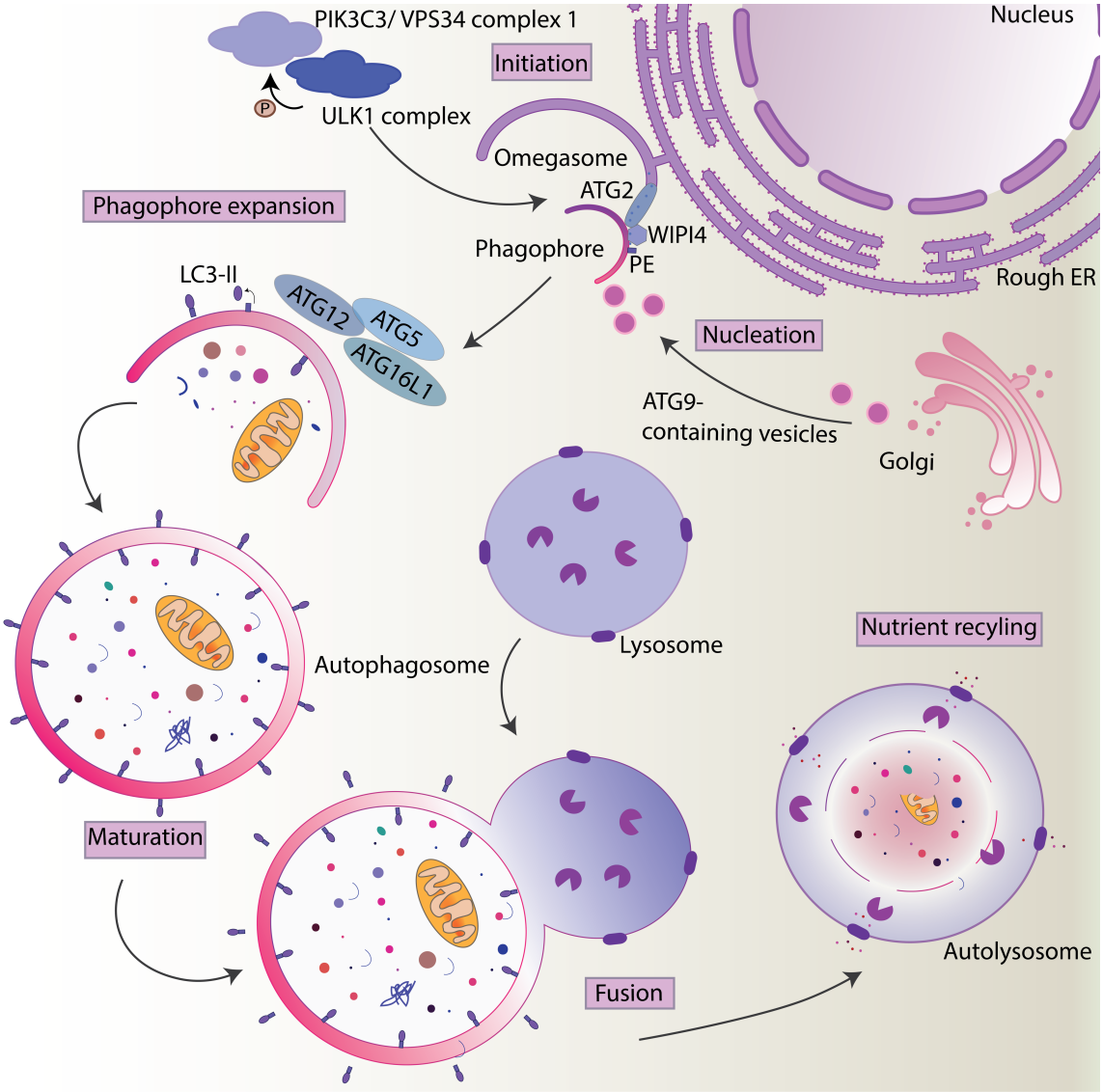
PIK3C3/ VPS34 complex 1
Initiation
ULK1 complex
Omegasome
ATG2
WIPI4
PE
Phagophore
Phagophore expansion
LC3-II
ATG12
ATG5
ATG16L1
Nucleation
ATG9-
containing vesicles
Golgi
Nucleus
Rough ER
Lysosome
Autophagosome
Nutrient recyling
Maturation
Fusion
Autolysosome

Figure 1: Overview of autophagy in mammalian cells.

Macroautophagy is initiated by the ULK1 and PIK3C3/Vps34 complexes which triggers the nucleation of the phagophore at the omegasome. The membrane sources required for phagophore biogenesis are supplied by ATG9-containing vesicles as well as phospholipids channeled from the ER into the growing phagophore by the ATG2-WDR45/WIPI4 complex. The two ubiquitin-like conjugation systems aid in phagophore expansion and closure. Subsequently, the autophagosome fuses with the lysosome where its contents are degraded, and the macromolecules generated are recycled.

1.2 Induction of Autophagy by the External Nutrient Environment

Here I explore the current understanding of nutrient-dependent signaling pathways that control autophagy. I focus specifically on studies that use *Saccharomyces cerevisiae* as the model system. I divide the section based on the specific nutrient limitations to contextualize the role of major signaling pathways that regulate autophagy. The complexity of biological systems means that that there are typically several nodes of intersection between and among signaling pathways; however, here I focus on signaling pathways that are primarily stimulated by the presence or lack of certain metabolites. By elucidating the molecular intricacies of nutrient-dependent regulation of autophagy, I can deepen our understanding of the role of autophagy in cellular adaptation and its potential implications for human health and disease.

1.2.1 Autophagy induction by nitrogen and amino acid starvation

Amino acids are important building blocks of proteins and therefore play significant roles in protein synthesis. Additionally, amino acids are central signaling metabolites capable of eliciting anabolic programs (Zhu et al., 2022). Amino acids exist in distinct pools in the cells, whose concentration is precisely regulated, especially by the vacuole (Kitamoto et al., 1988; Klionsky et al., 1990; Ohsumi & Anraku, 1981). The vacuolar amino acid pool is rich in basic and neutral amino acids, and glutamate is rapidly exchanged between the cytoplasmic and vacuolar compartments, where glutamate functions as fuel for the TCA cycle in the mitochondria (Klionsky et al., 1990; Ljungdahl & Daignan-Fornier, 2012). The methionine-derived co-factor, S-adenosyl methionine, is actively transported in and out of the vacuole and is an essential precursor for histone methylation and gene regulation. Furthermore, amino acids provide a nitrogen source and are precursors for carbon metabolism and nucleotide biosynthesis (Ljungdahl & Daignan-Fornier, 2012). Amino acids, therefore, are important signaling

molecules, and the vacuole plays a vital role in regulating the concentration of amino acid pools in the cell and actively communicating this information to metabolic sensing hubs such as TOR and SNF1. During external limitation of amino acids, autophagy is crucial in maintaining appropriate vacuolar amino acid levels to sustain life. During nitrogen and amino acid starvation, autophagy-deficient cells have lower levels of intracellular amino acids and therefore experience a dramatic loss in total protein synthesis. This in part explains the growth defects of autophagy-deficient cells under starvation conditions. Therefore, autophagy is crucial to maintain cellular homeostasis during starvation primarily by supplying amino acids for protein synthesis (Onodera & Ohsumi, 2005).

The earliest discoveries on the regulation of autophagy, much before the discovery and characterization of *ATG* genes, showed that this pathway is highly responsive to fluctuations in the external amino acids pool. In 1976, James Mitchener and colleagues observed by electron microscopy that depriving HeLa cells of serum and amino acids results in robust induction of autophagy (Mitchener et al., 1976). Pioneering work by Glenn Mortimore and colleagues showed that autophagosome numbers dramatically increased in perfused rate livers without amino acids (Mortimore & Schworer, 1977). In 1992, Kazuhiko Takeshige and colleagues showed that, under nitrogen-deprivation conditions, yeast cells accumulate autophagic bodies inside the vacuole, which gradually increase in number. These bodies contain cytoplasmic ribosomes, rough endoplasmic reticulum, mitochondria, and other cytoplasmic components, suggesting sequestration of the cytosol in the vacuoles in response to nitrogen and amino acid starvation (Takeshige et al., 1992). Just a year previously, in 1991, Joe Heitman, Rao Movva, and Michael Hall had published a seminal paper identifying the targets of the immunosuppressive drug rapamycin and named the components TOR proteins (Heitman et al.,

1991). Furthermore, in 1995, it was reported that rapamycin, an inhibitor of TOR, induces autophagy in rat hepatocytes and inhibits the phosphorylation of the ribosomal protein RPS6/S6 (Blommaart et al., 1995). In 1998, Yoshinori Ohsumi's group reported that rapamycin induces autophagy in yeast as well, with TOR being the upstream regulator, highlighting the conserved nature of this nutrient-dependent mechanism and setting the stage for investigating signaling pathways that regulate autophagy (Noda & Ohsumi, 1998).

With the discovery of TOR proteins as a regulator of autophagy, tremendous progress was made in the understanding of how autophagy is regulated under different nutrient conditions, the mechanisms of fine-tuning this process concomitant with the severity of the starvation, and the identification of other regulators that control autophagy. In the following sections, I briefly summarize our current understanding of how amino acids are sensed by TORC1 and the subsequent regulation of autophagy.

1.2.1.1 Amino acids activate TORC1

The target of rapamycin (TOR) kinase is a highly conserved central regulator responsible for integrating signals from many stress-inducing stimuli to coordinate cell growth and maintain homeostasis (Gonzalez & Hall, 2017; Wullschleger et al., 2006). TOR forms two complexes that differ in structure, function, and localization, TORC1 and TORC2. In *S. cerevisiae*, TORC1 has four components: either Tor1 or Tor2 kinase, Kog1, Lst8 and Tco89, while TORC2 consists of Tor2, Avo1, Avo2, Bit61, Lst8 and Tsc11. Tor2 is mainly located at the plasma membrane and on endosomes, where it regulates membrane homeostasis, and actin cytoskeleton polarity and dynamics (Gonzalez & Hall, 2017). Tor1 is primarily associated with the vacuole and is considered the master regulator of nutrient sensing, stimulating protein synthesis and other

anabolic programs while suppressing catabolic processes such as autophagy. While the mechanisms by which it may sense extracellular nutrients are unclear, several studies have suggested that TORC1 proteins sense intracellular availability of nitrogen and amino acids (Gonzalez & Hall, 2017).

Amino acid sufficiency is signaled to TORC1 via different mechanisms involving the conserved family of Rag GTPases (Powis & De Virgilio, 2016). In response to amino acids, these small GTPases modulate the localization and activity status of TORC1. These GTPases, Gtr1 and Gtr2, form heterodimers and are tethered on the vacuolar member by the palmitoylated and myristoylated EGO complexes (Binda et al., 2009; Dubouloz et al., 2005; Gong et al., 2011; Hirose et al., 1998; Powis et al., 2015; Zhang et al., 2012). In the presence of amino acids, Gtr1 is loaded with GTP, while Gtr2 is bound to GDP (Kim et al., 2008). The active $Gtr1^{GTP}$-$Gtr2^{GDP}$ heterodimers bind Kog1 to activate TORC1 (Binda et al., 2009; Hughes Hallett et al., 2015; Kira et al., 2016; Kira et al., 2014). GTPase activating proteins/GAPs and guanine nucleotide exchange factors/GEFs tightly regulate the nucleotide-binding status of Gtr1 and Gtr2 (Kim et al., 2008; Powis & De Virgilio, 2016; Shimobayashi & Hall, 2016). Vam6 has been proposed as the guanine nucleotide exchange factor while SEACIT (Seh1-associated subcomplex inhibiting TORC1; consisting of Npr2, Npr3, and Iml1) functions as the GTPase activating protein for Gtr1 (Neklesa & Davis, 2009). The SEACAT complex (Seh1-associated subcomplex activating TORC1; consisting of Sec13, Seh1, Sea2, Sea3, and Sea4) negatively regulates SEACIT and is critical for normal TORC1 function (Binda et al., 2009; Dokudovskaya & Rout, 2015; Panchaud et al., 2013; Shimobayashi & Hall, 2016).

In summary, when Gtr1 binds to GTP, it binds to Kog1 and Tco89; TORC1 is active and is localized all along the vacuolar membrane. When Gtr1 binds to GDP, TORC1 is inactive, and

its vacuolar localization becomes a singular punctate structure, now called the TORC1 body. Therefore, amino acids modulate the GTP binding status of the Rag GTPases, which enables vacuolar localization of TORC1 through Kog1. Consistently, the dynamic localization of TORC1 on the vacuole is correlated with nutrient condition (Kira et al., 2016; Kira et al., 2014; Noda, 2017). While the mechanism of how a change in TORC1 localization affects its downstream target is unknown, this single punctate structure of TORC1 under nutrient-starvation conditions may sequester it away from Atg13, a regulator of the Atg1 kinase, thus allowing the recruitment of Atg13 to the PAS (Noda, 2017). However, another study identified two spatially distinct pools of TORC1 with different targets; vacuolar TORC1 promotes protein synthesis via Sch9, whereas endosomal TORC1 phosphorylates Atg13 and Vps27 to inhibit macroautophagy and endosomal sorting complexes required for transport/ESCRT-driven microautophagy, respectively (Hatakeyama et al., 2019). Why TORC1 exists in these different pools is still being determined. Furthermore, it would be interesting to investigate if these distinct pools are activated differentially by regulatory elements and metabolic content on endosomes and vacuoles.

Individual amino acids activate TORC1. For example, leucine activates TORC1 by modulating the nucleotide binding status of Gtr1. Furthermore, leucine-bound tRNA synthetases/LeuRS also act as leucine sensors by binding to Gtr1 and mediating activation of TORC1. Glutamine also activates TORC1, however, this occurs in a Gtr1-independent manner and the exact mechanism by which glutamine is sensed and relayed to TORC1 remains elusive. In mammalian cells, individual amino acids activate MTORC1 via amino acid-specific sensors; however, such sensors have not yet been identified in yeast. It is possible that the mechanism of activation of TORC1 in yeast is entirely different from mammalian cells. Activated tRNA

synthetases and amino acid transporters may play a more prominent role in activating TORC1 in yeast. For example, the general amino acid control/GAAC signaling pathway that coordinates protein translation and amino acid availability intersects with the TORC1 pathway wherein TORC1 inhibits Gcn2 activation by uncharged tRNAs. However, a more detailed understanding as to how this interplay manifests is needed to elucidate the mechanism of TORC1 activation.

1.2.1.2 Mechanism of autophagy regulation by TORC1

While amino acids robustly activate TORC1, several other contexts also activate this regulatory complex. By sensing external stressors such as nutrient limitation (including nitrogen, carbon, glucose, amino acids and phosphate) or extreme environments (high temperature, hypoxia and redox imbalance) or internal stressors such as dysfunctional proteins, and superfluous or damaged organelles, signaling cascades are initiated which ultimately converge at TORC1 and the downstream effectors enable initiation of bulk autophagy. TORC1 exerts its regulatory control on autophagy by directly modulating the activity of the Atg1 kinase complex through phosphorylation (Hu et al., 2019). The main target of TORC1 is Atg13, a serine-rich protein that is phosphorylated at multiple residues (Kamada et al., 2010). Several sites are in or near the interaction domain with Atg1 and the scaffold protein Atg17 (Licheva et al., 2022). Phosphorylated residues in these sites enable weak binding of Atg13 and Atg17. However, these interactions are strengthened through dephosphorylation (Fujioka et al., 2014). Subsequently, the intermolecular bridges of Atg17-Atg31-Atg29 hexamers facilitate the formation of supramolecular complexes consisting of Atg13 and Atg17-Atg31-Atg29 (Yamamoto et al., 2016). Atg13 interacts with Atg1 at the MIT-interacting motif/MIM domains, an interaction which again is strengthened through dephosphorylation. While the Atg17-Atg31-Atg29

subcomplex is constitutively present at the PAS, its association with Atg1 and Atg13 is regulated by their phosphorylation status (Fujioka et al., 2014).

When nutrients are available, TORC1 directly represses the autophagy initiation complex by phosphorylating both Atg1 and Atg13. During nutrient limitation, TORC1 is inhibited, and Atg13 is rapidly dephosphorylated, which allows it to form an active Atg1-Atg13-Atg17 initiation complex to induce autophagy (Yamamoto et al., 2016). While over 40 phosphorylation sites have been mapped on Atg13, only some have been verified as direct TORC1 or Atg1 targets (Fujioka et al., 2014; Hu et al., 2019; Kamada et al., 2010). Ser428 and Ser429, targets of both TORC1 and Atg1, are involved in regulating the Atg13-Atg17 interaction, while Ser344, Ser437, and Ser581 have an effect on Atg13 interaction with the PAS (Fujioka et al., 2020; Hu et al., 2019; Rao et al., 2016). *In vivo* studies show that Ser646 is targeted by TORC1, and Ser496 and Ser535 are targets of Atg1. A phosphatase that dephosphorylates Atg13 in response to nutrient starvation has yet to be identified. However, several PP2A phosphatases have been implicated in dephosphorylating Atg13 (Janssens & Goris, 2001; Yeasmin et al., 2016). Double deletions of *PPH21* and *PPH22*, and *CDC55* and *RTS1* show defects in autophagy; however, the effect on dephosphorylation of Atg13 is not complete (Yeasmin et al., 2016). In contrast, another study investigating the role of PP2A in autophagy found that the inactivation of PP2A stimulates autophagy, and overexpression of its catalytic subunit blocks rapamycin-induced autophagy (Yorimitsu et al., 2009). Therefore, the role of PP2A in regulating autophagy is yet to be fully understood. Ptc2 and Ptc3, two of the PP2C phosphatases, also show a block in autophagy in a double-mutant background (Memisoglu et al., 2019). Furthermore, Atg13 remains hyperphosphorylated irrespective of TORC1 status, indicating that Ptc2 and Ptc3 are involved in the dephosphorylation of Atg13 (Memisoglu et al., 2019). Later, it was confirmed that Ptc2

dephosphorylates Atg13 at the Ser428 and Ser429 sites, enhancing the phase separation propensity of the Atg1 kinase complex (Fujioka et al., 2020).

Global proteomic analysis has revealed that TORC1 likely exerts control over several other Atg proteins, including Atg1, Atg2, Atg9, and Atg29, suggesting that not only does TORC1 control the initiation of autophagy but also downstream processes such as phagophore nucleation and expansion. Interestingly, these targets are shared with Atg1, suggesting an intimate relationship between TORC1 and Atg1 in coordinated control of autophagy initiation (Hu et al., 2019).

TORC1, therefore, exerts its regulatory effects on autophagy through phosphorylation. In particular, Atg13 and Atg1 have emerged as key proteins that undergo TORC1-dependent post-translational modification. While I have only discussed phosphorylation by TORC1, it is important to note that several other kinases phosphorylate a myriad of autophagy targets and are also dynamically regulated by phosphatases. These observations underpin the role of phospho-regulation of autophagy and highlight an opportunity for the development of kinase and phosphatase inhibitors to modulate autophagy in human diseases.

1.2.2 Autophagy induction by carbon starvation

Yeast can utilize a diverse array of carbon sources for energy generation and as precursors of anabolism. It exhibits a bias toward utilizing fermentable sugars like glucose or fructose, while showing less preference for non-fermentable carbon sources such as glycerol or ethanol. These hierarchical preferences achieved by allosteric regulation of various glycolytic and gluconeogenesis enzymes. Furthermore, glucose controls transcriptional regulatory networks where it suppresses genes responsible for the catabolism of non-fermentable sugars, including genes involved in oxidative phosphorylation (Fendt & Sauer, 2010; Kayikci & Nielsen, 2015).

Therefore, even in the presence of oxygen, yeast cells exclusively use glycolysis to obtain energy from glucose. This specific metabolic program, called the Warburg effect, is also adopted by cancer and stem cells (Diaz-Ruiz et al., 2011; Fiechter et al., 1981; van Dijken et al., 1993). Because ATP is mainly derived through glycolysis under these conditions, a precipitous drop in ATP is observed following glucose starvation (Lang et al., 2014). When the cell's energy status is disrupted due to glucose limitation, cells must proactively switch to utilizing an available alternate carbon source. The Snf1 complex is primarily involved in enabling this switch via transcriptional regulation and modulation of enzyme activity (Crozet et al., 2014). Thus, cells transition from a glucose to ethanol utilization phase (Perez-Samper et al., 2018).

Additionally, in the absence of reserves and limited ATP available for transporting catabolic substrates from external sources, it is highly probable that cells primarily depend on the hydrolysis of their own cellular components for sustenance during the initial stages of glucose starvation, enabled by autophagy. Interestingly, cytosolic degradation is dependent on Atg17, but not Atg11, another scaffold protein that functions primarily during growing conditions (Iwama & Ohsumi, 2019). Furthermore, nuclear and cytoplasmic ER is turned over by reticulophagy in an Atg39- and Atg40-dependent manner, respectively. Once the ethanol in the extracellular medium is depleted, cells begin to degrade excess mitochondria in an Atg11- and Atg32-dependent manner, suggesting that cells adapt the type of autophagy induction concomitant to carbon source availability (Iwama & Ohsumi, 2019). In parallel to autophagy, microautophagy is also induced in both the ethanol utilization and ethanol-depleted phases. Thus, a multifaceted autophagic response is initiated to different carbon sources and glucose limitation conditions wherein the metabolic states switch from glucose-driven rapid growth to respiratory growth and then survival without any carbon source (Iwama & Ohsumi, 2019). Future investigations into the

fine-tuning and regulating autophagic substrates will be critical in understanding how cells utilize autophagy to adapt to changing metabolic conditions.

Although autophagy induction is less pronounced under glucose limitation compared to nitrogen starvation, it remains crucial for efficient growth and adaptation to non-fermentable carbon sources. The availability of respiratory carbon sources is adequate to promptly trigger nonselective autophagy, and any disruption of this process leads to impaired mitochondrial metabolism. Serine, an amino acid supplied through autophagy, plays a supportive role in mitochondrial translation, function, and facilitates adaptation to respiratory growth. (May et al., 2020).

Given the different stages of metabolic and autophagic responses to carbon availability, experimental procedures wherein cells are shifted from growing conditions to glucose starvation (a complete lack of any carbon source or supplemented with glycerol or other non-fermentable carbon sources) may result in discrepancies in the autophagic responses observed (Gross & Graef, 2020). For example, when cells grown in glucose-rich media are shifted to carbon-free media, autophagy is induced (Adachi et al., 2017). In contrast, glucose depletion and nitrogen starvation inhibit autophagy (Lang et al., 2014). These findings indicate that the concentration of different metabolites' intracellular pools may modulate the strength of autophagy induction.

1.2.2.1 Glucose limitation activates Snf1

Snf1 is a protein kinase in the Snf1/AMPK family and was identified by Carlson et al. in 1981 when they performed a screen for mutants that were unable to utilize sucrose and other non-fermentable carbon sources (therefore, sucrose nonfermenting) (Carlson et al., 1981). It was later uncovered that the *SNF1* gene encodes the catalytic subunit of a serine-threonine kinase (Celenza & Carlson, 1984, 1986). Following studies identified the non-catalytic components, the

beta and the gamma subunits, demonstrating the Snf1 complex to be heterotrimeric. In yeast, three alternative beta subunits (Sip1, Sip2, Gal83) and one regulatory gamma subunit, Snf4, are present. Consequently, this results in the presence of three distinct Snf1 complexes (Yang et al., 1992; Erickson & Johnston, 1993; Celenza & Carlson, 1989; Celenza et al., 1989; Matsumoto et al., 1981; Neigeborn & Carlson, 1984; Schmidt & McCartney, 2000; Yang et al., 1994).

In response to glucose limitation, the catalytic subunit is activated by phosphorylation of Thr210 in the activation loop and is regulated by upstream kinases Sak1, Elm1, and Tos3 and the protein phosphatase PP1 (Hong et al., 2003; Sutherland et al., 2003; Sanz et al., 2000; Tu & Carlson, 1995). Unlike the mammalian AMPK, Snf1 is not allosterically activated by AMP, but the activation is correlated with a high AMP:ATP ratio (Mitchelhill et al., 1994; Adams et al., 2004; Wilson et al., 1996; Woods et al., 1994). Through adaptation to glucose limitation, Snf1 activity reduces to minimal levels required for continued growth (Hedbacker & Carlson, 2008). Other environmental conditions such as nitrogen starvation and rapamycin treatment also induces the phosphorylation of Snf1 (Orlova et al., 2006). While the beta subunits are not essential for glucose derepression, they are regarded as the scaffold for Snf1 complex assembly, as their C-terminal domains appear to bridge the catalytic and regulatory subunits. Furthermore, a functional regulatory gamma subunit is required for the kinase activity of Snf1 (Coccetti et al., 2018).

Additionally, the subcellular localization of the Snf1 complex is regulated by glucose availability (Vincent et al., 2001). In glucose-rich conditions, the Snf1 complex is cytoplasmic; however, when glucose is limiting, the beta subunits have a different localization pattern depending on their N-terminal sequences (Vincent et al., 2001); Sip1 relocates to the vacuolar membrane, Sip2 remains cytoplasmic, and Gal83 moves to the nucleus (Ghaemmaghami et al.,

2003; Hedbacker et al., 2004). These subunits, therefore, direct the localization of Snf1 (Hedbacker et al., 2004). However, the activation of Snf1 by the kinase Sak1 is required for Snf1-Gal83 to localize to the nucleus. (Hedbacker & Carlson, 2006). The Snf4 subunit is localized both in the cytoplasm, and the nucleus, and its localization is independent of the nutritional status of the cell (Vincent et al., 2001).

1.2.2.2 Mechanism of autophagy regulation by Snf1

Snf1 is a positive regulator of autophagy, and deletion of *SNF1* completely blocks autophagy induction (Wang et al., 2001). Snf1 directly phosphorylates Atg1, suggesting that Snf1 activates Atg1 during glucose starvation (Yao et al., 2020). Atg11, critical for the cytoplasm-to-vacuole targeting/Cvt pathway and selective autophagy, is also essential for autophagy under glucose-starvation conditions. By controlling the interaction of Snf1 and Atg1, and therefore, Snf1-dependent Atg1 phosphorylation, Atg11 modulates the kinase activity of Atg1 during glucose starvation (Yao et al., 2020). Atg11 also binds to Snf1; however, whether Snf1 phosphorylates Atg11 is unknown.

Glucose starvation induces the movement of Snf1 to the mitochondria, wherein Snf1 phosphorylates Mec1, an essential genome integrity checkpoint protein (Yi et al., 2017). Phosphorylated Mec1 interacts with Atg1, enabling its recruitment to the mitochondria and promoting glucose starvation-induced autophagy. As a DNA damage sensor, Mec1 is also essential for DNA-damage induced autophagy (Yao et al., 2023). Furthermore, Mec1 also localized to the mitochondria, providing a hint to its role in mitophagy. Additionally, the Snf1-Mec1-Atg1 axis maintains mitochondrial activity, which is crucial doe both the phosphorylation fo Mec1 and the interaction between Atg1 and Atg13 in response to glucose starvation.

Therefore, activated Snf1 supports mitochondrial respiration by phosphorylating Mec1 and promoting the binding of Atg1 and Atg13 to initiate autophagy (Yi et al., 2017).

Furthermore, Mec1 plays a pivotal role in recruiting Atg13 to the PAS and facilitates the interaction between mitochondria and autophagosomes through Ggc1 and Atg13 (Yao et al., 2023). Nevertheless, the specific necessity of the link between mitochondria and autophagosomes mediated by Mec1 to initiate autophagy during glucose scarcity remains unclear. One hypothesis posits that mitochondria might serve as a potential source of essential materials required for the formation of autophagosomes. Additionally, mitochondria serve as an energy center and supply ATP to Snf1, which resides in the mitochondria during glucose starvation. To adapt to the energy stress during glucose starvation, it is possible that cells transmit the signal from Snf1 to autophagy initiation via Mec1 (Wu et al., 2020).

Interestingly, mitochondria are the regulatory hub of glucose starvation-induced autophagy, analogous to the vacuole for nitrogen or amino acid starvation-induced autophagy (Yi et al., 2018). Mitochondrial respiration and mitochondrial fusion are necessary for the association between Snf1 and Mec1 and the subsequent recruitment of Atg protein to the PAS (Wu et al., 2020). Consequently, Atg1-Atg13 interacts with Snf1-Mec1, so it will be interesting to investigate if the PAS could be close to the mitochondrial network instead of the vacuole during glucose starvation-induced autophagy, drawing attention to the broader question of what determines the location of the PAS.

1.2.2.3 Glucose activates PKA

The Ras-cyclic AMP (cAMP)-dependent protein kinase A (PKA) is another crucial signal transduction pathway that governs autophagy in response to fluctuations in nutrient availability(Stephan et al., 2009). The PKA pathway plays a role in regulating cellular

metabolism and growth, working in tandem with glucose levels (Tamaki, 2007). Glucose activates the production of cAMP, which in turn activates the Ras-cAMP-PKA pathway, thereby mediating cellular functions such as cell growth, metabolism, and stress resistance in response to glucose (Tamaki, 2007). The G protein coupled receptor Gpr1 and secondary messenger cAMP control glucose-mediated activation of PKA (Peeters et al., 2017; Rolland et al., 2000). However, other nutrients, such as nitrogen, phosphate, and sulfate, activate PKA in starvation conditions without cAMP signaling (Van Zeebroeck et al., 2020).

The Ras GTPase family consists of the Ras1 and Ras2 proteins that coexist in their different nucleotide-bound states, influencing glucose availability (Van Zeebroeck et al., 2020). By shift from a non-fermentable carbon source to a fermentable carbon source, Ras proteins are activated, and they subsequently bind to the enzyme adenylate cyclase to promote cAMP production (Thevelein & de Winde, 1999). cAMP then promotes the dissociation of the catalytic subunits of PKA (Tpk1, Tpk2, and Tpk3) from the repressor Bcy1, thus activating PKA. Activated PKA continues the signaling cascade by phosphorylating its substrates, allowing adaptation to the new condition (Mitchener et al., 1976).

1.2.2.4 Interplay of the PKA and TORC1 pathways regulates autophagy

The Ras-PKA pathway negatively regulates autophagy (Budovskaya et al., 2004). Interestingly, simply blocking PKA kinase activity alone does not trigger the induction autophagy. It simultaneously requires the inhibition of Sch9, the TORC1 substrate. This highlights a cooperative role of PKA and TORC1 in regulating autophagy. Additionally, inhibition of TORC1 and PKA has a synergistic effect on autophagy induction. Thus, the signaling cascades of TORC1 and PKA need to be efficiently integrated to regulate autophagy, possibly at multiple regulatory nodes (Schmelzle et al., 2004).

One such node is at the level of Atg proteins. Sequence analysis revealed two potential PKA sites in Atg1, later confirmed by *in vitro* and *in vivo* studies(Budovskaya et al., 2005). However, mutations of these sites does not affect Atg1 kinase activity but alters its localization. The Atg1 variant that lacks the PKA sites is constitutively localized to the PAS irrespective of the nutritional status. Additionally, constitutively active PKA, utilizing the $Ras2^{G19V}$ allele, disrupts the localization of Atg1 to the PAS, suggesting that PKA negatively regulates autophagy by phosphorylating Atg1 and preventing its localization to the PAS by autophagy induction (Budovskaya et al., 2005).

In addition to Atg1, PKA also phosphorylates Atg13 (Stephan et al., 2009). This phosphorylation, distinct from the Tor1-dependent sites, regulates the localization of Atg13 to the PAS. Mutating PKA-dependent phosphorylation sites on Atg13 sequesters the protein at the PAS, irrespective of the nutritional state. Furthermore, the localization of Atg13 to the PAS is disrupted in the presence of constitutively active PKA, suggesting that PKA regulates autophagy at the early stages by controlling the localization of crucial autophagy induction proteins to the PAS (Stephan et al., 2009).

The second regulatory node is at the level of transcription. Rim15, a protein kinase, integrates signals from TORC1 and PKA to positively regulate autophagy (Yorimitsu et al., 2007). When nutrients are abundant, Rim15 is phosphorylated by TORC1 and PKA, thus inhibiting its nuclear translocation. In response to TORC1 inhibition, Rim15 is dephosphorylated and enters the nucleus. Here, it phosphorylates Ume6, a negative regulator of *ATG8* expression. Rim15-mediated phosphorylation inhibits Ume6, thus promoting *ATG8* transcription (Bartholomew et al., 2012). Similarly, Rim15-dependent phosphorylation of Rph1, a histone

demethylase and negative regulator of autophagy, inhibits it, thus enabling the transcription of *ATG1*, *ATG7*, *ATG8*, *ATG9*, *ATG14*, *ATG29*, and *ATG32* (Bernard et al., 2015).

Another regulatory node where TORC1 and PKA coordinate to suppress autophagy is at Ksp1 (Umekawa & Klionsky, 2012). Ksp1 has several consensus phosphorylation sites and is activated by PKA. Upon activation, Ksp1 activates TORC1, as evidenced by Atg13 hyperphosphorylation, inhibiting autophagy. However, a feedback mechanism may exist through PKA-independent phosphorylation because Ksp1 is also a target of TORC1 phosphorylation. Thus, together, TORC1 and PKA regulate autophagy based on the nutritional conditions within the cell (Umekawa & Klionsky, 2012).

1.3 Regulation of *ATG* gene expression

Signaling pathways that sense nutrient availability and influence autophagy provide deeper understanding how spatially separated processes are integrated to elicited a cellular response to external cues. However, tuning autophagy by modulating the activation/suppression of these pathway tend to be tedious due to various pleotropic effects. In order to specifically target and tune autophagy without disrupting other important cellular pathway, regulators that act directly on the autophagy-related gene product are best suited. Toward this, regulation of ATG expression at various stages such as transcription, post-transcription, translation and post translation can occur. In this thesis, I specifically look at post-transcriptional and translational mechanisms that regulate autophagy.

In the following sections, I provide a primer on RNA-binding proteins, the current understanding of post transcriptional regulation in yeast and mammalian systems, and post transcriptional regulators that influence autophagy in health and disease.

1.3.1 RNA-binding protein: primary drivers of mRNA life cycle

RNA-binding proteins engage with mRNA during every stage of its lifecycle, influencing its sysnthetis, modification, localization, translation and stability. They are critical effectors of post-transcriptional regulation of genes and the interplay of RNA and RBPs within dynamic ribonucleoproteins (RNPs) orchestrate the various facets of RNA biology. Distinct cellular contexts, therefore, utilize varying RBP repertoire with differential activates to respond to environmental cues. A subset of constitutive RNA-binding proteins may be ubiquitously active whereas many RBPs may have distinct expression pattern or activity based on specific PTMs.

RBP-RNA interactions can be single protein-RNA interaction or a dynamic assembly of an array of RBPs that interact with multiple regions of the RNA. The mechanism that defines the selectivity of RNA-RBP interaction is not known, however, several studies have identified different types of intermolecular interactions and preferred amino acid required for the interaction. RNA-binding domains in proteins are the modular units that bind to mRNA. Multiple types of domains can occur in one RBP or the same domain can be repeated multiple times. These modular arrangement coordinate, enhance and specify RNA-binding. These domains, more than 600 identified, are regularly linked by intrinsically disorder regions (IDR), able to bind RNA as well, but aid in the modular architecture of RNA-binding proteins. (Gerstberger et al., 2014). IDRs rich in serine and arginine (S.R) and arginine and glycine (R/G) were found to contribute to RNA-binding activity and co-occur with other types of RNA-binding domains.

The RNA Recognition Motif (RRM) is one of the most abundant RNA-binding domains (RBDs) in eukaryotes (Maris et al., 2005). In the human proteome, about 30% of the RBPs with RNA-binding function contain one or more RRM. RRM consistently also co-occur with other types of RBDs, with zinc fingers being the most common. Proteins that contain RRM are

involved in RNA metabolism, enriched in the spliceosome or mRNA surveillance. Interestingly, about 18% of RRM containing proteins are associated with human diseases suggesting the crucial role played by RRM in RNA biology and human physiology (Agarwal & Bahadur, 2023).

RBPs mainly function in two cellular compartments: nuclear, with a role in splicing of pre-mRNAs or cytoplasmic with a role in post transcriptional regulation. Some RBPs remain associated with mRNA throughout the life-time whereas others bind either at early or later stages of the mRNA life cycle (Choi et al., 2024; Coppin et al., 2018). These spatial and temporal interaction dynamics ensure specificity of RNA regulation while ensuring homeostatic processes to occur without disruption. Composition of mRNPs determines the fate of RNA in this spatiotemporal paradigm wherein the mRNA can be immediately translated or transported for storage or translation at local areas. mRNPs therefore undergo constant remodeling, aided by competitive RBP-RNA interactions and post-translational modifications to meet the demands of the cell.

1.3.1.1 Role of RNA-binding proteins in the nucleus

RBPs in the nucleus are primarily involved in co-transcriptional processes of the mRNA life cycle. Newly synthesized eukaryotic transcripts undergo maturation consisting of the addition of a 5' cap, a 3' poly(A) tail, and the removal of introns by splicing. Various RNA-binding proteins coordinate to complete the maturation process of mRNA while some interactions also control the mRNA export and fate of the mRNA in the cytoplasm. This predetermination is brought about my co-transcriptional imprinting of mRNA with proteins which in turn regulate the metabolism of the mRNA in the cytoplasm (Haimovich et al., 2013). For example, Rap1 binding to the promoter of a gene can alter the stability of the transcript in the cytoplasm by affecting the composition of the exported mRNP, which in turn regulates mRNA

decay in the cytoplasm (Bregman et al., 2011). This highlights the presence of a co-transcriptional mechanism that defines the mRNP assembly surrounding the newly synthesized transcript.

The nascent mRNA is thus surrounded with proteins that determine correct RNA processing, integrity, export and subsequent steps in the cytoplasm. Defective mRNP assembly, thus prevents the mRNA to be exported, leading to nuclear retention of the transcript and eventual degradation. In yeast, numerous factors ensure the biogenesis of export-competent mRNPs, including Npl3, the THO complex and Yra1. Npl3 is a major SR-like RNA-binding protein that is recruited to the newly synthesized transcript. Npl3 is found in the same complex with RNA Pol II and directly stimulates its elongation activity (Dermody et al., 2008). Mutations in Npl3 block mRNA export suggesting that Npl3 interacts with RNA co-transcriptionally and primes the transcript for export (Lei et al., 2001).

Following proper packing of the mRNA in the mRNP complex is released from the transcription site and transported to the cytoplasm by the mRNA export receptor: Mex67-Mtr2, that guide the complex through nuclear pore complexes that embed the nuclear envelope. Mex67-Mtr2 transcript across the NPC through interactions with several nnucleoporins that contain FG repeats. These FG repeats form a mesh in the NPC that selectively allows access for nuclear transport receptors. Once the mRNA reaches the cytoplasmic side of the NPC, Nup159 and Nup42 recruit Dbp5 that impart directionality to the export process by remodeling the mRNP in an ATP dependent manner. Dbp5 thus aides in the disassembly of the mRNP complex which prevent reentry to the cytoplasm before mRNA release. Mex67-Mtr2 then return to the nucleus to begin another round of mRNP export from nucleus to the cytoplasm. The essential role of both

Mex67 and Dbp5 requires there localization to the NPC (Adams & Wente, 2020; Derrer et al., 2019).

1.3.1.2 Role of RNA-binding proteins in the cytoplasm

The mRNP composition is remodeled close to the NPC before cytoplasmic release of mRNA but the mRNP continues to be dynamically remodeled in the cytoplasm. The new mRNP thus controls the fate of the mRNA and can control its localization, stability and translation.

Subcellular localization of mRNA provide precise control over the location of protein synthesis (Holt & Bullock, 2009). This spatial control results in the configuration of distinct subcellular compartments for specialized functions as seen in, for example, the synaptic activity of mammalian neurons (Mofatteh, 2020). Molecular motor-based transport is a predominant mechanism of localization, but RNA granules 'hitchhiking' onto membrane-bound organelles to traverse across the cellular plane is also quite common (Liao et al., 2019). Further understanding of RBP-motor protein interactions and pathways of transport will elucidate the spatial and temporal control of gene expression.

RNA-binding proteins have been shown to regulate several biological roles by modulating mRNA translation (Li et al., 2022). Eukaryotic mRNAs contain 5' and 3' untranslated regions that impose regulatory control on the fate of the mRNA by guiding RBP-RNA interactions. The 5' UTR, the entry point for ribosome recruitment during translation, can adopt complex secondary structures. At the 5' UTR, translation begins with the recruitment of the 43S preinitiation complex, containing a GTP bound eIF2 at the 5' cap. This recruitment is facilitated by the eIF4F complex containing eIF4E, eIF4G, eIF4A and the poly(A) binding protein, PABP. The PIC scans the mRNA 5' untranslated region until it finds the AUG triplet complementary to the anticodon of Met-tRNA. Upon recognition, the GTP bound to eIF2 hydrolyzes to produce a

stable 48S PIC. eIF5B then catalyzes the recruitment of 60s ribosome subunit followed by the release of eIF2-GDP. The newly formed 80S initiation complex thus begins translation process (Hinnebusch et al., 2016). Due to the importance of the 5' UTR in forming the pre-initiation complex, secondary structures in the region can influence the efficiency of translation initiation. In order to ensure smooth translation scanning, RNA-binding proteins called DEAD-box ATP dependent RNA helicases overcome structural hindrances to increase translation efficiency. eIF4E preferentially stimulates the translation of mRNAs containing secondary structures (Koromilas et al., 1992). Ded1/DDX3 plays a crucial role in resolving stable structures and this ensures efficient translation initiation (Abaeva et al., 2011).

RBPs bind to the 3' UTR cis elements and mediate recruitment of effector proteins. As RBPs interact with several different proteins, the 3' untranslated region of the mRNA provide a platform for defining RBP-RNA interactions that control crucial decisions such as translation and stability (Szostak & Gebauer, 2013). The cellular state also defines the RBP-3' UTR interactions and the function of the 3' UTR is context dependent based on the type of RBP that is bound. Therefore, the 3' UTR-RBP interactome is dynamic and is remodeled in response to environmental cues through changes in post-translational modifications and interaction with other RBPs (Berkovits & Mayr, 2015).

During nutrient and ribosomal stress, translation is inhibited wherein the mRNAs are released from ribosomes and bound to RBPs knowing to granules which consists of ribosomal subunits, translation factors, decay enzymes, helicases, scaffold proteins, and RNA-binding proteins. The two main types of granules are processing bodies (PBs) and stress granules (SGs). PBs facilitate mRNA degradation, while SGs inhibit translation by harboring stalled 48S initiation complexes. For instance, Pub1 and Dhh1 are involved in the assembly of these

granules, modulating translation during stress. These granules interact with the cytoskeleton, enabling their dynamic properties, and can exchange mRNAs. However, if the RBPs involved in granule formation also have other roles to may in the cellular mRNA metabolism is yet to be explored.

1.4 Post-transcriptional regulation of autophagy in yeast

Recently, *ATG1* has emerged as a transcript regulated by multiple players in a nutrient-dependent manner. Notably, under nutrient-rich conditions, the cytoplasmic exoribonuclease Xrn1 reduces the stability of *ATG1* mRNA, leading to its degradation (Delorme-Axford et al., 2018). During nitrogen deprivation, the Pat1-Lsm complex plays a protective role, preventing the degradation of *ATG1* mRNA by the exosome from the 3' to the 5' end, thereby maintaining its stability (Gatica et al., 2019). In the presence of ample nutrients, Dhh1, an RNA helicase, collaborates with Dcp2 to accelerate the breakdown of *ATG1* messages, leading to a decrease in autophagy (Hu et al., 2015). However, under prolonged nitrogen starvation, Dhh1 works with Eap1 to enhance *ATG1* mRNA translation, specifically targeting the structured region close to the start codon and promoting autophagy (Liu et al., 2019). The translation of *ATG1* mRNA is further enhanced during extended periods of nitrogen limitation by the RGG motif-bearing protein Psp2, which interacts with translation machinery components eIF4E and eIF4G2 and targets the 5' UTR of *ATG1*, independent from Dhh1 (Yin et al., 2019). Finally, Ded1, in conjunction with Rad53, upregulates Atg1 protein expression only in response to nitrogen starvation but not in amino acid starvation, suggesting the sensitivity of this regulatory network to minute changes in external nutrient environments (Lahiri et al., 2022). These novel insights point to a complex web of *ATG1* mRNA-protein interactions, suggesting extensive regulatory

oversight across its metabolic lifecycle. However, how these various factors, that make up P-bodies, coordinate to regulate the same mRNA is yet unknown.

1.5 Post-transcriptional regulation of autophagy in mammals

In searching for RBPs that regulate autophagy, a high throughput small interfering RNA screen targeting 1,530 RBPs in MCF-7 cells determined that ablation of the eukaryotic translation initiation factors 5A (EIF5A) and 4A3 (EIF4A3) causes a decrease in GFP-LC3B puncta in autophagy-inducing conditions (Lubas et al., 2018; Sakellariou et al., 2021) . Association of EIF5A with ribosomes increases during starvation conditions, suggesting that recruitment of EIF5A to ribosomes can reflect the repertoire of the actively translated pool of transcripts that promote autophagy. Analysis of newly synthesized proteins by LC-MS determined that ATG3 protein levels are decreased upon EIF5A ablation and revealed that EIF5A assists the translation of *ATG3* through a hard-to-translate motif called the DDG motif. This facilitates the lipidation of LC3B and thus the promotion of autophagosome biogenesis (Lubas et al., 2018). Interestingly, in B cells, the polyamine spermidine post-translationally modifies EIF5A by adding the unusual amino acid hypusine (Zhang et al., 2019). Hypusinated EIF5A is required for the translation of hard-to-read motifs and is also important for the translation of TFEB, a key autophagy regulator (Zhang et al., 2019).

The human embryonic lethal abnormal vision (ELAV/Hu) family is a highly conserved family of RBPs that consists of four members, ELAV like RNA-binding protein 1 (ELAVL1 also known as HuA or HuR), ELAVL2/HuB/Hel-N1, ELAVL3/HuC and ELAVL4/HuD. These RBPs are characterized by the presence of three RNA recognition motifs (RRMs), with RRM2 and RRM3 connected by a flexible linker region (Maris et al., 2005).The ELAV/Hu family RBPs stabilize

mRNAs and subsequently activate its translation. Analyses of their targets have revealed these RBPs regulate autophagy by stabilization and translational upregulation of *ATG* transcripts. For example, in pancreatic beta cells, ELAVL4 associates with *ATG5* mRNA (Kim et al., 2014; Lee et al., 2012). Here, ELAVL4 binds to the 3' UTR of *ATG5* mRNA. Ablation or overexpression of ELAVL4 does not affect endogenous *ATG5* mRNA levels; however, the protein levels of ATG5 are significantly reduced following silencing of ELAVL4 (Kim et al., 2014). Furthermore, analysis of translation of *ATG5* mRNA by polysome fractionation confirms that ELAVL4 enhances ATG5 translation by increasing its association with actively translating polysome fractions. ELAVL4 promotes autophagosome biogenesis by increasing ATG5 abundance, therefore acting as a positive regulator of autophagy (Kim et al., 2014). Furthermore, ELAVL1 was found to bind to *ATG5, ATG12* and *ATG16L1* mRNAs at their 3' UTR regions and regulates autophagy by enhancing translation of these transcripts (Ji et al., 2019). Studies focusing on elucidating the role of ELAVL1 in hypoxia-induced autophagy demonstrate that ELAVL1 binds to *ATG7* and *ATG16L1* in the coding and 3' UTR regions, respectively, which results in the upregulation of the protein levels and enhanced autophagosome formation (Palanisamy et al., 2019). Another study determined that ELAVL1 activates autophagy by stabilizing *ATG7* transcripts to suppress senescence in diabetic NP cells (Shao et al., 2021). Together, these studies show that ELAV proteins, such as ELAVL4 and ELAVL1, are important regulators of *ATG* mRNA stability and promote autophagy by enhancing *ATG* mRNA translation through association with their 3' UTRs. It is worth noting that *ATG* mRNAs can also be negatively regulated by RBPs. For instance, ZFP36/TTP binds to the 3' UTR of *ATG16L1* mRNA to recruit deadenylating and degradation factors during ferroptosis, thus acting as a negative regulator of autophagy (Zhang et al., 2020)

1.6 Outlook

The field of autophagy has made tremendous progress in the past 30 years, wherein over 40 genes involved in the autophagy pathway have been identified, and many of the morphological, molecular, and cellular mechanisms underlying autophagosome biogenesis have been elucidated (Feng et al., 2014; Khandia et al., 2019; Nakatogawa, 2020). When faced with changing metabolic environments, cells rely on autophagy to maintain homeostasis and generate building blocks to feed into processes and metabolic networks critical for survival. In utilizing available nutrients, cellular systems integrate complex metabolic and functional information to fine-tune the extent of autophagy induction and execution. In integrating the external nutrient cues to functional autophagy, cells utilize several signaling pathways, mainly TORC1, Snf1, and cAMP-PKA pathways, that exert control over multiple levels of cellular outputs (Russell et al., 2014). By sensing nutrient changes, sensors transduce information to master regulators. These regulators, usually kinases, act By effectors such as transcription factors spatially and temporally. Transcription factors target genes involved in nutrient import, vacuolar export, biosynthesis, and autophagy. Building blocks generated from autophagy are then reutilized. This perpetual feedback loop of activation-inactivation utilizing kinases, transcription factors, and import/export proteins defines the cellular survival mechanisms for adapting to external nutrient environments.

Physiologically, changes in external nutrient environments are more gradual. However, the experimental approaches currently use drastic switches from one condition to another. It will be interesting to investigate how cellular responses change and what signaling cascades are revealed when gradual nutrient limitation is employed. Additionally, these experimental

procedures only study single-nutrient limitations, whereas physiologically there may exist multiple starvation conditions at the same time. Therefore, it will be interesting to explore how autophagic processes are prioritized under such conditions. Studies have shown that the extent of autophagy is dependent on the severity of starvation. For example, nitrogen starvation induces a stronger autophagy response compared to amino acid starvation and glucose starvation. This subtle fine tuning of autophagy is driven by the post-transcriptional regulation of *ATG1* transcript by an RNA-binding protein, Ded1 (Lahiri et al., 2022). Furthermore, comparison of molecular and cellular changes in autophagic responses with regard to Atg protein utilization, PAS site formation, and organelle involvement to various external nutrient cues are yet to be investigated.

An intriguing aspect is the requirement for multiple signaling pathways in autophagy regulation. It is plausible that these pathways respond to different nutritional cues, resulting in distinct autophagy responses during various types of starvation within the cell. The existence of multiple inputs offers the cell increased adaptability to cope with dynamic environmental changes. Unraveling the impact of these pathways on the degradative process and understanding the coordination of their signaling activities represents significant areas for future research.

A fascinating nexus that needs further investigation is towards strategic utilization of nutrients during starvation conditions; global translation is downregulated via TORC1 and general amino acid control pathways. However, selectively driven translation of specific protein subsets, especially Atg proteins, is critical for cellular survival mechanisms (Hu et al., 2015). How this selectivity is achieved and how the translation of specific RNA subsets is enhanced are questions under investigation. To uncover this, I focus on an important Atg protein required for autophagy induction, Atg1. Despite the known involvement of RNA-binding proteins in

autophagy and RNA-binding proteins (RBPs) that interact with *ATG1* transcript, a comprehensive understanding of the *ATG1*-RBP interaction network is lacking. How *ATG1*-RBP interaction influences the lifecycle of ATG1 transcript, including export, interaction with translation factors and finally translation by ribosomes is yet to be comprehensively elucidated. Further, I are yet to understand how the translation of the *ATG1* transcript is modulated during different nutritional stresses. I address these questions in my thesis work.

1.7 References

1. Abeliovich, H., & Klionsky, D. J. (2001). Autophagy in yeast: mechanistic insights and physiological function. *Microbiol Mol Biol Rev*, *65*(3), 463-479, table of contents. https://doi.org/10.1128/MMBR.65.3.463-479.2001
2. Adachi, A., Koizumi, M., & Ohsumi, Y. (2017). Autophagy induction under carbon starvation conditions is negatively regulated by carbon catabolite repression. *J Biol Chem*, *292*(48), 19905-19918. https://doi.org/10.1074/jbc.M117.817510
3. Adams, J., Chen, Z. P., Van Denderen, B. J., Morton, C. J., Parker, M. W., Witters, L. A., Stapleton, D., & Kemp, B. E. (2004). Intrasteric control of AMPK via the gamma1 subunit AMP allosteric regulatory site. *Protein Sci*, *13*(1), 155-165. https://doi.org/10.1110/ps.03340004
4. Adams, R. L., & Wente, S. R. (2020). Dbp5 associates with RNA-bound Mex67 and Nab2 and its localization at the nuclear pore complex is sufficient for mRNP export and cell viability. *PLoS Genet*, *16*(10), e1009033. https://doi.org/10.1371/journal.pgen.1009033
5. Agarwal, A., & Bahadur, R. P. (2023). Modular architecture and functional annotation of human RNA-binding proteins containing RNA recognition motif. *Biochimie*, *209*, 116-130. https://doi.org/10.1016/j.biochi.2023.01.017
6. Apponi, L. H., Kelly, S. M., Harreman, M. T., Lehner, A. N., Corbett, A. H., & Valentini, S. R. (2007). An interaction between two RNA-binding proteins, Nab2 and Pub1, links mRNA processing/export and mRNA stability. *Mol Cell Biol*, *27*(18), 6569-6579. https://doi.org/10.1128/MCB.00881-07
7. Ariosa, A. R., Lahiri, V., Lei, Y., Yang, Y., Yin, Z., Zhang, Z., & Klionsky, D. J. (2021). A perspective on the role of autophagy in cancer. *Biochim Biophys Acta Mol Basis Dis*, *1867*(12), 166262. https://doi.org/10.1016/j.bbadis.2021.166262
8. Bartholomew, C. R., Suzuki, T., Du, Z., Backues, S. K., Jin, M., Lynch-Day, M. A., Umekawa, M., Kamath, A., Zhao, M., Xie, Z., Inoki, K., & Klionsky, D. J. (2012). Ume6 transcription factor is part of a signaling cascade that regulates autophagy. *Proc Natl Acad Sci U S A*, *109*(28), 11206-11210. https://doi.org/10.1073/pnas.1200313109
9. Berkovits, B. D., & Mayr, C. (2015). Alternative 3' UTRs act as scaffolds to regulate membrane protein localization. *Nature*, *522*(7556), 363-367. https://doi.org/10.1038/nature14321
10. Bernard, A., Jin, M., Gonzalez-Rodriguez, P., Fullgrabe, J., Delorme-Axford, E., Backues, S. K., Joseph, B., & Klionsky, D. J. (2015). Rph1/KDM4 mediates nutrient-limitation signaling that leads to the transcriptional induction of autophagy. *Curr Biol*, *25*(5), 546-555. https://doi.org/10.1016/j.cub.2014.12.049
11. Binda, M., Peli-Gulli, M. P., Bonfils, G., Panchaud, N., Urban, J., Sturgill, T. W., Loewith, R., & De Virgilio, C. (2009). The Vam6 GEF controls TORC1 by activating the EGO complex. *Mol Cell*, *35*(5), 563-573. https://doi.org/10.1016/j.molcel.2009.06.033

12. Blommaart, E. F., Luiken, J. J., Blommaart, P. J., van Woerkom, G. M., & Meijer, A. J. (1995). Phosphorylation of ribosomal protein S6 is inhibitory for autophagy in isolated rat hepatocytes. *J Biol Chem*, *270*(5), 2320-2326. https://doi.org/10.1074/jbc.270.5.2320
13. Bregman, A., Avraham-Kelbert, M., Barkai, O., Duek, L., Guterman, A., & Choder, M. (2011). Promoter elements regulate cytoplasmic mRNA decay. *Cell*, *147*(7), 1473-1483. https://doi.org/10.1016/j.cell.2011.12.005
14. Buchan, J. R., Kolaitis, R. M., Taylor, J. P., & Parker, R. (2013). Eukaryotic stress granules are cleared by autophagy and Cdc48/VCP function. *Cell*, *153*(7), 1461-1474. https://doi.org/10.1016/j.cell.2013.05.037
15. Budovskaya, Y. V., Stephan, J. S., Deminoff, S. J., & Herman, P. K. (2005). An evolutionary proteomics approach identifies substrates of the cAMP-dependent protein kinase. *Proc Natl Acad Sci U S A*, *102*(39), 13933-13938. https://doi.org/10.1073/pnas.0501046102
16. Budovskaya, Y. V., Stephan, J. S., Reggiori, F., Klionsky, D. J., & Herman, P. K. (2004). The Ras/cAMP-dependent protein kinase signaling pathway regulates an early step of the autophagy process in Saccharomyces cerevisiae. *J Biol Chem*, *279*(20), 20663-20671. https://doi.org/10.1074/jbc.M400272200
17. Carlson, M., Osmond, B. C., & Botstein, D. (1981). Mutants of yeast defective in sucrose utilization. *Genetics*, *98*(1), 25-40. https://doi.org/10.1093/genetics/98.1.25
18. Celenza, J. L., & Carlson, M. (1984). Cloning and genetic mapping of SNF1, a gene required for expression of glucose-repressible genes in Saccharomyces cerevisiae. *Mol Cell Biol*, *4*(1), 49-53. https://doi.org/10.1128/mcb.4.1.49-53.1984
19. Celenza, J. L., & Carlson, M. (1986). A yeast gene that is essential for release from glucose repression encodes a protein kinase. *Science*, *233*(4769), 1175-1180. https://doi.org/10.1126/science.3526554
20. Celenza, J. L., & Carlson, M. (1989). Mutational analysis of the Saccharomyces cerevisiae SNF1 protein kinase and evidence for functional interaction with the SNF4 protein. *Mol Cell Biol*, *9*(11), 5034-5044. https://doi.org/10.1128/mcb.9.11.5034-5044.1989
21. Celenza, J. L., Eng, F. J., & Carlson, M. (1989). Molecular analysis of the SNF4 gene of Saccharomyces cerevisiae: evidence for physical association of the SNF4 protein with the SNF1 protein kinase. *Mol Cell Biol*, *9*(11), 5045-5054. https://doi.org/10.1128/mcb.9.11.5045-5054.1989
22. Choi, Y., Um, B., Na, Y., Kim, J., Kim, J. S., & Kim, V. N. (2024). Time-resolved profiling of RNA-binding proteins throughout the mRNA life cycle. *Mol Cell*, *84*(9), 1764-1782 e1710. https://doi.org/10.1016/j.molcel.2024.03.012
23. Chomczynski, P., & Sacchi, N. (2006). The single-step method of RNA isolation by acid guanidinium thiocyanate-phenol-chloroform extraction: twenty-something years on. *Nat Protoc*, *1*(2), 581-585. https://doi.org/10.1038/nprot.2006.83
24. Chowdhury, S., Otomo, C., Leitner, A., Ohashi, K., Aebersold, R., Lander, G. C., & Otomo, T. (2018). Insights into autophagosome biogenesis from structural and biochemical analyses of the ATG2A-WIPI4 complex. *Proc Natl Acad Sci U S A*, *115*(42), E9792-E9801. https://doi.org/10.1073/pnas.1811874115
25. Chun, Y., & Kim, J. (2018). Autophagy: An Essential Degradation Program for Cellular Homeostasis and Life. *Cells*, *7*(12). https://doi.org/10.3390/cells7120278

26. Coccetti, P., Nicastro, R., & Tripodi, F. (2018). Conventional and emerging roles of the energy sensor Snf1/AMPK in Saccharomyces cerevisiae. *Microb Cell*, *5*(11), 482-494. https://doi.org/10.15698/mic2018.11.655
27. Conrad, M., Schothorst, J., Kankipati, H. N., Van Zeebroeck, G., Rubio-Texeira, M., & Thevelein, J. M. (2014). Nutrient sensing and signaling in the yeast Saccharomyces cerevisiae. *FEMS Microbiol Rev*, *38*(2), 254-299. https://doi.org/10.1111/1574-6976.12065
28. Coppin, L., Leclerc, J., Vincent, A., Porchet, N., & Pigny, P. (2018). Messenger RNA Life-Cycle in Cancer Cells: Emerging Role of Conventional and Non-Conventional RNA-Binding Proteins? *Int J Mol Sci*, *19*(3). https://doi.org/10.3390/ijms19030650
29. Crozet, P., Margalha, L., Confraria, A., Rodrigues, A., Martinho, C., Adamo, M., Elias, C. A., & Baena-Gonzalez, E. (2014). Mechanisms of regulation of SNF1/AMPK/SnRK1 protein kinases. *Front Plant Sci*, *5*, 190. https://doi.org/10.3389/fpls.2014.00190
30. Delorme-Axford, E., Abernathy, E., Lennemann, N. J., Bernard, A., Ariosa, A., Coyne, C. B., Kirkegaard, K., & Klionsky, D. J. (2018). The exoribonuclease Xrn1 is a post-transcriptional negative regulator of autophagy. *Autophagy*, *14*(5), 898-912. https://doi.org/10.1080/15548627.2018.1441648
31. Delorme-Axford, E., & Klionsky, D. J. (2018). Transcriptional and post-transcriptional regulation of autophagy in the yeast Saccharomyces cerevisiae. *J Biol Chem*, *293*(15), 5396-5403. https://doi.org/10.1074/jbc.R117.804641
32. Dermody, J. L., Dreyfuss, J. M., Villen, J., Ogundipe, B., Gygi, S. P., Park, P. J., Ponticelli, A. S., Moore, C. L., Buratowski, S., & Bucheli, M. E. (2008). Unphosphorylated SR-like protein Npl3 stimulates RNA polymerase II elongation. *PLoS One*, *3*(9), e3273. https://doi.org/10.1371/journal.pone.0003273
33. Derrer, C. P., Mancini, R., Vallotton, P., Huet, S., Weis, K., & Dultz, E. (2019). The RNA export factor Mex67 functions as a mobile nucleoporin. *J Cell Biol*, *218*(12), 3967-3976. https://doi.org/10.1083/jcb.201909028
34. Diaz-Ruiz, R., Rigoulet, M., & Devin, A. (2011). The Warburg and Crabtree effects: On the origin of cancer cell energy metabolism and of yeast glucose repression. *Biochim Biophys Acta*, *1807*(6), 568-576. https://doi.org/10.1016/j.bbabio.2010.08.010
35. Dibble, C. C., & Manning, B. D. (2013). Signal integration by mTORC1 coordinates nutrient input with biosynthetic output. *Nat Cell Biol*, *15*(6), 555-564. https://doi.org/10.1038/ncb2763
36. Dokudovskaya, S., & Rout, M. P. (2015). SEA you later alli-GATOR--a dynamic regulator of the TORC1 stress response pathway. *Journal of Cell Science*, *128*(12), 2219-2228. https://doi.org/10.1242/jcs.168922
37. Dubouloz, F., Deloche, O., Wanke, V., Cameroni, E., & De Virgilio, C. (2005). The TOR and EGO protein complexes orchestrate microautophagy in yeast. *Mol Cell*, *19*(1), 15-26. https://doi.org/10.1016/j.molcel.2005.05.020
38. Efeyan, A., Comb, W. C., & Sabatini, D. M. (2015). Nutrient-sensing mechanisms and pathways. *Nature*, *517*(7534), 302-310. https://doi.org/10.1038/nature14190
39. Erickson, J. R., & Johnston, M. (1993). Genetic and molecular characterization of GAL83: its interaction and similarities with other genes involved in glucose repression in Saccharomyces cerevisiae. *Genetics*, *135*(3), 655-664. https://doi.org/10.1093/genetics/135.3.655

40. Faza, M. B., Kemmler, S., Jimeno, S., Gonzalez-Aguilera, C., Aguilera, A., Hurt, E., & Panse, V. G. (2009). Sem1 is a functional component of the nuclear pore complex-associated messenger RNA export machinery. *J Cell Biol*, *184*(6), 833-846. https://doi.org/10.1083/jcb.200810059
41. Fendt, S. M., & Sauer, U. (2010). Transcriptional regulation of respiration in yeast metabolizing differently repressive carbon substrates. *BMC Syst Biol*, *4*, 12. https://doi.org/10.1186/1752-0509-4-12
42. Feng, Y., He, D., Yao, Z., & Klionsky, D. J. (2014). The machinery of macroautophagy. *Cell Res*, *24*(1), 24-41. https://doi.org/10.1038/cr.2013.168
43. Fiechter, A., Fuhrmann, G. F., & Kappeli, O. (1981). Regulation of glucose metabolism in growing yeast cells. *Adv Microb Physiol*, *22*, 123-183. https://doi.org/10.1016/s0065-2911(08)60327-6
44. Frankel, L. B., Lubas, M., & Lund, A. H. (2017). Emerging connections between RNA and autophagy. *Autophagy*, *13*(1), 3-23. https://doi.org/10.1080/15548627.2016.1222992
45. Fujioka, Y., Alam, J. M., Noshiro, D., Mouri, K., Ando, T., Okada, Y., May, A. I., Knorr, R. L., Suzuki, K., Ohsumi, Y., & Noda, N. N. (2020). Phase separation organizes the site of autophagosome formation. *Nature*, *578*(7794), 301-305. https://doi.org/10.1038/s41586-020-1977-6
46. Fujioka, Y., Suzuki, S. W., Yamamoto, H., Kondo-Kakuta, C., Kimura, Y., Hirano, H., Akada, R., Inagaki, F., Ohsumi, Y., & Noda, N. N. (2014). Structural basis of starvation-induced assembly of the autophagy initiation complex. *Nat Struct Mol Biol*, *21*(6), 513-521. https://doi.org/10.1038/nsmb.2822
47. Gatica, D., Chiong, M., Lavandero, S., & Klionsky, D. J. (2022). The role of autophagy in cardiovascular pathology. *Cardiovasc Res*, *118*(4), 934-950. https://doi.org/10.1093/cvr/cvab158
48. Gatica, D., Hu, G., Liu, X., Zhang, N., Williamson, P. R., & Klionsky, D. J. (2019). The Pat1-Lsm Complex Stabilizes ATG mRNA during Nitrogen Starvation-Induced Autophagy. *Mol Cell*, *73*(2), 314-324 e314. https://doi.org/10.1016/j.molcel.2018.11.002
49. Geng, J., & Klionsky, D. J. (2008). The Atg8 and Atg12 ubiquitin-like conjugation systems in macroautophagy. 'Protein modifications: beyond the usual suspects' review series. *EMBO Rep*, *9*(9), 859-864. https://doi.org/10.1038/embor.2008.163
50. Gerstberger, S., Hafner, M., & Tuschl, T. (2014). A census of human RNA-binding proteins. *Nat Rev Genet*, *15*(12), 829-845. https://doi.org/10.1038/nrg3813
51. Ghaemmaghami, S., Huh, W. K., Bower, K., Howson, R. W., Belle, A., Dephoure, N., O'Shea, E. K., & Weissman, J. S. (2003). Global analysis of protein expression in yeast. *Nature*, *425*(6959), 737-741. https://doi.org/10.1038/nature02046
52. Gilbert, W., Siebel, C. W., & Guthrie, C. (2001). Phosphorylation by Sky1p promotes Npl3p shuttling and mRNA dissociation. *RNA*, *7*(2), 302-313. https://doi.org/10.1017/s1355838201002369
53. Gong, R., Li, L., Liu, Y., Wang, P., Yang, H., Wang, L., Cheng, J., Guan, K. L., & Xu, Y. (2011). Crystal structure of the Gtr1p-Gtr2p complex reveals new insights into the amino acid-induced TORC1 activation. *Genes Dev*, *25*(16), 1668-1673. https://doi.org/10.1101/gad.16968011
54. Gonzalez, A., & Hall, M. N. (2017). Nutrient sensing and TOR signaling in yeast and mammals. *Embo Journal*, *36*(4), 397-408. https://doi.org/10.15252/embj.201696010

55. Gotor, N. L., Armaos, A., Calloni, G., Torrent Burgas, M., Vabulas, R. M., De Groot, N. S., & Tartaglia, G. G. (2020). RNA-binding and prion domains: the Yin and Yang of phase separation. *Nucleic Acids Res*, *48*(17), 9491-9504. https://doi.org/10.1093/nar/gkaa681
56. Gross, A. S., & Graef, M. (2020). Mechanisms of Autophagy in Metabolic Stress Response. *J Mol Biol*, *432*(1), 28-52. https://doi.org/10.1016/j.jmb.2019.09.005
57. Haimovich, G., Choder, M., Singer, R. H., & Trcek, T. (2013). The fate of the messenger is pre-determined: a new model for regulation of gene expression. *Biochim Biophys Acta*, *1829*(6-7), 643-653. https://doi.org/10.1016/j.bbagrm.2013.01.004
58. Hatakeyama, R., Peli-Gulli, M. P., Hu, Z., Jaquenoud, M., Garcia Osuna, G. M., Sardu, A., Dengjel, J., & De Virgilio, C. (2019). Spatially Distinct Pools of TORC1 Balance Protein Homeostasis. *Mol Cell*, *73*(2), 325-338 e328. https://doi.org/10.1016/j.molcel.2018.10.040
59. Hedbacker, K., & Carlson, M. (2006). Regulation of the nucleocytoplasmic distribution of Snf1-Gal83 protein kinase. *Eukaryot Cell*, *5*(12), 1950-1956. https://doi.org/10.1128/EC.00256-06
60. Hedbacker, K., & Carlson, M. (2008). SNF1/AMPK pathways in yeast. *Front Biosci*, *13*, 2408-2420. https://doi.org/10.2741/2854
61. Hedbacker, K., Hong, S. P., & Carlson, M. (2004). Pak1 protein kinase regulates activation and nuclear localization of Snf1-Gal83 protein kinase. *Mol Cell Biol*, *24*(18), 8255-8263. https://doi.org/10.1128/MCB.24.18.8255-8263.2004
62. Heitman, J., Movva, N. R., & Hall, M. N. (1991). Targets for cell cycle arrest by the immunosuppressant rapamycin in yeast. *Science*, *253*(5022), 905-909. https://doi.org/10.1126/science.1715094
63. Heyer, E. E., & Moore, M. J. (2016). Redefining the Translational Status of 80S Monosomes. *Cell*, *164*(4), 757-769. https://doi.org/10.1016/j.cell.2016.01.003
64. Hinnebusch, A. G., Ivanov, I. P., & Sonenberg, N. (2016). Translational control by 5'-untranslated regions of eukaryotic mRNAs. *Science*, *352*(6292), 1413-1416. https://doi.org/10.1126/science.aad9868
65. Hirose, E., Nakashima, N., Sekiguchi, T., & Nishimoto, T. (1998). RagA is a functional homologue of S. cerevisiae Gtr1p involved in the Ran/Gsp1-GTPase pathway. *Journal of Cell Science*, *111 (Pt 1)*, 11-21. https://doi.org/10.1242/jcs.111.1.11
66. Holcik, M., & Sonenberg, N. (2005). Translational control in stress and apoptosis. *Nat Rev Mol Cell Biol*, *6*(4), 318-327. https://doi.org/10.1038/nrm1618
67. Holt, C. E., & Bullock, S. L. (2009). Subcellular mRNA localization in animal cells and why it matters. *Science*, *326*(5957), 1212-1216. https://doi.org/10.1126/science.1176488
68. Hong, S. P., Leiper, F. C., Woods, A., Carling, D., & Carlson, M. (2003). Activation of yeast Snf1 and mammalian AMP-activated protein kinase by upstream kinases. *Proc Natl Acad Sci U S A*, *100*(15), 8839-8843. https://doi.org/10.1073/pnas.1533136100
69. Howell, J. J., & Manning, B. D. (2011). mTOR couples cellular nutrient sensing to organismal metabolic homeostasis. *Trends Endocrinol Metab*, *22*(3), 94-102. https://doi.org/10.1016/j.tem.2010.12.003
70. Hu, G., McQuiston, T., Bernard, A., Park, Y. D., Qiu, J., Vural, A., Zhang, N., Waterman, S. R., Blewett, N. H., Myers, T. G., Maraia, R. J., Kehrl, J. H., Uzel, G., Klionsky, D. J., & Williamson, P. R. (2015). A conserved mechanism of TOR-dependent

RCK-mediated mRNA degradation regulates autophagy. *Nat Cell Biol*, *17*(7), 930-942. https://doi.org/10.1038/ncb3189
71. Hu, Z., Raucci, S., Jaquenoud, M., Hatakeyama, R., Stumpe, M., Rohr, R., Reggiori, F., De Virgilio, C., & Dengjel, J. (2019). Multilayered Control of Protein Turnover by TORC1 and Atg1. *Cell Rep*, *28*(13), 3486-3496 e3486. https://doi.org/10.1016/j.celrep.2019.08.069
72. Hughes Hallett, J. E., Luo, X., & Capaldi, A. P. (2015). Snf1/AMPK promotes the formation of Kog1/Raptor-bodies to increase the activation threshold of TORC1 in budding yeast. *Elife*, *4*. https://doi.org/10.7554/eLife.09181
73. Hurley, J. H., & Young, L. N. (2017). Mechanisms of Autophagy Initiation. *Annu Rev Biochem*, *86*, 225-244. https://doi.org/10.1146/annurev-biochem-061516-044820
74. Hurt, E., Luo, M. J., Rother, S., Reed, R., & Strasser, K. (2004). Cotranscriptional recruitment of the serine-arginine-rich (SR)-like proteins Gbp2 and Hrb1 to nascent mRNA via the TREX complex. *Proc Natl Acad Sci U S A*, *101*(7), 1858-1862. https://doi.org/10.1073/pnas.0308663100
75. Infantino, V., Tutucci, E., Yeh Martin, N., Zihlmann, A., Garcia-Molinero, V., Silvano, G., Palancade, B., & Stutz, F. (2019). The mRNA export adaptor Yra1 contributes to DNA double-strand break repair through its C-box domain. *PLoS One*, *14*(4), e0206336. https://doi.org/10.1371/journal.pone.0206336
76. Iwama, R., & Ohsumi, Y. (2019). Analysis of autophagy activated during changes in carbon source availability in yeast cells. *J Biol Chem*, *294*(14), 5590-5603. https://doi.org/10.1074/jbc.RA118.005698
77. Janssens, V., & Goris, J. (2001). Protein phosphatase 2A: a highly regulated family of serine/threonine phosphatases implicated in cell growth and signalling. *Biochem J*, *353*(Pt 3), 417-439. https://doi.org/10.1042/0264-6021:3530417
78. Ji, E., Kim, C., Kang, H., Ahn, S., Jung, M., Hong, Y., Tak, H., Lee, S., Kim, W., & Lee, E. K. (2019). RNA-binding Protein HuR Promotes Autophagosome Formation by Regulating Expression of Autophagy-Related Proteins 5, 12, and 16 in Human Hepatocellular Carcinoma Cells. *Mol Cell Biol*, *39*(6). https://doi.org/10.1128/MCB.00508-18
79. Kamada, Y., Yoshino, K., Kondo, C., Kawamata, T., Oshiro, N., Yonezawa, K., & Ohsumi, Y. (2010). Tor directly controls the Atg1 kinase complex to regulate autophagy. *Mol Cell Biol*, *30*(4), 1049-1058. https://doi.org/10.1128/MCB.01344-09
80. Kayikci, O., & Nielsen, J. (2015). Glucose repression in Saccharomyces cerevisiae. *FEMS Yeast Res*, *15*(6). https://doi.org/10.1093/femsyr/fov068
81. Keil, P., Wulf, A., Kachariya, N., Reuscher, S., Huhn, K., Silbern, I., Altmuller, J., Keller, M., Stehle, R., Zarnack, K., Sattler, M., Urlaub, H., & Strasser, K. (2023). Npl3 functions in mRNP assembly by recruitment of mRNP components to the transcription site and their transfer onto the mRNA. *Nucleic Acids Res*, *51*(2), 831-851. https://doi.org/10.1093/nar/gkac1206
82. Khandia, R., Dadar, M., Munjal, A., Dhama, K., Karthik, K., Tiwari, R., Yatoo, M. I., Iqbal, H. M. N., Singh, K. P., Joshi, S. K., & Chaicumpa, W. (2019). A Comprehensive Review of Autophagy and Its Various Roles in Infectious, Non-Infectious, and Lifestyle Diseases: Current Knowledge and Prospects for Disease Prevention, Novel Drug Design, and Therapy. *Cells*, *8*(7). https://doi.org/10.3390/cells8070674

83. Kim, C., Kim, W., Lee, H., Ji, E., Choe, Y. J., Martindale, J. L., Akamatsu, W., Okano, H., Kim, H. S., Nam, S. W., Gorospe, M., & Lee, E. K. (2014). The RNA-binding protein HuD regulates autophagosome formation in pancreatic beta cells by promoting autophagy-related gene 5 expression. *J Biol Chem*, *289*(1), 112-121. https://doi.org/10.1074/jbc.M113.474700
84. Kim, E., Goraksha-Hicks, P., Li, L., Neufeld, T. P., & Guan, K. L. (2008). Regulation of TORC1 by Rag GTPases in nutrient response. *Nat Cell Biol*, *10*(8), 935-945. https://doi.org/10.1038/ncb1753
85. Kira, S., Kumano, Y., Ukai, H., Takeda, E., Matsuura, A., & Noda, T. (2016). Dynamic relocation of the TORC1-Gtr1/2-Ego1/2/3 complex is regulated by Gtr1 and Gtr2. *Mol Biol Cell*, *27*(2), 382-396. https://doi.org/10.1091/mbc.E15-07-0470
86. Kira, S., Tabata, K., Shirahama-Noda, K., Nozoe, A., Yoshimori, T., & Noda, T. (2014). Reciprocal conversion of Gtr1 and Gtr2 nucleotide-binding states by Npr2-Npr3 inactivates TORC1 and induces autophagy. *Autophagy*, *10*(9), 1565-1578. https://doi.org/10.4161/auto.29397
87. Kitamoto, K., Yoshizawa, K., Ohsumi, Y., & Anraku, Y. (1988). Dynamic aspects of vacuolar and cytosolic amino acid pools of Saccharomyces cerevisiae. *J Bacteriol*, *170*(6), 2683-2686. https://doi.org/10.1128/jb.170.6.2683-2686.1988
88. Klama, S., Hirsch, A. G., Schneider, U. M., Zander, G., Seel, A., & Krebber, H. (2022). A guard protein mediated quality control mechanism monitors 5'-capping of pre-mRNAs. *Nucleic Acids Res*, *50*(19), 11301-11314. https://doi.org/10.1093/nar/gkac952
89. Klionsky, D. J., Herman, P. K., & Emr, S. D. (1990). The fungal vacuole: composition, function, and biogenesis. *Microbiol Rev*, *54*(3), 266-292. https://doi.org/10.1128/mr.54.3.266-292.1990
90. Koromilas, A. E., Lazaris-Karatzas, A., & Sonenberg, N. (1992). mRNAs containing extensive secondary structure in their 5' non-coding region translate efficiently in cells overexpressing initiation factor eIF-4E. *Embo Journal*, *11*(11), 4153-4158. https://doi.org/10.1002/j.1460-2075.1992.tb05508.x
91. Kroschwald, S., Munder, M. C., Maharana, S., Franzmann, T. M., Richter, D., Ruer, M., Hyman, A. A., & Alberti, S. (2018). Different Material States of Pub1 Condensates Define Distinct Modes of Stress Adaptation and Recovery. *Cell Rep*, *23*(11), 3327-3339. https://doi.org/10.1016/j.celrep.2018.05.041
92. Lahiri, V., Metur, S. P., Hu, Z., Song, X., Mari, M., Hawkins, W. D., Bhattarai, J., Delorme-Axford, E., Reggiori, F., Tang, D., Dengjel, J., & Klionsky, D. J. (2022). Post-transcriptional regulation of ATG1 is a critical node that modulates autophagy during distinct nutrient stresses. *Autophagy*, *18*(7), 1694-1714. https://doi.org/10.1080/15548627.2021.1997305
93. Lang, M. J., Martinez-Marquez, J. Y., Prosser, D. C., Ganser, L. R., Buelto, D., Wendland, B., & Duncan, M. C. (2014). Glucose starvation inhibits autophagy via vacuolar hydrolysis and induces plasma membrane internalization by down-regulating recycling. *J Biol Chem*, *289*(24), 16736-16747. https://doi.org/10.1074/jbc.M113.525782
94. Lee, E. K., Kim, W., Tominaga, K., Martindale, J. L., Yang, X., Subaran, S. S., Carlson, O. D., Mercken, E. M., Kulkarni, R. N., Akamatsu, W., Okano, H., Perrone-Bizzozero, N. I., de Cabo, R., Egan, J. M., & Gorospe, M. (2012). RNA-binding protein HuD controls insulin translation. *Mol Cell*, *45*(6), 826-835. https://doi.org/10.1016/j.molcel.2012.01.016

95. Lei, E. P., Krebber, H., & Silver, P. A. (2001). Messenger RNAs are recruited for nuclear export during transcription. *Genes Dev*, *15*(14), 1771-1782. https://doi.org/10.1101/gad.892401
96. Lei, Y., Huang, Y., Wen, X., Yin, Z., Zhang, Z., & Klionsky, D. J. (2022). How Cells Deal with the Fluctuating Environment: Autophagy Regulation under Stress in Yeast and Mammalian Systems. *Antioxidants (Basel)*, *11*(2). https://doi.org/10.3390/antiox11020304
97. Li, W., Deng, X., & Chen, J. (2022). RNA-binding proteins in regulating mRNA stability and translation: roles and mechanisms in cancer. *Semin Cancer Biol*, *86*(Pt 2), 664-677. https://doi.org/10.1016/j.semcancer.2022.03.025
98. Li, X., Rayman, J. B., Kandel, E. R., & Derkatch, I. L. (2014). Functional role of Tia1/Pub1 and Sup35 prion domains: directing protein synthesis machinery to the tubulin cytoskeleton. *Mol Cell*, *55*(2), 305-318. https://doi.org/10.1016/j.molcel.2014.05.027
99. Liao, Y. C., Fernandopulle, M. S., Wang, G., Choi, H., Hao, L., Drerup, C. M., Patel, R., Qamar, S., Nixon-Abell, J., Shen, Y., Meadows, W., Vendruscolo, M., Knowles, T. P. J., Nelson, M., Czekalska, M. A., Musteikyte, G., Gachechiladze, M. A., Stephens, C. A., Pasolli, H. A., . . . Ward, M. E. (2019). RNA Granules Hitchhike on Lysosomes for Long-Distance Transport, Using Annexin A11 as a Molecular Tether. *Cell*, *179*(1), 147-164 e120. https://doi.org/10.1016/j.cell.2019.08.050
100. Licheva, M., Raman, B., Kraft, C., & Reggiori, F. (2022). Phosphoregulation of the autophagy machinery by kinases and phosphatases. *Autophagy*, *18*(1), 104-123. https://doi.org/10.1080/15548627.2021.1909407
101. Liu, X., Yao, Z., Jin, M., Namkoong, S., Yin, Z., Lee, J. H., & Klionsky, D. J. (2019). Dhh1 promotes autophagy-related protein translation during nitrogen starvation. *PLoS Biol*, *17*(4), e3000219. https://doi.org/10.1371/journal.pbio.3000219
102. Ljungdahl, P. O., & Daignan-Fornier, B. (2012). Regulation of amino acid, nucleotide, and phosphate metabolism in Saccharomyces cerevisiae. *Genetics*, *190*(3), 885-929. https://doi.org/10.1534/genetics.111.133306
103. Lubas, M., Harder, L. M., Kumsta, C., Tiessen, I., Hansen, M., Andersen, J. S., Lund, A. H., & Frankel, L. B. (2018). eIF5A is required for autophagy by mediating ATG3 translation. *EMBO Rep*, *19*(6). https://doi.org/10.15252/embr.201846072
104. Lukong, K. E., Chang, K. W., Khandjian, E. W., & Richard, S. (2008). RNA-binding proteins in human genetic disease. *Trends Genet*, *24*(8), 416-425. https://doi.org/10.1016/j.tig.2008.05.004
105. Ma, Q., Long, S., Gan, Z., Tettamanti, G., Li, K., & Tian, L. (2022). Transcriptional and Post-Transcriptional Regulation of Autophagy. *Cells*, *11*(3). https://doi.org/10.3390/cells11030441
106. Ma, W. K., Cloutier, S. C., & Tran, E. J. (2013). The DEAD-box protein Dbp2 functions with the RNA-binding protein Yra1 to promote mRNP assembly. *J Mol Biol*, *425*(20), 3824-3838. https://doi.org/10.1016/j.jmb.2013.05.016
107. MacKellar, A. L., & Greenleaf, A. L. (2011). Cotranscriptional association of mRNA export factor Yra1 with C-terminal domain of RNA polymerase II. *J Biol Chem*, *286*(42), 36385-36395. https://doi.org/10.1074/jbc.M111.268144
108. Mackenzie, I. R., Nicholson, A. M., Sarkar, M., Messing, J., Purice, M. D., Pottier, C., Annu, K., Baker, M., Perkerson, R. B., Kurti, A., Matchett, B. J., Mittag, T., Temirov, J., Hsiung, G. R., Krieger, C., Murray, M. E., Kato, M., Fryer, J. D., Petrucelli,

L., . . . Rademakers, R. (2017). TIA1 Mutations in Amyotrophic Lateral Sclerosis and Frontotemporal Dementia Promote Phase Separation and Alter Stress Granule Dynamics. *Neuron*, *95*(4), 808-816 e809. https://doi.org/10.1016/j.neuron.2017.07.025

109. Mao, K., Chew, L. H., Inoue-Aono, Y., Cheong, H., Nair, U., Popelka, H., Yip, C. K., & Klionsky, D. J. (2013). Atg29 phosphorylation regulates coordination of the Atg17-Atg31-Atg29 complex with the Atg11 scaffold during autophagy initiation. *Proc Natl Acad Sci U S A*, *110*(31), E2875-2884. https://doi.org/10.1073/pnas.1300064110

110. Mari, M., Griffith, J., Rieter, E., Krishnappa, L., Klionsky, D. J., & Reggiori, F. (2010). An Atg9-containing compartment that functions in the early steps of autophagosome biogenesis. *J Cell Biol*, *190*(6), 1005-1022. https://doi.org/10.1083/jcb.200912089

111. Maris, C., Dominguez, C., & Allain, F. H. (2005). The RNA recognition motif, a plastic RNA-binding platform to regulate post-transcriptional gene expression. *FEBS J*, *272*(9), 2118-2131. https://doi.org/10.1111/j.1742-4658.2005.04653.x

112. Martens, S., & Fracchiolla, D. (2020). Activation and targeting of ATG8 protein lipidation. *Cell Discov*, *6*, 23. https://doi.org/10.1038/s41421-020-0155-1

113. Matsumoto, K., Toh-e, A., & Oshima, Y. (1981). Isolation and characterization of dominant mutations resistant to carbon catabolite repression of galactokinase synthesis in Saccharomyces cerevisiae. *Mol Cell Biol*, *1*(2), 83-93. https://doi.org/10.1128/mcb.1.2.83-93.1981

114. May, A. I., Prescott, M., & Ohsumi, Y. (2020). Autophagy facilitates adaptation of budding yeast to respiratory growth by recycling serine for one-carbon metabolism. *Nat Commun*, *11*(1), 5052. https://doi.org/10.1038/s41467-020-18805-x

115. Memisoglu, G., Eapen, V. V., Yang, Y., Klionsky, D. J., & Haber, J. E. (2019). PP2C phosphatases promote autophagy by dephosphorylation of the Atg1 complex. *Proc Natl Acad Sci U S A*, *116*(5), 1613-1620. https://doi.org/10.1073/pnas.1817078116

116. Metur, S. P., & Klionsky, D. J. (2024). Nutrient-dependent signaling pathways that control autophagy in yeast. *FEBS Lett*, *598*(1), 32-47. https://doi.org/10.1002/1873-3468.14741

117. Metur, S. P., Lei, Y., Zhang, Z., & Klionsky, D. J. (2023). Regulation of autophagy gene expression and its implications in cancer. *Journal of Cell Science*, *136*(10). https://doi.org/10.1242/jcs.260631

118. Mitchelhill, K. I., Stapleton, D., Gao, G., House, C., Michell, B., Katsis, F., Witters, L. A., & Kemp, B. E. (1994). Mammalian AMP-activated protein kinase shares structural and functional homology with the catalytic domain of yeast Snf1 protein kinase. *J Biol Chem*, *269*(4), 2361-2364. https://www.ncbi.nlm.nih.gov/pubmed/7905477

119. Mitchener, J. S., Shelburne, J. D., Bradford, W. D., & Hawkins, H. K. (1976). Cellular autophagocytosis induced by deprivation of serum and amino acids in HeLa cells. *Am J Pathol*, *83*(3), 485-492. https://www.ncbi.nlm.nih.gov/pubmed/937509

120. Mizushima, N. (2010). The role of the Atg1/ULK1 complex in autophagy regulation. *Curr Opin Cell Biol*, *22*(2), 132-139. https://doi.org/10.1016/j.ceb.2009.12.004

121. Mofatteh, M. (2020). mRNA localization and local translation in neurons. *AIMS Neurosci*, *7*(3), 299-310. https://doi.org/10.3934/Neuroscience.2020016

122. Mortimore, G. E., & Schworer, C. M. (1977). Induction of autophagy by amino-acid deprivation in perfused rat liver. *Nature*, *270*(5633), 174-176. https://doi.org/10.1038/270174a0
123. Moursy, A., Clery, A., Gerhardy, S., Betz, K. M., Rao, S., Mazur, J., Campagne, S., Beusch, I., Duszczyk, M. M., Robinson, M. D., Panse, V. G., & Allain, F. H. (2023). RNA recognition by Npl3p reveals U2 snRNA-binding compatible with a chaperone role during splicing. *Nat Commun*, *14*(1), 7166. https://doi.org/10.1038/s41467-023-42962-4
124. Nair, U., Thumm, M., Klionsky, D. J., & Krick, R. (2011). GFP-Atg8 protease protection as a tool to monitor autophagosome biogenesis. *Autophagy*, *7*(12), 1546-1550. https://doi.org/10.4161/auto.7.12.18424
125. Nakatogawa, H. (2020). Mechanisms governing autophagosome biogenesis. *Nat Rev Mol Cell Biol*, *21*(8), 439-458. https://doi.org/10.1038/s41580-020-0241-0
126. Neigeborn, L., & Carlson, M. (1984). Genes affecting the regulation of SUC2 gene expression by glucose repression in Saccharomyces cerevisiae. *Genetics*, *108*(4), 845-858. https://doi.org/10.1093/genetics/108.4.845
127. Neklesa, T. K., & Davis, R. W. (2009). A genome-wide screen for regulators of TORC1 in response to amino acid starvation reveals a conserved Npr2/3 complex. *PLoS Genet*, *5*(6), e1000515. https://doi.org/10.1371/journal.pgen.1000515
128. Nishimura, T., & Tooze, S. A. (2020). Emerging roles of ATG proteins and membrane lipids in autophagosome formation. *Cell Discov*, *6*, 32. https://doi.org/10.1038/s41421-020-0161-3
129. Noda, N. N., & Fujioka, Y. (2015). Atg1 family kinases in autophagy initiation. *Cell Mol Life Sci*, *72*(16), 3083-3096. https://doi.org/10.1007/s00018-015-1917-z
130. Noda, T. (2017). Regulation of Autophagy through TORC1 and mTORC1. *Biomolecules*, *7*(3). https://doi.org/10.3390/biom7030052
131. Noda, T., & Klionsky, D. J. (2008). The quantitative Pho8Delta60 assay of nonspecific autophagy. *Methods Enzymol*, *451*, 33-42. https://doi.org/10.1016/S0076-6879(08)03203-5
132. Noda, T., & Ohsumi, Y. (1998). Tor, a phosphatidylinositol kinase homologue, controls autophagy in yeast. *J Biol Chem*, *273*(7), 3963-3966. https://doi.org/10.1074/jbc.273.7.3963
133. Ohsumi, Y. (2014). Historical landmarks of autophagy research. *Cell Res*, *24*(1), 9-23. https://doi.org/10.1038/cr.2013.169
134. Ohsumi, Y., & Anraku, Y. (1981). Active transport of basic amino acids driven by a proton motive force in vacuolar membrane vesicles of Saccharomyces cerevisiae. *J Biol Chem*, *256*(5), 2079-2082. https://www.ncbi.nlm.nih.gov/pubmed/6450764
135. Onodera, J., & Ohsumi, Y. (2005). Autophagy is required for maintenance of amino acid levels and protein synthesis under nitrogen starvation. *J Biol Chem*, *280*(36), 31582-31586. https://doi.org/10.1074/jbc.M506736200
136. Orlova, M., Kanter, E., Krakovich, D., & Kuchin, S. (2006). Nitrogen availability and TOR regulate the Snf1 protein kinase in Saccharomyces cerevisiae. *Eukaryot Cell*, *5*(11), 1831-1837. https://doi.org/10.1128/EC.00110-06
137. Palanisamy, K., Tsai, T. H., Yu, T. M., Sun, K. T., Yu, S. H., Lin, F. Y., Wang, I. K., & Li, C. Y. (2019). RNA-binding protein, human antigen R regulates hypoxia-induced autophagy by targeting ATG7/ATG16L1 expressions and autophagosome formation. *J Cell Physiol*, *234*(5), 7448-7458. https://doi.org/10.1002/jcp.27502

138. Panchaud, N., Peli-Gulli, M. P., & De Virgilio, C. (2013). SEACing the GAP that nEGOCiates TORC1 activation: evolutionary conservation of Rag GTPase regulation. *Cell Cycle*, *12*(18), 2948-2952. https://doi.org/10.4161/cc.26000
139. Park, H., Kang, J. H., & Lee, S. (2020). Autophagy in Neurodegenerative Diseases: A Hunter for Aggregates. *Int J Mol Sci*, *21*(9). https://doi.org/10.3390/ijms21093369
140. Parzych, K. R., & Klionsky, D. J. (2014). An overview of autophagy: morphology, mechanism, and regulation. *Antioxid Redox Signal*, *20*(3), 460-473. https://doi.org/10.1089/ars.2013.5371
141. Peeters, K., Van Leemputte, F., Fischer, B., Bonini, B. M., Quezada, H., Tsytlonok, M., Haesen, D., Vanthienen, W., Bernardes, N., Gonzalez-Blas, C. B., Janssens, V., Tompa, P., Versees, W., & Thevelein, J. M. (2017). Fructose-1,6-bisphosphate couples glycolytic flux to activation of Ras. *Nat Commun*, *8*(1), 922. https://doi.org/10.1038/s41467-017-01019-z
142. Perez-Samper, G., Cerulus, B., Jariani, A., Vermeersch, L., Barrajon Simancas, N., Bisschops, M. M. M., van den Brink, J., Solis-Escalante, D., Gallone, B., De Maeyer, D., van Bael, E., Wenseleers, T., Michiels, J., Marchal, K., Daran-Lapujade, P., & Verstrepen, K. J. (2018). The Crabtree Effect Shapes the Saccharomyces cerevisiae Lag Phase during the Switch between Different Carbon Sources. *mBio*, *9*(5). https://doi.org/10.1128/mBio.01331-18
143. Powis, K., & De Virgilio, C. (2016). Conserved regulators of Rag GTPases orchestrate amino acid-dependent TORC1 signaling. *Cell Discov*, *2*, 15049. https://doi.org/10.1038/celldisc.2015.49
144. Powis, K., Zhang, T., Panchaud, N., Wang, R., De Virgilio, C., & Ding, J. (2015). Crystal structure of the Ego1-Ego2-Ego3 complex and its role in promoting Rag GTPase-dependent TORC1 signaling. *Cell Res*, *25*(9), 1043-1059. https://doi.org/10.1038/cr.2015.86
145. Rao, Y., Perna, M. G., Hofmann, B., Beier, V., & Wollert, T. (2016). The Atg1-kinase complex tethers Atg9-vesicles to initiate autophagy. *Nat Commun*, *7*, 10338. https://doi.org/10.1038/ncomms10338
146. Rayman, J. B., Karl, K. A., & Kandel, E. R. (2018). TIA-1 Self-Multimerization, Phase Separation, and Recruitment into Stress Granules Are Dynamically Regulated by Zn(2). *Cell Rep*, *22*(1), 59-71. https://doi.org/10.1016/j.celrep.2017.12.036
147. Reggiori, F., Tucker, K. A., Stromhaug, P. E., & Klionsky, D. J. (2004). The Atg1-Atg13 complex regulates Atg9 and Atg23 retrieval transport from the pre-autophagosomal structure. *Dev Cell*, *6*(1), 79-90. https://doi.org/10.1016/s1534-5807(03)00402-7
148. Reynaud, K., McGeachy, A. M., Noble, D., Meacham, Z. A., & Ingolia, N. T. (2023). Surveying the global landscape of post-transcriptional regulators. *Nat Struct Mol Biol*, *30*(6), 740-752. https://doi.org/10.1038/s41594-023-00999-5
149. Robinson, J. S., Klionsky, D. J., Banta, L. M., & Emr, S. D. (1988). Protein sorting in Saccharomyces cerevisiae: isolation of mutants defective in the delivery and processing of multiple vacuolar hydrolases. *Mol Cell Biol*, *8*(11), 4936-4948. https://doi.org/10.1128/mcb.8.11.4936-4948.1988
150. Rolland, F., De Winde, J. H., Lemaire, K., Boles, E., Thevelein, J. M., & Winderickx, J. (2000). Glucose-induced cAMP signalling in yeast requires both a G-

protein coupled receptor system for extracellular glucose detection and a separable hexose kinase-dependent sensing process. *Mol Microbiol*, *38*(2), 348-358. https://doi.org/10.1046/j.1365-2958.2000.02125.x

151. Ruiz-Echevarria, M. J., & Peltz, S. W. (2000). The RNA-binding protein Pub1 modulates the stability of transcripts containing upstream open reading frames. *Cell*, *101*(7), 741-751. https://doi.org/10.1016/s0092-8674(00)80886-7

152. Russell, R. C., Yuan, H. X., & Guan, K. L. (2014). Autophagy regulation by nutrient signaling. *Cell Res*, *24*(1), 42-57. https://doi.org/10.1038/cr.2013.166

153. Ryter, S. W., Cloonan, S. M., & Choi, A. M. (2013). Autophagy: a critical regulator of cellular metabolism and homeostasis. *Mol Cells*, *36*(1), 7-16. https://doi.org/10.1007/s10059-013-0140-8

154. Sakellariou, D., Tiberti, M., Kleiber, T. H., Blazquez, L., Lopez, A. R., Abildgaard, M. H., Lubas, M., Bartek, J., Papaleo, E., & Frankel, L. B. (2021). eIF4A3 regulates the TFEB-mediated transcriptional response via GSK3B to control autophagy. *Cell Death Differ*, *28*(12), 3344-3356. https://doi.org/10.1038/s41418-021-00822-y

155. Santos-Pereira, J. M., Herrero, A. B., Moreno, S., & Aguilera, A. (2014). Npl3, a new link between RNA-binding proteins and the maintenance of genome integrity. *Cell Cycle*, *13*(10), 1524-1529. https://doi.org/10.4161/cc.28708

156. Sanz, P., Alms, G. R., Haystead, T. A., & Carlson, M. (2000). Regulatory interactions between the Reg1-Glc7 protein phosphatase and the Snf1 protein kinase. *Mol Cell Biol*, *20*(4), 1321-1328. https://doi.org/10.1128/MCB.20.4.1321-1328.2000

157. Schieweck, R., Ciccopiedi, G., Klau, K., & Popper, B. (2023). Monosomes buffer translational stress to allow for active ribosome elongation. *Front Mol Biosci*, *10*, 1158043. https://doi.org/10.3389/fmolb.2023.1158043

158. Schmelzle, T., Beck, T., Martin, D. E., & Hall, M. N. (2004). Activation of the RAS/cyclic AMP pathway suppresses a TOR deficiency in yeast. *Mol Cell Biol*, *24*(1), 338-351. https://doi.org/10.1128/MCB.24.1.338-351.2004

159. Schmidt, M. C., & McCartney, R. R. (2000). beta-subunits of Snf1 kinase are required for kinase function and substrate definition. *Embo Journal*, *19*(18), 4936-4943. https://doi.org/10.1093/emboj/19.18.4936

160. Shao, Z., Ni, L., Hu, S., Xu, T., Meftah, Z., Yu, Z., Tian, N., Wu, Y., Sun, L., Wu, A., Pan, Z., Chen, L., Gao, W., Zhou, Y., Zhang, X., & Wang, X. (2021). RNA-binding protein HuR suppresses senescence through Atg7 mediated autophagy activation in diabetic intervertebral disc degeneration. *Cell Prolif*, *54*(2), e12975. https://doi.org/10.1111/cpr.12975

161. Shimobayashi, M., & Hall, M. N. (2016). Multiple amino acid sensing inputs to mTORC1. *Cell Res*, *26*(1), 7-20. https://doi.org/10.1038/cr.2015.146

162. Stephan, J. S., Yeh, Y. Y., Ramachandran, V., Deminoff, S. J., & Herman, P. K. (2009). The Tor and PKA signaling pathways independently target the Atg1/Atg13 protein kinase complex to control autophagy. *Proc Natl Acad Sci U S A*, *106*(40), 17049-17054. https://doi.org/10.1073/pnas.0903316106

163. Sutherland, C. M., Hawley, S. A., McCartney, R. R., Leech, A., Stark, M. J., Schmidt, M. C., & Hardie, D. G. (2003). Elm1p is one of three upstream kinases for the Saccharomyces cerevisiae SNF1 complex. *Curr Biol*, *13*(15), 1299-1305. https://doi.org/10.1016/s0960-9822(03)00459-7

164. Suzuki, K., Kirisako, T., Kamada, Y., Mizushima, N., Noda, T., & Ohsumi, Y. (2001). The pre-autophagosomal structure organized by concerted functions of APG genes is essential for autophagosome formation. *Embo Journal*, *20*(21), 5971-5981. https://doi.org/10.1093/emboj/20.21.5971
165. Suzuki, S. W., Onodera, J., & Ohsumi, Y. (2011). Starvation induced cell death in autophagy-defective yeast mutants is caused by mitochondria dysfunction. *PLoS One*, *6*(2), e17412. https://doi.org/10.1371/journal.pone.0017412
166. Szostak, E., & Gebauer, F. (2013). Translational control by 3'-UTR-binding proteins. *Brief Funct Genomics*, *12*(1), 58-65. https://doi.org/10.1093/bfgp/els056
167. Takeshige, K., Baba, M., Tsuboi, S., Noda, T., & Ohsumi, Y. (1992). Autophagy in yeast demonstrated with proteinase-deficient mutants and conditions for its induction. *J Cell Biol*, *119*(2), 301-311. https://doi.org/10.1083/jcb.119.2.301
168. Tamaki, H. (2007). Glucose-stimulated cAMP-protein kinase A pathway in yeast Saccharomyces cerevisiae. *J Biosci Bioeng*, *104*(4), 245-250. https://doi.org/10.1263/jbb.104.245
169. Thevelein, J. M., & de Winde, J. H. (1999). Novel sensing mechanisms and targets for the cAMP-protein kinase A pathway in the yeast Saccharomyces cerevisiae. *Mol Microbiol*, *33*(5), 904-918. https://doi.org/10.1046/j.1365-2958.1999.01538.x
170. Tu, J., & Carlson, M. (1995). REG1 binds to protein phosphatase type 1 and regulates glucose repression in Saccharomyces cerevisiae. *Embo Journal*, *14*(23), 5939-5946. https://doi.org/10.1002/j.1460-2075.1995.tb00282.x
171. Umekawa, M., & Klionsky, D. J. (2012). Ksp1 kinase regulates autophagy via the target of rapamycin complex 1 (TORC1) pathway. *J Biol Chem*, *287*(20), 16300-16310. https://doi.org/10.1074/jbc.M112.344952
172. Valverde, D. P., Yu, S., Boggavarapu, V., Kumar, N., Lees, J. A., Walz, T., Reinisch, K. M., & Melia, T. J. (2019). ATG2 transports lipids to promote autophagosome biogenesis. *J Cell Biol*, *218*(6), 1787-1798. https://doi.org/10.1083/jcb.201811139
173. van Dijken, J. P., Weusthuis, R. A., & Pronk, J. T. (1993). Kinetics of growth and sugar consumption in yeasts. *Antonie Van Leeuwenhoek*, *63*(3-4), 343-352. https://doi.org/10.1007/BF00871229
174. Van Zeebroeck, G., Demuyser, L., Zhang, Z., Cottignie, I., & Thevelein, J. M. (2020). Nutrient sensing and cAMP signaling in yeast: G-protein coupled receptor versus transceptor activation of PKA. *Microb Cell*, *8*(1), 17-27. https://doi.org/10.15698/mic2021.01.740
175. Vincent, O., Townley, R., Kuchin, S., & Carlson, M. (2001). Subcellular localization of the Snf1 kinase is regulated by specific beta subunits and a novel glucose signaling mechanism. *Genes Dev*, *15*(9), 1104-1114. https://doi.org/10.1101/gad.879301
176. Wang, Z., Wilson, W. A., Fujino, M. A., & Roach, P. J. (2001). Antagonistic controls of autophagy and glycogen accumulation by Snf1p, the yeast homolog of AMP-activated protein kinase, and the cyclin-dependent kinase Pho85p. *Mol Cell Biol*, *21*(17), 5742-5752. https://doi.org/10.1128/MCB.21.17.5742-5752.2001
177. Wen, X., Gatica, D., Yin, Z., Hu, Z., Dengjel, J., & Klionsky, D. J. (2020). The transcription factor Spt4-Spt5 complex regulates the expression of ATG8 and ATG41. *Autophagy*, *16*(7), 1172-1185. https://doi.org/10.1080/15548627.2019.1659573

178. Wen, X., & Klionsky, D. J. (2016). An overview of macroautophagy in yeast. *J Mol Biol*, *428*(9 Pt A), 1681-1699. https://doi.org/10.1016/j.jmb.2016.02.021
179. Wilson, W. A., Hawley, S. A., & Hardie, D. G. (1996). Glucose repression/derepression in budding yeast: SNF1 protein kinase is activated by phosphorylation under derepressing conditions, and this correlates with a high AMP:ATP ratio. *Curr Biol*, *6*(11), 1426-1434. https://doi.org/10.1016/s0960-9822(96)00747-6
180. Woods, A., Munday, M. R., Scott, J., Yang, X., Carlson, M., & Carling, D. (1994). Yeast SNF1 is functionally related to mammalian AMP-activated protein kinase and regulates acetyl-CoA carboxylase in vivo. *J Biol Chem*, *269*(30), 19509-19515. https://www.ncbi.nlm.nih.gov/pubmed/7913470
181. Wu, C., Yao, W., Kai, W., Liu, W., Wang, W., Li, S., Chen, Y., Wu, X., Wang, L., Li, Y., Tong, J., Qian, J., Zhang, L., Hong, Z., & Yi, C. (2020). Mitochondrial Fusion Machinery Specifically Involved in Energy Deprivation-Induced Autophagy. *Front Cell Dev Biol*, *8*, 221. https://doi.org/10.3389/fcell.2020.00221
182. Wullschleger, S., Loewith, R., & Hall, M. N. (2006). TOR signaling in growth and metabolism. *Cell*, *124*(3), 471-484. https://doi.org/10.1016/j.cell.2006.01.016
183. Yamamoto, H., Fujioka, Y., Suzuki, S. W., Noshiro, D., Suzuki, H., Kondo-Kakuta, C., Kimura, Y., Hirano, H., Ando, T., Noda, N. N., & Ohsumi, Y. (2016). The Intrinsically Disordered Protein Atg13 Mediates Supramolecular Assembly of Autophagy Initiation Complexes. *Dev Cell*, *38*(1), 86-99. https://doi.org/10.1016/j.devcel.2016.06.015
184. Yang, X., Hubbard, E. J., & Carlson, M. (1992). A protein kinase substrate identified by the two-hybrid system. *Science*, *257*(5070), 680-682. https://doi.org/10.1126/science.1496382
185. Yang, X., Jiang, R., & Carlson, M. (1994). A family of proteins containing a conserved domain that mediates interaction with the yeast SNF1 protein kinase complex. *Embo Journal*, *13*(24), 5878-5886. https://doi.org/10.1002/j.1460-2075.1994.tb06933.x
186. Yang, Z., & Klionsky, D. J. (2009). An overview of the molecular mechanism of autophagy. *Curr Top Microbiol Immunol*, *335*, 1-32. https://doi.org/10.1007/978-3-642-00302-8_1
187. Yao, W., Li, Y., Chen, Y., Chen, Y., Zhao, P., Zhang, Y., Jiang, Q., Feng, Y., Yang, F., Wu, C., Zhong, H., Zhou, Y., Sun, Q., Zhang, L., Liu, W., & Yi, C. (2023). Mec1 regulates PAS recruitment of Atg13 via direct binding with Atg13 during glucose starvation-induced autophagy. *Proc Natl Acad Sci U S A*, *120*(1), e2215126120. https://doi.org/10.1073/pnas.2215126120
188. Yao, W., Li, Y., Wu, L., Wu, C., Zhang, Y., Liu, J., He, Z., Wu, X., Lu, C., Wang, L., Zhong, H., Hong, Z., Xu, S., Liu, W., & Yi, C. (2020). Atg11 is required for initiation of glucose starvation-induced autophagy. *Autophagy*, *16*(12), 2206-2218. https://doi.org/10.1080/15548627.2020.1719724
189. Yeasmin, A. M., Waliullah, T. M., Kondo, A., Kaneko, A., Koike, N., & Ushimaru, T. (2016). Orchestrated Action of PP2A Antagonizes Atg13 Phosphorylation and Promotes Autophagy after the Inactivation of TORC1. *PLoS One*, *11*(12), e0166636. https://doi.org/10.1371/journal.pone.0166636
190. Yi, C., Tong, J., Lu, P., Wang, Y., Zhang, J., Sun, C., Yuan, K., Xue, R., Zou, B., Li, N., Xiao, S., Dai, C., Huang, Y., Xu, L., Li, L., Chen, S., Miao, D., Deng, H., Li, H., & Yu, L. (2017). Formation of a Snf1-Mec1-Atg1 Module on Mitochondria Governs

Energy Deprivation-Induced Autophagy by Regulating Mitochondrial Respiration. *Dev Cell*, *41*(1), 59-71 e54. https://doi.org/10.1016/j.devcel.2017.03.007
191. Yi, C., Tong, J. J., & Yu, L. (2018). Mitochondria: The hub of energy deprivation-induced autophagy. *Autophagy*, *14*(6), 1084-1085. https://doi.org/10.1080/15548627.2017.1382785
192. Yim, W. W., & Mizushima, N. (2020). Lysosome biology in autophagy. *Cell Discov*, *6*, 6. https://doi.org/10.1038/s41421-020-0141-7
193. Yin, Z., Liu, X., Ariosa, A., Huang, H., Jin, M., Karbstein, K., & Klionsky, D. J. (2019). Psp2, a novel regulator of autophagy that promotes autophagy-related protein translation. *Cell Res*, *29*(12), 994-1008. https://doi.org/10.1038/s41422-019-0246-4
194. Yin, Z., Popelka, H., Lei, Y., Yang, Y., & Klionsky, D. J. (2020). The Roles of Ubiquitin in Mediating Autophagy. *Cells*, *9*(9). https://doi.org/10.3390/cells9092025
195. Yorimitsu, T., He, C., Wang, K., & Klionsky, D. J. (2009). Tap42-associated protein phosphatase type 2A negatively regulates induction of autophagy. *Autophagy*, *5*(5), 616-624. https://doi.org/10.4161/auto.5.5.8091
196. Yorimitsu, T., Zaman, S., Broach, J. R., & Klionsky, D. J. (2007). Protein kinase A and Sch9 cooperatively regulate induction of autophagy in Saccharomyces cerevisiae. *Mol Biol Cell*, *18*(10), 4180-4189. https://doi.org/10.1091/mbc.e07-05-0485
197. Yu, L., Chen, Y., & Tooze, S. A. (2018). Autophagy pathway: Cellular and molecular mechanisms. *Autophagy*, *14*(2), 207-215. https://doi.org/10.1080/15548627.2017.1378838
198. Yu, X., Long, Y. C., & Shen, H. M. (2015). Differential regulatory functions of three classes of phosphatidylinositol and phosphoinositide 3-kinases in autophagy. *Autophagy*, *11*(10), 1711-1728. https://doi.org/10.1080/15548627.2015.1043076
199. Zhang, H., Alsaleh, G., Feltham, J., Sun, Y., Napolitano, G., Riffelmacher, T., Charles, P., Frau, L., Hublitz, P., Yu, Z., Mohammed, S., Ballabio, A., Balabanov, S., Mellor, J., & Simon, A. K. (2019). Polyamines Control eIF5A Hypusination, TFEB Translation, and Autophagy to Reverse B Cell Senescence. *Mol Cell*, *76*(1), 110-125 e119. https://doi.org/10.1016/j.molcel.2019.08.005
200. Zhang, T., Peli-Gulli, M. P., Yang, H., De Virgilio, C., & Ding, J. (2012). Ego3 functions as a homodimer to mediate the interaction between Gtr1-Gtr2 and Ego1 in the ego complex to activate TORC1. *Structure*, *20*(12), 2151-2160. https://doi.org/10.1016/j.str.2012.09.019
201. Zhang, Z., Guo, M., Li, Y., Shen, M., Kong, D., Shao, J., Ding, H., Tan, S., Chen, A., Zhang, F., & Zheng, S. (2020). RNA-binding protein ZFP36/TTP protects against ferroptosis by regulating autophagy signaling pathway in hepatic stellate cells. *Autophagy*, *16*(8), 1482-1505. https://doi.org/10.1080/15548627.2019.1687985
202. Zhu, J., & Thompson, C. B. (2019). Metabolic regulation of cell growth and proliferation. *Nat Rev Mol Cell Biol*, *20*(7), 436-450. https://doi.org/10.1038/s41580-019-0123-5
203. Zhu, J., Wang, H., & Jiang, X. (2022). mTORC1 beyond anabolic metabolism: Regulation of cell death. *J Cell Biol*, *221*(12). https://doi.org/10.1083/jcb.202208103

Chapter 2 : Identification of Translational Regulators of Autophagy

Macroautophagy/autophagy is crucial for maintaining metabolic homeostasis and cell survival during nutrient starvation. Autophagy requires the coordinated function of several Atg proteins, especially Atg1, for efficient induction and execution. Recently, several RNA-binding proteins have been shown to interact with the *ATG1* transcript. However, a comprehensive understanding of the interaction network has yet to be elucidated. Here, I developed and utilized an approach to identify RNA-binding proteins that specifically interact with *ATG1* untranslated regions. Our investigation revealed Npl3 and Pub1 as novel regulators of autophagy, and Atg1 protein translation by targeting its 5' UTR and 3' UTR, respectively. I show that Npl3 is required for the Pub1-*ATG1* interaction and export to the cytoplasm. Subsequently, Pub1 interacts with the translational machinery and facilitates recruitment of polysomes to the *ATG1* transcript, promoting its translation and thus autophagy induction. Significantly, in non-small cell lung cancer cell lines, TIA1 upregulates ULK1 protein expression at the post-transcriptional level, thereby positively regulating autophagy. Overall, our study highlights the intricate regulatory landscape that fine-tunes *ATG1* mRNA export and translation, thereby uncovering several novel regulators of the autophagy process.

Metur, S.P., Song, X., Mehta, S., Yin, Z., Tong, D., Klionsky, D. (2024). Yeast TIA-1 coordinates with Npl3 to promotes ULK1/Atg1 and autophagy. *This manuscript is in review.*

2.1 Introduction

A fundamental challenge all living organisms face is adapting to ever-changing external environments, with fluctuations in nutrient availability being the most critical and ubiquitous of these changes (Howell & Manning, 2011). In response to nutrient scarcity, cellular decisions are made to strategically utilize available metabolic nutrients to ensure survival. This response is characterized by the upregulation of macroautophagy (hereafter, autophagy), a critical process that plays a central role in adapting to metabolic perturbations (Ryter et al., 2013).

Autophagy is an evolutionarily conserved catabolic mechanism in eukaryotes designed to maintain cellular homeostasis in response to changes in the nutrient composition of the external environment (Metur & Klionsky, 2024). A characteristic feature of autophagy is the formation of double-membraned structures called phagophores, which engulf cytoplasmic cargo; the phagophores mature into autophagosomes that deliver the cargo to the vacuole for degradation (Parzych & Klionsky, 2014). Following degradation, metabolic building blocks are released to the cytosol, which mitigates the metabolic strain brought on by nutrient depletion, ensuring survival during periods of starvation (Abeliovich & Klionsky, 2001). Moreover, this mechanism is crucial for the clearance of damaged organelles and misfolded proteins, the accumulation of which has been shown to cause cancer, neurodegenerative diseases, and various metabolic disorders. Therefore, autophagy is not only an essential cytoprotective process that eliminates superfluous materials but also a key player in maintaining metabolic homeostasis and preventing the onset of various diseases.

Autophagy is primarily a degradative process and, therefore, must be fine-tuned to meet cellular requirements while avoiding unnecessary breakdown of the cytoplasm (Metur et al., 2023). Therefore, autophagy is subject to regulation by a complex interplay of several nutrient

responders that control its induction and execution. These nutrient responders act at multiple levels that upregulate autophagy by directly modulating the expression of essential autophagy genes, both at the level of transcription and translation. While several studies have described the transcriptional regulation of autophagy, I are only now beginning to discover novel post-transcriptional and translational regulators of autophagy (Ma et al., 2022).

Atg1/ULK1 is a crucial autophagy protein in yeast and mammalian cells; it is an essential Ser/Thr kinase for initiating autophagy and the only protein kinase among the core autophagy machinery that is required for autophagosome formation (Noda & Fujioka, 2015). Immediately By the induction of starvation-dependent autophagy, both *ATG1* mRNA and protein levels of Atg1 are upregulated (Lahiri et al., 2022). However, during nitrogen starvation, global translation is downregulated. How *ATG1* transcripts escape this global repression still remains elusive. RNA-binding proteins (RBPs) are effective nutrient responders that link external nutrient cues with post-transcriptional regulation (Lukong et al., 2008). Recent studies have identified several RBPs interacting with *ATG1* mRNA, influencing its stability and association with translation initiation factors. These interactions have significant implications for autophagy regulation (Lahiri et al., 2022; Liu et al., 2019; Yin et al., 2019). Furthermore, these studies allude to the intricate network of interactions involving *ATG1* mRNA, hinting at layers of potential regulatory control that span the multiple stages of its biosynthesis and usage. Therefore, I hypothesized the presence of a dynamic RBP interactome with *ATG1* transcripts in response to changing nutrient cues that regulate Atg1 protein expression, uncovering potential regulators of autophagy.

To comprehensively understand the nutrient-responsive regulatory paradigm of *ATG1* transcripts, I profiled the RNA-binding proteome of the *ATG1* 5' and 3' untranslated region

(UTR) in response to nutrient-rich and nitrogen-starvation conditions (Lahiri et al., 2022). I identified Npl3 and Pub1 as interacting partners of the *ATG1* transcript at the 5' UTR and 3' UTR, respectively and also showed that they are positive regulators of autophagy. I further characterized the role of Npl3 in conjunction with Pub1, a stress granule protein, in regulating *ATG1* mRNA export and ribosome association to promote its translation during nitrogen starvation. Intriguingly, the mammalian homolog of Pub1, TIA1, also positively regulates ULK1 expression at the post-transcriptional level, thereby promoting autophagy in response to nutrient starvation. This finding not only underscores the evolutionary importance of this regulatory pathway but also highlights the potential for translatability of this mechanism. Taken together, I provide insights into the intricate network of protein interaction linked with *ATG1* mRNA that governs the expression of the Atg1 protein and, thus, autophagy.

2.2 Results

2.2.1 An in vitro interactome capture reveals several new binding partners of ATG1 mRNA

To identify potential RNA-binding proteins involved in autophagy regulation at the level of the *ATG1* transcript, I performed an in vitro transcribed *ATG1* 5' UTR RNA affinity isolation followed by western blot and proteomics to identify interactors in nitrogen-rich (+N) and nitrogen-limited (-N) conditions (Figure 2a). I verified through western blot that Dhh1 and Ded1, known interactors with the *ATG1* 5' UTR (Figure 3a), were enriched only in the presence of labeled *ATG1* 5' UTR RNA (Fig 3). Proteomic profiling of the affinity isolate identified previously known interacting proteins of the *ATG1* 5' UTR, such as Eap1 and Psp2, under nitrogen-starvation conditions (Figure 3b), further validating the utility of this method to identify potential RBPs that could regulate autophagy at the level of *ATG1* mRNA. I identified 13 RBPs that were significantly enriched on the *ATG1* 5' UTR during nitrogen starvation relative to

growth in rich medium (Figure 2b). Out of the 13, I decided to test three non-essential proteins with a previously unknown role in regulating autophagy (Table 1). Accordingly, I created genomic deletion strains of *SRO9, NPL3,* and *MLF3* and tested them for effects on Atg1 protein expression using immunoblotting (Figure 2c). I found that *NPL3* deletion severely abrogated the increase in Atg1 protein levels seen in the wild-type (WT) strain under nitrogen-starvation conditions, suggesting a potential role of Npl3 in regulating Atg1 expression. In contrast, the other two deletion strains caused no obvious change in Atg1 levels relative to the WT.

2.2.2 Npl3 is a novel regulator of Atg1 protein expression and autophagy.

To confirm that Npl3 does indeed bind to the *ATG1* transcript, I performed an Npl3 immunoprecipitation followed by RT-qPCR to measure *ATG1* transcript levels and determine if the transcript was enriched. Our results show that Npl3 bound to both the 5' UTR (-290) and the coding region (+35) but not the 3' UTR (Figure 2d), revealing that Npl3 is indeed an interactor with the *ATG1 5'UTR*. I hypothesized that this interaction is crucial for the upregulation of Atg1 protein levels during nitrogen starvation-induced autophagy. To rule out the possibility that increased protein turnover results in lowered Atg1 protein levels in Npl3 mutants, I performed a cycloheximide (CHX) chase assay where Atg1 protein levels were allowed to accumulate during 6 h of nitrogen starvation, following which CHX was added. The Atg1 protein levels were then chased in nitrogen starvation medium for another 1 and 2 h and measured by immunoblotting using an Atg1-specific antibody. The results show that the turnover of Atg1 protein levels in both WT and *npl3*Δ strains was similar, and therefore, the regulation was upstream of protein degradation (Figure 2e, 2f). Next, I measured the mRNA levels of the *ATG1* transcript in WT and *npl3*Δ cells to assess if the lowered amount of Atg1 protein is due to a decrease in *ATG1*

mRNA levels and, therefore, a form of transcriptional regulation by Npl3. However, both WT and *npl3*Δ strains had similar levels of *ATG1* mRNA transcript (Figure 2g), suggesting that Npl3 regulates Atg1 protein levels at the post-transcriptional/translational level.

The decline in Atg1 protein levels By ablation of the *NPL3* gene led us to test if the decrease affects autophagy activity. Toward this end, I tested GFP-Atg8 processing. Atg8, or green fluorescent protein (GFP)-tagged Atg8, is attached to both sides of the phagophore via conjugation to phosphatidylethanolamine. After autophagosome maturation, Atg8/GFP-Atg8 is removed from the autophagosome outer membrane and recycled; in contrast, the protein on the inner surface is delivered to the vacuole after fusion with the autophagosome (Nair et al., 2011). Atg8 is degraded within the vacuole lumen, whereas GFP is relatively stable and accumulates within the vacuole. Thus, the generation of free GFP is an indication of autophagy activity. I determined that deletion of *NPL3* resulted in decreased GFP-Atg8 processing after 6 h of nitrogen starvation and, therefore, a lower level of autophagy activity (Figure 2h, 2i).

Finally, autophagy is required for yeast cell viability during starvation; autophagy mutants display decreased viability under starvation conditions (Suzuki et al., 2011). Thus, resistance to starvation is another measure of functional autophagy. The *npl3* deletion resulted in decreased cellular viability during long-term starvation compared to the WT strain (Figure 2j). This result suggests that Npl3 is an essential factor required for survival during nitrogen starvation and that it acts by promoting Atg1 protein levels and autophagy activity.

Figure 2

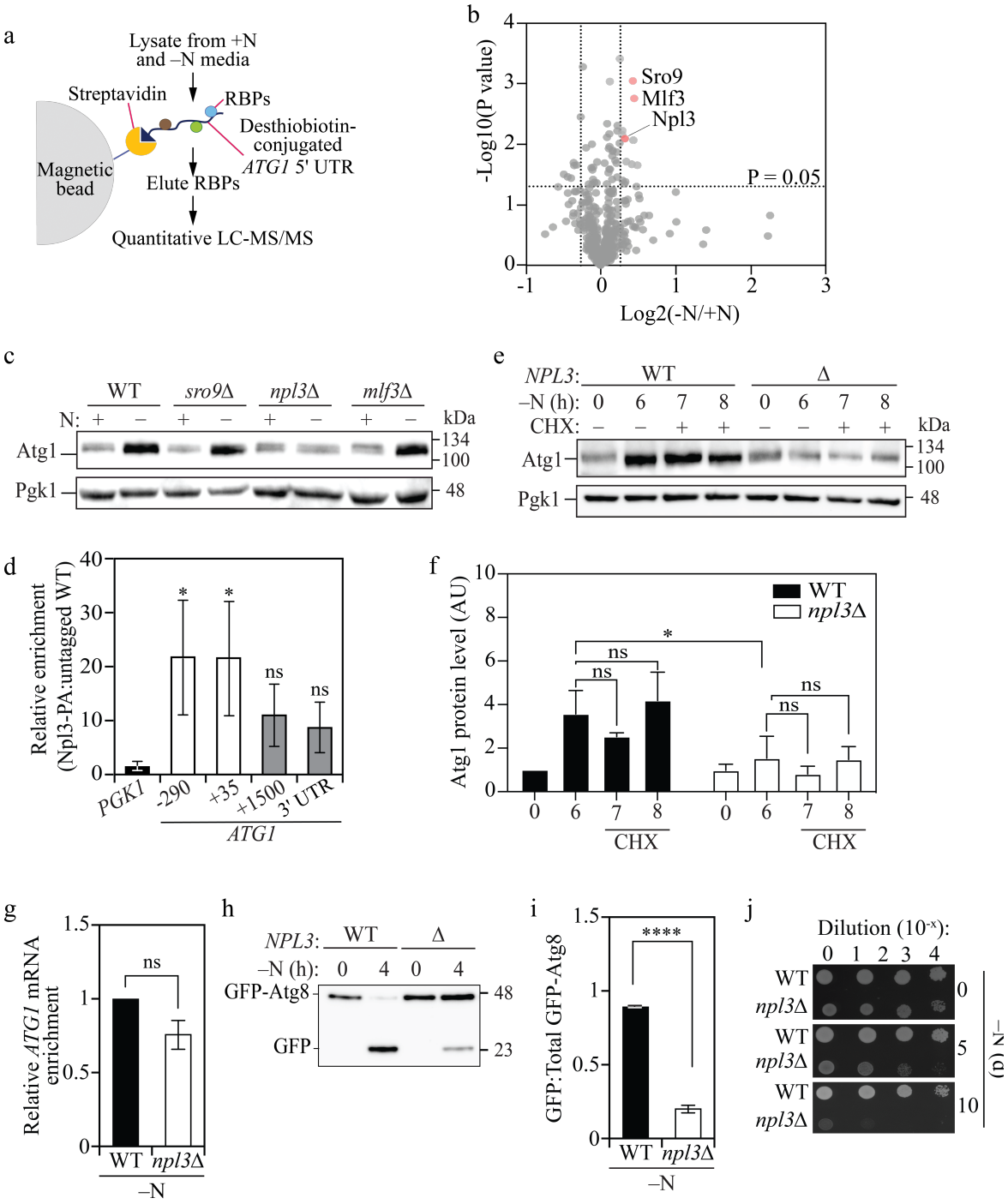
a
Lysate from +N and –N media
Streptavidin
RBPs
Desthiobiotin-conjugated ATG1 5' UTR
Magnetic bead
Elute RBPs
Quantitative LC-MS/MS
b
-Log10(P value)
Log2(-N/+N)
Sro9
Mlf3
Npl3
P = 0.05
c
WT
sro9Δ
npl3Δ
mlf3Δ
N:
kDa
Atg1
Pgk1
134
100
48
e
NPL3:
WT
Δ
–N (h):
CHX:
kDa
Atg1
Pgk1
d
Relative enrichment (Npl3-PA:untagged WT)
PGK1
-290
+35
+1500
3' UTR
ATG1
ns
f
Atg1 protein level (AU)
WT
npl3Δ
CHX
g
Relative ATG1 mRNA enrichment
WT
npl3Δ
–N
h
NPL3:
–N (h):
GFP-Atg8
GFP
i
GFP:Total GFP-Atg8
****
WT
npl3Δ
–N
j
Dilution (10-x):
WT
npl3Δ
–N (d)

Figure 2: Exploring *ATG1*-RBP interactions reveals Npl3 as a novel regulator of autophagy.

a. Schematic of in vitro *ATG1* mRNA interactome capture: Lysates from rich medium (+N) and nitrogen starvation medium (-N) were incubated with streptavidin beads conjugated with desthiobiotin-tagged *ATG1* 5' UTR. The beads were washed and the RBPs bound to the beads were identified by mass spectrometry.

b. RBP-5' UTR interaction reveals novel binding partners of *ATG1*: Volcano plot of RBPs interacting with the *ATG1* 5' UTR in -N compared to +N. Results from 3 biological replicates are plotted. Student's t test between -N and +N condition was performed to identify statistically significant enrichments.

c. Npl3 is a novel regulator of Atg1 expression: WT (WLY176) and RBP deletion strains were grown in +N media and shifted to -N for 6 h, following which lysates were analyzed by immunoblotting to measure Atg1 protein levels using Atg1-specific antibody. Pgk1 was used as a loading control.

d. RNA-IP confirms Npl3 interaction with *ATG1*: Npl3 tagged with PA (YZY312) was affinity isolated using IgG Sepharose beads and bound mRNA was extracted and quantified by qRT-PCR. The region of interaction was determined using primers specific to different regions of the *ATG1* mRNA as indicated. *PGK1* was used as an internal control, and an untagged strain (SEY6210) was used for normalization. Data are representative of three independent biological replicates, showing mean +/- SD. One-way ANOVA was used to determine statistical significance. * p value = 0.028.

e. The *npl3* deletion does not increase turnover of the Atg1 protein: WT (WLY176) and *npl3*Δ (SPY77) cells were grown in +N and transferred to -N for 6 h, then treated with cycloheximide (CHX). Following treatment, cells were harvested at the indicated time

points. Atg1 protein levels were measured by immunoblotting. Pgk1 was used as a loading control.

f. Quantification of e, representing data from two biological replicates, mean +/- SD. Two-way ANOVA was used to determine statistical significance, * p value = 0.0124.

g. Npl3 does not regulate *ATG1* at the level of transcription: WT (WLY176) and *npl3*Δ (SPY77) strains were subjected to nitrogen starvation for 6 h, then total RNA was extracted and cDNA synthesized. qRT-PCR was performed to quantify the abundance of *ATG1* mRNA. Data are representative of three biological replicates. Student's t test was performed to determine statistical significance. ns = not significant.

h. Ablation of *NPL3* results in reduced autophagic flux: WT (JMY347) and *npl3*Δ (YZY311) cells expressing genomically tagged Atg8-GFP were starved for nitrogen, harvested after 4 h and assessed by immunoblotting.

i. Quantification of h. The ratio of the free GFP to total GFP is a measure of autophagic flux. Data is representative of three biological replicates, showing mean +/- SD. Student's t test was performed to determine the statistical significance. **** p value < 0.0001.

j. Loss of Npl3 leads to reduced cell survival during nitrogen starvation: WT (SEY6210) and *npl3*Δ (SPY77) cells were grown in +N and then starved for the indicated time points. The indicated dilutions were grown on YPD plates for 2 days at 30°C.

Figure 3

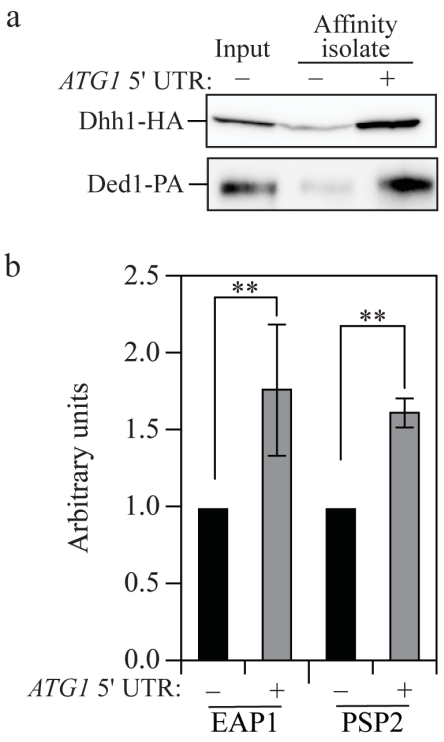
a
Input
Affinity isolate
ATG1 5' UTR: – – +
Dhh1-HA
Ded1-PA
b
Arbitrary units
2.5
2.0
1.5
1.0
0.5
0.0
**
**
ATG1 5' UTR: – + – +
EAP1
PSP2

Figure 3: An *ATG1* 5' UTR in vitro mRNA interactome capture identifies previously known interactions.

a. Dhh1 and Ded1 interact with in vitro transcribed *ATG1* 5' UTR: Epitope-tagged Dhh1 (XLY345) and Ded1 (VLY017) cells were subjected to nitrogen starvation and harvested. The lysates were incubated with streptavidin beads conjugated with or without desthiobiotin-tagged *ATG1* 5' UTR RNA. The beads were boiled, and the affinity isolation was monitored by immunoblotting.
b. Mass spectrometry following *ATG1* 5' UTR affinity isolation identified Eap1 and Psp2: The abundance of RNA-binding proteins identified during mass spectrometry is shown. Data are representative of two independent biological replicates. Two-way ANOVA was performed to determine the statistical significance. ** p value < 0.001.

2.2.3 Npl3 regulates ATG1 expression and autophagy in an RRM-dependent manner.

Npl3 belongs to a family of serine-arginine/SR proteins, well studied for its role in mRNA splicing. Npl3 has also been implicated in various stages of gene expression such as transcription elongation, termination, and mRNA splicing. The *ATG1* transcript in *Saccharomyces cerevisiae* does not contain any introns and because the depletion of *NPL3* did not affect *ATG1* mRNA levels but only the Atg1 protein level, I asked if 1) export and 2) translational efficiency of *ATG1* mRNA was affected. To test if there was defect in mRNA export, I isolated total mRNA from nuclear and cytoplasmic fractions from WT and *npl3*Δ cells after nitrogen starvation and, measured the percentage of *ATG1* mRNA. The percentage of *ATG1* mRNA in the nuclear fraction was significantly higher in *npl3*Δ cells compared to the wild type, whereas there was no significant difference seen with *PGK1* suggesting a specific defect in *ATG1* mRNA export (Figure 3a).

For this defect to subsequently affect Atg1 protein expression, I hypothesized that the translational efficiency of the transcript should be affected in *npl3*Δ cells. Accordingly, I assessed the translational efficiency by measuring ribosome occupancy of *ATG1* mRNA during nitrogen starvation, carrying out polysome profiling of WT and *npl3*Δ cells followed by qRT-PCR to determine the localization of the transcript in free and ribosome-bound fractions. The resulting polysome profiles showed a negligible increase in the 60S and 80S fractions; however, there was no significant change in the polysome fraction suggesting that the global translation remained unaffected in *npl3*Δ cells during nitrogen starvation (Figure 4a). Higher translational efficiency is a factor of higher ribosome occupancy, which localizes the transcript in the heavier polysome fractions. *ATG1* has high ribosome occupancy in WT cells during nitrogen starvation, as evidenced by the recruitment of 2 or more ribosomes on the transcript (Figure 4b).

Furthermore, almost 40% of *ATG1* mRNA was occupied by 1 ribosome, suggesting the importance of monosomes in translating stress-responsive genes (Heyer & Moore, 2016; Schieweck et al., 2023). In contrast, *npl3*Δ cells had a significant decrease in the abundance of *ATG1* mRNA in the polysome fraction, compared to the WT, where two or more ribosomes occupy the transcript. There was a modest yet significant decrease in monosome loading and a proportional increase in the mRNA in the free mRNA-protein complexes (mRNP) fraction in the *npl3*Δ strain, suggesting that depletion of *NPL3* reduced the ribosome loading onto the *ATG1* transcript; this effect was exacerbated in the polysome fractions. In contrast, the localization of the control mRNA, *PGK1*, was not drastically different in the mutant cells in the polysome fraction, with a modest decrease in the monosome and the free mRNP fractions (Figure 5b). Together, our data suggest that a decrease in Atg1 protein levels By *npl3* deletion is due a deficiency in *ATG1* mRNA export and therefore a subsequent decrease in ribosome accessibility of the *ATG1* transcript.

Npl3 is an RNA-binding protein with three potential RNA-binding motifs: 2 RNA recognition motifs (RRMs) and a C-terminal arginine-serine/RS domain containing an Arg-Gly-Gly (RGG) domain (Santos-Pereira et al., 2014). Genetic interactions analyzing the RNA recognition mechanism of Npl3 highlight the role of RRM1 during chromatin remodeling while RRM2 might be linked to the regulation of a specific transcript (Moursy et al., 2023). Furthermore, RRM2 recognizes a 5'-GNGG-3' motif, which is present in the 5' UTR of *ATG1* starting at position 65 (Figure 4c). Therefore, I sought to determine if Npl3 interacted with *ATG1* via its RRM2 domain. I deleted the Npl3 residues between 200 and 275 and tested the effect of this truncation on *ATG1* interaction and Atg1 protein levels. I performed RNA immunoprecipitation with protein A (PA)-tagged WT Npl3 and Npl3 ΔRRM2 and analyzed the

interaction with *ATG1* transcript fragments by qRT-PCR. Deleting RRM2 led to a significant reduction in *ATG1* mRNA enrichment compared to WT Npl3 (Figure 4c). Next, I tested the effect of deleting RRM2 on Atg1 protein levels using immunoblotting. Compared to the WT, the ΔRRM2 mutant showed significantly reduced Atg1 protein levels (Figure 4d-c). In contrast, *ATG1* mRNA levels remained unchanged (Figure 3f), suggesting that the RRM2 motif is essential for Npl3 to promote Atg1 protein expression but not for *ATG1* transcription. Finally, I asked if this reduced binding in the ΔRRM2 mutant led to reduced accessibility for ribosome recruitment on the *ATG1* transcript. Indeed, the recruitment of both monosomes and polysomes on the *ATG1* transcript was significantly reduced in ΔRRM2 mutants compared to the WT, with a proportional increase in the percentage of *ATG1* in the free mRNP fraction (Figure 4g).

When the global translational status was profiled, I noticed a modest decrease in polysomes in the ΔRRM2 mutant during nitrogen starvation (Figure 5d), suggests potential functional redundancy that may compensate for the loss of the complete protein (i.e., *npl3*Δ) but not for the RRM2 deletion alone and further suggests a weak dominant negative effect of the ΔRRM2 protein. Additionally, compared to WT, the control mRNA *PGK1* had a similar effect on the monosome and the free mRNP fractions, however, had no effect on polysomes. (Figure 5e). These results suggest that Npl3 interacts with *ATG1* mRNA in an RRM2-dependent manner, and this interaction is necessary for the export and the subsequent recruitment of ribosomes and, thus, translational upregulation of Atg1 during nitrogen starvation. Together, I have identified Npl3 as a novel post transcriptional regulator of *ATG1* mRNA during nitrogen starvation.

Figure 4

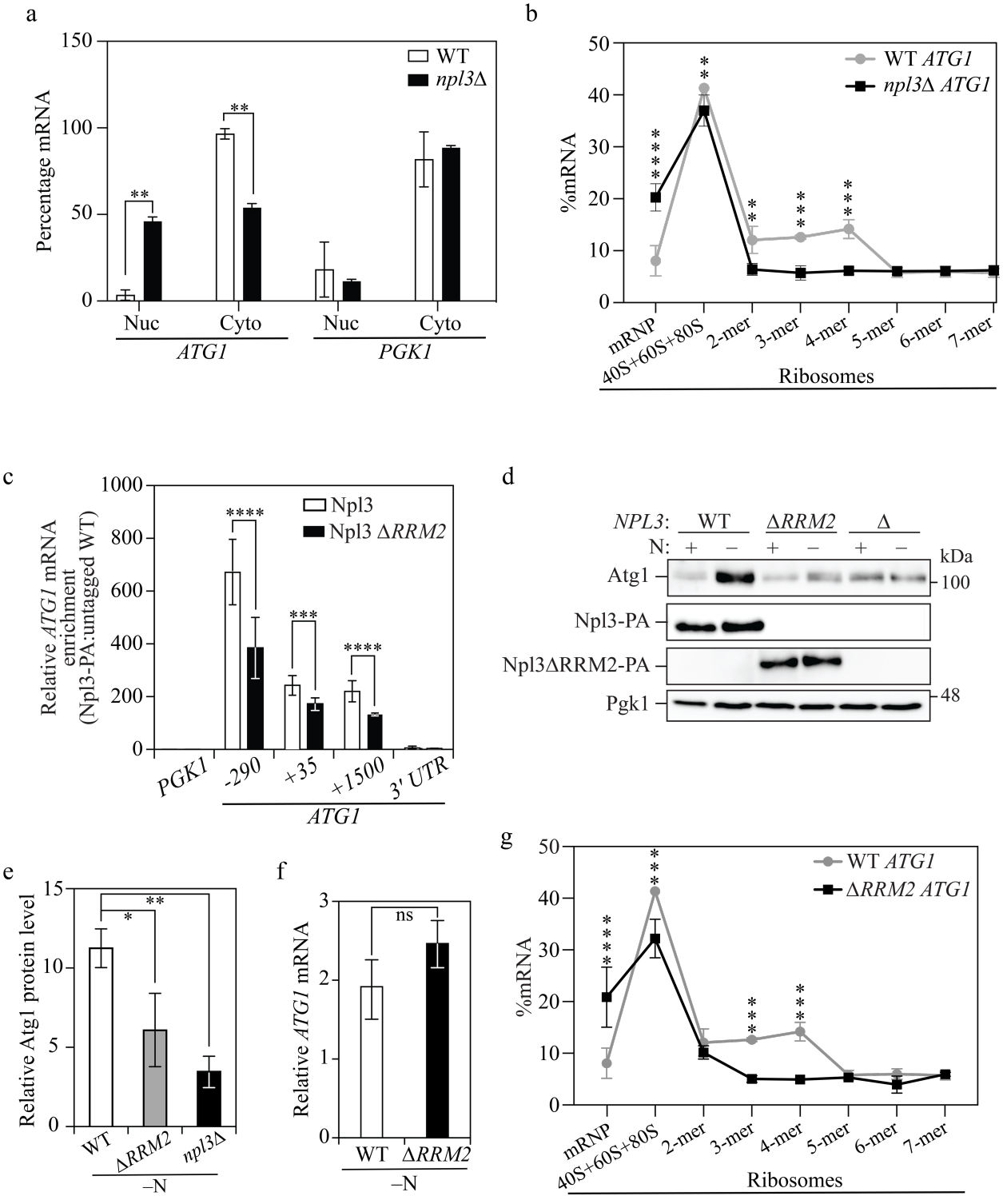
a
Percentage mRNA
150
100
50
0
WT
npl3Δ
**
**
Nuc
Cyto
Nuc
Cyto
ATG1
PGK1
b
%mRNA
50
40
30
20
10
0
WT ATG1
npl3Δ ATG1
mRNP
40S+60S+80S
2-mer
3-mer
4-mer
5-mer
6-mer
7-mer
Ribosomes
c
Relative ATG1 mRNA enrichment (Npl3-PA:untagged WT)
1000
800
600
400
200
0
Npl3
Npl3 ΔRRM2
****
***
****
PGK1
-290
+35
+1500
3' UTR
ATG1
d
NPL3: WT ΔRRM2 Δ
N: + − + − + −
kDa
Atg1
100
Npl3-PA
Npl3ΔRRM2-PA
Pgk1
48
e
Relative Atg1 protein level
15
10
5
0
*
**
WT
ΔRRM2
npl3Δ
–N
f
Relative ATG1 mRNA
3
2
1
0
ns
WT
ΔRRM2
–N
g
%mRNA
50
40
30
20
10
0
WT ATG1
ΔRRM2 ATG1
mRNP
40S+60S+80S
2-mer
3-mer
4-mer
5-mer
6-mer
7-mer
Ribosomes

Figure 4: Npl3 promotes *ATG1* translation and autophagy through an RRM-motif dependent mechanism.

a. Npl3 is required for export of *ATG1* mRNA: WT (SEY6210) and *npl3*Δ (SPY77) strains were starved for nitrogen for 4 h and fractionated to obtain nuclear and cytoplasmic fractions. Then 20 pg of spike-in control RNA was added, and total RNA was extracted. qRT-PCR was performed to quantify the percentage of *ATG1* mRNA in the two fractions. *PGK1* was used as a control RNA, showing the specificity of this regulation. The spike-in RNA was used for normalization. Data are representative of three biological replicates, showing mean +/- SD. Two-way ANOVA was performed to determine the statistical significance. ** p value = 0.0388

b. Polysome recruitment onto *ATG1* mRNA is reduced when *NPL3* is deleted: WT (SEY6210) and *npl3*Δ (SPY077) cells were subject to nitrogen starvation. Lysates were fractionated in a sucrose gradient and the abundance of *ATG1* transcript was analyzed by qRT-PCR. Data are representative of two independent biological replicates, showing mean +/- SD. Two-way ANOVA was performed to determine the statistical significance. **** p value <0.0001, *** p value <0.0005, ** p value < 0.01.

c. Npl3 interacts with *ATG1* in an RRM2-dependent manner: RNA immunoprecipitation of WT (untagged, SEY6210), Npl3-PA (SPY060) and Npl3 ΔRRM2-PA (SPY062) was performed to quantify the abundance of *ATG1* mRNA interaction during nitrogen starvation. Data are representative of three biological replicates, showing mean +/- SD. Two-way ANOVA was performed to determine statistical significance. **** p value <0.0001, *** p value = 0.0001.

d. The Npl3 RRM2 is required for upregulation of Atg1 protein during nitrogen starvation: WT (SEY6210), Npl3 ΔRRM2 (SPY060) and *npl3*Δ (SPY077) strains were subjected to

nitrogen starvation for 6 h and Atg1 protein levels were determined by immunoblotting. Pgk1 was used as a loading control.

e. Quantification of d. Two-way ANOVA was performed to determine statistical significance. ** p value = 0.0043, * p value = 0.0239.

f. Npl3 RRM2 truncation does not affect *ATG1* mRNA transcription: WT (SEY6210) and Npl3 ΔRRM2 (SPY060) cells were subjected to nitrogen starvation for 4 h and the abundance of *ATG1* mRNA was determined. Student's t test was performed to determine statistical significance.

g. Polysome profiling shows that *ATG1* mRNA localization in cells expressing the Npl3 RRM2 deletion phenocopies *npl3*Δ during nitrogen starvation: *ATG1* mRNA abundance in different polysome fractions was quantified in the WT (SEY6210) and Npl3 ΔRRM2 strains. Two-way ANOVA was performed to determine the statistical significance. ****p value <0.0001, *** p value < 0.001.

Figure 5

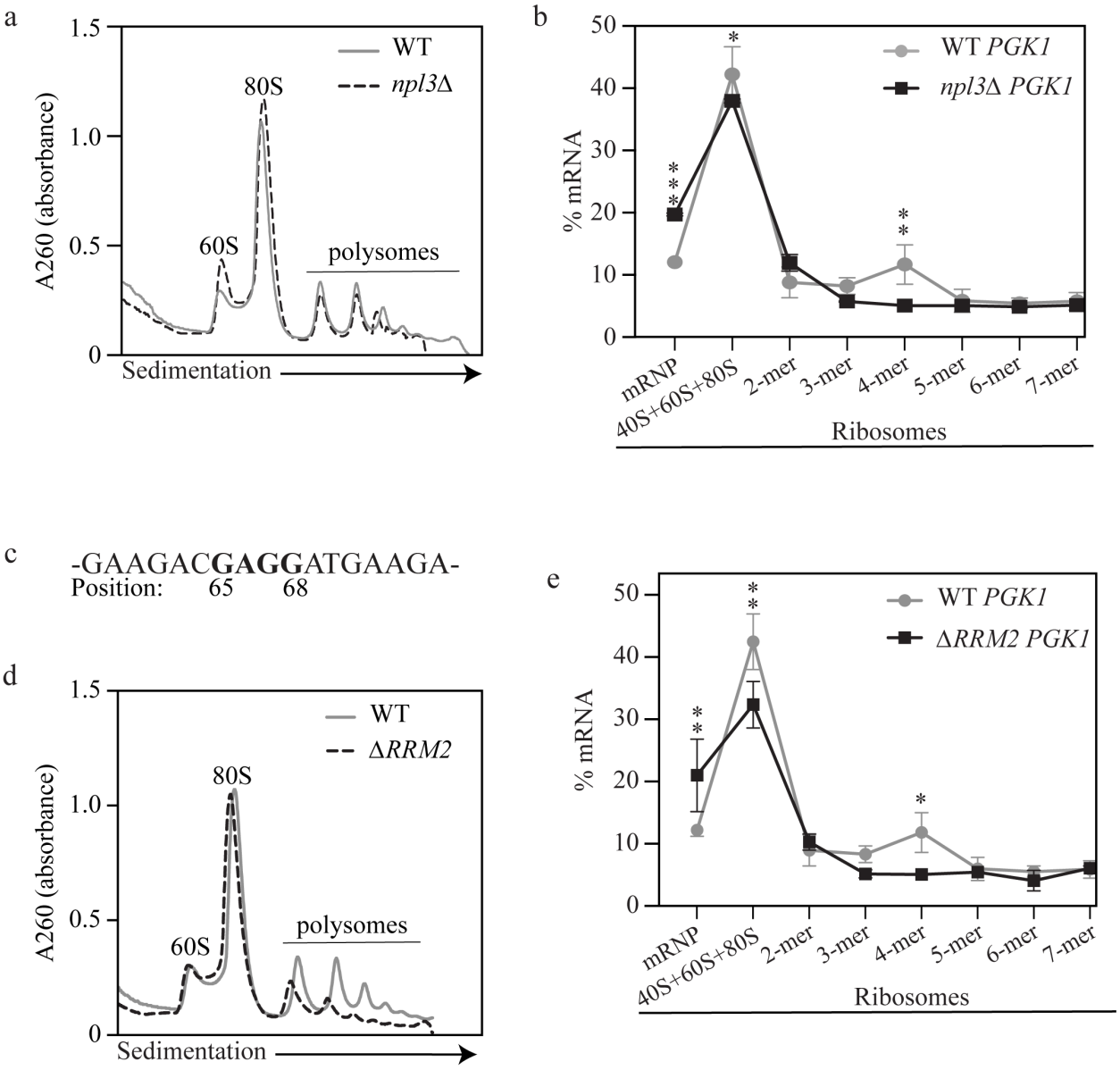
a
1.5
1.0
0.5
0
A260 (absorbance)
WT
npl3Δ
80S
60S
polysomes
Sedimentation
b
50
40
30
20
10
0
% mRNA
WT PGK1
npl3Δ PGK1
mRNP
40S+60S+80S
2-mer
3-mer
4-mer
5-mer
6-mer
7-mer
Ribosomes
c
-GAAGACGAGGATGAAGA-
Position: 65 68
d
1.5
1.0
0.5
0
A260 (absorbance)
WT
ΔRRM2
80S
60S
polysomes
Sedimentation
e
50
40
30
20
10
0
% mRNA
WT PGK1
ΔRRM2 PGK1
mRNP
40S+60S+80S
2-mer
3-mer
4-mer
5-mer
6-mer
7-mer
Ribosomes

Figure 5: Npl3 mutants do not affect global translation during nitrogen starvation.

a. The polysome profile of the *npl3*Δ strain is similar to the WT: WT and *npl3*Δ cells were subjected to nitrogen starvation and the polysome profiles were analyzed using a gradient fractionator.
b. The distribution of *PGK1* is minimally changed in the polysome fractions due to loss of Npl3: WT and *npl3*Δ cells were subjected to nitrogen starvation and equal amounts of different ribosomal fractions were collected using a gradient fractionator. The abundance of *PGK1* mRNA was determined using qRT-PCR.
c. The position of the -GNGG- motif in the *ATG1* 5' UTR is shown.
d. Polysome profile of WT and Npl3 ΔRRM2: WT and Npl3 ΔRRM2 cells were subjected to nitrogen starvation and the polysome profiles were analyzed using a gradient fractionator.
e. The distribution of *PGK1* is minimally changed in the polysome fractions due to the loss of the Npl3 RRM2: WT and Npl3 ΔRRM2 cells were subjected to nitrogen starvation and equal amounts of different ribosomal fractions were collected using a gradient fractionator. The abundance of *PGK1* mRNA was determined using qRT-PCR.

2.2.4 Pub1 promotes the translation of ATG1 mRNA and autophagy.

Now that I had mapped the interaction network of the *ATG1* 5' UTR, I were interested in analyzing the 3' UTR. The *ATG1* 3' UTR region binds to the Pat1-Lsm complex that protects the transcript from decay (Gatica et al., 2019). Specific RBP-3' UTR interactions also influence association with translational machinery and ribosome components (Szostak & Gebauer, 2013). I employed the mRNA affinity-isolation approach followed by a proteomics analysis utilizing the labeled 3' UTR of the *ATG1* transcript. Proteomics identification revealed that the *ATG1* 3' UTR interacted with the 5'-3' exonuclease Xrn1, previously shown to regulate Atg1 and autophagy (Delorme-Axford et al., 2018) (Figure 6a). In addition, I found that the Npl3-interacting protein Gbp2, involved with the nuclear export of transcripts, also associated with *ATG1*. Hrb1, a paralog of Gbp2, was similarly identified as an interactor of the *ATG1* 3' UTR (Data File 2) (Hurt et al., 2004). Furthermore, I identified ribosome component Rps27A, suggesting the crucial role of the 3' UTR in regulating *ATG1* mRNA stability, export, and translation (Data File 2).

The stress granule core protein Pub1 was also identified as interacting with the 3' UTR of *ATG1* (Fig 3a). Pub1 is not previously implicated in autophagy, and therefore I were curious as to the significance of the Pub1 interaction with *ATG1* mRNA. To confirm this interaction, I immunoprecipitated Pub1-sfGFP, expressed on a plasmid and tested if it interacted with *ATG1* mRNA. I found significant enrichment of the *ATG1* 3' UTR, with additional binding in the 5' UTR, suggesting that Pub1 indeed interacted with *ATG1* (Figure 6b).

As an interactor of the *ATG1* 3' UTR, I next asked whether Pub1 regulates the expression of Atg1. From immunoblot analysis, I determined that *pub1*Δ cells did not upregulate Atg1 protein levels compared to the WT (Figure 6c). However, the transcript levels of *ATG1* remained similar

to WT (Figure 6d). This result suggests that Pub1, similar to Npl3, regulates *ATG1* at the post-transcriptional level. To confirm this hypothesis, I performed polysome profiling and analyzed the distribution of *ATG1* transcript in the different polysome fractions as I did for the *npl3*Δ strain. The polysome profiles confirmed that *pub1* deletion did not significantly affect the global translation (Figure 7a). However, *PUB1* deletion did significantly reduce the localization of *ATG1* transcript in the polysome fractions, with a significant increase in the free mRNP fraction, suggesting a failure to recruit polysomes in the absence of Pub1 (Figure 6e).

In contrast, the control RNA *PGK1* did not show a drastic change in localization compared to the WT in the polysome fraction (Figure 7b). The difference in *ATG1* translation and, therefore, Atg1 protein expression resulted in a difference in autophagy activity as measured by Pho8Δ60 activity (Figure 6f), an enzymatic assay that monitors autophagic flux (Noda & Klionsky, 2008). Finally, *pub1* deletion drastically reduced the viability of the cells during long-term starvation, providing insights into the critical role of Pub1 in ensuring cell survival during nutrition limitation (Figure 6g).

Figure 6

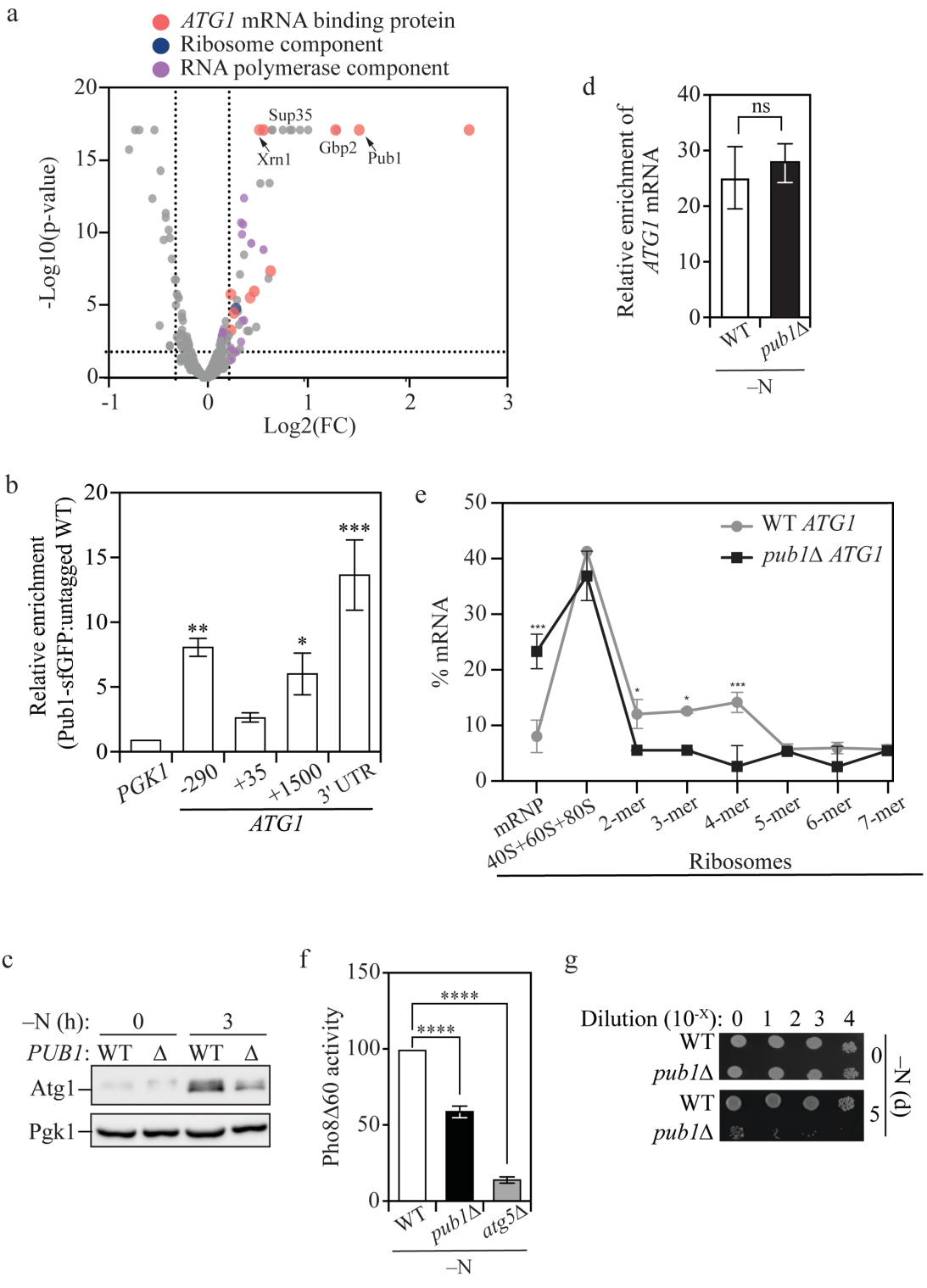
a
ATG1 mRNA binding protein
Ribosome component
RNA polymerase component
-Log10(p-value)
Log2(FC)
Sup35
Xrn1
Gbp2
Pub1
d
Relative enrichment of ATG1 mRNA
ns
WT
pub1Δ
–N
b
Relative enrichment (Pub1-sfGFP:untagged WT)
PGK1
-290
+35
+1500
3' UTR
ATG1
e
% mRNA
WT ATG1
pub1Δ ATG1
mRNP
40S+60S+80S
2-mer
3-mer
4-mer
5-mer
6-mer
7-mer
Ribosomes
c
–N (h): 0 3
PUB1: WT Δ WT Δ
Atg1
Pgk1
f
Pho8Δ60 activity
WT
pub1Δ
atg5Δ
–N
g
Dilution (10-X): 0 1 2 3 4
WT
pub1Δ
WT
pub1Δ
0
5
–N (d)

Figure 6: Nuclear localization of Npl3 is necessary for *ATG1* mRNA interaction and Atg1 protein expression.

a. An analysis of *ATG1* 3' UTR interaction network reveals novel interactors: Volcano plot showing RBPs interacting with the *ATG1* 3' UTR compared to *PGK1* as a control. The data show Npl3 interacting partners such as the previously identified Gbp2, and novel *ATG1* binding partners such as Xrn1 and Pub1 (highlighted in salmon). Data are representative of two independent biological replicates, mean +/- SD. Student's t test was performed to determine statistical significance. P values above 0.05 were considered significant.

b. Pub1 interacts with the 3' UTR of *ATG1* during nitrogen starvation: Pub1-sfGFP was expressed using a centromeric plasmid in a WT (SEY6210) strain and subjected to RNA immunoprecipitation following nitrogen starvation for 4 h. *ATG1* mRNA bound to Pub1 was quantified through qRT-PCR using primers specific to different regions on the transcript. Data are representative of two independent biological replicates, showing mean+/- SD. One-way ANOVA was performed to determine statistical significance. **** p value = 0.0003, ** p value = 0.0043, * p value = 0.0164.

c. Loss of Pub1 reduces Atg1 protein expression: WT (WLY176) and *pub1*Δ (SPY006) strains were subjected to nitrogen starvation for 3 h and Atg1 protein levels were determined by immunoblotting. Pgk1 was used as a loading control.

d. Loss of Pub1 does not affect *ATG1* transcription: WT (WLY176) and *pub1*Δ (SPY006) cells were subjected to nitrogen starvation for 3 h and the abundance of *ATG1* mRNA was determined by qRT-PCR. Data are representative of three independent biological replicates, showing mean +/- SD. Student's t test was performed to determine statistical significance.

e. Pub1 recruits polysomes onto the *ATG1* transcript during nitrogen starvation: WT (WLY176) and *pub1*Δ (SPY006) strains were subjected to nitrogen starvation for 3 h and the abundance of *ATG1* transcript in the different polysome fractions were determined using qRT-PCR. Data are representative from two independent biological replicates, showing SD+/- mean. Two-way ANOVA was used to determine statistical significance. *** p value = 0.0004, ** p value = 0.0022, * p value < 0.05.

f. Pub1 is a positive regulator of autophagy during nitrogen starvation: WT (WLY176) and *pub1*Δ (SPY006) strains were subjected to nitrogen starvation for 4 h and assayed to determine Pho8Δ60 activity. Data are representative of three independent biological replicates, showing mean +/- SD. One-way ANOVA was performed to determine statistical significance. **** p value <0.0001

g. Loss of Pub1 reduces viability during long-term nitrogen starvation: WT (WLY176) and *pub1*Δ (SPY006) strains were subjected to nitrogen starvation for the indicated times and the indicated dilutions were spotted on YPD plates and grown for 3 days at 30°C.

Figure 7

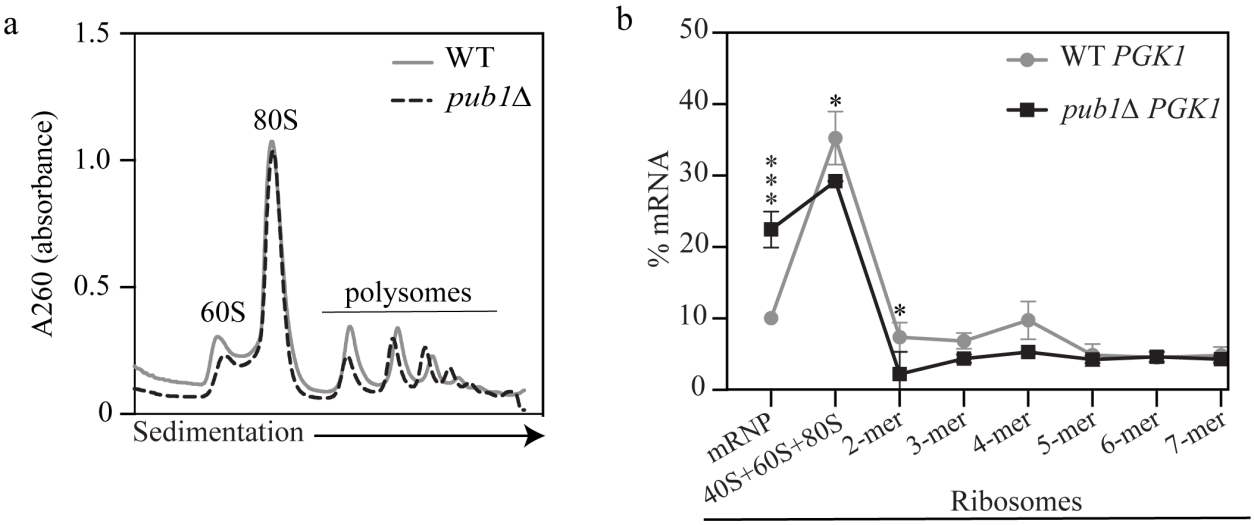
a
1.5
1.0
0.5
0
A260 (absorbance)
WT
pub1Δ
80S
60S
polysomes
Sedimentation
b
50
40
30
20
10
0
% mRNA
WT PGK1
pub1Δ PGK1
***
*
*
mRNP
40S+60S+80S
2-mer
3-mer
4-mer
5-mer
6-mer
7-mer
Ribosomes

Figure 7: Loss of Pub1 does not affect global translation during nitrogen starvation.

a. The polysome profile of *pub1*Δ is similar to WT: WT and *pub1*Δ strains were subjected to nitrogen starvation and the polysome profiles were analyzed using a gradient fractionator.
b. The distribution of *PGK1* is minimally changed in the polysome fractions due to loss of Pub1: WT and *pub1*Δ cells were subjected to nitrogen starvation and equal amounts of different ribosomal fractions were collected using a gradient fractionator. The abundance of *PGK1* mRNA was determined using qRT-PCR.

2.2.5 TIA1 promotes ULK1 expression and autophagy

To explore the conservation of Pub1's role, a protein I have shown here to regulate Atg1 expression, I studied the capacity of TIA1, its mammalian counterpart, to influence ULK1 (a homolog of Atg1) protein expression. I used a non-small cell lung cancer cell line, Calu-1, to test the effect of TIA1 on ULK1 levels and autophagy. I found that the knockdown of TIA1 led to a reduction in protein levels of ULK1 (Figure 8a, 8b). Crucially, stable knockdown of TIA1 using siRNA had no effect on the transcript levels of *ULK1*, suggesting post-transcriptional regulation (Figure 8c). Next, I analyzed MAP1LC3B/LC3B-II levels using immunoblotting, which showed a consistent decrease post-knockdown of TIA1 following serum starvation (Figure 8a, 8d). Treatment with bafilomycin A_1 blocks a late stage of autophagy and resulted in a substantial increase in ULK1 in the WT cells. In contrast, this treatment resulted in a significantly reduced accumulation of LC3B-II in TIA1 KD cells, indicating the reduction of autophagy in these cells as a result of lowered ULK1 levels (Figure 8d). Finally, I investigated whether TIA1 directly interacted with *ULK1* mRNA. Indeed, TIA1 showed significant enrichment at the 3' UTR of *ULK1*, similar to Pub1 (Figure 8e). Taken together, these results indicate that TIA1 plays a significant role in regulating ULK1 expression and autophagy, emphasizing the conserved nature of the regulation at the 3' UTR of both *ATG1* and *ULK1* via Pub1 and TIA1, respectively.

Figure 8

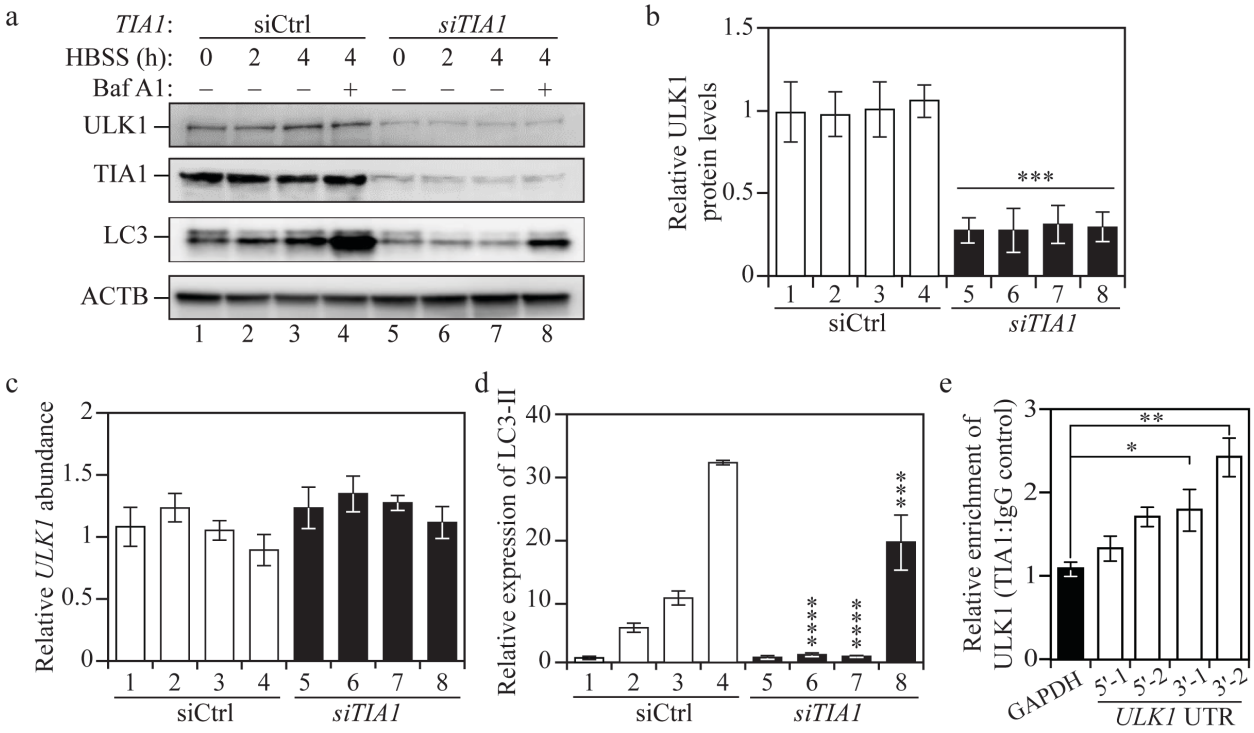
a
TIA1: siCtrl siTIA1
HBSS (h): 0 2 4 4 0 2 4 4
Baf A1: – – – + – – – +
ULK1
TIA1
LC3
ACTB
1 2 3 4 5 6 7 8
b
Relative ULK1 protein levels
1.5
1
0.5
0
***
1 2 3 4 5 6 7 8
siCtrl
siTIA1
c
Relative ULK1 abundance
2
1.5
1
0.5
0
1 2 3 4 5 6 7 8
siCtrl
siTIA1
d
Relative expression of LC3-II
40
30
20
10
0
****
****
***
1 2 3 4 5 6 7 8
siCtrl
siTIA1
e
Relative enrichment of ULK1 (TIA1:IgG control)
3
2
1
0
**
*
GAPDH
5'-1
5'-2
3'-1
3'-2
ULK1 UTR

Figure 8: TIA1 promotes ULK1 protein expression and autophagy during nutrient starvation.

a. Loss of TIA reduces ULK1 protein expression and autophagy: Calu-1 cells transfected with either siRNA (control) or siRNA specific to *TIA1* were subjected to serum starvation for the indicated times with or without treatment with bafilomycin A_1. Cells were harvested after the indicated times and protein levels of ULK1, TIA1 and LC3 were determined by immunoblotting. ACTB was used as a loading control.
b. Quantification of ULK1 protein levels in a. Data are representative of three independent biological replicates, showing mean +/- SD. **** p value <0.001.
c. TIA1 knockdown does not affect *ULK1* transcription: Total RNA was extracted from cells harvested under the conditions indicated in a and *ULK1* mRNA abundance was determined by qRT-PCR. *GAPDH* was used as a control. Data are representative of three independent biological replicates.
d. Quantification of LC3-II levels in a. Data are representative of three independent biological replicates, showing mean +/- SD. Two-way ANOVA was used to determine statistical significance. **** p value < 0.01, *** p value <0.05.
e. TIA1 binds to the 3' UTR of *ULK1*: RNA immunoprecipitation was performed using TIA1-specific antibody and the mRNA bound to the protein was quantified by qRT-PCR using two primers spanning different regions in the 5' UTR and 3' UTR. Data are representative of three independent biological replicates, showing mean +/- SD. One-way ANOVA was performed to determine statistical significance. ** p value = 0.0013, * p value = 0.0358.

2.2.6 Npl3 coordinates with Pub1 to export ATG1 mRNA and recruit polysomes for translation

Our investigations into the *ATG1* mRNA interactome revealed Npl3 and Pub1 as post-transcriptional regulators. Previous high-throughput studies have shown that Npl3 interacts with Pub1 (Gotor et al., 2020). This led us to ask whether Pub1 and Npl3 coordinate to enhance the translation of *ATG1* during nitrogen starvation. To examine this, I performed co-immunoprecipitation of Npl3 tagged with PA and determined the interaction of Pub1-tagged with sfGFP using immunoblot. Consistently, Npl3 interacted with Pub1 during nitrogen-starvation conditions (Figure 9a). Furthermore, this interaction was dependent on RNA; RNase treatment of the cell lysate prior to immunoprecipitation essentially eliminated the interaction between the two proteins. This finding suggests that Npl3 and Pub1 might coordinate to post-transcriptionally regulate the *ATG1* transcript. Therefore, I tested if the two proteins worked together in the polysome fraction. Towards this end, I tested the localization of Npl3 and Pub1 in the different fractions of free mRNPs, monosomes and polysomes. Npl3 showed no enrichment in the monosome and polysome fractions (Figure 9b). In contrast, Pub1 interacted with both monosome and polysome fractions during nitrogen starvation, suggesting a more direct role in translational regulation of *ATG1*.

Considering that Npl3 did not interact with polysome components, I were interested to further dissect its role and localization in regulating *ATG1* at the posttranscriptional. In line with this, I found that following growth in nutrient-rich conditions and during nitrogen starvation, Npl3 was predominantly localized to the nucleus (Figure 9c). Previously, studies have shown that the point mutation E409K results in a protein predominantly localized to the cytosol (Lei et al., 2001). I constructed a strain containing this mutation and asked if the E409K mutant showed defects in Atg1 expression. Indeed, $Npl3^{E409K}$ had lowered Atg1 protein but not *ATG1* mRNA levels (Figure 10a-c). This defect resulted from the severe reduction in *ATG1* mRNA-binding

exhibited by the E409K mutant (Figure 9d). Npl3 interacts with the transcription machinery and loads transcripts onto mRNPs responsible for transcript export, underscoring its pivotal role in the nucleus (Keil et al., 2023). These findings suggest a mechanism where the surveillance protein Npl3 recruits Pub1 onto the *ATG1* transcript. Therefore, I asked if the interaction of *ATG1* mRNA and Pub1 is dependent on the presence of Npl3. RNA immunoprecipitation of Pub1 in WT and *npl3*Δ backgrounds, showed that the interaction of Pub1 and the *ATG1* 3' UTR was severely reduced in the absence of *NPL3* (Figure 9e). Given that localization of Npl3 in the nucleus is critical for the Npl3-*ATG1* interaction and Npl3 is required for Pub1-*ATG1* interaction, I hypothesized that *ATG1* loading onto Pub1 by Npl3 is required to export *ATG1* transcript to the cytosol. Therefore, I asked if *pub1*Δ cells also have an export defect of *ATG1* mRNA. I found that the percentage of mRNA in the nuclear fraction was much higher in the absence of Pub1 compared to the WT (Figure 9f), thus phenocopying *npl3*Δ cells.

An obvious question was, does Pub1 link *ATG1* mRNA export and translation? Pub1 interacts with polysomes, and several independent studies have shown that it also can interact with mRNA export proteins (Apponi et al., 2007). However, Pub1 is also a core stress granule component, with primary functions in the cytoplasm. Therefore, I wanted to determine all the interactions of Pub1 during nitrogen starvation, and thus I performed immunoprecipitation of Pub1-sfGFP followed by mass spectrometry analysis to identify the factors that interact with Pub1 (Figure 9g). From this analysis, I confirmed the interaction of Pub1 with Npl3. Furthermore, I found that Pub1 interacted with several mRNA export proteins, along with Npl3. Notably, Pub1 interacted with Yra1 and Sem1, whose role in mRNA export from the nucleus has been long established (MacKellar & Greenleaf, 2011). I found that Pub1 bound to over 40 ribosome components, including large and small subunits, and interacted with translation factors

such as Sui1 and Gcd1, involved in translation initiation, as well as Yef3, a translation elongation factor, thus suggesting that Pub1 indeed shuttles between the nucleus and the cytoplasm, linking mRNA export and translational machinery. Furthermore, Pub1 interacted with known RBPs that influence Atg1 protein levels, such as Dhh1, Pat1, Ded1, and Cdc33 (Data File 3), confirming that Pub1 links the *ATG1* mRNA-protein interactome to the translational machinery and ribosome components to aid in translation. These results also suggest that Pub1 mediates two spatially separated processes of nuclear mRNP loading and cytoplasmic translation, providing a unifying mechanism of how previously identified interactors of *ATG1* help to deliver the transcript to translating ribosomes to enhance the Atg1 production needed to sustain starvation-dependent autophagy.

Figure 9

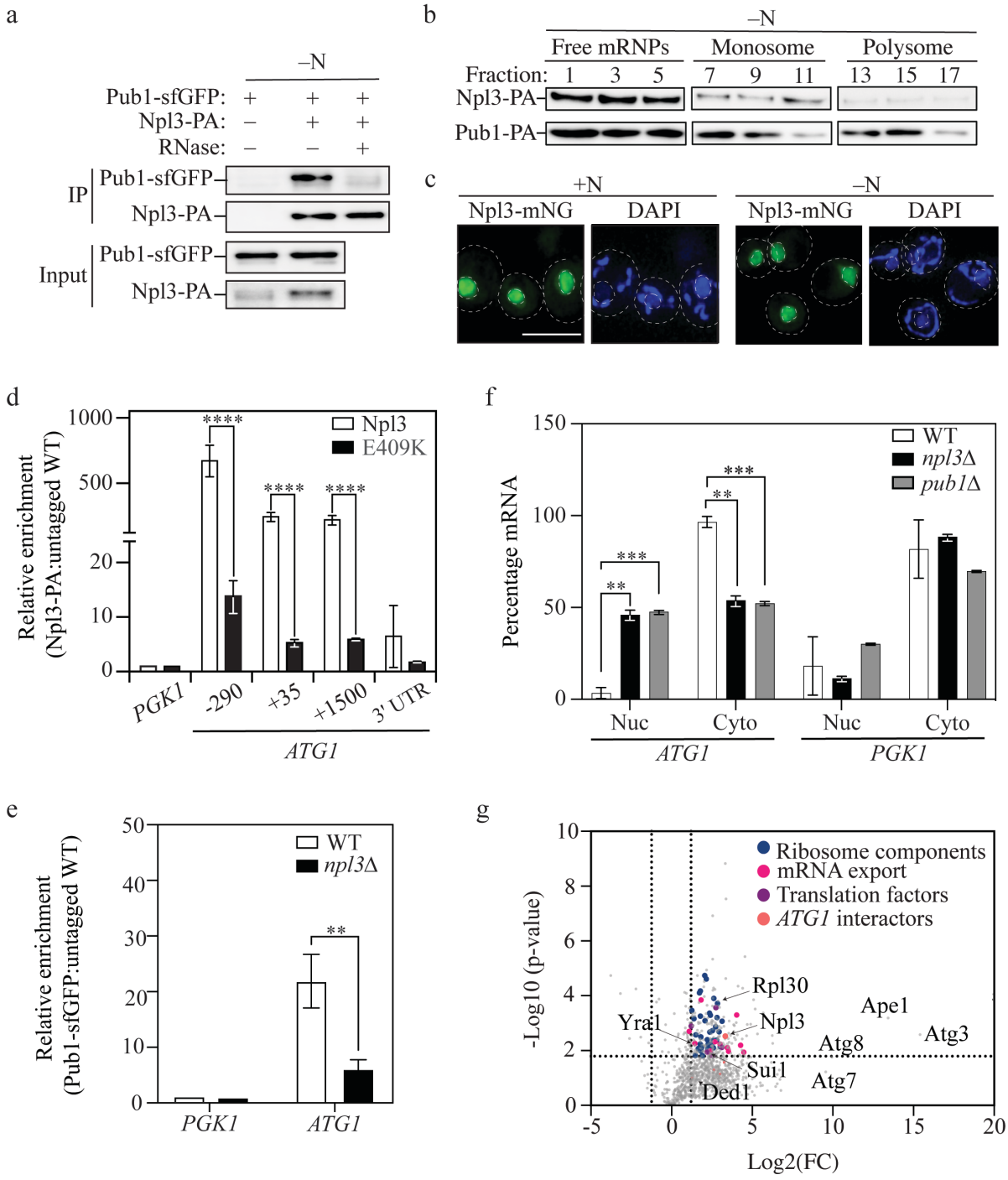
a
–N
Pub1-sfGFP: + + +
Npl3-PA: – + +
RNase: – – +
IP
Pub1-sfGFP
Npl3-PA
Input
Pub1-sfGFP
Npl3-PA
b
–N
Free mRNPs
Monosome
Polysome
Fraction: 1 3 5 7 9 11 13 15 17
Npl3-PA
Pub1-PA
c
+N
–N
Npl3-mNG
DAPI
Npl3-mNG
DAPI
d
Relative enrichment (Npl3-PA:untagged WT)
1000
500
20
10
0
Npl3
E409K
****
****
****
PGK1
-290
+35
+1500
3' UTR
ATG1
e
Relative enrichment (Pub1-sfGFP:untagged WT)
50
40
30
20
10
0
WT
npl3Δ
**
PGK1
ATG1
f
Percentage mRNA
150
100
50
0
WT
npl3Δ
pub1Δ
***
**
***
**
Nuc
Cyto
Nuc
Cyto
ATG1
PGK1
g
-Log10 (p-value)
10
8
6
4
2
0
Ribosome components
mRNA export
Translation factors
ATG1 interactors
Rpl30
Ape1
Yra1
Npl3
Atg3
Atg8
Sui1
Atg7
Ded1
-5
0
5
10
15
20
Log2(FC)

Figure 9: Pub1 links *ATG1* mRNA export and translation.

a. Npl3 and Pub1 interaction is RNA dependent: An Npl3-PA tagged strain expressing a centromeric Pub1-sfGFP was subjected to nitrogen starvation and harvested after 4 h. Npl3-PA was affinity isolated using IgG Sepharose beads with or without RNase and immunoblotted to determine Npl3 and Pub1 interaction.

b. Npl3 and Pub1 localize to different ribosome compartments: Npl3-PA (SPY060) and Pub1-PA (SPY034) strains were subjected to nitrogen starvation for 4 h and equal fractions were collected by polysome profiling. Two consecutive fractions were combined, and proteins were analyzed by immunoblotting.

c. Npl3 is predominantly localized to the nucleus: Npl3 was tagged with mNeongreen (SPY067) and imaged under rich medium (+N) and nitrogen starvation medium (-N) conditions. DAPI was used to stain DNA. Data are representative of 200 cells analyzed. Scale bar: 5 μm.

d. Nuclear localization of Npl3 is required for it to bind to *ATG1* mRNA: RNA immunoprecipitation was performed using WT (untagged, SEY6210), Npl3-PA (SPY060) and $Npl3^{E409K}$-PA (SPY057) strains and *ATG1* mRNA abundance was determined by qRT-PCR. Data are representative of three independent replicates, showing mean +/-SD. **** p value <0.0001.

e. Loss of Pub1 causes defects in *ATG1* mRNA export, similar to *npl3*Δ: WT (WLY176), *npl3*Δ (SPY077) and *pub1*Δ (SPY006) strains were subjected to nitrogen starvation for 4 h and fractionated to obtain nuclear and cytoplasmic fractions. *ATG1* abundance was determined by qRT-PCR. *PGK1* was used as a control. Two-way ANOVA was performed to determine statistical significance. **** p value = 0.0005, *** p value = 0.0097.

f. Npl3 is required for Pub1-*ATG1* interaction during nitrogen starvation: A centromeric plasmid harboring Pub1-sfGFP was expressed in WT (WLY176) and *npl3*Δ (SPY077) strains and subjected to nitrogen starvation for 4 h, following which GFP-trap nanobeads were used to immunoprecipitate Pub1. Untagged WLY176 was used as a control. *ATG1* 3' UTR abundance was determined by qRT-PCR. Data are representative of three independent biological replicates, showing mean +/- SD. Two-way ANOVA was performed to determine statistical significance. ** p value = 0.0095.

g. Pub1 interacts with ribosomal components and translation factors during nitrogen starvation: A Pub1-sf-GFP-expressing and untagged WT (SEY6210) strain were subjected to nitrogen starvation for 4 h and immunoprecipitated using GFP-trap nanobeads. The interactome of Pub1 was identified by mass spectrometry. Data are representative of two independent replicates. Student's t test was used to determine statistical significance. A p value above 0.05 was considered significant.

Figure 10

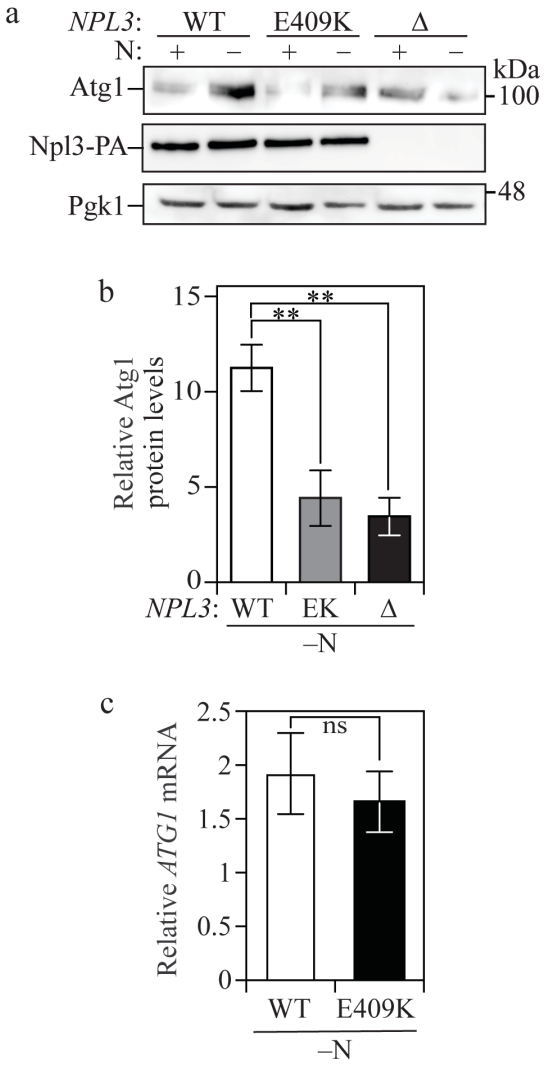
a
NPL3: WT E409K Δ
N: + – + – + –
kDa
Atg1
100
Npl3-PA
Pgk1
48
b
Relative Atg1 protein levels
15
10
5
0
**
**
NPL3: WT EK Δ
–N
c
Relative ATG1 mRNA
2.5
2
1.5
1
0.5
0
ns
WT E409K
–N

Figure 10: Nuclear localization of Npl3 is required to upregulate Atg1 protein expression.

a. The loss of nuclear localization of Npl3 results in reduced Atg1 protein levels: WT and *npl3*Δ strains and cells expressing the $Npl3^{E409K}$ mutant were subjected to nitrogen starvation for 6 h and Atg1 protein levels were monitored by immunoblotting. Pgk1 was used as a loading control.
b. Quantification of a. Data are representative of three independent biological replicates. One-way ANOVA was performed to determine statistical significance. ** p value <0.01.
c. Nuclear localization is not required for *ATG1* mRNA transcription: Cells expressing Npl3 WT and the E409K mutant were subjected to nitrogen starvation for 1 h and *ATG1* mRNA abundance was determined by qRT-PCR.

2.3 Discussion

2.3.1 ATG1 mRNA-protein interaction landscape

Understanding how cells fine-tune autophagy concomitant with the severity of metabolic stress continues to be a significant question in studying cell survival during nutrient starvation (Chun & Kim, 2018). Accumulating evidence has shown that an intricate interplay of nutrient-sensitive signaling cascades such as the TOR, general amino acid control/GAAC, and Snf1 pathways up to complex regulatory networks at multiple layers of molecular regulation work together to affect autophagy in response to nutrition limitation (Conrad et al., 2014). During nutrient limitation, cells, with the intention of conserving the limited energy and metabolite reserves, downregulate all energy-intensive processes, especially protein translation (Holcik & Sonenberg, 2005). How *ATG* transcripts escape the global repression of translation in order to elicit the required autophagy levels is an exciting question in the field. This question forces us to think about the regulatory architecture of autophagy at a detailed molecular level. This granular approach allows us to uncover regulators that specifically target autophagy without the pleiotropic effects that may result from interfering with major signaling pathways. One such class of regulators that have gained prominence over the last few years is the RNA-binding proteins that act at the post-transcriptional and translational level of autophagy (Frankel et al., 2017). These regulators target different stages of mRNA metabolism in a nutrient-dependent manner, thus allowing for autophagy activation and deactivation mechanisms.

To understand this process at the molecular level, I focused on *ATG1* mRNA in *S. cerevisiae*. Atg1, a serine/threonine kinase, plays a central role in the autophagy process. This protein orchestrates the initiation and regulation of autophagy by integrating signals of nutrient status and cellular energy, leading to the phosphorylation of autophagy machinery components

that function in the formation of autophagosomes. Beyond its pivotal role in cellular degradation and recycling, Atg1 also interfaces with other critical cellular processes, such as the cell cycle, apoptosis, and stress response, underlining its importance in maintaining cellular homeostasis and responding to environmental stresses (Noda & Fujioka, 2015). Recently, *ATG1* has emerged as a transcript regulated by multiple players in a nutrient-dependent manner. Notably, under nutrient-rich conditions, the cytoplasmic exoribonuclease Xrn1 reduces the stability of *ATG1* mRNA, leading to its degradation (Delorme-Axford et al., 2018). During nitrogen deprivation, the Pat1-Lsm complex plays a protective role, preventing the degradation of *ATG1* mRNA by the exosome from the 3′ to the 5′ end, thereby maintaining its stability (Gatica et al., 2019). In the presence of ample nutrients, Dhh1, an RNA helicase, collaborates with Dcp2 to accelerate the breakdown of *ATG1* messages, leading to a decrease in autophagy (Hu et al., 2015). However, under prolonged nitrogen starvation, Dhh1 works with Eap1 to enhance *ATG1* mRNA translation, specifically targeting the structured region close to the start codon and promoting autophagy (Liu et al., 2019). The translation of *ATG1* mRNA is further enhanced during extended periods of nitrogen limitation by the RGG motif-bearing protein Psp2, which interacts with translation machinery components eIF4E and eIF4G2 and targets the 5' UTR of *ATG1*, independent from Dhh1 (Yin et al., 2019). Finally, Ded1, in conjunction with Rad53, upregulates Atg1 protein expression only in response to nitrogen starvation but not in amino acid starvation, suggesting the sensitivity of this regulatory network to minute changes in external nutrient environments (Lahiri et al., 2022). These novel insights point to a complex web of *ATG1* mRNA-protein interactions, suggesting extensive regulatory oversight across its metabolic lifecycle. However, how these various factors, that make up P-bodies, coordinate to regulate the same mRNA is yet unknown. I propose a dynamic assembly of RNA-binding proteins linked to

ATG1 mRNA, adjusting to shifts in nutritional signals to manage Atg1 protein synthesis, potentially identifying new autophagy modulators. Our research suggests that the stress granule protein Pub1 links the export of *ATG1* transcript and these previously identified regulators to upregulate *ATG1* translation.

Our research strategy involved in vitro transcription of the *ATG1* 5' and 3' UTRs, followed by labelling with desthiobiotin. This labelled RNA served as bait for affinity-isolation assays, enabling the identification via mass spectrometry of proteins that interact with the *ATG1* UTRs. Our investigation into the protein network associated with *ATG1* UTRs, under both nutrient-rich conditions and nitrogen starvation, unveiled 36 interactors specific to nitrogen starvation, and 62 interactors specific to growing conditions at the 5' UTR. Notably, 26 of these proteins were previously shown to have mRNA-binding capacity. Furthermore, I identified 18 RNA-binding proteins interacting with the 3' UTR of *ATG1* mRNA (Table 1). Screening the interactors enriched specifically in nitrogen starvation at the 5' UTR and 3' UTR, I discovered Npl3 and Pub1 as significant interacting partners of the *ATG1* transcript, which emerged as crucial promoters of autophagy and survival during nitrogen starvation.

2.3.2 The Npl3-Pub1 axis facilitates ATG1 mRNA export and translation

Npl3 is an mRNA surveillance protein involved in multiple events immediately after the transcription of messenger RNA. Previous reports have shown that Npl3 directly binds to RNA polymerase II components and facilitates transcription elongation (Santos-Pereira et al., 2014). Npl3 is then involved in ensuring proper processing of the newly synthesized transcript. For example, Npl3 monitors proper 5' capping of the transcript, wherein uncapped mRNAs are subject to degradation by the nuclear exosome complex (Keil et al., 2023; Klama et al., 2022).

Evidence suggests that following proper processing, Npl3 recruits export-competent mRNPs. Our research reveals that deletion of *NPL3* leads to accumulation of the *ATG1* transcript in the nucleus, suggesting its role in the export of the transcript. Furthermore, Pub1 is a key protein recruited by Npl3 onto the *ATG1* transcript to facilitate *ATG1* export, and thus increase accessibility to ribosomes in the cytosol for translation. The diminished autophagy activity and lowered cell survival in cells lacking *NPL3* are likely tied to the reduced translation of Atg1. However, the potential upregulation of other autophagy-related or regulatory proteins by Npl3 cannot be dismissed, as our study focused primarily on Atg1 regulation. I found that Npl3 directly binds to the *ATG1* transcript through its RRM motif, providing a new perspective on the role of Npl3 in autophagy regulation.

Furthermore, phosphorylation of Npl3 by Sky1 promotes Npl3 shuttling to the cytosol and mRNA dissociation (Gilbert et al., 2001). However, our experiments showed that Sky1 did not affect Atg1 protein levels, suggesting that its role in the phosphorylation of Npl3 is not relevant to the export and translation of *ATG1* during nitrogen starvation (Figure 11a). Consistent with this, I found that mutations that prevent proper nuclear localization of Npl3 led to a decrease in *ATG1* binding and expression with a concomitant decrease in autophagy. Therefore, while Npl3 is a known nuclear-to-cytosol shuttling protein, in the context of nutrient starvation it predominantly functions in the nucleus and facilitates priming of *ATG1* mRNA for export by Pub1.

2.3.3 Possible dual role of Pub1 in response to nutrient stress

Pub1 is an RBP known for its role in stabilizing stress-responsive mRNA and facilitating its translation; one such example is seen with Gcn4 (Ruiz-Echevarria & Peltz, 2000). Here, I

show that the deletion of *PUB1* does not affect the stability of *ATG1* mRNA; however, it directly affects its translation. Most importantly, I discovered that Npl3 binds to Pub1 in an RNA-dependent manner during nitrogen starvation. Using immunoprecipitation combined with mass spectrometry, I identified the interactors of Pub1 in nitrogen starvation. Pub1 interacts with export proteins such as Yra1 and Sem1, and likely escorts *ATG1* transcripts to the cytosol, where it interacts with several translation factors, including initiation and elongation factors, as well as over 40 ribosomal components. (Faza et al., 2009; Infantino et al., 2019) Additionally, I found that Mex67, Dbp2 and Nab2 interact with the *ATG1* 5' UTR (Figure 11b). Dbp2 is required for the assembly of export components such as Nab2, Mex67 and Yra1 onto the RNA (Ma et al., 2013). This complex may also include Pub1. However, the interaction of Pub1 and Nab2 is independent of RNA (Apponi et al., 2007). Interestingly, I showed that Pub1 also interacts with previously known *ATG1* interactors mentioned above, either directly or indirectly via the *ATG1* transcript (Data File 3). This finding suggests that the proteome components of the *ATG1* transcript function in close proximity to each other.

Crucially, I found this role to be conserved in humans as well via TIA1, a homolog of Pub1. Depletion of TIA1 results in the decrease of ULK1 protein levels and autophagy levels while not affecting the mRNA levels of *ULK1*. Finally, similar to Pub1, I found that TIA1 interacts with ULK1 at the 3' UTR. Mutations in the *TIA1* gene have been linked to various neurodegenerative disorders. For instance, some studies have associated TIA1 mutations with amyotrophic lateral sclerosis/ALS and frontotemporal dementia/FTD, suggesting that these mutations may disrupt normal protein aggregation and RNA metabolism processes in neurons (Mackenzie et al., 2017). The ability of TIA1 to influence autophagy, therefore, has significant implications for diseases where autophagy is dysregulated. For instance, in neurodegenerative

diseases altered autophagy can contribute to the accumulation of toxic protein aggregates (Park et al., 2020). Modulating TIA1 function could potentially offer therapeutic strategies to enhance autophagy and mitigate disease progression.

Pub1 and its mammalian equivalent TIA1 interact with Sup35 and GSPT2 (Li et al., 2014). Our study reveals that the *ATG1* 3' UTR binds to Sup35 (Figure 6a), suggesting a novel mechanism where Pub1-Sup35 could facilitate local translation of autophagy-related proteins, akin to their proposed function in cytoskeleton integrity via tubulin translation. Interestingly, I found that Pub1 physically interacts with Atg3, Atg7, Atg8, and the marker for the phagophore assembly site, precursor Ape1 (Fig 5g). This presents us with two intriguing possibilities: One is the potential for local translation of autophagy-related proteins at the site of autophagosome formation. The second possibility is that these interactions are critical for "granulophagy," which involves autophagy's selective degradation of stress granules (Buchan et al., 2013). Further investigation is necessary to tease apart the importance of these interactions.

Meanwhile, Pub1/TIA1's role in forming phase-separated stress granules is well established (Kroschwald et al., 2018; Rayman et al., 2018). Here, in nitrogen starvation, typically not associated with phase-separated stress granule formation, I show that Pub1 shuttles between the nucleus and cytosol to aid in *ATG1* translation by recruiting translation initiation and elongation factors and both large and small ribosome subunits, suggesting the importance of its stress granule-independent role. Interestingly, TIA1 mutations exhibited in patients with amyotrophic lateral sclerosis increase the propensity of the protein to undergo phase transition, possibly removing its interaction with *ULK1* and its positive influence on autophagy, leading to autophagy defects (Mackenzie et al., 2017). This dual functionality of Pub1/TIA1 may represent

the robustness of the system wherein the *ATG1*/*ULK1* transcript is primed to switch between translation and storage depending on the severity of the nutrient starvation.

2.3.4 Modularity of ATG regulation

Our study has unveiled a trove of novel interactors of the *ATG1* mRNA transcript at the 5' and 3' UTR regions and has brought to light two previously unknown regulators of autophagy, with Pub1's role conserved in mammalian cells. The sheer diversity of the *ATG1* mRNA-protein interactome hints at the modular nature of *ATG1* transcript regulation; different regulators can function independently, enabling nutritional control, but can also operate interchangeably, underscoring the redundancy of the system, thereby bolstering its robustness (Reynaud et al., 2023). Crucially, these independent regulators can collaborate in a coordinated manner to achieve synergistic regulation. The modular architecture of the system has allowed us to identify individual regulators, but it is only now that I are beginning to fathom the true complexity of the process. Utilizing our approach of mRNA affinity isolation followed by proteomics, I can now map the protein interaction landscape of other *ATG* transcripts to comprehensively understand the interaction network that regulates not only Atg protein expression but also autophagy. Together, our study found that following transcription, Npl3 loads *ATG1* transcript onto Pub1, which then exports it to the cytosol. In the cytosol, Pub1 interacts with several translational factors and previously identified *ATG1* interactors to recruit ribosomal components onto the *ATG1* transcript and facilitate its translation and autophagy during nitrogen starvation.

The *ATG1* transcript, with its myriad interactions, highlights the cell's ingenious strategy to maintain homeostasis and prepare for uncertain metabolic landscapes, showcasing the elegance and complexity of autophagic regulation. Through this lens, I begin to appreciate the

exquisite sensitivity of cells to their environment and the sophisticated mechanisms they employ to thrive in the face of metabolic adversity.

Figure 11

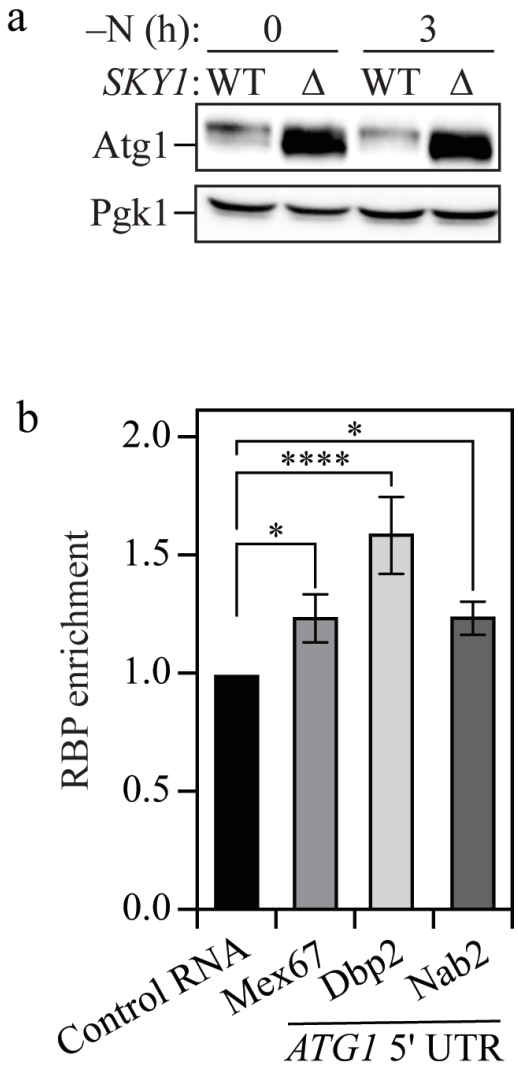
a
–N (h): 0 3
SKY1: WT Δ WT Δ
Atg1
Pgk1
b
RBP enrichment
2.0
1.5
1.0
0.5
0.0
*
****
*
Control RNA
Mex67
Dbp2
Nab2
ATG1 5' UTR

Figure 11: Pub1 interactors bind to the *ATG1* 5' UTR.

a. Established export proteins and Pub1 interactors bind to the *ATG1* 5' UTR: RBP enrichment of Mex67, Dbp2 and Nab2 as determined by mass spectrometry is shown from two independent biological replicates. One-way ANOVA was performed to determine statistical significance. **** p value <0.001, * p value <0.05.
b. Sky1, which phosphorylates Npl3, is not a regulator of Atg1 protein expression: WT and *sky1*Δ cells were subjected to nitrogen starvation for the indicated times. The Atg1 level in protein extracts was then determined by immunoblotting. Pgk1 was used as a loading control.

2.4 Materials and Methods

2.4.1 Yeast Methods

Yeast strains, media and growth conditions

Yeast strains used in this study are listed in Table S1. Standard methods were used to generate gene deletions and tagging.

Yeast cells were grown in rich media, YPD (1% yeast extract, 2% peptone and 2% glucose), until the OD reached 0.8-1.0. An appropriate volume of cells was collected by centrifugation, washed with water and transferred to nitrogen starvation medium (-N; 0.17% yeast nitrogen base without ammonium sulfate or amino acid, 2% glucose) for the indicated times to induce starvation-dependent autophagy

Plasmids

pUC19-*ATG1* 5' UTR has been described previously (Yin et al., 2019) , consisting of 500 base pairs (bp) upstream of the *ATG1* start codon. pUC19-*ATG1* 3' UTR was constructed by amplifying the ~600 bp downstream of the *ATG1* stop codon and inserting the fragment into the pUC19 plasmid containing the T7 promoter. pUC19-PGK1 5' UTR was constructed by amplifying 500 bp upstream of the *PGK1* start codon and inserting the fragment into the pUC19 plasmid. Centromeric Pub1sf-GFP was described previously (Kroschwald et al., 2018).

2.4.2 RNA methods

mRNA invitro transcription

This method was carried out using the pUC19 plasmids as described above. Briefly, the plasmids were linearized using HindIII at 37°C for 2 h. One ug of linearized plasmid was then subject to in vitro transcription using the HiScribe T7 Quick High Yield RNA Synthesis Kit (NEB). The resulting RNA was purified using an RNA clean-up kit (New England Biolabs, T2050)) and quantified.

RNA labeling and affinity isolation

In vitro transcribed RNA (50 pmols) was used for a single labeling reaction with the desthiobiotin RNA labelling kit (Thermo, 20164) according to the manufacturer's instructions. The labeled RNA was then conjugated with streptavidin beads (Thermo, 20164)). Cells (200 OD_{600} units) grown in the appropriate medium was used for a single affinity-isolation reaction. Cells were lysed with polysome buffer (10 mM Tris-HCl, pH 7, 0.1 M NaCl, 30 mM $MgCl_2$, supplemented with a cOmplete protease inhibitor tablet [Roche, 11836170001] and 40 units of RNase inhibitor [Promega, N2611]) and protein was quantified using the BCA assay. Equal amounts of protein were incubated with *ATG1* and *PGK1* RNA-conjugated beads at 4°C overnight on a rocking platform. The beads were then washed with wash buffer (provided in the kit) and sent to the Proteomics core in the Pathology Department, University of Michigan for on-beads digestion and protein identification. For analysis by immunoblotting, the beads were boiled in an equal volume of 2x MURB buffer (Liu et al., 2019) and loaded onto SDS-PAGE gels and quantified by western blot.

Polysome profiling

All buffers were prepared using DEPC-treated water and cells and polysome fractions were kept on ice throughout the procedure. WT and mutant cells were grown in 125 mL of an appropriate rich medium to an OD_{600} of 0.8-1.0, and shifted to nitrogen starvation medium. To the cells, 100 µg/mL cycloheximide was added and the culture was continuously shaken for 15 min at 250 rpm at 30°C. The cells were collected and lysed in a buffer containing 80 µg/mL cycloheximide, 200 µg/mL heparin, 0.2% DEPC, 10 mM Tris-HCl, pH 7.5, 0.1 M NaCl, 30 mM $MgCl_2$, and RNAse inhibitor. The lysates were centrifuged at 16,000g for 10 min at 4°C and the supernatant collected. Sucrose gradients for ultracentrifugation were prepared a day in advance with 7% to 47% sucrose solutions, including 20 mM Tris-HCl, pH 7.5, 140 mM KCl, 5 mM $MgCl_2$, 50 µg/mL cycloheximide, 0.1 mg/mL heparin, and 0.5 mM DTT. Equal amount of RNA across different experimental conditions were loaded onto the gradients and centrifuged at 35,000 rpm for 3 h at 4°C in an SW41Ti rotor. Following centrifugation, 500 µl fractions were collected in microcentrifuge tubes using a Brandel density gradient fractionator. Equal volumes of 100% ethanol, 0.2 ng/µl of *FLuc* mRNA and 5 µl of Glycoblue (Thermo, Am9516) were added to each fraction and stored overnight at -80°C. The fractions were centrifuged at 16,000g for 15 min at 4°C. The resulting pellet was dissolved in 100 µl of water and RNA was extracted using a standard acid phenol and chloroform method(Chomczynski & Sacchi, 2006) , followed by isopropanol and ethanol precipitation. The pellet was washed with 70% EtOH and air dried, then dissolved in 30 µl DEPC-treated water. A portion of this RNA (8 µl) was treated with TURBO DNase according to the manufacturer's instructions. A 9.6-µl aliquot of this reaction was used to convert to cDNA and the resulting cDNA was used to perform qPCR using a previously published protocol (Hu et al., 2015). Each gene was normalized first to *FFLuc* mRNA to account for differences in capture and precipitation of each sample. Next, the abundance of each mRNA

in each fraction was normalized to the total amount of that mRNA on the gradient. These data were then used to determine the percentage abundance of RNA in each fraction.

RNA immunoprecipitation

The RNA immunoprecipitation protocol was adapted from earlier methods documented in several studies(Liu et al., 2019; Yin et al., 2019) . To explore the interaction between Npl3 and *ATG1* mRNA, strains with Npl3 tagged with PA in the genome and untagged control strains were grown to mid-log phase (~100 OD_{600} units of cells) and then subjected to nitrogen starvation for 3 h. Formaldehyde was at a final concentration of 0.8%, and the cultures were gently agitated for 10 min at room temperature to facilitate cross-linking. This reaction was quenched by adding glycine to a final concentration of 0.2 M and shaking for 5 more min. Afterward, the cultures were harvested, rinsed with PBS, and lysed in FA buffer (50 mM HEPES, pH 7.5, 150 mM NaCl, 1 mM EDTA, 1% Triton X-100, 0.1% sodium deoxycholate, 0.1% SDS) supplemented with 5 mM PMSF, a complete protease inhibitor cocktail tablet, PhoSTOP (Roche, Phoss-RO) and RNasin® PLUS RNase inhibitor (Promega, N2611). Cells were lysed by the addition of glass beads and mixing with a vortex at 4°C. The lysates were sonicated and subsequently divided into input and immunoprecipitation (IP) fractions. The IP fractions were incubated overnight with IgG Sepharose 6 Fast Flow beads (Cytiva, 17096901)) at 4°C, while input samples were stored at −80°C. After multiple washes with FA buffer, IP fractions were eluted in RIP elution buffer (50 mM Tris-HCl [pH 7.5], 10 mM EDTA, 1% SDS)and treated with proteinase K in the presence of RNase inhibitor, at 42°C for 1 h followed by 65°C for 1 h to allow for the reversal of RNA-protein crosslinks. Samples were then subjected to acid phenol-chloroform extraction, and the aqueous phase was treated with sodium acetate,

Glycoblue and ethanol to precipitate RNA. After incubation at −80°C, the RNA was pelleted, washed, dried, and resuspended in nuclease-free water. DNase treatment was used to remove any contaminating DNA, followed by qRT-PCR analysis as detailed in prior publications. For the analysis of Pub1-GFP interaction with *ATG1*, the same protocol was followed, except the lysates (after sonication and centrifugation) were incubated with GFP-trap nanobeads from Chromtek for 3 h before being washed with FA lysis buffer and proteinase K treatment as described above.

RNA extraction from nuclear and cytoplasmic fractions

Cells were grown in rich medium until they reach OD_{600} = 0.8 and shifted to nitrogen starvation medium for 4 h. Cells (50 OD_{600} units) were collected, and the nuclear and cytoplasmic fractions were isolated using the Abcam Yeast Nuclei Isolation Kit (ab206997). To the nuclear and cytoplasmic fractions, 2 pg of *FFLuc* mRNA was added as internal control and total RNA was extracted using the standard acid phenol-chloroform method as described above.

Total RNA extraction, cDNA synthesis and qPCR

Total RNA was extracted using the Nucleo Spin RNA kit from Macherey Nagel, which includes DNAse treatment. One µg of total RNA was used to convert to cDNA using the High-capacity cDNA Reverse Transcription kit (Applied Biosystems). The transcript abundance in each sample was determined using methods and primers previously described. For comparison between wild type and mutants, the geometric mean of *Taf10*, *Tfc1* and *Cdc34/Ubc3* or *Sld3* was used as reference.

2.4.3 Protein methods

Protein extraction and immunoblotting

For analysis of Atg1 levels and other proteins, 1.2 OD_{600} units of yeast cells in the appropriate condition were precipitated with 10% trichloroacetic acid, followed by washing the cell pellet with acetone and air drying. The dried pellets were then lysed by adding glass beads in MURB buffer (50 mM sodium phosphate, pH 7.0, 25 mM MES, 1% SDS [w:v], 3 M urea, 1 mM NaN3, 1% β-mercaptoethanol, 0.01% bromophenol blue) and mixing on a vortex for 5 min. After lysis, samples were heated at 55°C for 15 min and then centrifuged at 10,000xg for 3 min to collect the supernatant for use in immunoblotting. Immunoblotting involved standard SDS-PAGE under denaturing conditions, followed by transfer using a Trans-Blot® SD Semi-Dry Transfer Cell (Bio-Rad). The membrane was blocked with TBST containing 5% skim milk for 1 h and incubated with appropriate antibodies. Signal detection was performed using Clarity and Clarity Max ECL Western Blotting Substrates (Bio-Rad) and imaged with a ChemiDoc Touch Imaging System (Bio-Rad), then quantified using Bio-Rad image lab.

2.4.4 Mammalian methods

Mammalian cell culture and RNA immunoprecipitation

Calu-1 cells were cultured in Dulbecco's modified eagle's medium with 10% heat inactivated FBS, and antibiotics. TIA1 knockdown was performed by si-RNA (Sigma, SASI-Hs01-0007018) using Lipofectamine RNAiMAX (Invitrogen, 13778030). For serum starvation, cells were transferred to Hanks' balanced salt solution for the specified time and collected for western blot. For RNA immunoprecipitation, I used a Magna RIP kit from Millipore Sigma.

2.4.5 Statistical methods

Statistical analysis was done using GraphPad Prism from 2-3 independent biological replicates using either Student's t test, one-way ANOVA or two-way ANOVA, corrected for multiple comparisons using Turkey's test. For all figures, P value <0.05 were considered significant.

2.5 Tables

Table 1. Significantly enriched RBPs on the *ATG1* 5'UTR.

Gene	Role	Null mutant
Crz1	Transcription factor	Viable
Yol107w	Unknown function	Viable
Mlf3	Unknown function	Viable
Jsn1	RNA-binding protein	Viable
Sro9	RNA-binding protein	Viable
Yml6	Mitochondrial ribosomal protein	
Nab2	RNA-binding protein	Inviable
Npl3	RNA-binding protein	Viable
Ymr045C	Retrotransposon TYA Gag	
Rrp40	RNA-binding protein	Inviable
Yet3	Unknown function	Viable
Rna14	RNA-binding protein	Inviable
Sbp1	RNA-binding protein	Viable

Table 2. Strains used in this study.

Name	Genotype	Ref
JMY347	SEY6210, *ZEO1p-pho13Δ pho8Δ60, CUP1p-GFP-ATG8(405)::LEU2*	(Wen et al., 2020)
SEY6210	MATα *leu2-3,112 ura3-52 his3-Δ200 trp1-Δ901 suc2-Δ9 lys2-801 GAL*	(Robinson et al., 1988)
SPY006	*WLY176 pub1Δ*	This study
SPY034	SEY6210 *PUB1-PA*	This study
SPY067	SEY6210 *NPL3-mNeonGreen*	This study
SPY077	WLY176 *npl3Δ*	This study
SPY100	SEY6210 *sky1Δ*	This study
VLY017	SEY6210 *DED1-3xPA*	(Lahiri et al., 2022)
WLY176	SEY6210 *pho13Δ pho8::pho8Δ60*	(Mao et al., 2013)
XLY345	SEY6210 *DHH1-HA*	(Liu et al., 2019)
YZY311	JMY347 *npl3Δ*	This study
YZY312	JMY347 *NPL3-PA*	This study
YZY313	JMY347 *NPL3ΔRRM2-PA*	This study
YZY315	JMY347 *NPL3-E409K-PA*	This study

2.6 References

1. Howell, J.J. and B.D. Manning, *mTOR couples cellular nutrient sensing to organismal metabolic homeostasis.* Trends Endocrinol Metab, 2011. **22**(3): p. 94-102.
2. Ryter, S.W., S.M. Cloonan, and A.M. Choi, *Autophagy: a critical regulator of cellular metabolism and homeostasis.* Mol Cells, 2013. **36**(1): p. 7-16.
3. Metur, S.P. and D.J. Klionsky, *Nutrient-dependent signaling pathways that control autophagy in yeast.* FEBS Lett, 2024. **598**(1): p. 32-47.
4. Parzych, K.R. and D.J. Klionsky, *An overview of autophagy: morphology, mechanism, and regulation.* Antioxid Redox Signal, 2014. **20**(3): p. 460-73.
5. Abeliovich, H. and D.J. Klionsky, *Autophagy in yeast: mechanistic insights and physiological function.* Microbiol Mol Biol Rev, 2001. **65**(3): p. 463-79, table of contents.
6. Metur, S.P., et al., *Regulation of autophagy gene expression and its implications in cancer.* J Cell Sci, 2023. **136**(10).
7. Ma, Q., et al., *Transcriptional and Post-Transcriptional Regulation of Autophagy.* Cells, 2022. **11**(3).
8. Noda, N.N. and Y. Fujioka, *Atg1 family kinases in autophagy initiation.* Cell Mol Life Sci, 2015. **72**(16): p. 3083-96.
9. Lahiri, V., et al., *Post-transcriptional regulation of ATG1 is a critical node that modulates autophagy during distinct nutrient stresses.* Autophagy, 2022. **18**(7): p. 1694-1714.
10. Lukong, K.E., et al., *RNA-binding proteins in human genetic disease.* Trends Genet, 2008. **24**(8): p. 416-25.
11. Liu, X., et al., *Dhh1 promotes autophagy-related protein translation during nitrogen starvation.* PLoS Biol, 2019. **17**(4): p. e3000219.
12. Yin, Z., et al., *Psp2, a novel regulator of autophagy that promotes autophagy-related protein translation.* Cell Res, 2019. **29**(12): p. 994-1008.
13. Nair, U., et al., *GFP-Atg8 protease protection as a tool to monitor autophagosome biogenesis.* Autophagy, 2011. **7**(12): p. 1546-50.
14. Suzuki, S.W., J. Onodera, and Y. Ohsumi, *Starvation induced cell death in autophagy-defective yeast mutants is caused by mitochondria dysfunction.* PLoS One, 2011. **6**(2): p. e17412.

15. Heyer, E.E. and M.J. Moore, *Redefining the Translational Status of 80S Monosomes.* Cell, 2016. **164**(4): p. 757-69.

16. Schieweck, R., et al., *Monosomes buffer translational stress to allow for active ribosome elongation.* Front Mol Biosci, 2023. **10**: p. 1158043.

17. Santos-Pereira, J.M., et al., *Npl3, a new link between RNA-binding proteins and the maintenance of genome integrity.* Cell Cycle, 2014. **13**(10): p. 1524-9.

18. Moursy, A., et al., *RNA recognition by Npl3p reveals U2 snRNA-binding compatible with a chaperone role during splicing.* Nat Commun, 2023. **14**(1): p. 7166.

19. Gatica, D., et al., *The Pat1-Lsm Complex Stabilizes ATG mRNA during Nitrogen Starvation-Induced Autophagy.* Mol Cell, 2019. **73**(2): p. 314-324 e4.

20. Szostak, E. and F. Gebauer, *Translational control by 3'-UTR-binding proteins.* Brief Funct Genomics, 2013. **12**(1): p. 58-65.

21. Delorme-Axford, E., et al., *The exoribonuclease Xrn1 is a post-transcriptional negative regulator of autophagy.* Autophagy, 2018. **14**(5): p. 898-912.

22. Hurt, E., et al., *Cotranscriptional recruitment of the serine-arginine-rich (SR)-like proteins Gbp2 and Hrb1 to nascent mRNA via the TREX complex.* Proc Natl Acad Sci U S A, 2004. **101**(7): p. 1858-62.

23. Noda, T. and D.J. Klionsky, *The quantitative Pho8Delta60 assay of nonspecific autophagy.* Methods Enzymol, 2008. **451**: p. 33-42.

24. Gotor, N.L., et al., *RNA-binding and prion domains: the Yin and Yang of phase separation.* Nucleic Acids Res, 2020. **48**(17): p. 9491-9504.

25. Lei, E.P., H. Krebber, and P.A. Silver, *Messenger RNAs are recruited for nuclear export during transcription.* Genes Dev, 2001. **15**(14): p. 1771-82.

26. Keil, P., et al., *Npl3 functions in mRNP assembly by recruitment of mRNP components to the transcription site and their transfer onto the mRNA.* Nucleic Acids Res, 2023. **51**(2): p. 831-851.

27. Apponi, L.H., et al., *An interaction between two RNA-binding proteins, Nab2 and Pub1, links mRNA processing/export and mRNA stability.* Mol Cell Biol, 2007. **27**(18): p. 6569-79.

28. MacKellar, A.L. and A.L. Greenleaf, *Cotranscriptional association of mRNA export factor Yra1 with C-terminal domain of RNA polymerase II.* J Biol Chem, 2011. **286**(42): p. 36385-95.

29. Chun, Y. and J. Kim, *Autophagy: An Essential Degradation Program for Cellular Homeostasis and Life.* Cells, 2018. **7**(12).

30. Conrad, M., et al., *Nutrient sensing and signaling in the yeast Saccharomyces cerevisiae.* FEMS Microbiol Rev, 2014. **38**(2): p. 254-99.

31. Holcik, M. and N. Sonenberg, *Translational control in stress and apoptosis.* Nat Rev Mol Cell Biol, 2005. **6**(4): p. 318-27.

32. Frankel, L.B., M. Lubas, and A.H. Lund, *Emerging connections between RNA and autophagy.* Autophagy, 2017. **13**(1): p. 3-23.

33. Hu, G., et al., *A conserved mechanism of TOR-dependent RCK-mediated mRNA degradation regulates autophagy.* Nat Cell Biol, 2015. **17**(7): p. 930-942.

34. Klama, S., et al., *A guard protein mediated quality control mechanism monitors 5'-capping of pre-mRNAs.* Nucleic Acids Res, 2022. **50**(19): p. 11301-11314.

35. Gilbert, W., C.W. Siebel, and C. Guthrie, *Phosphorylation by Sky1p promotes Npl3p shuttling and mRNA dissociation.* RNA, 2001. **7**(2): p. 302-13.

36. Ruiz-Echevarria, M.J. and S.W. Peltz, *The RNA-binding protein Pub1 modulates the stability of transcripts containing upstream open reading frames.* Cell, 2000. **101**(7): p. 741-51.

37. Infantino, V., et al., *The mRNA export adaptor Yra1 contributes to DNA double-strand break repair through its C-box domain.* PLoS One, 2019. **14**(4): p. e0206336.

38. Faza, M.B., et al., *Sem1 is a functional component of the nuclear pore complex-associated messenger RNA export machinery.* J Cell Biol, 2009. **184**(6): p. 833-46.

39. Ma, W.K., S.C. Cloutier, and E.J. Tran, *The DEAD-box protein Dbp2 functions with the RNA-binding protein Yra1 to promote mRNP assembly.* J Mol Biol, 2013. **425**(20): p. 3824-38.

40. Mackenzie, I.R., et al., *TIA1 Mutations in Amyotrophic Lateral Sclerosis and Frontotemporal Dementia Promote Phase Separation and Alter Stress Granule Dynamics.* Neuron, 2017. **95**(4): p. 808-816 e9.

41. Park, H., J.H. Kang, and S. Lee, *Autophagy in Neurodegenerative Diseases: A Hunter for Aggregates.* Int J Mol Sci, 2020. **21**(9).

42. Li, X., et al., *Functional role of Tia1/Pub1 and Sup35 prion domains: directing protein synthesis machinery to the tubulin cytoskeleton.* Mol Cell, 2014. **55**(2): p. 305-18.

43. Buchan, J.R., et al., *Eukaryotic stress granules are cleared by autophagy and Cdc48/VCP function.* Cell, 2013. **153**(7): p. 1461-74.

44. Kroschwald, S., et al., *Different Material States of Pub1 Condensates Define Distinct Modes of Stress Adaptation and Recovery.* Cell Rep, 2018. **23**(11): p. 3327-3339.

45. Rayman, J.B., K.A. Karl, and E.R. Kandel, *TIA-1 Self-Multimerization, Phase Separation, and Recruitment into Stress Granules Are Dynamically Regulated by Zn(2).* Cell Rep, 2018. **22**(1): p. 59-71.

46. Reynaud, K., et al., *Surveying the global landscape of post-transcriptional regulators.* Nat Struct Mol Biol, 2023. **30**(6): p. 740-752.

47. Chomczynski, P. and N. Sacchi, *The single-step method of RNA isolation by acid guanidinium thiocyanate-phenol-chloroform extraction: twenty-something years on.* Nat Protoc, 2006. **1**(2): p. 581-5.

Chapter 3 : Translational Regulation of Macroautophagy During Distinct Nutrient Stress

Macroautophagy/autophagy is a highly conserved nutrient-recycling pathway that eukaryotes utilize to combat diverse stresses including nutrient depletion. Dysregulation of autophagy disrupts cellular homeostasis leading to starvation susceptibility in yeast and disease development in humans. In yeast, the robust autophagy response to starvation is controlled by the upregulation of *ATG* genes, via regulatory processes involving multiple levels of gene expression. Despite the identification of several regulators through genetic studies, the predominant mechanism of regulation modulating the autophagy response to subtle differences in nutrient status remains undefined. Here, I report the unexpected finding that subtle changes in nutrient availability can cause large differences in autophagy flux, governed by hitherto unknown post-transcriptional regulatory mechanisms affecting the expression of the key autophagy inducing kinase Atg1 (ULK1/ULK2 in mammals). I have identified two novel post-transcriptional regulators of *ATG1* expression, the kinase Rad53 and the RNA-binding protein Ded1 (DDX3 in mammals). Furthermore, I show that DDX3 regulates ULK1 expression post-transcriptionally, establishing mechanistic conservation and highlighting the power of yeast biology in uncovering regulatory mechanisms that can inform therapeutic approaches.

Lahiri, V., Metur, S. P., Hu, Z., Song, X., Mari, M., Hawkins, W. D., ... & Klionsky, D. J. (2022). Post-transcriptional regulation of *ATG1* is a critical node that modulates autophagy during distinct nutrient stresses. *Autophagy*, *18*(7), 1694-1714.

3.1 Introduction

Macroautophagy (hereafter, autophagy) is a nutrient-recycling pathway conserved among eukaryotes (Gatica et al., 2018). The hallmark of autophagy is the de novo synthesis of a transient membranous structure which expands to form the double-membrane autophagosome (Chang et al., 2021; Melia et al., 2020). Autophagy occurs basally to maintain homeostasis but is induced in response to various cues, including nutrient-depletion; this type of stress promotes the nonselective sequestration of cytoplasm leading to its subsequent engulfment within the lumen of autophagosomes (Corona Velazquez and Jackson, 2018; Nakatogawa, 2020). Autophagosomes subsequently fuse with the lysosomes or vacuole, to promote cargo degradation leading to the generation of simple metabolites that, upon efflux back into the cytosol, act as an alternative source of nutrients (Liu et al., 2021; May et al., 2020; White et al., 2015). The ability to provide nutrients makes autophagy a critical survival pathway in cancer cells (Amaravadi et al., 2016; White, 2015). Mutant KRAS-driven pancreatic cancers require autophagy-derived nutrients for survival (Guo et al., 2011; Lock et al., 2011; Mulcahy Levy and Thorburn, 2020). In pancreatic ductal adenocarcinoma, pancreatic stellate cells, present in the tumor microenvironment, upregulate autophagy to generate alanine, which is supplied to the tumor cells to meet their metabolic requirements (Fu et al., 2018; Sousa et al., 2016). The identification of autophagy inhibitors has, therefore, gained importance as a therapeutic tool (Amaravadi et al., 2019; Mulcahy Levy and Thorburn, 2020).

Autophagy inhibition for therapeutic purposes needs to be nuanced because a complete block of autophagy compromises survival (Karsli-Uzunbas et al., 2014; Mizushima and Levine, 2020). This necessitates the need to understand the subtle aspects of autophagy regulation. Even in a simple eukaryote – the budding yeast Saccharomyces cerevisiae – the autophagy pathway is

complex and requires the concerted activity of several Atg (autophagy related) proteins. (Feng et al., 2014; Yin et al., 2016). Because autophagy is initiated in response to stresses such as nutrient depletion, the induction of *ATG* gene expression contrasts with that of most other genes. In yeast and mammalian cells, starvation leads to the activation of several pathways that suppress general transcription and translation but promotes that of *ATG* genes (Gross and Graef, 2020; Kim et al., 2011; Russell et al., 2014). Furthermore, because it is primarily a degradative process, the cell needs to fine-tune autophagy to meet cellular requirements while preventing unnecessary breakdown of the cytoplasm. The expression of *ATG* genes is, therefore, subject to a complex regulatory network that acts at transcriptional, post-transcriptional and translational levels (Abildgaard et al., 2020; Delorme-Axford and Klionsky, 2018; Lahiri et al., 2019). Additionally, Atg protein function is extensively regulated by post-translational modifications allowing for the exquisite regulation of autophagy in response to starvation (McEwan and Dikic, 2011; Xie et al., 2015).

Previous investigations, focused on genetically modulating the transcription of individual *ATG* genes, demonstrated that *ATG8* (Xie et al., 2008) and *ATG9* (Jin et al., 2014) expression levels are directly correlated with the size and frequency of autophagosome formation respectively. However, whether these mechanisms are the predominant physiological response to different nutritional challenges remains untested. Here, I study how autophagy is modulated in response to subtle differences in nutrient availability. I do so by comparing autophagy flux during nitrogen and amino acid starvation – two related but distinct starvation conditions ¬– and show that modulation of autophagy under these conditions occurs primarily via post-transcriptional regulation of *ATG* gene expression, particularly that of *ATG1*. Atg1 (ULK1 in mammals) is a Ser/Thr kinase that is critical in the initiation of autophagy and the activation of Atg9 function

through phosphorylation. I explore regulation of *ATG1* expression under these conditions and identify the kinase Rad53, as a post-transcriptional regulator of starvation-induced autophagy. Furthermore, I have identified a second novel regulator of *ATG1* expression, the RNA-helicase Ded1. I show that Ded1 directly binds to the 5' UTR of *ATG1* preferentially during nitrogen starvation, where it likely functions to resolve secondary structures in the *ATG1* mRNA to facilitate efficient translation (Sen et al., 2019; Sen et al., 2015). In agreement with this, I show that the loss of Ded1 leads to a greater reduction in Atg1 expression and autophagy during nitrogen starvation relative to amino acid starvation. Crucially, this mode of regulation is conserved – DDX3 (the mammalian homolog of Ded1) positively regulates *ULK1* expression post-transcriptionally to promote autophagy in mammalian cells. Consistently, knockdown of DDX3 leads to a reduction in, but not a complete block of, autophagy, thereby making this protein with previously characterized pro-tumorigenic functions (Botlagunta et al., 2008; Chen et al., 2015; Wilky et al., 2016) an attractive candidate for therapeutic exploration.

3.2 Results

3.2.1 Differential autophagy flux during distinct nutrient stresses is not determined by ATG *transcription*

In yeast, autophagy is initiated in response to loss of nutrient availability (Cebollero and Reggiori, 2009). However, how different starvation stresses differentially modulate regulators to influence autophagy flux is unclear. To shed light on these mechanisms, I investigated the effect of differential nutrient availability on autophagy regulation by comparing complete nitrogen starvation with amino acid starvation (Conrad et al., 2014). Yeast cells subjected to nitrogen starvation were starved of organic nitrogen and limited for inorganic nitrogen, whereas amino-acid starved cells were deprived only of amino acids. I chose these two conditions for our study because

despite being similar stresses overall, they represent the subtle differences that are frequently associated with divergence from homeostasis that promotes physiological responses. Additionally, while these two conditions have been studied in yeast (Ecker et al., 2010), this is, to the best of our knowledge, the first large-scale comparison of the autophagy response between these conditions, thus providing the potential for novel discoveries. The transcription factor Gcn4 is a master regulator of gene expression in response to general amino acid deprivation (Natarajan et al., 2001). Cytoplasmic dearth of amino acids activates the eIF2 kinase Gcn2 which promotes the efficient translation of Gcn4 (Dever et al., 1992). Because both nitrogen and amino acid starvation lead to an amino acid deficit, the expression of Gcn4 was increased to very similar levels in cells subjected to either nitrogen starvation ("-N") or amino acid starvation ("-A") treatment compared to those grown in the nutrient-rich YPD medium ("+") (Figure 12A and 12B), highlighting the similar nature of both conditions. To compare autophagy flux between these starvation treatments, I utilized the GFP-Atg8 processing assay as an end-point measurement. I found that nitrogen starvation led to the robust activation of autophagy flux with the autophagy response being significantly lower with amino acid starvation (Figure 12C and 12D). This finding was corroborated by the prApe1 maturation assay for autophagy flux (Huang et al., 2014), which measures the autophagy-dependent maturation of precursor aminopeptidase I (prApe1; Figures 13A and 13B). To assess the long-term effect of both starvation treatments, I carried out a longer time-course analysis using the Pho8Δ60 activity assay as an end-point measurement (Klionsky, 2007). Extended nitrogen starvation elicited a significantly stronger autophagy response compared to extended amino acid starvation (Figure 12E) while both starvation treatments showed increased autophagy relative to nutrient-rich conditions.

I then sought to directly examine the characteristics—frequency and size—of autophagosome formation under these starvation conditions (Backues et al., 2014). Autophagosomes were monitored by the accumulation of autophagic bodies (ABs; the single-membrane vesicle generated by fusion of an autophagosome with a vacuole) within the vacuole lumen of yeast cells lacking the major vacuolar protease Pep4 (to prevent autophagic body degradation) and Vps4 (to block the accumulation of multivesicular bodies). Consistent with biochemical assays, transmission electron microscopy (TEM) analyses revealed that ABs were more numerous in cells subjected to nitrogen starvation compared to amino acid starvation (Figure 12F and 12G). In addition, ABs in nitrogen-starved cells were significantly larger than in amino-acid starved cells (Figures 12F and 12C). Because the SEY6210 strain, used as the parent for constructing strains for autophagy flux analysis, is an auxotroph, I confirmed the autophagy responses to nitrogen and amino acid starvation using the prototrophic strain CEN.PK (Kummel et al., 2010). Consistent with the autophagy phenotype in SEY6210, I found that nitrogen starvation led to increased Atg8-lipidation. Furthermore, this difference was aggravated upon treatment with the protease inhibitor PMSF, confirming that reduced flux was not responsible for the increased abundance of lipidated Atg8 (Figure 13D).

Autophagy in yeast is robustly regulated by transcriptional control (Backues et al., 2012; Bernard et al., 2015b; Delorme-Axford and Klionsky, 2018; Jin et al., 2014; Jin and Klionsky, 2014), so I hypothesized a differential ATG transcriptome under these starvation conditions. I tested our hypothesis by carrying out RNA-sequencing analysis for both sets of treatments. For high-confidence identification of DEGs (differentially expressed genes), I used the following significance parameters: 2-fold enrichment with an associated $p < 0.05$ cut-off. Contrary to our expectations, the core *ATG* genes were not identified among the DEGs (Figure 12H), with the

majority of DEGs involved in translation and metabolism (Figure 13E). *ATG31* was the only core autophagy gene along with *ATG32* and *ATG39*, involved in mitophagy (Kanki et al., 2009) and reticulophagy (Mochida et al., 2015), respectively, differentially expressed with higher expression in nitrogen starvation (Figures 13F and 13G, and data not shown). I confirmed that the transcriptional response did not vary with time by measuring the transcriptional upregulation of two genes crucial to the induction of autophagy: *ATG1* (Mizushima, 2010) and *ATG9* (Matoba et al., 2020). At both 1 h and 6 h post-starvation, nitrogen and amino acid starvation elicited similar levels of transcriptional response for both *ATG1* (Figures 12I and 12J) and *ATG9* (Figures 13H and 13I) consistent with our findings from the RNA-sequencing experiments. Taken together, these data suggest that differential autophagy flux during nitrogen and amino acid starvation is not due to differential transcriptional activation of *ATG* genes.

Figure 12

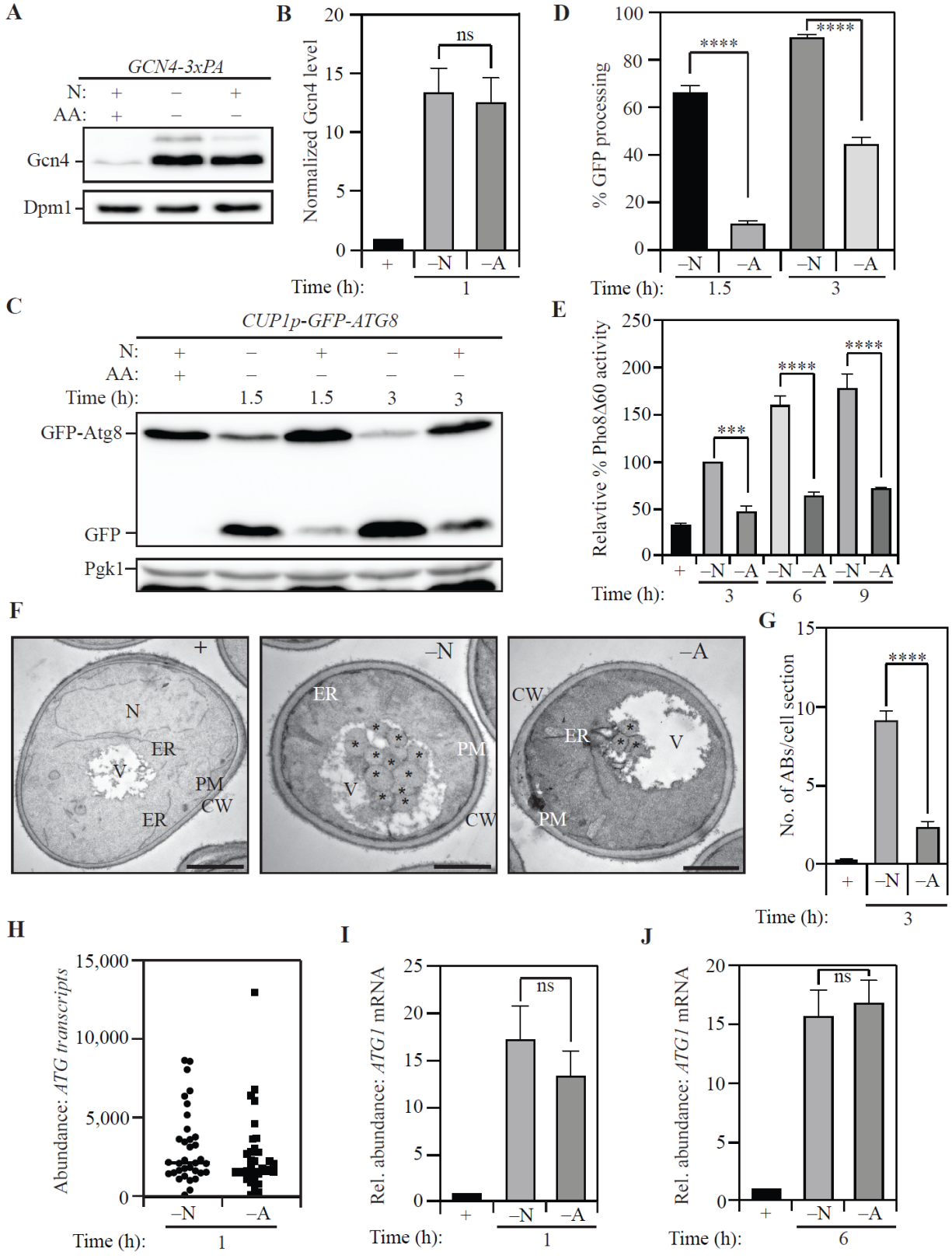
A
GCN4-3xPA
N: + – +
AA: + – –
Gcn4
Dpm1
B
Normalized Gcn4 level
ns
Time (h): 1
C
CUP1p-GFP-ATG8
N: + – + – +
AA: + – – – –
Time (h): 1.5 1.5 3 3
GFP-Atg8
GFP
Pgk1
D
% GFP processing
****
****
Time (h): 1.5 3
E
Relavtive % Pho8Δ60 activity
***
****
****
Time (h): 3 6 9
F
+
N
ER
V
PM
CW
ER
–N
ER
PM
V
CW
–A
CW
ER
V
PM
G
No. of ABs/cell section
****
Time (h): 3
H
Abundance: ATG transcripts
Time (h): 1
I
Rel. abundance: ATG1 mRNA
ns
Time (h): 1
J
Rel. abundance: ATG1 mRNA
ns
Time (h): 6

Figure 12: Differential autophagy flux during distinct nutrient stresses is not determined by ATG transcription.

a. Gcn4 expression is upregulated during both nitrogen and amino acid starvation: WT (SEY6210) cells with C-terminally 3x-PA tagged Gcn4 were harvested in nutrient-replete conditions or after starvation for the indicated time and examined by western blot. Gcn4 was detected using the anti-PA antibody and Dpm1 was used as a loading control.
b. Densitometric analysis for (a) from three independent biological replicates.
c. The GFP-Atg8 processing assay demonstrates increased autophagy flux during nitrogen starvation relative to amino acid starvation: WT (WLY176) cells with integrated *CUP1p-GFP-ATG8* were harvested in nutrient-replete conditions or after starvation for the indicated times and assessed by western blot. The appearance of free GFP indicates autophagy flux. Pgk1 was used as a loading control.
d. Densitometric analysis of (c) from three independent biological replicates.
e. Autophagy flux is higher during nitrogen starvation compared to amino acid starvation as assessed by the Pho8Δ60 assay: WT (WLY176) cells were harvested in nutrient-replete conditions or after starvation for the indicated times and Pho8Δ60 enzyme activity was measured by colorimetry. An increase in Pho8Δ60 activity indicates increased autophagic flux. Data from three independent biological replicates.
f. Autophagosome formation is more frequent during nitrogen starvation compared to amino acid starvation: WT (SEY6210) *pep4*Δ *vps4*Δ cells were harvested in nutrient-replete conditions or after starvation for 3 h. The cells were fixed, stained and ultrastructural analysis was used to visualize the number of ABs.

g. Quantification of the number of ABs from 100 randomly selected cell profiles from two independent biological replicates.

h. RNA-Sequencing reveals similar abundance of *ATG* transcripts during nitrogen and amino acid starvation: DESeq2 analysis of *ATG* transcriptome during nitrogen and amino acid starvation. The plot represents the mean of three independent biological replicates from WT (SEY6210) cells.

i. There is a similar abundance of *ATG1* transcript in cells subjected to nitrogen or amino acid starvation: qRT-PCR detection of *ATG1* mRNA in WT (SEY6210) cells after 1 h of starvation.

j. qRT-PCR detection of *ATG1* mRNA in WT (SEY6210) cells after 6 h of starvation. *ALG9* was used as a reference gene for normalization. Data from three independent biological replicates.

Data in (b), (d), (e), (g), (h), (i) and (j) represent mean ± SEM from the indicated number of replicates. Statistical analysis for (b), (g), (i) and (j) was carried out using unpaired Student's t-test while (d) and (e) were analyzed using one-way analysis of variance (ANOVA). Multiple comparisons were carried out using Tukey's multiple comparisons test. *$p < 0.05$, **$p < 0.005$, ***$p < 0.001$, ****$p < 0.0001$ ns: not significant.

Figure 13

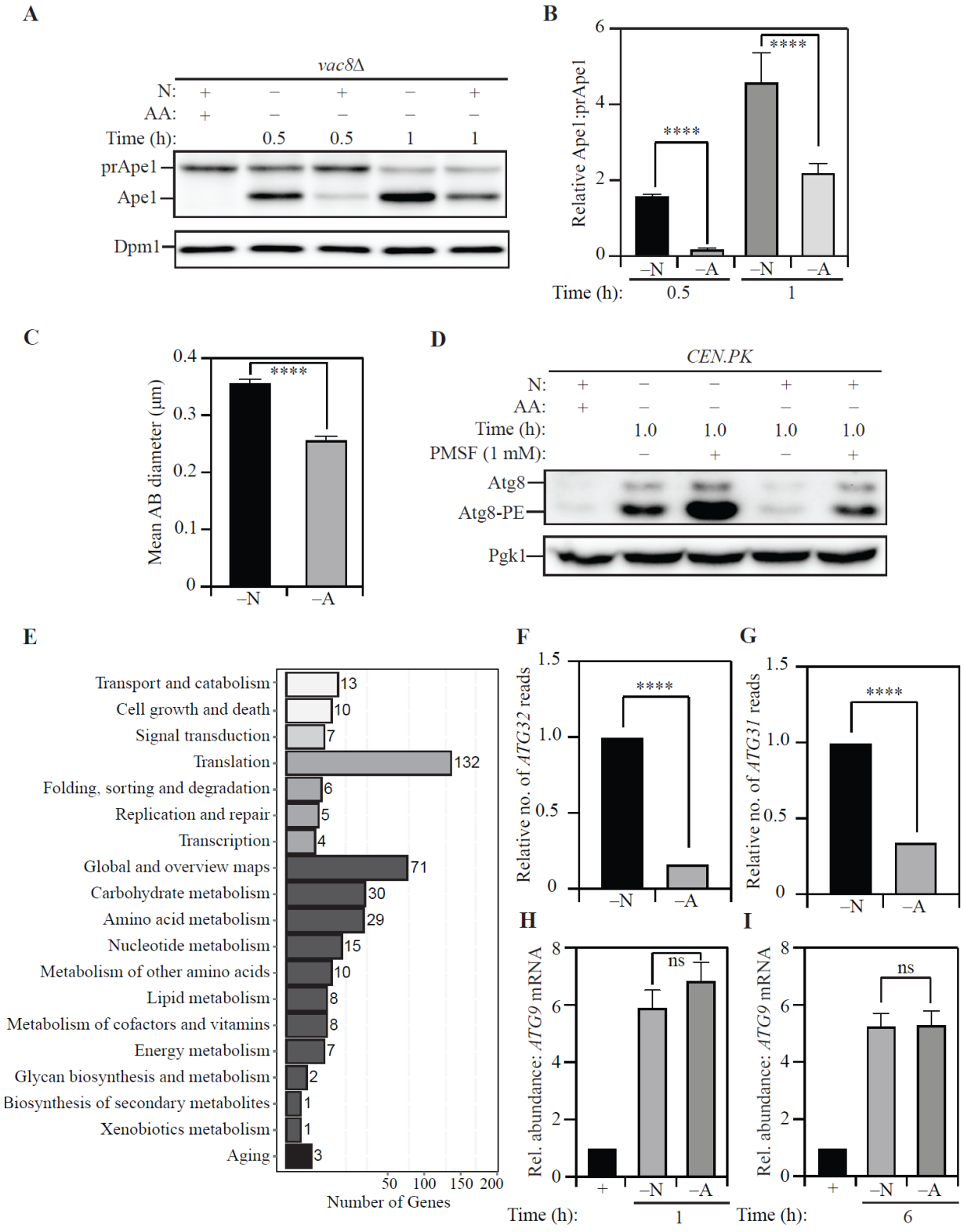
A
vac8Δ
N:
AA:
Time (h):
prApe1
Ape1
Dpm1
B
Relative Ape1:prApe1
****
Time (h):
–N
–A
C
Mean AB diameter (μm)
D
CEN.PK
PMSF (1 mM):
Atg8
Atg8-PE
Pgk1
E
Transport and catabolism
Cell growth and death
Signal transduction
Translation
Folding, sorting and degradation
Replication and repair
Transcription
Global and overview maps
Carbohydrate metabolism
Amino acid metabolism
Nucleotide metabolism
Metabolism of other amino acids
Lipid metabolism
Metabolism of cofactors and vitamins
Energy metabolism
Glycan biosynthesis and metabolism
Biosynthesis of secondary metabolites
Xenobiotics metabolism
Aging
Number of Genes
F
Relative no. of ATG32 reads
G
Relative no. of ATG31 reads
H
Rel. abundance: ATG9 mRNA
ns
I
Rel. abundance: ATG9 mRNA
ns

Figure 13: Differential autophagy flux during distinct nutrient stresses is not determined by ATG transcription.

a. Higher autophagy flux during nitrogen starvation compared to amino acid starvation, demonstrated by the precursor Ape1 (prApe1) maturation assay: SEY6210 *vac8*Δ cells were harvested in nutrient-replete conditions or after starvation for the indicated times. Conversion of prApe1 to Ape1 indicates autophagy flux. Dpm1 was used as a loading control
b. Densitometric analysis of (a) from three independent biological replicates.
c. The size of autophagosomes is larger during nitrogen starvation relative to amino acid starvation: Quantification of the diameter of autophagic bodies from SEY6210 *pep4*Δ *vps4*Δ cells starved for nitrogen or amino acids. Data from 100 cell profiles per condition across two independent biological replicates.
d. Elevated Atg8-lipidation in nitrogen starvation relative to amino acid starvation in the absence and presence of the serine protease inhibitor PMSF: CEN.PK cells were harvested in nutrient-replete conditions or after starvation for the indicated times. Pgk1 was used as a loading control.
e. Identified DEGs were grouped according to cellular function.
f. Abundance of *ATG32* transcripts is significantly lower in amino acid starvation relative to nitrogen starvation as determined by RNA-Sequencing. Data represent the mean of three independent biological replicates.
g. Abundance of *ATG31* transcripts is significantly lower in amino acid starvation relative to nitrogen starvation as determined by RNA-Sequencing. Data represent the mean of three independent biological replicates.

h. Transcriptional upregulation of *ATG9* is similar during nitrogen and amino acid starvation: qRT-PCR-based detection of *ATG9* mRNA in WT (SEY6210) cells after 1 h of starvation.

i. Transcriptional upregulation of *ATG9* is similar during nitrogen and amino acid starvation: qRT-PCR-based detection of *ATG9* mRNA in WT (SEY6210) cells after 6 h of starvation. *ALG9* was used as a reference gene for normalization. Data are from three independent biological replicates.

Data in (b), (c), (h) and (i) represent mean ± SEM from indicated number of replicates. Statistical analysis for (b) was carried out using one-way analysis of variance (ANOVA) while (c), (h) and (i) were analyzed using an unpaired Student's t-test. Data in (f) and (g) represent mean from indicated number of replicates. Statistical analysis for (f) and (g) was carried out using one-way analysis of variance (ANOVA). Multiple comparisons were carried out using Tukey's multiple comparisons test. *$p < 0.05$, **$p < 0.005$, ***$p < 0.001$, ****$p < 0.0001$ ns: not significant.

3.2.2 Post-transcriptional activation of **ATG** *gene expression is a critical node determining autophagy during nitrogen starvation*

The induction of autophagy upon starvation depends on the synthesis of key Atg proteins. For example, Atg1, which is critical for the initiation of autophagy, is robustly synthesized in response to starvation (Yin et al., 2019). Because *ATG* transcription was not differentially affected I investigated differential expression of Atg proteins that could contribute to the differential autophagy flux. To this end, I compared the proteome of cells subjected to nitrogen starvation and amino acid starvation using stable isotope labelling with amino acids in culture (SILAC) (Figure 9A) (Deng et al., 2019). SILAC analysis revealed that several Atg proteins were differentially expressed, with increased expression in nitrogen starvation (Figure 14A). The proteins with the largest and most consistent differential expression were Atg1 and Atg9 (Figure 14A). The expression of Atg9, a protein responsible for lipid delivery and transfer for phagophore formation (Matoba et al., 2020), was ~45% lower in amino acid starvation compared to in nitrogen starvation. I confirmed this observation with immunoblotting for endogenous Atg9 protein and, consistent with our SILAC analysis, found a ~50% reduction in amino acid starvation relative to nitrogen starvation (Figure 15B and 15C). This outcome is consistent with previous findings that suggest Atg9 levels are directly correlated with the frequency of autophagosome formation (Jin et al., 2014).

In our SILAC analysis, amino-acid starved cells showed an ~50% reduction in Atg1 expression compared to nitrogen-starved cells. In contrast, other components of the Atg1 complex such as Atg13 and Atg17 did not exhibit significant differential expression, prompting us to focus on Atg1. I confirmed differential Atg1 expression by examining endogenous Atg1 levels by immunoblotting. In agreement with our SILAC data, Atg1 levels were found to be 50% lower

during amino acid starvation compared to nitrogen starvation at 2 h (Figures 14B and 15D) and ~65% lower at 6 h post-starvation (Figures 14C and 14D). A similar response was observed in the prototrophic CEN.PK strain where nitrogen starvation led to elevated Atg1 expression relative to amino acid starvation (Figure 15E). Taken together, these data suggest that post-transcriptional control is a critical node in the regulation of *ATG* gene expression that contributes to differential responses in autophagy flux. To rule out the possibility that *ATG* mRNA transcription is generally increased in response to any type of nutrient depletion, I compared the transcriptional induction of *ATG1* and *ATG9* during glucose starvation, which fails to significantly stimulate autophagy (Lang et al., 2014). Expectedly, I found no transcriptional response for either *ATG1* (Figure 14E) or *ATG9* (Figure 15F), consistent with autophagy flux not being significantly induced, as assessed by the Pho8Δ60 assay (Figure 14F).

To investigate the mechanism of differential regulation further, I focused on *ATG1*, because Atg1 is responsible for autophagy initiation and regulating Atg9 activity through phosphorylation. I compared the stability of *ATG1* mRNA in nitrogen starvation to that in amino acid starvation, to confirm that reduced protein expression during amino acid starvation is not due to mRNA instability. I induced *ATG1* transcription with a pulse of nitrogen starvation, following which I treated the cells with the transcriptional inhibitor 1,10-phenanthroline (Gatica et al., 2019). Cells were then either allowed to recover in rich medium (YPD) or starved in nitrogen starvation or amino acid starvation medium to monitor *ATG1* mRNA stability (Figure 15G). While recovery in YPD ("+" in Figure 14G) led to a significant reduction in the levels of *ATG1* mRNA, there was no decrease in either nitrogen starvation ("–N") or amino acid starvation ("–A") media highlighting that *ATG1* mRNA was similarly stable under both conditions. Furthermore, to rule out the possibility that the difference in Atg1 levels is due to post-translational instability of the

corresponding proteins during amino acid starvation, I used a cycloheximide chase assay. Because Atg1 levels are low during growing conditions and Atg1 is synthesized in response to starvation, I took advantage of constitutive Atg1 expression when measuring Atg1 stability. A strain expressing Atg1 from a *CUP1* promoter was treated with cycloheximide and Atg1 protein level was followed by immunoblotting after 2, 4 and 6 h of treatment (Figure 15H). I found no significant difference in the stability of Atg1 protein between nitrogen and amino acid starvation (Figures 14H and 14I). Taken together, these findings further suggest that a post-transcriptional mechanism promotes the translation of *ATG1* mRNA during nitrogen starvation.

Figure 14

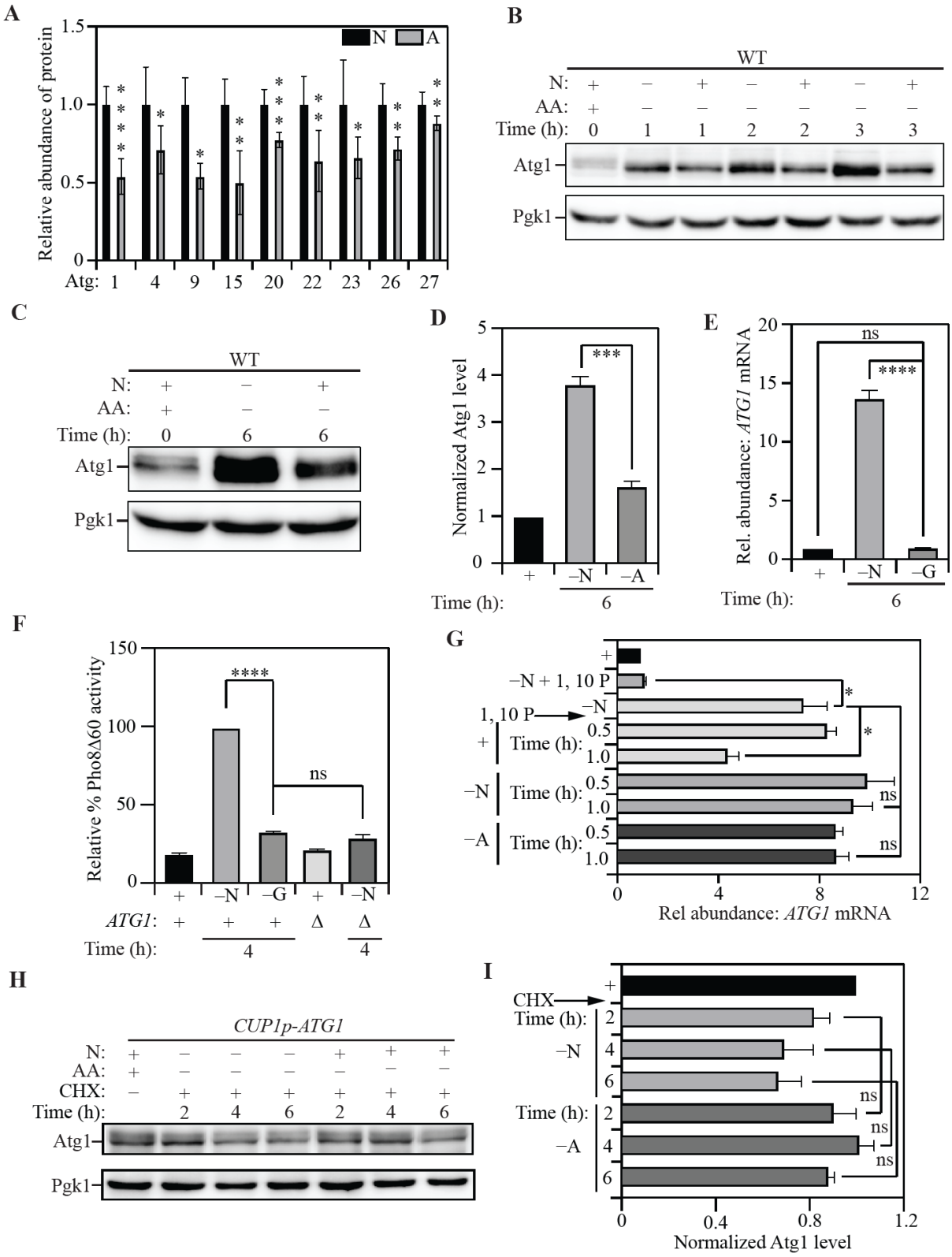
A
Relative abundance of protein
N
A
Atg: 1 4 9 15 20 22 23 26 27
B
WT
N:
AA:
Time (h): 0 1 1 2 2 3 3
Atg1
Pgk1
C
WT
N:
AA:
Time (h): 0 6 6
Atg1
Pgk1
D
Normalized Atg1 level
Time (h): 6
E
Rel. abundance: ATG1 mRNA
Time (h): 6
F
Relative % Pho8Δ60 activity
ATG1:
Time (h): 4 4
G
Rel abundance: ATG1 mRNA
H
CUP1p-ATG1
N:
AA:
CHX:
Time (h): 2 4 6 2 4 6
Atg1
Pgk1
I
Normalized Atg1 level

Figure 14: Post-transcriptional activation of *ATG* gene expression is a critical node determining autophagy during nitrogen starvation.

a. The Atg proteome is significantly different during nitrogen starvation compared to amino acid starvation: Triplex-SILAC labeling was used to compare the Atg protein abundance between nutrient-replete, nitrogen starvation and amino-acid starvation conditions in SEY6210 *arg4*Δ cells using LC-MS/MS. The plot shows the levels of differentially expressed Atg proteins during amino acid starvation (gray bars) relative to nitrogen starvation (black bars). Individual proteins were normalized to the total protein input. Data from at least three independent biological replicates. Significant differences are highlighted.
b. Atg1 levels increase substantially more during nitrogen versus amino acid starvation. WT (SEY6210) cells were harvested in nutrient-replete conditions or after starvation for the indicated times and protein levels analyzed by western blot. Pgk1 was used as a loading control.
c. Atg1 levels increase substantially more during nitrogen versus amino acid starvation. WT (SEY6210) cells were harvested in nutrient-replete conditions or after starvation for 6 hand protein levels analyzed by western blot. Pgk1 was used as a loading control.
d. Densitometric analysis of (c) from three independent biological replicates.
e. Transcriptional upregulation of *ATG1* occurs during nitrogen, but not glucose, starvation: qRT-PCR detection of *ATG1* mRNA in WT (SEY6210) cells after 1 h of starvation. *ALG9* was used as a reference gene for normalization. Data from three independent biological replicates.

f. Autophagy flux is upregulated during nitrogen, but not glucose, starvation: WT (WLY176) cells were harvested in nutrient-replete conditions or after starvation for the indicated times and Pho8Δ60 enzyme activity was measured by colorimetry. An increase in Pho8Δ60 activity indicates increased autophagic flux. Negative control: SEY6210 *atg1*Δ cells. Data from three independent biological replicates.

g. *ATG1* mRNA is stable under conditions of nitrogen and amino acid starvation: WT (SEY6210) cells were pulsed with nitrogen starvation to induce *ATG1* transcription and/or treated with the transcriptional inhibitor 1,10-phenanthroline (1,10 P) to stop transcription. Cells were then kept in nitrogen-starvation medium or transferred to nutrient-replete medium or amino acid starvation for the indicated times. At each time point *ATG1* mRNA abundance was measured by qRT-PCR. *ALG9* was used as the reference gene for normalization. Data are from three independent biological replicates.

h. Atg1 protein is not preferentially degraded during amino acid starvation relative to nitrogen starvation: WT (SEY6210) cells harboring a centromeric *CUP1p-ATG1* (constitutive Atg1 expression) plasmid were grown in nutrient-replete conditions and treated with cycloheximide (CHX). Following treatment, cells were transferred to nitrogen or amino acid starvation medium and harvested at the indicated time points. Atg1 abundance was measured by western blot. Pgk1 was used as a loading control.

i. Data from three independent biological replicates represented in (h).

Data in (a), (d), (e), (f), (g) and (i) represent mean ± SEM from indicated number of replicates. Statistical analysis for (a) and (d) was carried out using unpaired Student's t-test while (e), (f), (g) and (i) were analyzed using one-way analysis of variance (ANOVA).

Multiple comparisons were carried out using Tukey's multiple comparisons test. *$p < 0.05$, **$p < 0.005$, ***$p < 0.001$, ****$p < 0.0001$ ns: not significant.

Figure 15

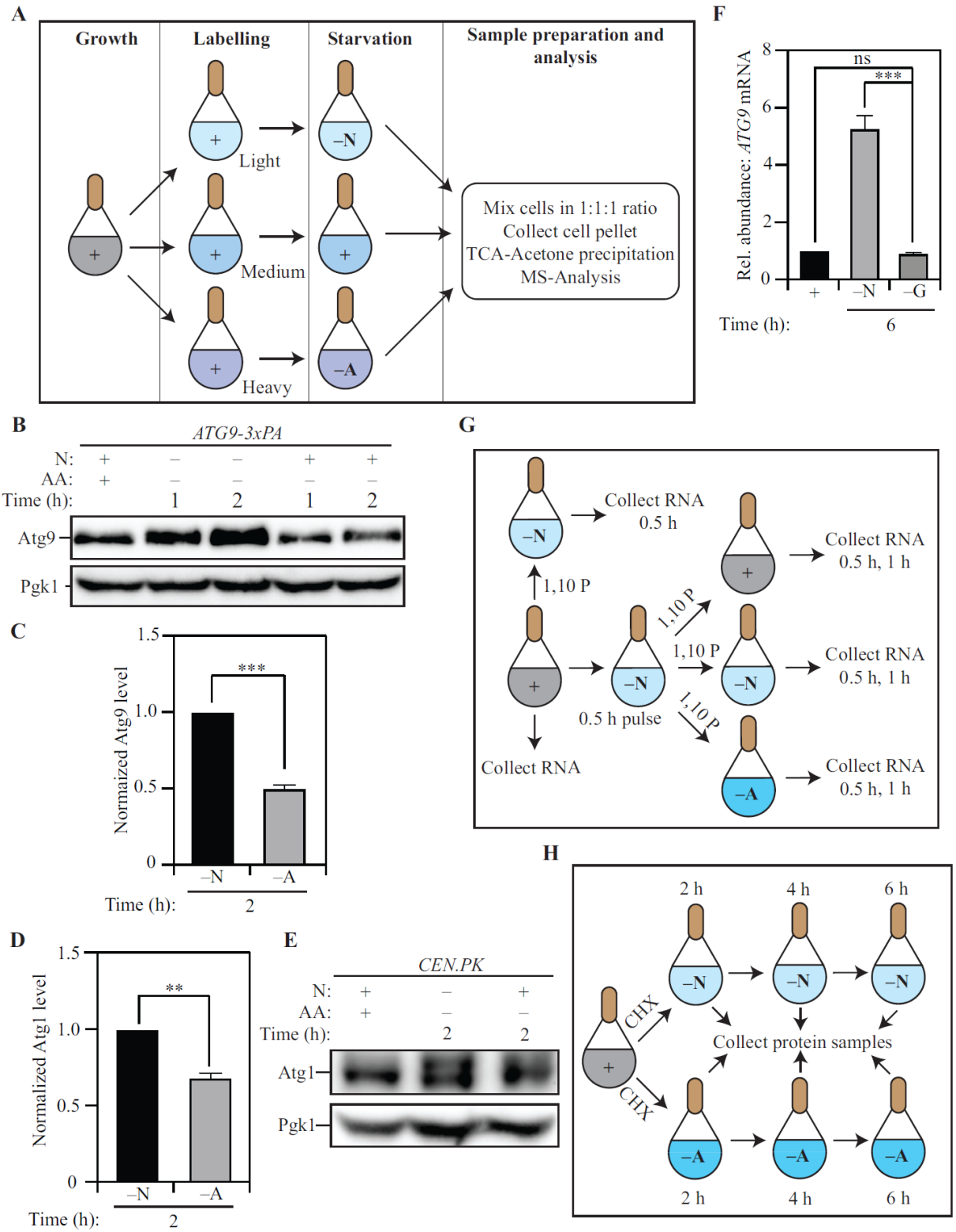
A
Growth
Labelling
Starvation
Sample preparation and analysis
Light
Medium
Heavy
Mix cells in 1:1:1 ratio
Collect cell pellet
TCA-Acetone precipitation
MS-Analysis
F
Rel. abundance: ATG9 mRNA
ns
***
Time (h):
6
B
ATG9-3xPA
N:
AA:
Time (h):
Atg9
Pgk1
C
Normaized Atg9 level
***
Time (h):
2
D
Normalized Atg1 level
**
Time (h):
2
E
CEN.PK
N:
AA:
Time (h):
Atg1
Pgk1
G
Collect RNA
0.5 h
1,10 P
0.5 h pulse
Collect RNA
0.5 h, 1 h
H
2 h
4 h
6 h
CHX
Collect protein samples

Figure 15: Post-transcriptional activation of *ATG* gene expression is a critical node determining autophagy during nitrogen starvation.

a. Scheme of the triplex SILAC experiment. “Light”, “Medium” and “Heavy” refer to the nature of arginine and lysine isotopes present in the media. Across different biological replicates, the nature of the medium used for growing cells for each treatment (nutrient-replete, nitrogen starvation or amino acid starvation) was alternated.
b. Atg9 levels are higher during nitrogen starvation compared to amino acid starvation: WT (SEY6210) cells were harvested in nutrient-replete conditions or after starvation for the indicated times and Atg9 protein levels were assessed by western blot. Pgk1 was used as a loading control.
c. Densitometric analysis of (b) from three independent biological replicates.
d. Densitometric analysis of Atg1 levels in WT cells after 2 h of nitrogen or amino acid starvation (from Figure 8B) from three independent biological replicates.
e. Atg1 levels increase substantially more during nitrogen versus amino acid starvation: CEN.PK cells were harvested in nutrient-replete conditions or after starvation for the indicated times and protein levels analyzed by western blot. Pgk1 was used as a loading control.
f. Transcriptional upregulation of *ATG9* mRNA occurs during nitrogen, but not glucose, starvation: qRT-PCR-based detection of *ATG9* mRNA in WT cells after 1 h of starvation. *ALG9* was used as a reference gene for normalization. Data are from three independent biological replicates.
g. Schematic for *ATG1* mRNA stability assay by 1,10-phenanthroline (1,10 P) chase
h. Schematic for Atg1 stability assay by cycloheximide chase (Figures 8H and 8I). Data in (C), (D) and (F) represent mean ± SEM from indicated number of replicates. Statistical analysis

for (C) and (D) was carried out using an unpaired Student's t-test while (F) was analyzed using one-way analysis of variance (ANOVA). Multiple comparisons were carried out using Tukey's multiple comparisons test. $p < 0.05$, $^{**}p < 0.005$, $^{***}p < 0.001$, $^{****}p < 0.0001$ ns: not significant.

3.2.3 Post-transcriptional regulation of ATG1 expression by Rad53 facilitates nitrogen starvation-induced autophagy

Higher Atg1 levels are correlated with the increased autophagy flux. To identify the molecular basis for increased Atg1 expression, I sought to identify regulators that specifically promote autophagy and Atg1 expression during nitrogen starvation. Because kinases are known to be involved in autophagy regulation (Licheva et al., 2021), I performed a screen to identify kinases that affected autophagy during nitrogen starvation. A Saccharomyces cerevisiae kinase deletion library, constructed in the BY4742 strain background, was utilized for this screen. Kinase deletion mutants were compared to wild-type BY4742 for identification of differences in autophagy flux. Autophagy flux was monitored by measuring the relative Atg8 degradation rate in the absence or presence of the serine protease inhibitor phenylmethylsulfonyl fluoride (PMSF). In brief, PMSF blocks the vacuolar degradation of Atg8 causing an increased accumulation of Atg8–PE when autophagy flux is high (Steinfeld et al., 2021). From this preliminary analysis I determined that the DNA damage response-related kinase Rad53 (Jung et al., 2019; Szyjka et al., 2008) is a potential regulator of autophagy and that the loss of Rad53 led to a 40% decrease in autophagy flux during nitrogen starvation (Figure 17A and 17B; data for other kinases not shown). Whereas Rad53 has been previously identified as a regulator of genotoxic-stress induced autophagy, its role in starvation-induced autophagy is unexplored (Eapen et al., 2017). Consistent with this finding, compared to wild-type (WT) cells, rad53Δ sml1Δ cells (deletion of SML1 is essential for the viability of the rad53Δ strain) exhibited ~50% lower levels of Atg1 after nitrogen starvation, while the expression of Atg1 during amino acid starvation was not significantly affected (Figure 16A and 16B). During genotoxic stress, the regulation of autophagy by Rad53 occurs at the

transcriptional level (Eapen et al., 2017). To determine if the effect on Atg1 expression was post-transcriptional, I probed the level of *ATG1* mRNA in WT and rad53Δ sml1Δ cells using qRT-PCR and found that the steady state levels of *ATG1* transcript was not affected by the deletion of *RAD53* during nitrogen starvation (Figure 16C). To investigate the effect of the rad53Δ sml1Δ deletion on autophagy flux, I used the Pho8Δ60 assay and found that while the loss of Rad53 led to a 25% reduction in autophagy during nitrogen starvation, it had no effect on autophagy during amino acid starvation (Figure 17C and 17D). Next, I utilized the accumulation of free GFP resulting from the nitrogen-starvation induced degradation of Pgi1-GFP as a marker for autophagy activity upon prolonged starvation (Liu et al., 2019). Pgi1-GFP has a longer half-life as an autophagy substrate during starvation relative to GFP-Atg8, preventing substrate exhaustion. Compared to WT cells or sml1Δ cells, rad53Δ sml1Δ cells showed 40% lower Pgi1-GFP processing activity (Figure 16D and 16E) after starvation, confirming that the autophagy phenotype is strictly due to the deletion of RAD53 and not SML1.

Next, I utilized the differential Atg8 degradation assay to demonstrate that the kinase activity of Rad53 is responsible for its stimulatory effect on autophagy. The kinase-dead Rad53^{DK227A,D339A} mutant of Rad53 (Holzen and Sclafani, 2010) exhibited a similar defect in autophagy as the rad53Δ sml1Δ strain (Figure 17E and 17F). To ensure that the autophagy phenotype of the rad53Δ sml1Δ strain is not due to chronic stress caused by the loss of Rad53, I used the auxin-inducible degron (AID) system to achieve tight temporal control of Rad53 loss (Morawska and Ulrich, 2013). Rad53-AID was degraded swiftly upon treatment with IAA (auxin) (Figure 10F; last two lanes). Compared to Rad53-AID cells treated with DMSO (vehicle), IAA-treated Rad53-AID cells showed an ~40% reduction in Atg1 expression (Figure 16F and 16G).

Consistent with the results from the *rad53*Δ *sml1*Δ cells, the Pho8Δ60 activity was reduced by ~25% in Rad53-AID cells treated with IAA, compared to those treated with DMSO (Figure 10H).

The canonical activation of Rad53 occurs downstream of the DNA damage response by the Mec1 kinase (Sweeney et al., 2005). Therefore, I tested whether Mec1 has any role in autophagy during nitrogen starvation. Accordingly, I constructed a MEC1-AID strain to probe if Mec1 plays a role in starvation-induced autophagy. IAA treatment in this strain did not result in decreased Atg1 expression (Figures 18A and 18B), or reduced autophagy flux as measured by the Pho8Δ60 activity assay (Figure 18C), compared to treatment with DMSO. This contrasts with DNA damage-induced autophagy where Mec1 is involved in autophagy regulation (Eapen et al., 2017), highlighting the fact that the role of Rad53 in nitrogen-starvation induced autophagy is distinct from its role in DNA-damage induced autophagy.

To probe selective Rad53 activation during nitrogen starvation I looked at differential phosphorylation of Rad53 between the two starvation conditions. The S175 site of Rad53 was previously identified by several large-scale phosphoproteome studies (Albuquerque et al., 2008; Chen et al., 2014), but the kinase responsible for the phosphorylation remains unclear (Schleker et al., 2010). Furthermore, a recent study demonstrated that unlike Rad53 S560, which is phosphorylated extensively in response to DNA damage, Rad53 S175 is only modestly phosphorylated, suggesting a distinct regulatory function for this site (Lanz et al., 2021). Our SILAC analysis identified S175 on Rad53 as a site that was more strongly phosphorylated during nitrogen starvation relative to amino acid starvation (Figure 16I). I reasoned that if this phosphorylation is critical for the autophagy-stimulating effect of Rad53, mutation of the residue to an alanine should dampen autophagy during nitrogen starvation. Indeed, the plasmid-based re-introduction of the phospho-dead Rad53^{S175A} mutant in a *rad53*Δ *sml1*Δ background revealed a

partial ~25% reduction in autophagy flux, as measured by the Pgi1-GFP processing assay, compared to the re-introduction of WT Rad53 (Figure 16J and 16K). This finding indicates that the S175 site is likely an important site for Rad53 activation during nitrogen starvation but may not be the sole activation site for Rad53. In-silico analysis suggested that the S175 residue is likely to be phosphorylated by a proline-directed kinase. Because the proline-directed kinase Cdc28 is known to regulate Rad53 phosphorylation (Abreu et al., 2013; Schleker et al., 2010), I examined whether Cdc28 is responsible for regulating *ATG1* expression during nitrogen-starvation induced autophagy. Treatment of a *CDC28*-AID strain with IAA led to complete loss of Cdc28 (Figure 12D; last two lanes) but had no effect on Atg1 levels (Figures 18D and 18E) or autophagy flux (Figure 18F) indicating that Cdc28 is not involved in nitrogen starvation-induced autophagy. Taken together, these data suggest that an unconventional mode of Rad53 activation promotes Atg1 expression and autophagy during nitrogen starvation.

Figure 16

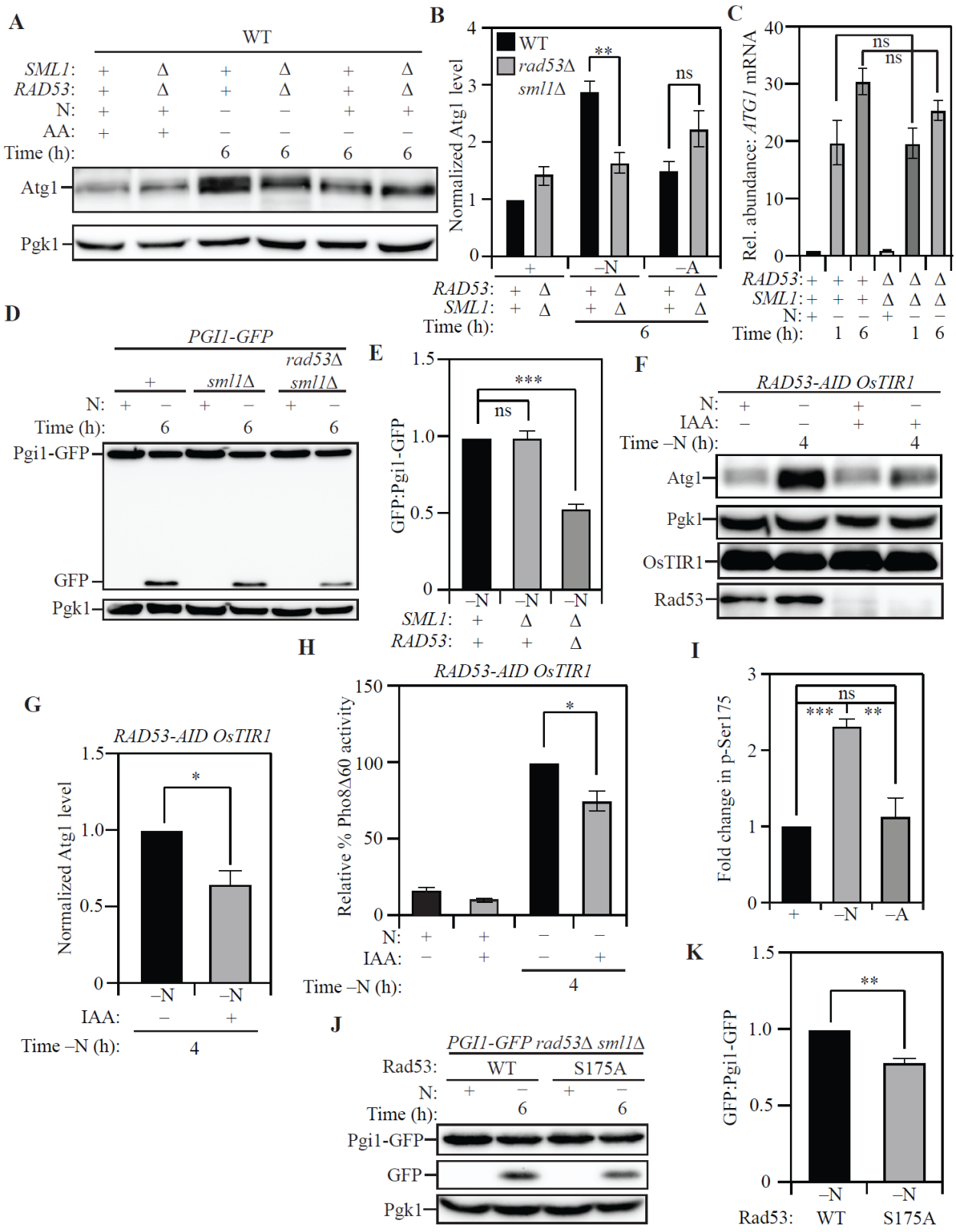
A
WT
SML1: + Δ + Δ + Δ
RAD53: + Δ + Δ + Δ
N: + + – – + +
AA: + + – – – –
Time (h): 6 6 6 6
Atg1
Pgk1
B
WT
rad53Δ sml1Δ
Normalized Atg1 level
**
ns
+ –N –A
RAD53: + Δ + Δ + Δ
SML1: + Δ + Δ + Δ
Time (h): 6
C
Rel. abundance: ATG1 mRNA
ns
ns
RAD53: + + + Δ Δ Δ
SML1: + + + Δ Δ Δ
N: + – – + – –
Time (h): 1 6 1 6
D
PGI1-GFP
rad53Δ sml1Δ
+ sml1Δ
N: + – + – + –
Time (h): 6 6 6
Pgi1-GFP
GFP
Pgk1
E
GFP:Pgi1-GFP
***
ns
–N –N –N
SML1: + Δ Δ
RAD53: + + Δ
F
RAD53-AID OsTIR1
N: + – + –
IAA: – – + +
Time –N (h): 4 4
Atg1
Pgk1
OsTIR1
Rad53
G
RAD53-AID OsTIR1
Normalized Atg1 level
*
–N –N
IAA: – +
Time –N (h): 4
H
RAD53-AID OsTIR1
Relative % Pho8Δ60 activity
*
N: + + – –
IAA: – + – +
Time –N (h): 4
I
Fold change in p-Ser175
ns
*** **
+ –N –A
J
PGI1-GFP rad53Δ sml1Δ
Rad53: WT S175A
N: + – + –
Time (h): 6 6
Pgi1-GFP
GFP
Pgk1
K
GFP:Pgi1-GFP
**
–N –N
Rad53: WT S175A

Figure 16: Post-transcriptional regulation of *ATG1* expression by Rad53 facilitates nitrogen starvation-induced autophagy.

a. Atg1 levels exhibit a significantly greater increase in WT (SEY6210) cells relative to *rad53*Δ *sml1*Δ cells upon nitrogen starvation but not upon amino acid starvation: Cells of the indicated genotypes were harvested during nutrient-replete conditions or after nitrogen or amino acid starvation for the indicated times and protein level examined by western blot. Pgk1 was used as a loading control.
b. Densitometric analyses for (a) from three independent biological replicates.
c. A similar abundance of *ATG1* transcript was detected in WT (SEY6210) and *rad53*Δ *sml1*Δ cells after nitrogen starvation: Cells of the indicated genotypes were harvested during nutrient-replete conditions or after starvation. qRT-PCR was used to determine *ATG1* transcript abundance using *ALG9* as the reference gene for normalization. Data from three independent biological replicates.
d. Autophagy flux during nitrogen starvation, assessed by the Pgi1-GFP processing assay, is reduced in *rad53*Δ *sml1*Δ cells compared to WT (SEY6210) and *sml1*Δ cells: Cells of the indicated genotypes, expressing chromosomally tagged Pgi1-GFP were harvested and examined as in (a). The appearance of free GFP indicates autophagy flux.
e. Densitometric analysis of (d) from three independent biological replicates.
f. The acute loss of Rad53 leads to a reduction in Atg1 expression during nitrogen starvation: WT (WLY176) *RAD53-AID* cells expressing the OsTIR1 ubiquitin ligase were treated with either IAA or DMSO and harvested during nutrient-replete conditions or after nitrogen starvation for the indicated times. IAA treatment activates the ligase activity and targets Rad53-AID for proteasomal degradation. Pgk1 was used as a loading control.

g. Densitometric analysis of (f) from three independent biological replicates.

h. The Pho8Δ60 assay reveals a reduction in autophagy flux during nitrogen starvation caused by the acute loss of Rad53: WT (WLY176) *RAD53-AID OsTIR1* cells were harvested during nutrient-replete conditions or after starvation for the indicated times with or without IAA treatment, and Pho8Δ60 enzyme activity was measured by colorimetry. An increase in Pho8Δ60 activity indicates increased autophagic flux. Data are from three independent biological replicates.

i. Rad53 S175 phosphorylation levels are significantly higher in nitrogen starvation compared to amino acid starvation or nutrient-replete conditions: Phosphoproteome analysis of SEY6210 *arg4*Δ cells comparing nitrogen and amino acid starvation using triplex-SILAC labelling and LC-MS/MS analysis. The plot represents data from four independent biological replicates.

j. A phospho-dead mutation of Rad53 S175 ($Rad53^{S175A}$) reduces autophagy flux during nitrogen starvation, as examined by the Pgi1-GFP processing assay: WT (SEY6210) *rad53*Δ *sml1*Δ *PGI1-GFP* cells expressing either Rad53 or $Rad53^{S175A}$ were harvested during nutrient-replete conditions or after starvation for the indicated times. The appearance of free GFP indicates autophagy flux. Pgk1 used as loading control.

k. Densitometric analysis of (j) from three independent biological replicates.

Data in (b), (c), (e), (g), (h), (i) and (k) represent the mean ± SEM from the indicated number of replicates. Statistical analysis for (b), (c), (e) and (h) was carried out using one-way analysis of variance (ANOVA). (g) and (k) were analyzed using unpaired Student's t-test while (i) was analyzed using paired Student's t-test. Multiple comparisons were carried out using Tukey's

multiple comparisons test. *p < 0.05, **p < 0.005, ***p < 0.001, ****p < 0.0001 ns: not significant.

Figure 17

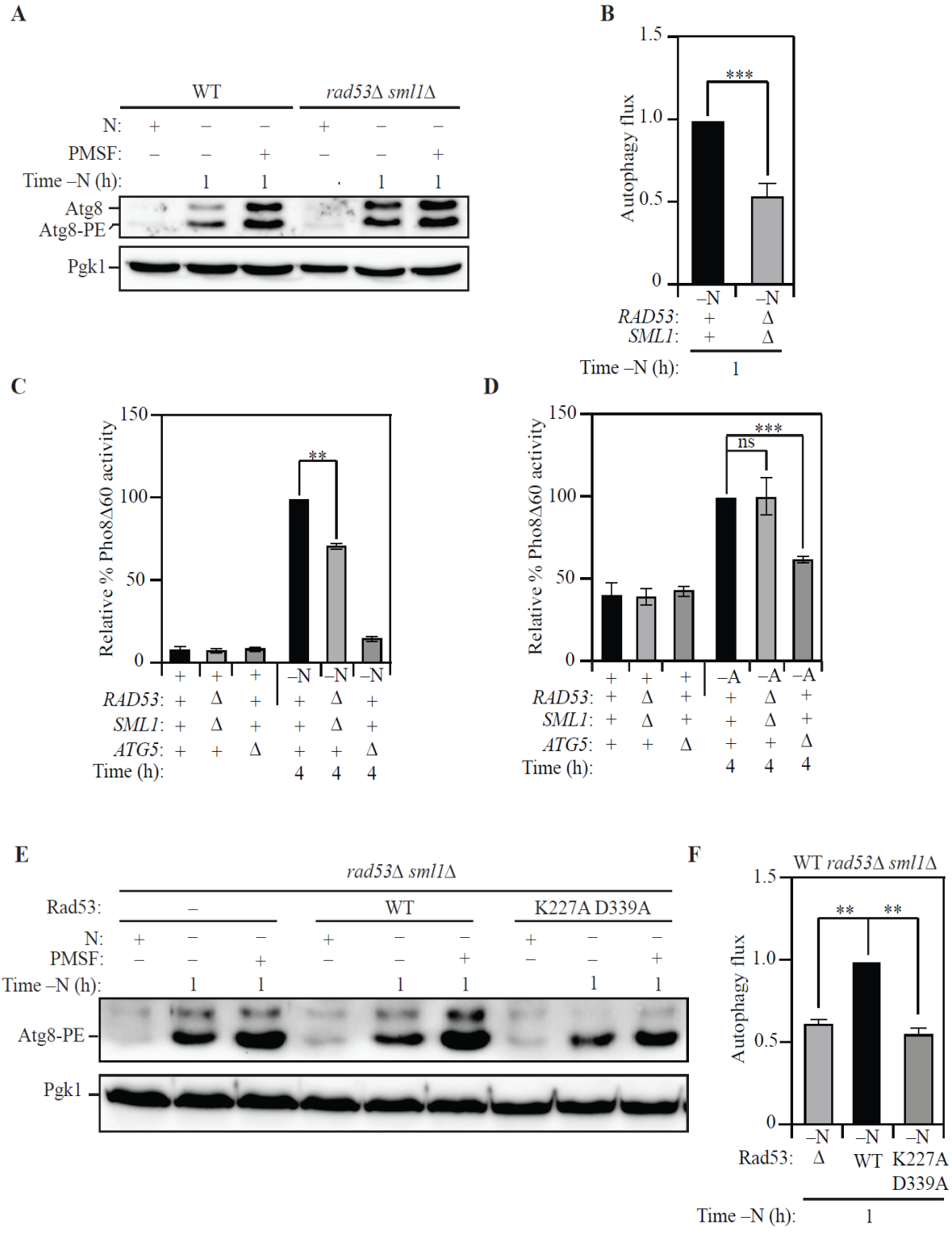
A
WT
rad53Δ sml1Δ
N:
PMSF:
Time –N (h):
Atg8
Atg8-PE
Pgk1
B
Autophagy flux
***
RAD53:
SML1:
Time –N (h):
C
Relative % Pho8Δ60 activity
**
RAD53:
SML1:
ATG5:
Time (h):
D
Relative % Pho8Δ60 activity
***
ns
RAD53:
SML1:
ATG5:
Time (h):
E
rad53Δ sml1Δ
Rad53:
WT
K227A D339A
N:
PMSF:
Time –N (h):
Atg8-PE
Pgk1
F
WT rad53Δ sml1Δ
Autophagy flux
**
**
Rad53:
WT
K227A D339A
Time –N (h):

Figure 17: Post-transcriptional regulation of *ATG1* expression by Rad53 facilitates nitrogen starvation-induced autophagy.

a. The loss of Rad53 function impairs autophagy during nitrogen starvation as demonstrated by the Atg8-lipidation assay: WT (SEY6210) and *rad53*Δ *sml1*Δ cells were harvested during nutrient-replete conditions or after starvation with or without PMSF treatment. Increased Atg8–PE accumulation upon PMSF treatment (relative to no treatment control) indicates autophagy flux.
b. Densitometry analysis of (a) from three biological replicates.
c. The loss of Rad53 function reduces autophagy flux during nitrogen starvation but not amino acid starvation, as demonstrated by the Pho8Δ60 assay: WT (WLY176) and *rad53*Δ *sml1*Δ cells were harvested during nutrient-replete conditions or after nitrogen starvation starvation for the indicated times. Pho8Δ60 enzyme activity was measured by colorimetry. An increase in Pho8Δ60 activity indicates increased autophagic flux. Negative control: SEY6210 *atg5*Δ cells. Data from three independent biological replicates.
d. WT (WLY176) and *rad53*Δ *sml1*Δ cells were harvested during nutrient-replete conditions or after amino acid starvation for the indicated times. Pho8Δ60 enzyme activity was measured by colorimetry. An increase in Pho8Δ60 activity indicates increased autophagic flux. Negative control: SEY6210 *atg5*Δ cells. Data from three independent biological replicates.
e. Abolishing Rad53 kinase activity reduces autophagy flux during nitrogen starvation: WLY176 *rad53*Δ *sml1*Δ cells expressing either Rad53 or Rad53^{K227A,D339A} (kinase-dead Rad53) from a centromeric plasmid were harvested during nutrient-replete conditions or after starvation with or without PMSF treatment. Increased Atg8–PE accumulation upon PMSF treatment (relative to the no-treatment control) indicates autophagy flux.

f. Densitometric analysis of (e) from three independent biological replicates.

Data in (a), (b), (d) and (f) represent mean ± SEM from the indicated number of replicates. Statistical analysis for (a) and (b) was carried out using two-way analysis of variance (ANOVA) while (d) was analyzed using an unpaired Student's t-test. Statistical analysis for (f) was carried out using one-way analysis of variance (ANOVA). Multiple comparisons were carried out using Tukey's multiple comparisons test. *$p < 0.05$, **$p < 0.005$, ***$p < 0.001$, ****$p < 0.0001$ ns: not significant.

Figure 18

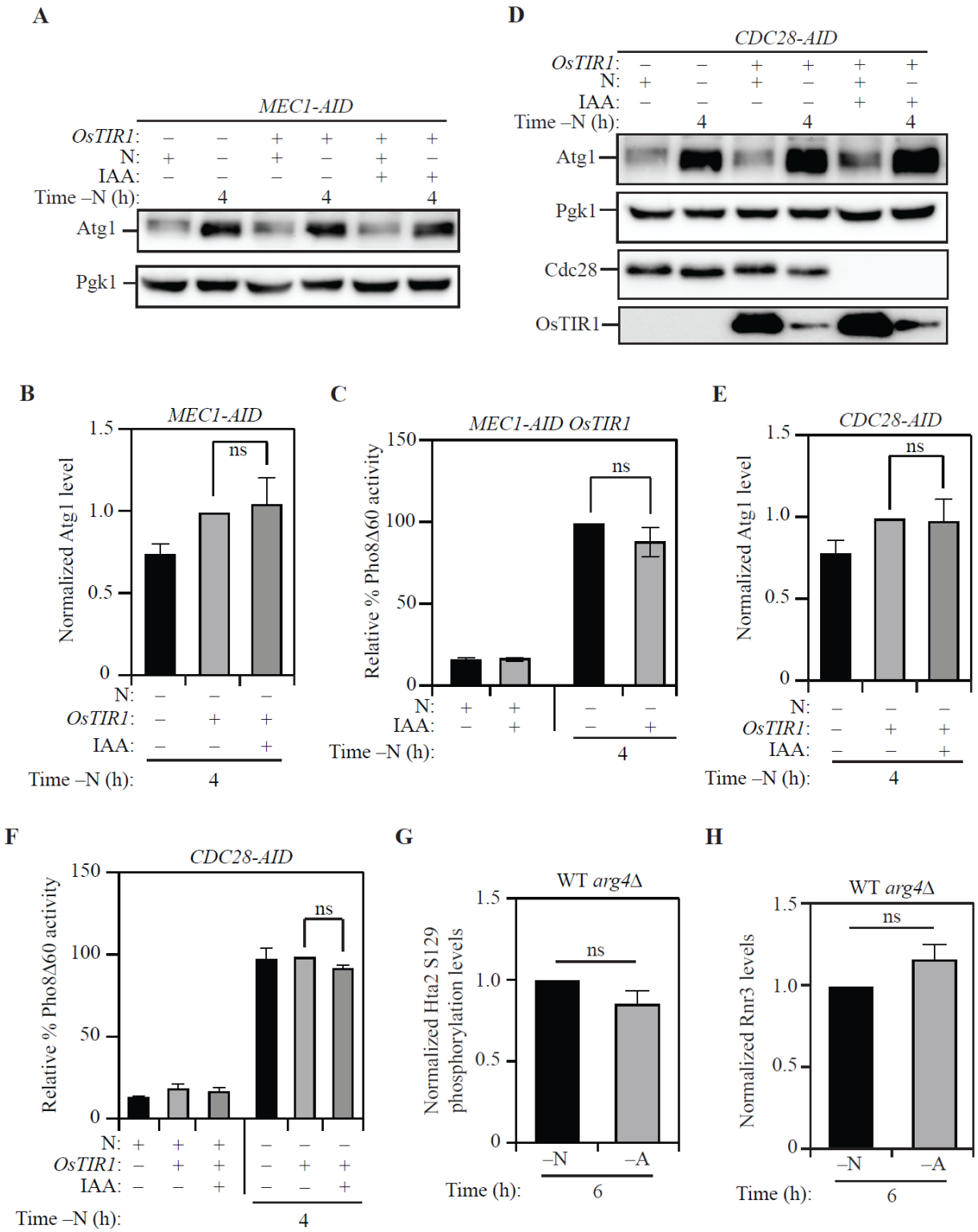
A
MEC1-AID
OsTIR1: – – + + + +
N: + – + – + –
IAA: – – – – + +
Time –N (h): 4 4 4
Atg1
Pgk1
D
CDC28-AID
OsTIR1: – – + + + +
N: + – + – + –
IAA: – – – – + +
Time –N (h): 4 4 4
Atg1
Pgk1
Cdc28
OsTIR1
B
MEC1-AID
Normalized Atg1 level
1.5
1.0
0.5
0
ns
N: – – –
OsTIR1: – + +
IAA: – – +
Time –N (h): 4
C
MEC1-AID OsTIR1
Relative % Pho8Δ60 activity
150
100
50
0
ns
N: + + – –
IAA: – + – +
Time –N (h): 4
E
CDC28-AID
Normalized Atg1 level
1.5
1.0
0.5
0
ns
N: – – –
OsTIR1: – + +
IAA: – – +
Time –N (h): 4
F
CDC28-AID
Relative % Pho8Δ60 activity
150
100
50
0
ns
N: + + + – – –
OsTIR1: – + + – + +
IAA: – – + – – +
Time –N (h): 4
G
WT arg4Δ
Normalized Hta2 S129 phosphorylation levels
1.5
1.0
0.5
0
ns
–N –A
Time (h): 6
H
WT arg4Δ
Normalized Rnr3 levels
1.5
1.0
0.5
0
ns
–N –A
Time (h): 6

Figure 18: Mec1 and Cdc28 are not involved in Rad53 activation during nitrogen starvation-induced autophagy.

a. The acute loss of Mec1 has no effect on Atg1 expression during nitrogen starvation: WT (WLY176) *CUP1p-GFP-ATG8 MEC1-AID* cells without OsTIR1 expression and WT *CUP1p-GFP-ATG8 MEC1-AID OsTIR1* cells were harvested during nutrient-replete conditions or after nitrogen starvation with or without IAA treatment. Atg1 proteins levels were examined by western blot. Pgk1 was used as a loading control.
b. Densitometric analysis of three independent biological replicates from (a).
c. The acute loss of Mec1 does not affect autophagy flux during nitrogen starvation: WLY176 *CUP1p-GFP-ATG8 MEC1-AID OsTIR1* cells were harvested as in (a) and Pho8Δ60 enzyme activity was measured by colorimetry. An increase in Pho8Δ60 activity indicates increased autophagic flux. Data from three independent biological replicates.
d. The acute loss of Cdc28 has no effect on Atg1 expression: WT *CUP1p-GFP-ATG8 CDC28-AID* cells without OsTIR1 expression and WT *CUP1p-GFP-ATG8 CDC28-AID OsTIR1* cells were harvested and examined as in (a). Pgk1 was used as a loading control.
e. Densitometric analysis of three independent biological replicates from (d).
f. The acute loss of Cdc28 does not affect autophagy flux during nitrogen starvation: WLY176 *CUP1p-GFP-ATG8 CDC28-AID OsTIR1* cells were harvested and measured as in (c). Data from three independent biological replicates.
g. No differential DNA damage in nitrogen starvation relative to amino acid starvation. Hta2 S129 phosphorylation level is similar during nitrogen and amino acid starvation (see text for details).

h. No differential DNA damage in nitrogen starvation relative to amino acid starvation. Rnr3 phosphorylation level is similar during nitrogen and amino acid starvation (see text for details).

Data in (b), (c), and (e-h) represent the mean ± SEM from the indicated number of replicates. Statistical analysis for (b) and (e) was carried out using one-way analysis of variance/ANOVA. Statistical analysis for (c) and (f) was carried out using two-way analysis of variance. Statistical analysis for (g) and (h) was carried out using Unpaired t-test. Multiple comparisons were carried out using Tukey's multiple comparisons test. *$p < 0.05$, **$p < 0.005$, ***$p < 0.001$, ****$p < 0.0001$, ns: not significant.

3.2.4 Ded1 binds ATG1 mRNA to promote Atg1 expression

Our results indicated that post-transcriptional mechanisms promote the expression of Atg1 during nitrogen starvation relative to amino acid starvation. Therefore, I hypothesized that the regulation occurs via an RNA-binding protein (RBP), which binds *ATG1* mRNA preferentially during nitrogen starvation and facilitates its translation. Accordingly, I carried out an unbiased preliminary screen for proteins that bind the 5' UTR of *ATG1* which identified Ded1 in addition to several previously characterized *ATG1* mRNA-binding proteins (see Materials and Methods for details on the screen methodology).

Ded1 is an essential RNA-helicase that is involved in promoting translation initiation under nutrient-rich conditions (de la Cruz et al., 1997) that has recently been demonstrated to be a Rad53 substrate (Lao et al., 2018). Because Ded1 was identified from a single large-scale dataset, I used RNA-immunoprecipitation (RNA-IP) to verify that Ded1 binds *ATG1* mRNA in vivo during nitrogen starvation. For this purpose, I tagged Ded1 with a 3xPA-tag and affinity isolated Ded1-PA, harvested from cells subjected to nitrogen starvation, using IgG-Sepharose beads. This affinity isolation was followed by the extraction of bound RNA and detection using qRT-PCR. As a control, I used a strain where Ded1 was not epitope-tagged with PA, which served as the background to eliminate non-specific isolates (Gatica et al., 2018; Liu et al., 2019). Using PGK1 mRNA as an internal control, and normalizing detection to the untagged strain, I found that Ded1 specifically associates with the 5' UTR of *ATG1* mRNA in vivo (Figure 13A). I validated this interaction using a reciprocal approach: I synthesized 500 bp of the 5' UTR of *ATG1* mRNA immediately upstream of the ORF and labeled the synthesized RNA with desthiobiotin. I incubated this RNA with nitrogen-starved yeast cell lysates. Following cross-linking and streptavidin affinity isolation, I probed the interaction between the in vitro synthesized *ATG1* 5' UTR fragment (*ATG1*

fragment) and endogenous epitope-tagged Ded1 (Ded1-PA) from nitrogen starved cell lysates by immunoblotting. Indeed, I found that Ded1-PA exhibited a 4-fold enrichment when affinity isolated with the *ATG1* fragment compared to the control RNA fragment (Figures 19B and 19C), indicating specific binding to the *ATG1* fragment.

I next tested whether Ded1 has a stimulatory role in Atg1 expression during nitrogen starvation. Because *DED1* is an essential gene, I used a temperature sensitive *ded1-95* strain (*ded1^{ts}*) to investigate Atg1 expression at permissive (23°C) and non-permissive (35°C) temperatures relative to WT (Burckin et al., 2005). At both temperatures, the expression of Atg1 was significantly reduced in the *ded1^{ts}* strain with a severe 80% reduction at the non-permissive temperature (Figure 21A and 21B). This reduction was post-transcriptional because the steady state levels of *ATG1* mRNA were essentially unchanged between the wild-type and the *ded1^{ts}* strains (Figure 21C).

Contrary to the reduction in Atg1 levels, a significant reduction was not noticed in the levels of Atg9 in the *ded1^{ts}* strain, which highlights the specificity of Ded1 for *ATG1* mRNA (Figures 21D and 21E). To eliminate the possibility of the defects being caused due to chronic stress in the *ded1^{ts}* strain, I generated an auxin-inducible Ded1 (Ded1-AID) strain to temporally control the loss of Ded1. Treatment with IAA led to degradation of cellular Ded1 (Figure 19D, last lane). I used this strain to probe for differences in Atg1 expression upon Ded1 degradation. Relative to DMSO treatment, degradation of Ded1 by IAA treatment led to an 80% reduction in Atg1 expression (Figures 19D and 19E), consistent with the reduction observed in the *ded1^{ts}* strain. Once again, loss of Ded1 by IAA treatment did not affect *ATG1* mRNA levels (Figure 19F) indicating post-transcriptional regulation. To ensure that the acute loss of Ded1 did not affect general translation, I used Coomassie Brilliant Blue staining to compare total protein profiles of

Ded1-AID cells treated with or without IAA after nitrogen starvation (Figure 21F). Quantification of lane profiles indicated that there was no significant decrease in the total protein content upon IAA-mediated Ded1 degradation (Figure 21G).

Next, I tested whether the strength of the interaction between Ded1 and the 5' UTR of the *ATG1* mRNA differed in amino acid starvation relative to nitrogen starvation. Using epitope-tagged Ded1 (Ded1-13xMYC) for RNA-IP, I investigated this interaction in cells subjected to nitrogen starvation and amino acid starvation. Consistent with our hypothesis, Ded1 binding to the 5'-UTR of the *ATG1* mRNA was reduced by ~60% in amino acid starvation relative to nitrogen starvation (Figure 19G). This was not due to reduced Ded1 expression because Ded1 levels were higher during amino acid starvation relative to nitrogen starvation (Figure 19H). This finding suggests that while a basal level of Ded1-*ATG1* mRNA interaction is present during amino acid starvation, increased Ded1 binding to the *ATG1* mRNA promotes increased Atg1 synthesis during nitrogen starvation. Indeed, when probing the levels of Atg1 after amino acid starvation in the Ded1-AID strain, I observed an ~35% reduction in Atg1 level upon Ded1 degradation by IAA (Figures 19I and 19J), compared to the ~75% reduction observed during nitrogen starvation. This result highlights the fact that Ded1 promotes Atg1 expression preferentially during nitrogen starvation.

Finally, to investigate whether Rad53 promotes the binding of Ded1 to *ATG1* mRNA, I compared the ability of epitope-tagged Ded1 (Ded1-13xMYC) to bind the 5' UTR of *ATG1* mRNA in WT and *rad53*Δ *sml1*Δ cells using RNA-IP. Using *PGK1* mRNA as an internal control, I determined that the ability of Ded1 to bind the 5' UTR of *ATG1* mRNA was reduced by 65% in a *rad53*Δ *sml1*Δ background (Figure 19K), mirroring the reduction in binding in amino-acid relative to nitrogen-starvation conditions. Taken together, these findings indicate that Ded1 binds the 5'

UTR of *ATG1* mRNA. Moreover, they also reveal that this binding preferentially occurs during nitrogen starvation and is mediated, at least in part, by Rad53.

Having determined that Ded1 regulates Atg1 expression, I investigated the role of Ded1 in autophagy. To measure the impact of Ded1 on autophagy flux, I transformed WT and *ded1*^{ts} cells with an *ATG8*-promoter driven GFP-Atg8 plasmid and followed the appearance of free GFP after nitrogen starvation. Autophagy flux was reduced in the *ded1*^{ts} strain at both permissive and non-permissive temperatures, relative to WT (Figures 21H and 21I). I confirmed this phenotype with biochemical assays utilizing the Ded1-AID strain chromosomally expressing a CUP1 promoter-driven GFP-Atg8, where treatment with IAA led to a 70% reduction in autophagy flux compared to treatment with DMSO (Figure 20A and 20B). This was corroborated by the Pho8Δ60 activity assay, where the loss of Ded1 led to a 60% reduction in autophagy flux (Figure 20C). Mirroring its effect on Atg1 expression during amino acid starvation relative to nitrogen starvation, loss of Ded1 by IAA treatment led to a smaller (~30%) reduction in autophagy flux, as assessed by the Pho8Δ60 activity assay (Figure 20D). Next, I used a *pep4*Δ *vps4*Δ Ded1-AID strain to directly compare autophagosome formation in the presence and absence of Ded1 (Figure 20E) after nitrogen starvation using TEM. The loss of Ded1 by IAA treatment caused a severe reduction in the number of ABs accumulated within the vacuole, indicating a lower frequency of autophagosome formation (Figures 20F and 20G). The size of the ABs was also reduced in the IAA-treated Ded1-AID cells (Figure 14H). Taken together, these findings implicate Ded1 in the regulation of autophagy flux through the regulation of Atg1 expression (Figure 20I).

Figure 19

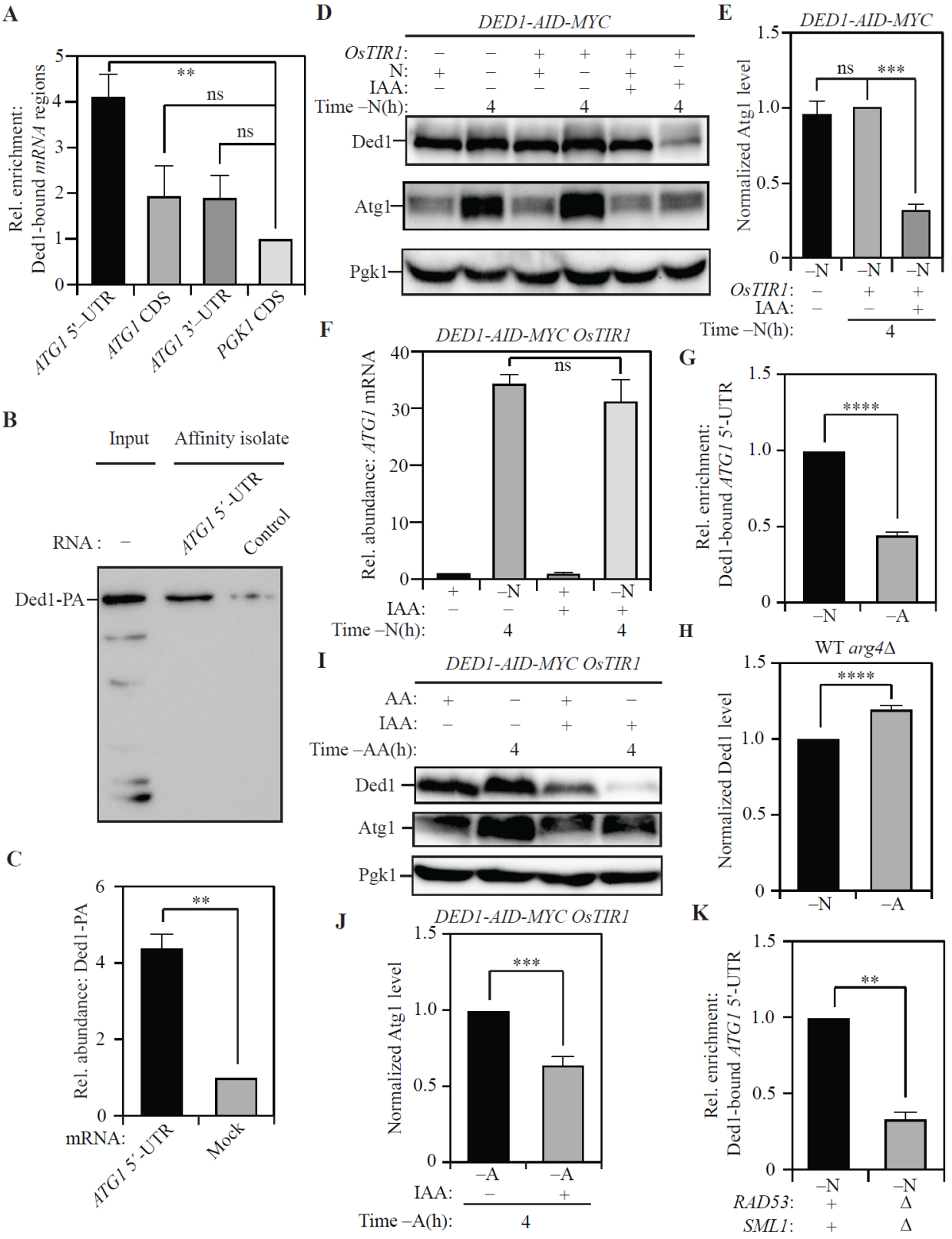
A
Rel. enrichment: Ded1-bound mRNA regions
**
ns
ns
ATG1 5′-UTR
ATG1 CDS
ATG1 3′-UTR
PGK1 CDS
B
Input
Affinity isolate
RNA :
ATG1 5′-UTR
Control
Ded1-PA
C
Rel. abundance: Ded1-PA
**
mRNA:
ATG1 5′-UTR
Mock
D
DED1-AID-MYC
OsTIR1:
N:
IAA:
Time –N(h):
Ded1
Atg1
Pgk1
E
DED1-AID-MYC
Normalized Atg1 level
ns
***
–N
OsTIR1:
IAA:
Time –N(h):
F
DED1-AID-MYC OsTIR1
Rel. abundance: ATG1 mRNA
ns
IAA:
Time –N(h):
G
Rel. enrichment: Ded1-bound ATG1 5′-UTR
****
–N
–A
H
WT arg4Δ
Normalized Ded1 level
****
I
DED1-AID-MYC OsTIR1
AA:
IAA:
Time –AA(h):
Ded1
Atg1
Pgk1
J
DED1-AID-MYC OsTIR1
Normalized Atg1 level
***
IAA:
Time –A(h):
K
Rel. enrichment: Ded1-bound ATG1 5′-UTR
**
RAD53:
SML1:

Figure 19: Ded1 binds *ATG1* mRNA to promote Atg1 expression.

a. RNA-IP analysis demonstrates Ded1 binding to the 5'-UTR of *ATG1* mRNA during nitrogen starvation: PA-tagged Ded1 was immunoprecipitated using IgG-Sepharose beads and bound RNA was amplified and detected by qRT-PCR. Specific primers were used to identify the relative enrichment of the indicated regions of the *ATG1* mRNA. Primers targeting the *PGK1* mRNA coding sequence (CDS) were used as an internal control. A strain with untagged Ded1 was used as a control for normalization.
b. In vitro RNA affinity isolation confirms interaction between Ded1 and the 5' UTR of *ATG1* mRNA during nitrogen starvation: The sequence of bases from 500 bp upstream of the *ATG1* mRNA up to the coding sequence of *ATG1* mRNA was synthesized *in vitro* and labelled with desthibiotin (*ATG1* 5' UTR fragment). The fragment was incubated with lysates from WT (SEY6210) Ded1-13xMYC cells. The RNA was affinity isolated using streptavidin, and Ded1 was probed by immunoblotting using anti-MYC antibody. The presence of Ded1 indicates binding to the *ATG1* 5' UTR fragment. Mock fragment (random sequence) used as a control
c. Data for (b) from three independent biological replicates.
d. The acute loss of Ded1 leads to reduced Atg1 expression during nitrogen starvation: WT (WLY176) *CUP1p-GFP-ATG8 DED1*-AID cells without OsTIR1 expression and WT (WLY176) *CUP1p-GFP-ATG8 DED1-AID OsTIR1* cells were harvested during nutrient-replete conditions or after nitrogen starvation with or without IAA treatment and protein levels were examined by western blot. Pgk1 was used as a loading control.
e. Densitometric analysis of Atg1 levels from (d) from three independent biological replicates.

f. The acute loss of Ded1 has no effect on *ATG1* transcription during nitrogen starvation: Total RNA was isolated from WT (WLY176) *CUP1p-GFP-ATG8 DED1-AID OsTIR1* cells during nutrient-replete conditions or after nitrogen starvation with or without IAA treatment. qRT-PCR analysis was used to measure the *ATG1* transcript level with *ALG9* as a reference gene. Data from three independent biological replicates.

g. The interaction between Ded1 and the 5' UTR of *ATG1* mRNA is stronger during nitrogen starvation compared to amino acid starvation, as demonstrated by RNA-IP analysis. Data are representative of three independent biological replicates.

h. Ded1 levels are higher during amino acid starvation relative to nitrogen starvation: Ded1 levels were measured in WT (SEY6210) *arg4*Δ cells using SILAC and normalized to total protein input per sample.

i. The acute loss of Ded1 leads to a partial decrease in Atg1 expression during amino acid starvation: WT (WLY176) *CUP1p-GFP-ATG8 DED1-AID OsTIR1* cells were harvested during nutrient-replete conditions or after amino acid starvation with or without IAA treatment and protein levels examined by western blot. Pgk1 was used as a loading control.

j. Densitometric analysis of Atg1 levels in (i) from three independent biological replicates.

k. The interaction between Ded1 and *ATG1* mRNA is weaker in *rad53*Δ *sml1*Δ cells relative to WT (SEY6210) cells during nitrogen starvation, as demonstrated by RNA-IP analysis. Data are representative of three independent biological replicates.

Data in (a), (c), (e), (f), (g), (i) and (j) represent the mean ± SEM from the indicated number of replicates. Statistical analysis for (a), (e) and (f) was carried out using one-way analysis of variance (ANOVA) while (c), (g), (i) and (j) were analyzed using unpaired Student's t-

test. Multiple comparisons were carried out using Tukey's multiple comparisons test. *p < 0.05, **p < 0.005, ***p < 0.001, ****p < 0.0001 ns: not significant.

Figure 20

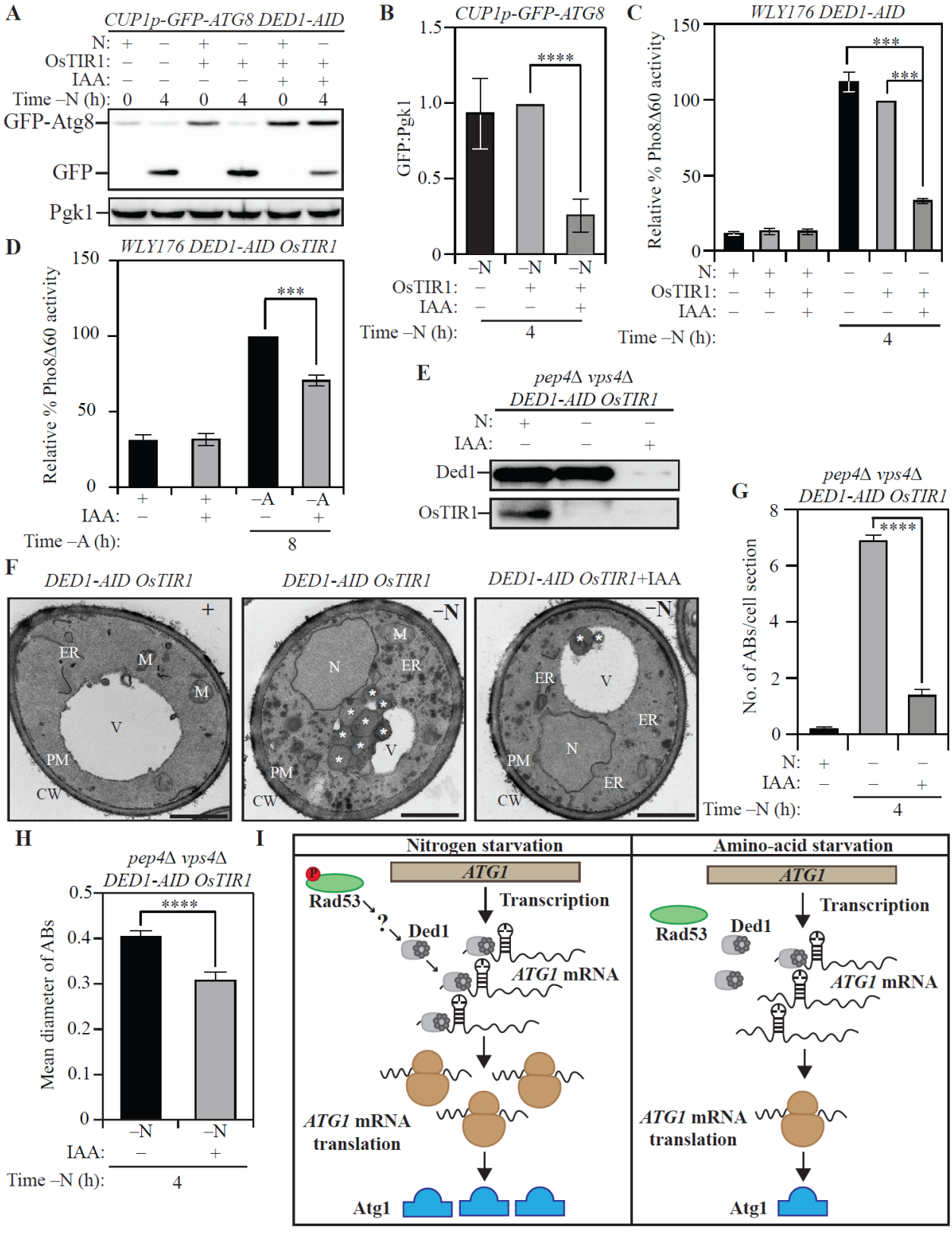
A
CUP1p-GFP-ATG8 DED1-AID
N:
OsTIR1:
IAA:
Time –N (h): 0 4 0 4 0 4
GFP-Atg8
GFP
Pgk1
B
CUP1p-GFP-ATG8
GFP:Pgk1
****
–N –N –N
OsTIR1:
IAA:
Time –N (h): 4
C
WLY176 DED1-AID
Relative % Pho8Δ60 activity
***
***
N:
OsTIR1:
IAA:
Time –N (h): 4
D
WLY176 DED1-AID OsTIR1
Relative % Pho8Δ60 activity
***
–A –A
IAA:
Time –A (h): 8
E
pep4Δ vps4Δ
DED1-AID OsTIR1
N:
IAA:
Ded1
OsTIR1
F
DED1-AID OsTIR1
DED1-AID OsTIR1
DED1-AID OsTIR1+IAA
+
–N
–N
ER
M
V
PM
CW
N
G
pep4Δ vps4Δ
DED1-AID OsTIR1
No. of ABs/cell section
****
N:
IAA:
Time –N (h): 4
H
pep4Δ vps4Δ
DED1-AID OsTIR1
Mean diameter of ABs
****
–N –N
IAA:
Time –N (h): 4
I
Nitrogen starvation
Amino-acid starvation
ATG1
Transcription
Rad53
?
Ded1
ATG1 mRNA
ATG1 mRNA translation
Atg1

Figure 20: Ded1 regulates autophagy in yeast.

a. The acute loss of Ded1 causes a reduction in autophagy flux during nitrogen starvation as assessed by the GFP-Atg8 processing assay: WT (WLY176) *CUP1p-GFP-ATG8 DED1-AID* cells lacking OsTIR1 and WT (WLY176) *CUP1p-GFP-ATG8 DED1-AID OsTIR1* cells were harvested during nutrient-replete conditions or after nitrogen starvation with or without IAA treatment and examined by western blot. The appearance of free GFP indicates autophagy flux.
b. Densitometric analysis of (a) from three independent biological replicates.
c. The acute loss of Ded1 reduces autophagy flux significantly more during nitrogen starvation than amino acid starvation as demonstrated by the Pho8Δ60 assay: WT (WLY176) *CUP1p-GFP-ATG8 DED1-AID* cells and WT (WLY176) *CUP1p-GFP-ATG8 DED1-AID OsTIR1* cells were harvested during nutrient-replete and nitrogen starvation conditions and Pho8Δ60 enzyme activity was measured by colorimetry. An increase in Pho8Δ60 activity indicates increased autophagic flux. Data are from three independent biological replicates.
d. WT (WLY176) *CUP1p-GFP-ATG8 DED1-AID* cells and WT (WLY176) *CUP1p-GFP-ATG8 DED1-AID OsTIR1* cells were harvested during nutrient-replete and amino acid starvation conditions and Pho8Δ60 enzyme activity was measured by colorimetry. An increase in Pho8Δ60 activity indicates increased autophagic flux. Data are from three independent biological replicates.
e. Degradation of Ded1-AID upon IAA treatment in SEY6210 *pep4*Δ *vps4*Δ *DED1-AID OsTIR1* cells.

f. Defects in autophagosome formation during nitrogen starvation due to acute loss of Ded1: (F) SEY6210 *pep4*Δ *vps4*Δ *DED1-AID OsTIR1* cells were harvested during nutrient-replete conditions or after 3-h nitrogen starvation with or without IAA treatment. The cells were fixed, stained and ultrastructural analysis was used to visualize the number and size of ABs.

g. Quantification of the number of ABs from 100 randomly selected cell profiles from two independent biological replicates.

h. Quantification of the diameter of ABs counted in (g).

i. Schematic depicting the proposed post-transcriptional regulation of *ATG1* expression that regulates autophagy differentially between nitrogen and amino acid starvation.

Data in (b), (c), (d), (g) and (h) represent mean ± SEM from the indicated number of replicates. Statistical analysis was carried out using one-way analysis of variance (ANOVA) Multiple comparisons were carried out using Tukey's multiple comparisons test. *$p < 0.05$, **$p < 0.005$, ***$p < 0.001$, ****$p < 0.0001$ ns: not significant.

Figure 21

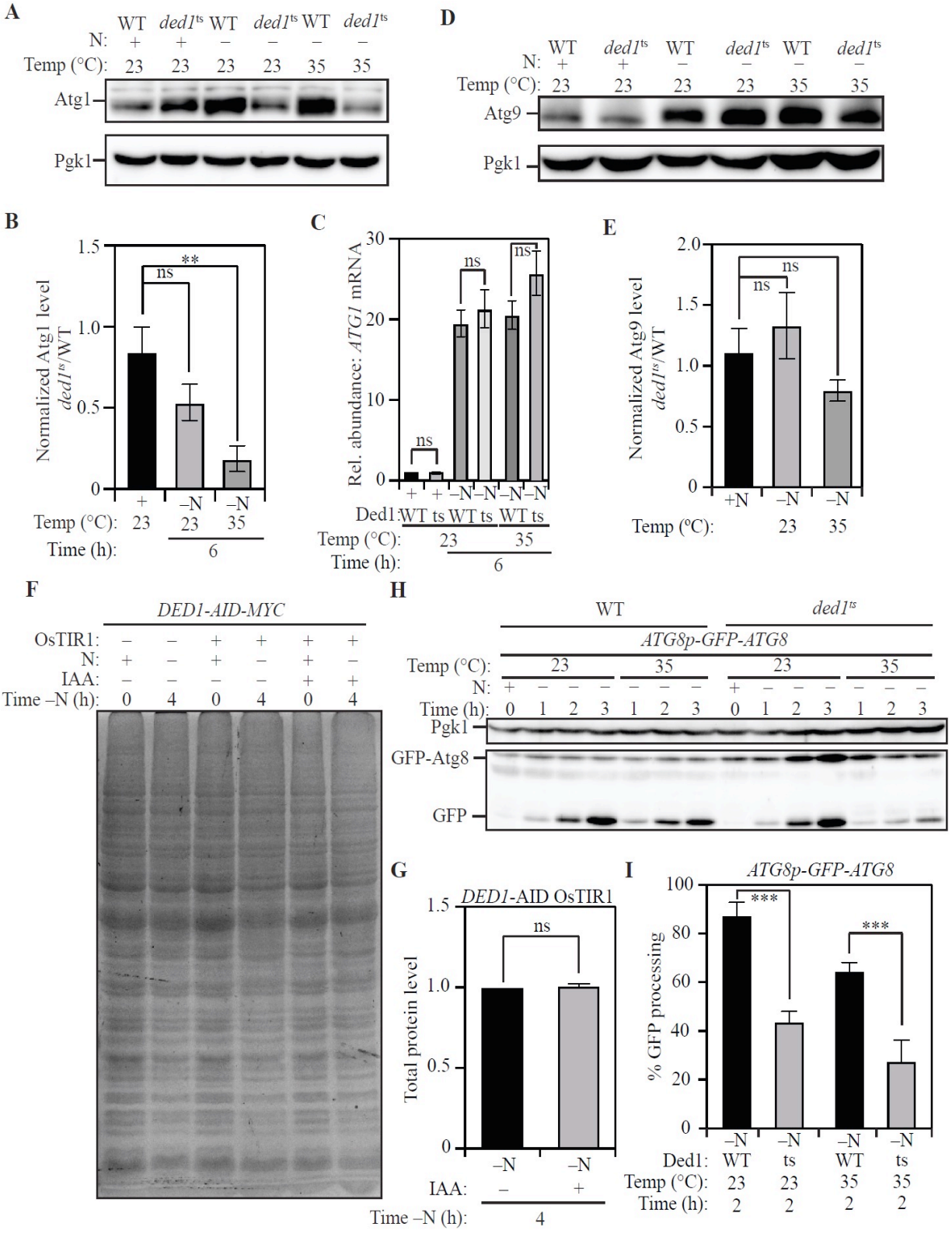
A
WT ded1ts WT ded1ts WT ded1ts
N: + + – – – –
Temp (°C): 23 23 23 23 35 35
Atg1
Pgk1
D
WT ded1ts WT ded1ts WT ded1ts
N: + + – – – –
Temp (°C): 23 23 23 23 35 35
Atg9
Pgk1
B
Normalized Atg1 level ded1ts/WT
1.5
1.0
0.5
0
**
ns
+ –N –N
Temp (°C): 23 23 35
Time (h): 6
C
Rel. abundance: ATG1 mRNA
30
20
10
0
ns
ns
ns
+ + –N –N –N –N
Ded1: WT ts WT ts WT ts
Temp (°C): 23 35
Time (h): 6
E
Normalized Atg9 level ded1ts/WT
2.0
1.5
1.0
0.5
0
ns
ns
+N –N –N
Temp (°C): 23 35
F
DED1-AID-MYC
OsTIR1: – – + + + +
N: + – + – + –
IAA: – – – – + +
Time –N (h): 0 4 0 4 0 4
H
WT ded1ts
ATG8p-GFP-ATG8
Temp (°C): 23 35 23 35
N: + – – – – – – – + – – – – – – –
Time (h): 0 1 2 3 1 2 3 0 1 2 3 1 2 3
Pgk1
GFP-Atg8
GFP
G
DED1-AID OsTIR1
Total protein level
1.5
1.0
0.5
0
ns
–N –N
IAA: – +
Time –N (h): 4
I
ATG8p-GFP-ATG8
% GFP processing
100
80
60
40
20
0
***
***
–N –N –N –N
Ded1: WT ts WT ts
Temp (°C): 23 23 35 35
Time (h): 2 2 2 2

Figure 21: Ded1 regulates Atg1 expression and autophagy in yeast. (A) The loss of Ded1 activity impairs Atg1 expression during nitrogen starvation.

a. WT (SEY6210) or *ded1*^{ts} (non-permissive temperature: 35°C) strains were harvested during nutrient-replete conditions or after nitrogen starvation at 23°C or 35°C. Atg1 levels were examined using western blot. Pgk1 was used as a loading control.
b. Densitometric analyses of Atg1 expression in *ded1*^{ts} relative to SEY6210 from three independent biological replicates.
c. The loss of Ded1 activity has no effect on *ATG1* transcription during nitrogen starvation: Strains and conditions as in (a) were used to measure the levels of *ATG1* mRNA by qRT-PCR. *ALG9* was used as a reference gene for normalization. Data from three independent biological replicates.
d. The loss of Ded1 activity has no effect on Atg9 expression: WT (SEY6210) or *ded1*^{ts} strains were harvested as in (a). Atg9 levels were examined using western blot. Pgk1 was used as a loading control.
e. Densitometric analyses of Atg9 expression in *ded1*^{ts} relative to the WT (SEY6210) from three independent biological replicates.
f. Total protein profile reveals that the loss of Ded1 activity does not promote changes in general translation during nitrogen starvation: WT (WLY176) *CUP1p-GFP-ATG8 DED1-AID* cells without OsTIR1 expression and WT (WLY176) *CUP1p-GFP-ATG8 DED1-AID OsTIR1* cells harvested during nutrient-replete conditions or after nitrogen starvation with or without IAA treatment. Proteins were stained using Coomassie Brilliant Blue.
g. Total protein quantified by densitometric analysis of five prominent bands from the total profile across three independent biological replicates.

h. The loss of Ded1 activity impairs autophagy flux during nitrogen starvation, assessed by the GFP-Atg8 processing assay: WT (SEY6210) or *ded1*^{ts} (non-permissive temperature: 35°C) cells were transformed with an *ATG8p-GFP-ATG8* plasmid (expressing *ATG8* under the control of the endogenous promoter) and harvested in nutrient-replete conditions or after starvation for the indicated times at either 23°C or 35°C. Proteins were examined by western blot. The appearance of free GFP indicates autophagy flux. Pgk1 was used as a loading control.

i. Densitometric analysis from three independent biological replicates.

Data in (b), (c), (e), (g) and (i) represent the mean ± SEM from the indicated number of replicates. Statistical analysis for (b), (c), (e) and (i) was carried out using one-way analysis of variance (ANOVA). Statistical analysis for (g) was carried out using an unpaired Student's t-test. Multiple comparisons were carried out using Tukey's multiple comparisons test. *$p < 0.05$, **$p < 0.005$, ***$p < 0.001$, ****$p < 0.0001$ ns: not significant.

3.2.5 DDX3 regulates ULK1 expression and autophagy in mammalian cells

To examine whether the function of Ded1 is conserved, I investigated the ability of DDX3, the mammalian homolog of Ded1 (Tarn and Chang, 2009), to regulate ULK1 expression. I used the pancreatic ductal cancer-derived cell line PANC-1 as well as the fibrosarcoma-derived cell line HT-1080 to probe for a role of DDX3 in autophagy regulation. I found that stable knockdown (KD) of DDX3 led to a reduction in the level of ULK1 protein (Figure 22A) in PANC-1 cells. Crucially, the reduction in ULK1 levels occurred without reduction in the level of *ULK1* mRNA (Figure 22B) indicating post-transcriptional regulation. To measure changes in autophagy caused by DDX3 KD, PANC-1 cells were treated with the MTOR inhibitor rapamycin for up to 4 h. At all the time points tested (0.5, 2 and 4 h), DDX3 KD cells (Figure 22C and 22D) showed reduced ULK1 expression (Figure 22C and 22E) and reduced LC3-lipidation ratio (LC3-II:LC3-I; Figure 22C and 22F) relative to control cells. Additionally, co-treatment with bafilomycin A1 enhanced the LC3 lipidation ratio in both control and DDX3 KD cells, with control cells still exhibiting significantly higher levels of lipidated LC3 compared to DDX3 KD. This finding highlighted the fact that the decreased LC3 lipidation ratio in shDDX3 cells could not be attributed to accelerated autophagy flux but was caused be an overall reduction in autophagy (Klionsky et al., 2021) (Figure 22C and 22F). Finally, the increased accumulation of SQSTM1 in DDX3 KD cells relative to control cells confirmed that autophagy flux was reduced upon loss of DDX3 (Bjorkoy et al., 2009) (Figure 22C and 22G). In contrast, the level of ATG5 was unaffected upon DDX3 KD highlighting the fact that DDX3 loss did not affect general *ATG* gene expression (Figures 22C and 22A). The phenotypes observed in PANC-1 cells were consistent in HT-1080 cells: stable DDX3 KD (Figures 17B and 17C) led to a reduction in ULK1 levels without alteration of *ULK1* mRNA (Figures 23B,

23D and 23E), as well as a reduction in the LC3 lipidation ratio (both with and without bafilomycin A_1; Figures 23B and 23F). Similarly, DDX3 KD caused an increased accumulation of SQSTM1 following rapamycin treatment, but no further increase with bafilomycin A_1, indicating a reduction in autophagy rather than accelerated flux (Figures 23B and 23G) without affecting ATG5 levels (Figures 23B and 23H). Taken together, these data indicate that DDX3 plays a selective role in modulating ULK1 expression and regulating autophagy in mammalian cells.

Figure 22

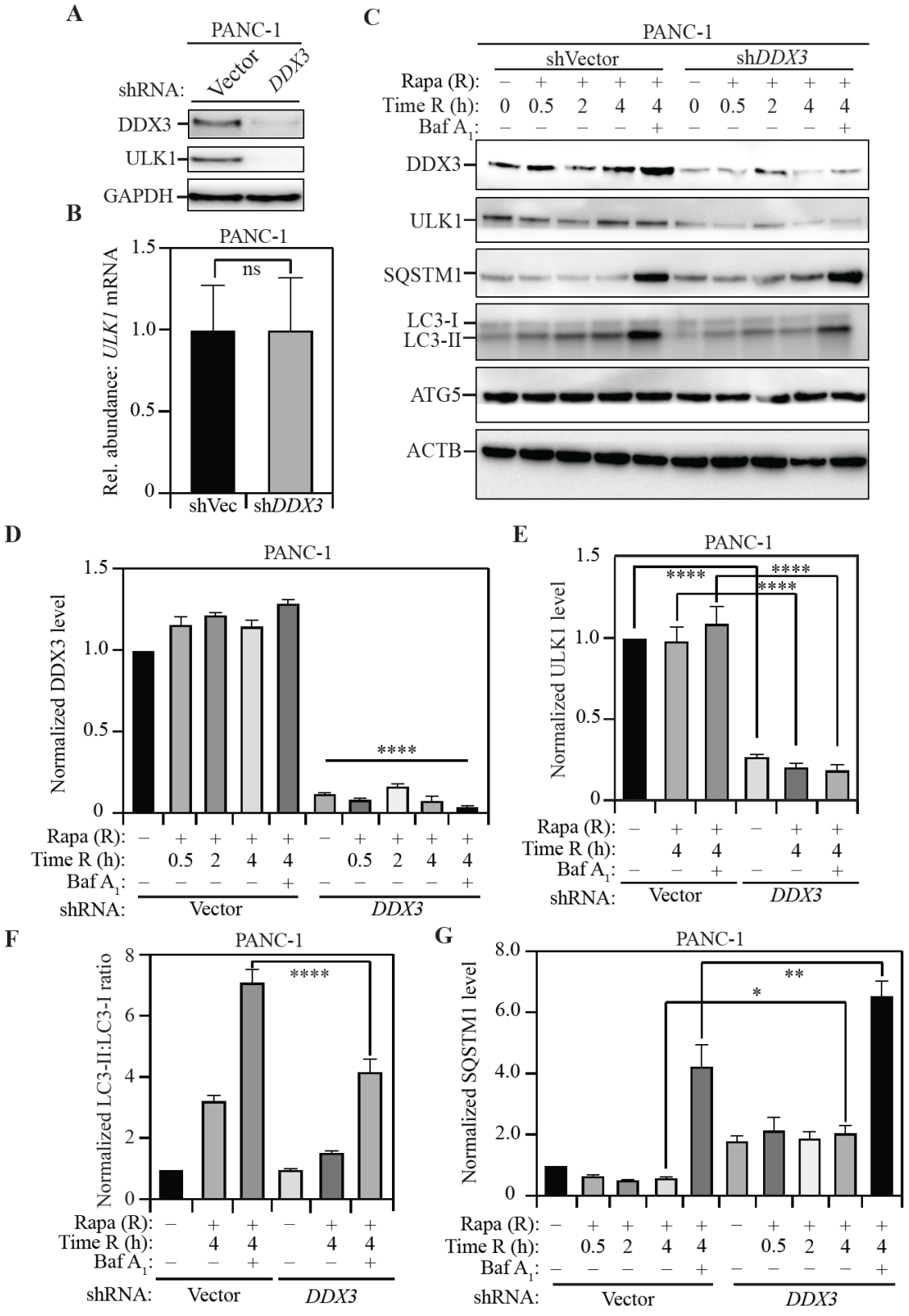
A
PANC-1
shRNA:
Vector
DDX3
DDX3
ULK1
GAPDH
B
PANC-1
Rel. abundance: ULK1 mRNA
ns
shVec
shDDX3
C
PANC-1
shVector
shDDX3
Rapa (R):
Time R (h):
Baf A1:
DDX3
ULK1
SQSTM1
LC3-I
LC3-II
ATG5
ACTB
D
PANC-1
Normalized DDX3 level
****
Rapa (R):
Time R (h):
Baf A1:
shRNA:
Vector
DDX3
E
PANC-1
Normalized ULK1 level
****
****
****
Rapa (R):
Time R (h):
Baf A1:
shRNA:
Vector
DDX3
F
PANC-1
Normalized LC3-II:LC3-I ratio
****
Rapa (R):
Time R (h):
Baf A1:
shRNA:
Vector
DDX3
G
PANC-1
Normalized SQSTM1 level
**
*
Rapa (R):
Time R (h):
Baf A1:
shRNA:
Vector
DDX3

Figure 22: DDX3 regulates autophagy in mammalian cells.

a. Stable shRNA-mediated knockdown of DDX3 in PANC-1 cells: Western blotting to probe for DDX3 and ULK1 levels in cells transfected with shVector (control) or sh*DDX3*. GAPDH was used as a loading control.
b. Relative abundance of *ULK1* mRNA in sh*DDX3* cells compared to control cells. *GAPDH* was used as a reference gene. Data represent three independent biological replicates.
c. The loss of DDX3 leads to a reduction in ULK1 levels and autophagy in mammalian cells: PANC-1 cells, stably transfected with either vector shRNA (control) or shRNA targeting *DDX3*, were treated with rapamycin (Rapa; R) for the indicated times with or without co-treatment with bafilomycin A_1 (Baf A_1). A representative blot shows the levels of DDX3, ULK1, SQSTM1, LC3-I, LC3-II, and ATG5 with ACTB as a loading control, upon harvesting cells at the indicated time points after rapamycin treatment.
d. Normalized DDX3 levels at the indicated time points with the indicated treatments. Data represent three independent biological replicates.
e. Normalized ULK1 levels at the indicated time points with the indicated treatments. Data represent three independent biological replicates.
f. Normalized LC3-II:LC3-I ratio at the indicated time points with the indicated treatments. Decreased LC3-II:LC3-I ratio in the presence of bafilomycin A_1 indicates reduced autophagy flux. Data represent three independent biological replicates.
g. Normalized SQSTM1 level at the indicated time points with the indicated treatments. Increased SQSTM1 accumulation indicates reduced autophagy flux. Data represent three independent biological replicates.

Data in (b), (d), (e), (f) and (g) represent mean ± SEM from indicated number of replicates. (b) was analyzed using unpaired Student's t-test while the statistical analysis for (d), (e), (f) and (g) was carried out using one-way analysis of variance (ANOVA). Multiple comparisons were carried out using Tukey's multiple comparisons test. *$p < 0.05$, **$p < 0.005$, ***$p < 0.001$, ****$p < 0.0001$ ns: not significant.

Figure 23

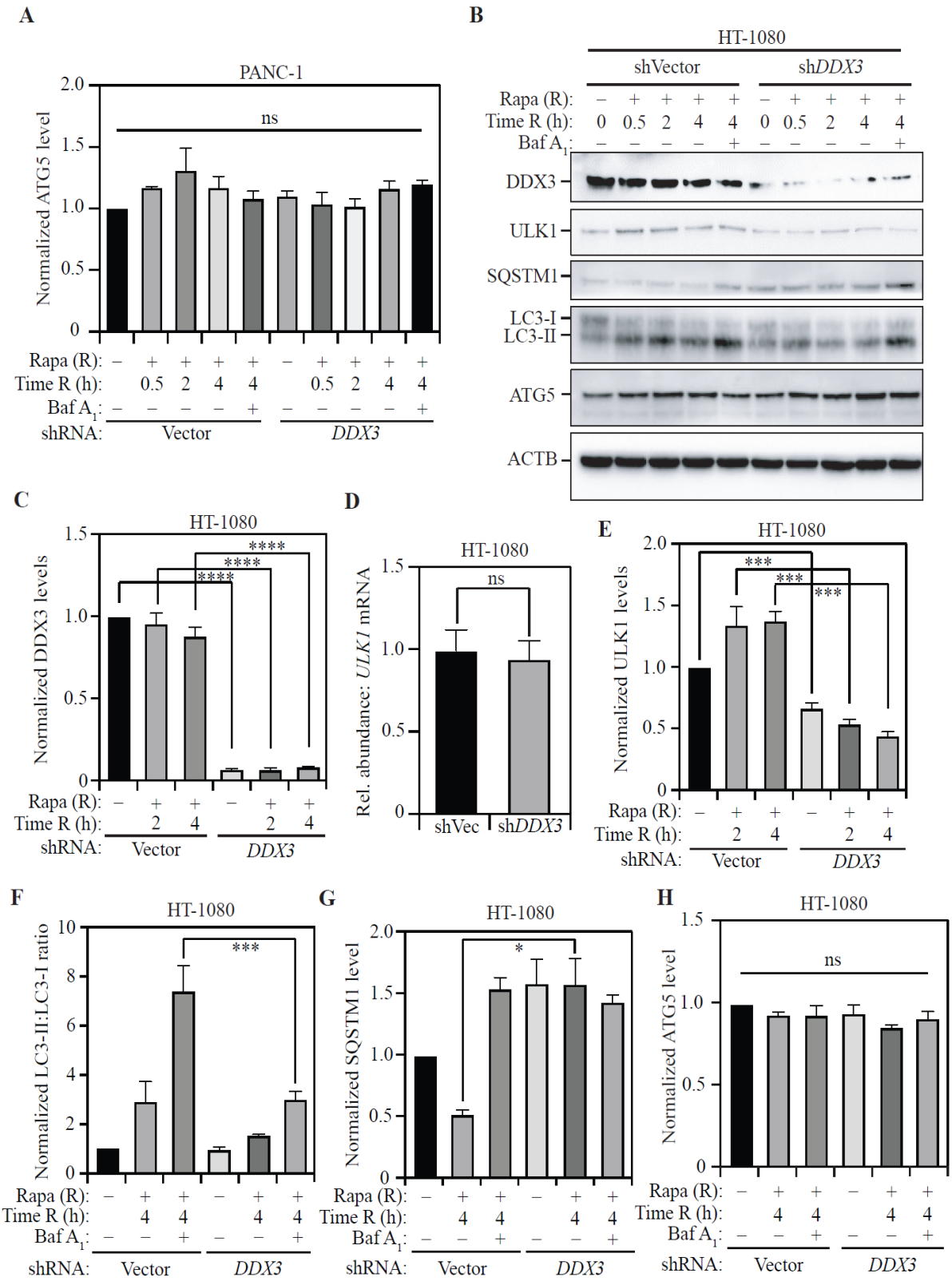
A
PANC-1
Normalized ATG5 level
ns
Rapa (R):
Time R (h):
Baf A1:
shRNA:
Vector
DDX3
B
HT-1080
shVector
shDDX3
Rapa (R):
Time R (h):
Baf A1:
DDX3
ULK1
SQSTM1
LC3-I
LC3-II
ATG5
ACTB
C
HT-1080
Normalized DDX3 levels
****
Rapa (R):
Time R (h):
shRNA:
Vector
DDX3
D
HT-1080
Rel. abundance: ULK1 mRNA
ns
shVec
shDDX3
E
HT-1080
Normalized ULK1 levels
***
Rapa (R):
Time R (h):
shRNA:
Vector
DDX3
F
HT-1080
Normalized LC3-II:LC3-I ratio
***
Rapa (R):
Time R (h):
Baf A1:
shRNA:
Vector
DDX3
G
HT-1080
Normalized SQSTM1 level
*
Rapa (R):
Time R (h):
Baf A1:
shRNA:
Vector
DDX3
H
HT-1080
Normalized ATG5 level
ns
Rapa (R):
Time R (h):
Baf A1:
shRNA:
Vector
DDX3

Figure 23: DDX3 regulates autophagy in mammalian cells.

a. The loss of DDX3 has no effect on ATG5 expression: PANC-1 cells, stably transfected with either vector shRNA (control) or shRNA targeting *DDX3*, were treated with rapamycin (Rapa) for the indicated times with or without co-treatment with bafilomycin A_1 (Baf A_1). Normalized ATG5 level at the indicated time points with the indicated treatments.
b. The loss of DDX3 impairs ULK1 expression and autophagy in mammalian cells: HT-1080 cells, stably transfected with either vector shRNA (control) or shRNA targeting *DDX3*, were treated with rapamycin for the indicated times with or without co-treatment with bafilomycin A_1. A representative blot shows the levels of DDX3, ULK1, SQSTM1, LC3-I and LC3-II, and ATG5 with ACTB as a loading control, upon harvesting cells at the indicated time points after rapamycin treatment.
c. Normalized DDX3 levels at the indicated time points with the indicated treatments. Data represent three independent biological replicates.
d. Relative abundance of *ULK1* mRNA in sh*DDX3* cells compared to control cells. *GAPDH* was used as a reference gene. Data represent three independent biological replicates.
e. Normalized DDX3 levels at the indicated time points with the indicated treatments. Data represent three independent biological replicates.
f. Normalized LC3-II:LC3-I ratio at the indicated time points with the indicated treatments. Decreased LC3-II:LC3-I ratio in the presence of bafilomycin A_1 indicates reduced autophagy flux.
g. Normalized SQSTM1 level at the indicated time points with the indicated treatments. An increased SQSTM1 accumulation indicates reduced autophagy flux.

h. Normalized ATG5 level at the indicated time points with the indicated treatments. Data represent three independent biological replicates.

Data in (a), and (c-h) represent mean ± SEM from the indicated number of replicates. Statistical analysis for (a), (c), and (e-h) was carried out using one-way analysis of variance (ANOVA) while (d) was analyzed using an unpaired Student's t-test. Multiple comparisons were carried out using Tukey's multiple comparisons test. *$p < 0.05$, **$p < 0.005$, ***$p < 0.001$, ****$p < 0.0001$ ns: not significant.

3.3 Discussion

Autophagy is a highly complex process, and genetic studies in the model yeast system have been crucial in identifying regulators of autophagy. The expression of *ATG1*, which encodes the Ser/Thr kinase responsible for autophagy initiation, is subject to multiple levels of regulation. *ATG1* is transcriptionally regulated by Gcn4 (Bernard et al., 2015b), Pho23 (Jin et al., 2014) and Rph1 (Bernard et al., 2015a): Gcn4 promotes *ATG1* transcription during nitrogen starvation, whereas Pho23 and Rph1 repress transcription during nutrient-replete conditions. The cytoplasmic exoribonuclease Xrn1 regulates the stability of the *ATG1* mRNA, mediating its degradation during nutrient-replete conditions (Delorme-Axford et al., 2018). In contrast, the Pat1-Lsm complex prevents 3'-5' degradation of *ATG1* mRNA by the exosome during nitrogen starvation, thereby stabilizing the *ATG1* mRNA (Gatica et al., 2019). In nutrient-replete conditions, the RNA helicase Dhh1 associates with Dcp2 to facilitate the degradation of *ATG1* transcripts to reduce autophagy (Hu et al., 2015), while associating with Eap1 to promote *ATG1* translation and autophagy during sustained nitrogen starvation (Liu et al., 2019). Atg1 expression is enhanced during long-term nitrogen starvation by the RGG motif-containing protein Psp2, which associates with components of the translational machinery eIF4E and eIF4G2, to promote the translation of *ATG1* mRNA (Yin et al., 2019). However, several questions remain unanswered including which of these mechanisms of regulation is physiologically critical and whether there are yet unknown regulators of *ATG1* expression.

I have compared two different nutrient-starvation treatments to uncover the fact that autophagy is physiologically regulated at the level of post-transcriptional control in yeast. *ATG1* undergoes transcriptional upregulation during both amino acid starvation and nitrogen starvation

but post-transcriptional mechanisms that allow facile translation of the *ATG1* mRNA occur simultaneously only during nitrogen starvation. While the physiological rationale driving the disconnect between *ATG1* transcription and translation during amino acid starvation is unclear, an attractive hypothesis is as follows: nitrogen starvation imposes a stricter nutrient stress response that warrants swift autophagy activation, but the milder amino acid starvation initiates transcriptional priming without promoting unnecessary self-consumption.

In the process of elucidating cellular mechanisms that promote autophagy during nitrogen starvation, I have uncovered the kinase Rad53 as a post-transcriptional regulator of *ATG1* expression. While Rad53 has previously been implicated in regulating autophagy transcriptionally in response to genotoxic stress (Eapen et al., 2017), a role in promoting Atg1 expression post-transcriptionally during nitrogen starvation is novel. I confirmed that there was no differential DNA damage in nitrogen starvation, relative to amino acid starvation, which would be responsible for differential Rad53 activation. Results from our SILAC analysis indicated that conventional markers for DNA damage in yeast including S129 phosphorylation of Hta2 (Downs et al., 2000) and the expression of RNR3 (ribonucleotide reductase 3) (Tkach et al., 2012) were not significantly different between nitrogen and amino acid starvation (Figure 18G and 18H). Additionally, I found no evidence of a role for Mec1 – a key mediator of the DNA-damage response pathway that activates Rad53 – in nitrogen-starvation induced autophagy. Consistent with this novel function of Rad53, I found that a previously identified but incompletely characterized phosphorylation site on Rad53 – Ser175 – was more abundantly phosphorylated during nitrogen starvation compared to amino acid starvation. Indeed, the $Rad53^{S175A}$ mutant exhibited reduced autophagy flux during nitrogen starvation, supporting selective activation of Rad53 during nitrogen starvation. Previous studies suggest that Rad53 S175 phosphorylation is

independent of DNA damage or spindle checkpoint responses and is a proline-directed site likely to be phosphorylated by Cdc28. However, I found that Cdc28 was not involved in autophagy regulation during nitrogen starvation, indicating that Rad53 S175 phosphorylation during nitrogen starvation was not mediated by Cdc28. Our future analyses will focus on the identification of the kinase responsible for this phosphorylation.

I also identified the RNA-helicase Ded1 as a downstream effector that regulates the expression of *ATG1* mRNA. The *ATG1* mRNA is a highly structured mRNA with stem-loop structures in the 5' UTR and the 5' UTR proximal CDS (Liu et al., 2019). I hypothesized that Ded1 would bind the 5' UTR of *ATG1* where it would function to resolve secondary structures to promote facile translation (Sen et al., 2019; Sen et al., 2015). Using RNA-immunoprecipitation, I confirmed that Ded1 binds to the 5' UTR of *ATG1* mRNA. Consistent with its hypothesized role in promoting *ATG1* translation during nitrogen starvation, the loss of Ded1 activity led to a reduction in Atg1 expression after nitrogen starvation, without affecting general translation. I also demonstrated that the Ded1-*ATG1* mRNA interaction is 60% lower in amino acid starvation relative to nitrogen starvation, highlighting the fact that increased Ded1 binding likely drives increased *ATG1* translation during nitrogen starvation. Ded1 has previously been identified as a Rad53 substrate (Lao et al., 2018), indicating the possibility that Ded1 is regulated differentially by Rad53 during distinct nutrient-starvation conditions. Indeed, I show that in cells lacking Rad53, the interaction between Ded1 and *ATG1* mRNA during nitrogen starvation is reduced by ~65%, consistent with the difference seen between the two starvation treatments. TEM analysis revealed a reduction in number and size of autophagosomes following nitrogen starvation in cells suffering transient loss of Ded1, indicating its importance in mediating the autophagy response.

Our study demonstrates an intriguing role for Ded1 within the landscape of regulators identified to modulate *ATG1* expression. Whereas negative regulators like Xrn1 prevent unnecessary *ATG1* expression during nutrient-rich conditions, positive regulators such as Pat1 and Psp2 promote *ATG1* expression during starvation by stabilizing *ATG1* mRNA and promoting *ATG1* mRNA translation, respectively. Dhh1 switches from a negative regulatory role to a positive regulatory role as nutrient levels diminish. However, there is a temporal delay among these processes: whereas Pat1 stabilizes *ATG1* mRNA shortly after cells are exposed to nitrogen starvation (1-2 h), the roles of Psp2 and Dhh1 in promoting *ATG1* mRNA translation occur after extended starvation (24 h). This difference suggests that another regulator is involved in promoting *ATG1* translation within this time window, and our data suggest that this regulator is Ded1. Accordingly, strong binding of Ded1 to *ATG1* mRNA promotes translation during nitrogen starvation, whereas weaker binding during amino acid starvation leads to decreased Atg1 expression. What happens to the *ATG1* transcripts during amino acid starvation is an intriguing question. It is probable that the *ATG1* mRNA are sequestered in specialized RNA-containing structures such as stress granules or P-bodies. Because stress granules and P-bodies have largely been studied in the context of glucose starvation, this will be a challenging but interesting subject of investigation for a subsequent study.

Our study also demonstrated that DDX3, the human homolog of Ded1 (Tarn and Chang, 2009), is involved in the post-transcriptional activation of ULK1 expression, highlighting a conservation of function. DDX3 is a DEAD-box protein involved in RNA metabolism (Soto-Rifo and Ohlmann, 2013), influencing several cellular pathways including cell cycle regulation (Heerma van Voss et al., 2018; Lai et al., 2010), WNT signaling (Cruciat et al., 2013; Heerma van Voss et al., 2015; Zhao et al., 2016) and apoptosis (Sun et al., 2013). DDX3 has been implicated

in stimulatory roles in the development of several cancers including breast cancer, lung cancer and colorectal cancer (Ariumi, 2014; Bol et al., 2015; Botlagunta et al., 2008; Heerma van Voss et al., 2015; Wilky et al., 2016). DDX3 knockdown reduces cell migration and metastasis highlighting the oncogenic role of DDX3 in malignant cancers (Chen et al., 2015). Using pancreatic cancer- and fibrosarcoma-derived human cell lines, I show that DDX3 is also responsible for mediating the autophagy response; cells lacking DDX3 function exhibited reduced ULK1 expression and autophagy flux as assessed by LC3-lipidation and SQSTM1 accumulation assays. In mammalian cells, ULK1 and ULK2 show some functional redundancy. It is possible that DDX3 may not regulate ULK2 expression, which may explain why I saw a limited reduction of LC3-II and partial block in autophagy in the knockdown cells. Indeed, a partial block in autophagy may be therapeutically more desirable than a complete block. Additionally, targeting ULK1 for autophagy inhibition is an approach that had already been adopted. For example, SBI-0206965, a small-molecule kinase inhibitor of ULK1, has shown promise in pre-clinical studies in cellular models of cancer (Egan et al., 2015). Therefore, targeting DDX3 function, which would compromise both autophagy-dependent and autophagy-independent tumor survival pathways, could be an attractive therapeutic avenue for treating autophagy-addicted tumors.

3.4 Materials and Methods

3.4.1 Yeast growth and starvation media

Yeast cells were cultured in YPD (Bacto-yeast extract 10 g; Bacto-peptone 20 g; 2% dextrose; double-distilled H2O to 1 L) to mid-log phase (O.D = 0.8 – 1.0) before harvesting. For SILAC experiments yeast cells were cultures in SMD (0.67% yeast nitrogen base without amino acids; 2% D-glucose; and appropriate amino acids and nucleic acid bases) with light, medium or heavy lysine and arginine. Strains of interest carrying centromeric plasmids were grown in SMD

selective medium in which the appropriate amino acids and/or nucleic acid bases were omitted. Nitrogen starvation was carried out in SD(-N) medium (0.17% yeast nitrogen base without amino acids and ammonium sulfate, with 2% glucose). Amino acid starvation was carried out in SD(-A) medium (0.67% yeast nitrogen base without amino acids; 2% D-glucose; and appropriate nucleic acid bases). If the strain of interest was a temperature-sensitive mutant, cells were grown at a permissive temperature and shifted to a nonpermissive temperature for an appropriate period before the final harvesting.

3.4.2 Protein sample preparation and Immunoblotting

For yeast samples, proteins were precipitated using 10% TCA and the cell pellet was washed with acetone and dried. Dried, precipitated cell pellets were lysed by vortexing with glass beads in MURB buffer (50 mM sodium phosphate, pH 7.0, 25 mM MES, 1% SDS [w:v], 3 M urea, 1 mM NaN3, 1% β-mercaptoethanol, 0.01% bromophenol blue) for 5 min. Lysed samples were incubated at 55°C for 15 min before being collected by centrifugation at 10,000xg for 3 min. The supernatant was used as the sample for immunoblotting. Immunoblotting was carried out with standard denaturing SDS-PAGE followed by a semi-dry transfer using Trans-Blot® SD Semi-Dry Transfer Cell (Bio-Rad). After blocking with TBST containing 5% skim milk for 1 h, the membrane was incubated overnight at 4°C with various primary antibodies (1:1000). After incubation with peroxidase-conjugated secondary antibodies (goat anti-rabbit IgG secondary antibody [Fisher, ICN55676; 1:1000]; rabbit anti-mouse IgG secondary antibody [Jackson; 1:1000]) for 1 h at room temperature, the signals were visualized by chemiluminescence using Clarity and Clarity Max ECL Western Blotting Substrates (Bio-Rad) on a ChemiDoc Touch Imaging System (Bio-Rad).

For mammalian samples, cells were lysed in 1× cell lysis buffer (Cell Signaling Technology, 9803) containing protease inhibitor (Roche, 11836153001) on ice for 10 min. After centrifugation at 14,000 × g for 15 min at 4°C, the supernatants were collected and quantified using the BCA assay (Thermo Fisher Scientific, 23225). The 30 μg of each sample were resolved on 4–12% Criterion XT Bis–Tris gels (Bio-Rad, 3450124) in XT MES running buffer (Bio-Rad, 1610789) and transferred to PVDF membranes (Bio-Rad, 1620233) using the Trans-Blot Turbo Transfer Pack and System (Bio-Rad). After blocking with TBST containing 5% skim milk for 1 h, the membrane was incubated overnight at 4°C with various primary antibodies (1:1000). After incubation with peroxidase-conjugated secondary antibodies (goat anti-rabbit IgG secondary antibody [Cell Signaling Technology, 7074; 1:1000]; rabbit anti-goat IgG secondary antibody [Abcam, ab6741; 1:1000]) for 1 h at room temperature, the signals were visualized by chemiluminescence using SuperSignal™ West Femto Maximum Sensitivity Substrate (Thermo Fisher Scientific, 34095). I collected protein from each cell line in three biologically independent samples and mixed them together for western blot analysis. The relative intensities of the bands of western blots from three regions were automatically analyzed and normalized to a loading control using the ChemiDoc Touch Imaging System Version 1.2 (Bio-Rad).

3.4.3 RNA isolation, RNA-Sequencing, and qRT-PCR

The RNA extraction protocol and qPCR primers are published previously (Hu et al., 2015). In brief, RNA isolation was performed using the Macherey-Nagel Mini kit for RNA purification. For RNA-Sequencing, isolated RNA was frozen and submitted to BGI Genomics Inc. Transcriptome profiling was carried out using the DNBSeq™ technology and bioinformatics analysis was done using three well-established workflows: DESeq2, EBSeq and NOIseq.

For qRT-PCR using yeast cells, cDNA synthesis was carried out using random primers and the High-Capacity cDNA Reverse Transcription Kit (Applied Biosystems™). cDNA samples were analyzed using a Bio-Rad CFX Connect Real-Time System. Samples were tested in Hard-Shell 96-clear well black shell plates (Bio-Rad). The reaction mix (15 µl final volume) consisted of 7.5 µl Radiant Green Lo-ROX qPCR kit (Radiant), 0.6 µl each primer (400 nM final concentration), 1.3 µl H2O, and 5 µl of a 1:5 dilution of the cDNA preparation. The thermocycling program consisted of an initial hold at 95°C for 3 min, followed by 40 cycles of 5 s at 95°C and 25 s at 62°C. After completion, a melting curve was generated to verify PCR specificity, as well as the absence of contamination and primer dimers. The transcript abundance in samples was determined using the CFX Manager Software regression method. Relative abundance of reference mRNAs and normalization for different total RNA amounts was carried out as described previously (Hu et al., 2015).

For qRT-PCR using mammalian cells, total RNA was extracted and purified from cultured cells using the RNA extraction kit (E.Z.N.A.® HP Total RNA Kit, R6812, Omega, Biotek) according to the manufacturer's instructions. The RNA was quantified by determining absorbance at 260 nm. One microgram of total RNA from each sample was reverse transcribed into cDNA using the iScript cDNA synthesis kit (Bio-Rad, 1708890) in a volume of 20 µl; cDNA from cell samples was amplified. The qPCR was performed using 2X SYBR Green q-PCR master mix (Bimake, B21202) on the C1000 Touch Thermocycler CFX96 Real-Time System (Bio-Rad) according to the manufacturer's protocol. Analysis was performed using Bio-Rad CFX Manager software 3.1 (Bio-Rad). The gene expression was calculated via the $2^{-\Delta\Delta Ct}$ method and normalized to GAPDH. The relative concentrations of mRNA were expressed in arbitrary units based on the untreated group, which was assigned a value of 1.

3.4.4 SILAC sample preparation and LC-MS/MS analysis

Samples were prepared as described previously (Hu et al., 2019a). Briefly, dried TCA-treated cell pellets (50 mg) of each labeling were mixed and lysed in urea buffer (8 M urea, 50 mM Tris-HCl, pH 8.0). Proteins were then alkylated by treatment with 5 mM iodoacetamide for 30 min and digested by Lys-C (Lysyl Endopeptidase, WAKO Chemicals) for 4 h. The concentration of urea was diluted to 1 M and digested with trypsin (Promega) overnight. On the following day, peptides were acidified and purified by SPE using HR-X columns in combination with C18 cartridges (Macherey-Nagel). Buffers used were as follows: Buffer A, 0.1% formic acid in deionized water; Buffer B, 80% acetonitrile and 0.1% formic acid in deionized water. Elutes were frozen in liquid nitrogen and lyophilized overnight. On the third day, peptides were fractionated by HpH reversed phase chromatography (Batth et al., 2014). The dry peptide powder was suspended 5% ammonium hydroxide and fractionated using a Waters XBridge BEH130 C18 3.5 µm 4.6 × 250 mm column on an Ultimate 3000 HPLC (Thermo Scientific). Peptides were loaded with 100% HpH buffer A containing 10 mM ammonium formate in deionized water (pH 10) and fractionated by increasing acetonitrile concentration from 1% to 40% using buffer B (10 mM ammonium formate and 90% acetonitrile;pH 10) in 25 min. Ninety-six fractions were collected in a 96-deep well plate. Fractions were mixed with an interval of 12 to yield 8 final fractions. The peptides were acidified, frozen in liquid nitrogen and lyophilized overnight. On the fourth day, the dry peptides were suspended in 200 µl 80% acetonitrile with 0.1% TFA. Phosphopeptides were enriched either by TiO2 beads (GL Sciences) manually (Zarei et al., 2016) or by Fe(III)-NTA cartridges (Agilent) automatically using the Bravo Automated Liquid Handling Platform (Agilent) (Post et al., 2017). Samples were concentrated by vacuum concentration and resuspended in 20 µL of 0.1% formic acid for LC-MS/MS analysis. The tip flow-through was stored at −80°C for proteome analysis.

LC-MS/MS measurements were performed on a QExactive (QE) Plus and HF-X mass spectrometer coupled to an EasyLC 1000 and EasyLC 1200 nanoflow-HPLC, respectively (all Thermo Scientific). Peptides were fractionated on a fused silica HPLC-column tip (I.D. 75 µm, New Objective, self-packed with ReproSil-Pur 120 C18-AQ, 1.9 µm (Dr. Maisch) to a length of 20 cm) using a gradient of A (0.1% formic acid in water) and B (0.1% formic acid in 80% acetonitrile in water): samples were loaded with 0% B with a flow rate of 600 nL/min; peptides were separated by 5%–30% B within 85 min with a flow rate of 250 nL/min. Spray voltage was set to 2.3 kV and the ion-transfer tube temperature to 250°C; no sheath and auxiliary gas were used. Mass spectrometers were operated in the data-dependent mode; after each MS scan (mass range m/z = 370 – 1750; resolution: 70,000 for QE Plus and 120,000 for HF-X) a maximum of ten, or twelve MS/MS scans were performed using a normalized collision energy of 25%, a target value of 1,000 (QE Plus)/5,000 (HF-X) and a resolution of 17,500 for QE Plus and 30,000 for HF-X. MS raw files were analyzed using MaxQuant (version 1.6.2.10) (Cox and Mann, 2008b; Cox and Mann, 2008a) using a Uniprot full-length S. cerevisiae database (March, 2016) and common contaminants such as keratins and enzymes used for in-gel digestion as reference. Carbamidomethylcysteine was set as fixed modification and protein amino-terminal acetylation, serine-, threonine- and tyrosine- (heavy) phosphorylation, and oxidation of methionine were set as variable modifications. The MS/MS tolerance was set to 20 ppm and three missed cleavages were allowed using trypsin/P as enzyme specificity. Peptide, site, and protein FDR based on a forward-reverse database were set to 0.01, minimum peptide length was set to 7, the minimum score for modified peptides was 40, and minimum number of peptides for identification of proteins was set to one, which must be unique. The “match-between-run” option was used with a time window of 0.7 min. MaxQuant results were analyzed using Perseus (Tyanova et al., 2016).

3.4.5 Ultrastructural analysis

The sample preparation protocol for TEM analysis was adapted from a previously described protocol (Backues et al., 2014). SEY6210 pep4Δ vps4Δ or SEY6210 pep4Δ vps4Δ DED1-AID-Myc OsTIR1-MYC cells were cultured in YPD, with or without auxin, and 20 OD600 unit equivalents of cells in log phase were harvested by centrifugation at 3,000 g for 5 min at room temperature (RT). Cells were then washed once with 10 ml of distilled water. Cell pellets were subsequently resuspended in 1 ml of freshly prepared ice-cold 1.5% KMnO4 (Sigma Aldrich, 223468-25G) and transferred into microcentrifuge tubes. The microcentrifuge tubes were entirely filled completely with ice-cold 1.5% KMnO4 to exclude air and incubated on a slow-moving rotating wheel for 30 min at 4°C. Cells were then centrifuged at 3,000 x g for 3 min at 4°C and the supernatant discarded. Pellets were again resuspended in 1.5 ml of ice-cold 1.5% KMnO4 and microcentrifuge tubes incubated on a rotating wheel overnight at 4°C. After 5 washes with 1 ml of distilled water, cells were collected by centrifugation at 5,000 x g for 3 min.

Dehydration was performed by incubating the cells in 1 ml of 10, 30, 50, 70, 90 and 95% acetone (acetone for analysis ENSURE®; MERCK, 1.00014.2500) with at least 20 min incubation at RT. Between each incubation steps, cells were collected by centrifugation at 5,000 x g for 4 min. Cells were then incubated 3 times in 1 ml of water-free acetone (dried acetone; MERCK, 1.00299.0500) for at least 20 min each time, on a slow motion rotating wheel at RT. This was followed by incubation in 33% freshly made Spurr's resin (11.8 g nonenyl succinic anhydride [Ted Pella, 18301], 8.2 g ERL 4221 epoxide resin [Ted Pella, 18306-4221], 1.9 g diglycidyl ether of poly [propylene glycol] 736 [Ted Pella, 18310], 0.2 g dimethylaminoethanol [Ted Pella, 18315]) on a slow-motion rotating wheel for at least 1 h at RT. Cells were collected by centrifugation at 5,000 x g for 5 min and the supernatants discarded. Following this, cells were incubated in 100%

Spurr's resin on a rotating wheel overnight at RT and collected by centrifugation at 5,000 x g for 5 min and the supernatant discarded. Incubation in 100% Spurr's resin was repeated for 8 h at RT and the samples transferred to conic embedding capsules (BEEM embedding capsules size 00, EMS, 70010-B). The capsules were centrifuged at 5,000 x g for 5 min and the supernatant discarded. The tubes were then topped with fresh 100% Spurr's resin and heated at 65˚C for 4 days to polymerize the resin.

Ultra-thin 55-nm sections were cut using a Leica ultramicrotome (Leica Microsystems) and collected on formvar carbon-coated 50 mesh copper grids (EMS). Cell sections were stained with a filtered lead-citrate solution (80 mM lead nitrate, 120 mM sodium citrate, pH 12) for 2 min at RT. Sections were viewed either in either a CM100bio TEM or a Talos F200i (FEI). The average number of ABs per cell section was determined by counting 100 randomly selected cell profiles over 3 grids for each analyzed condition. The average diameter of ABs was measured using the ImageJ software (Schneider et al., 2012) and examining at least 100 ABs profiles randomly selected.

3.4.6 Auxin-inducible degradation

S. cerevisiae SEY6210 cells were first transformed with the plasmid pNHK53 (ADH1p-OsTIR1-9MYC). Genes of interest (DED1, RAD53, CDC28 and MEC1) was then tagged with AID-9MYC by homologous recombination. The DNA fragments used for transformation were amplified with pHIS3-AID*-9MYC (Addgene, 99524; deposited by Dr. Helle Ulrich) as the template DNA. The auxin-inducible degron refers to the 71-116 amino acids of the AT1G04250/ATIAA17 protein in plants. To deplete target protein levels, the cells were treated with 500 mM 3-indoleacetic acid (IAA/auxin; Sigma) or DMSO (vehicle) during mid-log phase growth in YPD medium for 60-90

min (depending on the protein of interest) to induce degradation of target protein. Subsequently, samples were collected for downstream analyses: enzymatic assays, immunoblots or qRT-PCR.

3.4.7 RNA Immunoprecipitation

The RNA immunoprecipitation protocol was modified from previously published procedures (Liu et al., 2019; Selth et al., 2009). For determining Ded1-*ATG1* mRNA interaction, a Ded1-PA tagged strain and an untagged (control) strain were cultured to mid-log phase and subjected to nitrogen starvation for 4 h. Cross-linking was performed by adding formaldehyde, to a final concentration of 0.8%, and shaking slowly for 10 min at room temperature. Cross-linking was halted with glycine treatment, to a final concentration of 0.2 M, with shaking for 5 min. Cultures were then harvested, washed in PBS, and resuspended in FA lysis buffer (50 mM HEPES, pH 7.5, 150 mM NaCl, 1 mM EDTA, 1% Triton X-100 [Sigma, T8787], 0.1% sodium deoxycholate [Sigma, D6750], 0.1% SDS), containing 5 mM PMSF, 1 tablet of complete protease inhibitor cocktail (Roche, 1873580) and RNasin® PLUS RNase inhibitor (Promega/Fisher Scientific, PRN2615). Yeast cells were lysed by vortexing with glass beads (USA Scientific, 7400-2405) at 4°C, centrifuged (5000 x g, 1 min) and the supernatant was collected. Samples were sonicated at 4°C using three 15-s pulses of 45% amplitude, with 60-s pauses for cooling on ice. Sonicated samples were collected by centrifugation (10,000 x g, 10 min), and the supernatant was collected and divided into input and IP fractions. IP fractions were incubated with IgG Sepharose 6 Fast Flow beads (GE healthcare Life Sciences), overnight with shaking at 4°C, while input fractions were frozen in liquid nitrogen and left at -80°C. IP fractions were washed with FA lysis buffer several times, resuspended in RIP elution buffer (50 mM Tris-HCl, pH 7.5, 10 mM EDTA, 1% SDS) and incubated at 70°C for 10 min with intermittent vortexing. IP supernatant and input samples were collected and incubated

with a combination of proteinase K and RNase inhibitor at 42°C for 1 h, followed by 1 h at 65°C to ensure degradation of proteins bound to RNA.

Next, the samples were treated with equal volume of acid phenol-chloroform, mixed by vortexing and centrifuged. The aqueous layer of each sample was recovered and treated with 25 ml 3 M sodium acetate, 20 mg glycogen (Roche/Sigma, 10901393001), and 625 ml ice-cold 100% ethanol to precipitate the RNA. Samples were incubated for 1 h to overnight at -80°C, following which they were centrifuged, washed with 70% ethanol, and dried for 15 min. Pellets were resuspended in 90 ml of nuclease-free water and treated with DNase (10 ml TURBO DNase buffer, 2 ml TURBO DNase [TURBO DNA-free kit; Invitrogen/Fisher Scientific, AM1907]) with 0.5 ml of RNasin® PLUS RNase inhibitor (Promega/Fisher Scientific, PRN2615). Samples were incubated for 45 min at 37°C to eliminate DNA. Following incubation, DNase was inhibited using the DNase inactivation reagent (TURBO DNA-free kit). Samples were then subjected to qRT-PCR as described in the qRT-PCR method section.

For determining Ded1-*ATG1* mRNA interaction in the WT or *rad53*Δ *sml1*Δ background, the procedure followed was the same as described in the earlier paragraph except for the following: 1) Ded1 was tagged C-terminally with 13xMYC; 2) IP fractions were incubated with MYC magnetic beads (Pierce™/Fisher Scientific, 88843) overnight with shaking at 4°C; and 3) magnetic separation was used for collecting beads during the incubation, washing and elution processes.

3.4.8 In vitro RNA interactome capture screen/mRNA IP

RNA in vitro transcription was performed as previously described (Yin et al., 2019). The linearized pUC19-ATG1-5' UTR was used as template to carry out RNA transcription using the

HiScribe T7 High Yield RNA synthesis kit (NEB, E2040S). The yield of the resulting RNA was measured using a nanodrop and the 3'-end was labelled with desthiobiotin according to manufacturer's instructions using the Pierce 3'-End desthiobiotinylation kit (Thermo Fisher Scientific, 20163). The labelled mRNA was used in the in vitro RNA immunoprecipitation.

Cell pellets were resuspended in lysis buffer (10 mM Tris-HCl, pH 7.5, 0.1 M Nacl, 30 mM MgCl2, 1% Triton X-100, RNasin® PLUS RNase inhibitor (Promega/Fisher Scientific, PRN2615) and Roche complete protease inhibitor cocktail (Roche, 1873580) and mechanically lysed used acid washed beads for 5 min at 4°C. The lysates were centrifuged at 12,000 xg for 10 min and the supernatant was collected. The affinity isolation was set up according to the manufacturer's instructions (Thermo Fisher Scientific, 20164). Protein enrichment in labeled RNA reaction was measured either using MS analysis (for preliminary screen leading to Ded1 identification) or monitored by immunoblotting (for confirming interaction between Ded1 and *ATG1* 5' UTR).

3.4.9 Mammalian cell culture, transfection, and infection

The PANC-1 (CRL-1469) and HT1080 (CCL-121) cell lines were obtained from the American Type Culture Collection. These cells were cultured in Dulbecco's modified Eagle's medium (Thermo Fisher Scientific, 11995073) supplemented with 10% heat-inactivated fetal bovine serum (Thermo Fisher Scientific, A3840001) and 1% penicillin and streptomycin (Thermo Fisher Scientific, 15070-063) at 37°C, with 95% humidity, and 5% CO2. Lentiviral particles were generated by transfection of the DDX3 shRNA (Sigma, TRCN0000000002 and TRCN0000000003), and the 2nd generation lentiviral systems (viral packaging psPAX2 and viral envelope pMD2G) were collected, mixed with polybrene, and added into 293-T cells using Lipofectamine 2000 (Life Technologies) for transfection. Culture media were harvested 48 h after

transfection and filtered through 0.45-μm filters. Upon infection, the stable cell lines were established by selecting with 2-5 μg/ml puromycin.

3.4.10 Quantification and statistical analyses

Western blot images were quantified using Bio-Rad ImageLab software. Statistical analyses were performed using GraphPad Prism 9.1.0. Statistical significance was determined in all cases from at least 3 independent biological replicates using either Student's t test, one-way ANOVA or two-way ANOVA followed by Tukey's multiple comparisons test. Differences with a P value < 0.05 or lower were considered significant. $*p < 0.05$, $**p < 0.01$, $***p < 0.001$. Number of independent experiments (n), statistical tests utilized, dispersion of measurements and significance are also described in the figure legends.

3.5 Acknowledgements

I thank members of the Klionsky group for their constructive suggestions during the study, and BGI Americas Corp for their collaboration on the RNA-Sequencing experiment. I would like to thank Rishav Mitra for insightful comments aiding manuscript preparation. I would like to thank Subhechha Roy for help with figure preparation. This work was supported by NIGMS grant GM131919 (DJK), by the Swiss National Science Foundation and the canton and University of Fribourg (JD), ENW KLEIN-1 OCENW.KLEIN.118 (FR), ZonMW TOP 91217002 (FR), and NCI grant R01CA160417 (DT). M.M. is supported by an ALW Open Programme (ALWOP.355).

3.6 Tables

Table 3. Yeast strains used in this study.

Strain	Genotype	Reference

SEY6210	*MATα leu2-3,112 ura3-52 his3-Δ200 trp1-Δ901 suc2-Δ9 lys2-801; GAL*	[61]
VLY001	SEY6210 *GCN4-3xPA::TRP1*	This study
VLY002	WLY176 *CUP1p-GFP-ATG8::LEU2*	This study
VLY003	SEY6210 pep4Δ*::KAN*	This study
VLY004	SEY6210 pep4Δ*::KAN vps4Δ::LEU2*	This study
VLY005	SEY6210 vac8Δ*::KAN*	This study
VLY006	SEY6210 arg4Δ*::HIS*	This study
VLY007	SEY6210 ATG9-*3xPA::TRP1*	This study
VLY008	SEY6210 *atg1Δ::HIS3*	This study
VLY009	SEY6210 *sml1Δ::HIS3*	This study
VLY010	SEY6210 *sml1Δ::HIS3 rad53Δ::URA3*	This study
VLY011	SEY6210 *PGI1-GFP::TRP1*	[58]
VLY012	SEY6210 *sml1Δ::HIS3 PGI1-GFP::TRP1*	This study
VLY013	SEY6210 *sml1Δ::HIS3 rad53Δ::URA3 PGI1-GFP::TRP1*	This study
VLY014	WLY176 *RAD53-AID-MYC::HIS3*	This study
VLY015	VLY014 *pNHK53::URA3*	This study
VLY016	VLY002 *MEC1-AID-MYC::HIS3*	This study
VLY017	VLY016 *pNHK53::URA3*	This study
VLY018	VLY002 *CDC28-AID-MYC::HIS3*	This study
VLY019	VLY018 *pNHK53::URA3*	This study
VLY020	SEY6210 *DED1-3xPA::TRP1*	This study
VLY021	SEY6210 *DED1-13xMYC::HIS3*	This study
VLY022	VLY010 *DED1-13xMYC::HIS3*	This study
	ded1-95	[113]
VLY022	VLY002 *DED1-AID-MYC::HIS3*	This study
VLY023	VLY022 *pNHK53::URA3*	This study
VLY024	VLY004 *DED1-AID-MYC::HIS3*	This study
VLY025	VLY024 *pNHK53::URA3*	This study
WLY176	SEY6210 *pho13Δ pho8*::*pho8Δ*60	[30]

Table 4. Primers for yeast genetics.

Name	Sequence (5'-3')
GCN4 T F	AAATGAGGTTGCCAGATTAAAGAAATTAGTTGGCGAACGCCGGATCCCCGGGTTAATTAA
GCN4 T R	GAGAATGAAATAAAAAATATAAAATAAAAGGTAAATGAAAGAATTCGAGCTCGTTTAAAC
GCN4 T C	TCCACTGAAGAAGTTTCTCT
PEP4 D F	AAAGAAAAAAAAAAAGCCTAGTGACCTAGTATTTAATCCAAATAAAATTCAAACAAAAACCAAAACTAACCGGATCCCCGGGTTAATTAA
PEP4 D R	TTGTTATCTACTTATAAAAGCTCTCTAGATGGCAGAAAAGGATAGGGCGGAGAAGTAAGAAAAGTTTAGCGAATTCGAGCTCGTTTAAAC
PEP4 D C	CGTTTTCAATATCTTGAGCTCCTCAATTGTATTTG
VPS4 D F	TTGAGGACATGGAAGACAAAAATAAAGCAGCATAGAGTGCCTATAGTAGATGGGGTACAACAGCTGAAGCTTCGTACGC
VPS4 D R	TTTTTTTATTTTTTATTTTCATGTACACAAGAAATCTACATTAGCACGTTAATCAATTGAGCATAGGCCACTAGTGGATCTG
VPS4 D C	GTGTCATCTGTTGCAGTCG
VAC8 D F	CAGGAACTGAGCAAACTATAAGGGTGTTCTTTCTTCTGTACTATATATACATTTGCAACTCAGCTGAAGCTTCGTACGC
VAC8 D R	AACTTCTGAGAAGAAAATTTTGATAAAAATTATAATGCCTAGTCCCGCTTTTGAAGAAAAGCATAGGCCACTAGTGGAT
VAC8 D C	GAGCCCTTAAGGAGGACTC
ARG4 D F	GCTCAAAAGCAGGTAACTATATAACAAGACTAAGGCAAACCAGCTGAAGCTTCGTACGC
ARG4 D R	CCAGACCTGATGAAATTCTTGCGCATAACGTCGCCATCTGGCATAGGCCACTAGTGGATCTG

ARG4 D C	CAGCGGTAGATGTAAGCC
ATG9 T F	CTTGTTAAAGAGTATTACAAGAAGTCTGACGTCGGAAGACGGATCC CCGGGTTAATTAA
ATG9 T R	ATATAGTTATATTGGATGATGTACACGACACAGTCTGCCGAATTCGA GCTCGTTTAAAC
ATG9 T C	CCGAAGACCATAGCGATAAAG
ATG1 D F	ATTTGAAGCTACCCCATATTTTCAAATCTCTTTTACAACACCAGACG AGAAATTAAGAAACAGCTGAAGCTTCGTACGC
ATG1 D R	AGATACTTGAAAATATAGCAGGTCATTTGTACTTAATAAGAAAACC ATATTATGCATCACGCATAGGCCACTAGTGGATCTG
ATG1 D C	TCCCCCATCAGCATCAGTTTGTG
SML1 D F	CCTTTGTGATCTTACGGTCTCACTAACCTCTCTTCAACTGCTCAATAA TTTCCCGCTCAGCTGAAGCTTCGTACGC
SML1 D R	GAAAAGAACAGAACTAGTGGGAAATGGAAAGAGAAAAGAAAAGAG TATGAAAGGAACTGCATAGGCCACTAGTGGATCTG
SML1 D C	CATTGCCGTCGAACGTC
RAD53 D F	TCTTAAGCTTTAAAAGAGAGAATAGTGAGAAAAGATAGTGTTACAC AACATCAACTAAAACAGCTGAAGCTTCGTACGC
RAD53 D R	GGTATCTACCATCTTCTCTCTTAAAAAGGGGCAGCATTTTCTATGGG TATTTGTCCTTGGGCATAGGCCACTAGTGGATCTG
RAD53 D C	GCTCAGCACCTACCTAAATG
RAD53 A F	GGTTAAAAGGGCAAAATTGGACCAAACCTCAAAAGGCCCCGAGAAT TTGCAATTTTCGCTTCGTACGCTGCAGGTCGA
RAD53 A R	TATCTACCATCTTCTCTCTTAAAAAGGGGCAGCATTTTCTATGGGTA TTTGTCCTTGGCATCGATGAATTCGAGCTCG

RAD53 AC	GCATGTATGAATCTCCGGC
MEC1 AF	AGAAGCAACATCAGAAGACAATCTAAGCAAGATGTATATTGGTTGGCTTCCATTTTGGCTTCGTACGCTGCAGGTCGA
MEC1 AR	TGCAGTGATGGTTAGATCAAGAGGAAGTTCGTCTGTTGCCGAAAATGGTGGAAAGTCGCATCGATGAATTCGAGCTCG
MEC1 AC	CATGGAACAGGTAGATAAATTTCC
CDC28 AF	CCCTATTAACCGGATTAGCGCCAGAAGAGCAGCCATCCACCCCTACTTCCAAGAATCACTTCGTACGCTGCAGGTCGA
CDC28 AR	AGGCTATAATGACAGTGCAGTAGCATTTGTAATATAATAGCGAAATAGATTATAATGCCATCGATGAATTCGAGCTCG
CDC28 AC	GGACCAACCGTTAGGAGC
DED1 AF	TGGGGTAACAGCGGTGGTTCAAACAACTCTTCTTGGTGGCTTCGTACGCTGCAGGTCGA
DED1 AR	GCAGAAAACGAAGAATCCTCACCCTAGTTTGTCTGAAACATCGATGAATTCGAGCTCG
DED1 AC	GAGCTACCGCCATTCATG
RA	TCGACCTGCAGCGTACGAAG
RD	GCGTACGAAGCTTCAGCTG
RT	TTAATTAACCCGGGGATCCG

A, AID tagging; C, PCR-based forward detection primer; D, deletion; F, forward primer; R, reverse primer; RA, PCR-based reverse detection primer for AID tagging; RD, PCR-based reverse detection primer for deletion; RT, PCR-based reverse detection primer for tagging; T, tagging.

Table 5. Primers for qRT-PCR.

Name	Sequence (5'-3')
ATG1 F	ATCTAAGATGGCCGCACATATG
ATG1 R	AGGGTAGTCACCATAGGCATTC
ATG9 F	CGTACTAACAGAGTCTTTCCTTG
ATG9 R	CTAAGACACCACCCTTATTGAG
ALG9 F	CACGGATAGTGGCTTTGGTGAACAATTAC
ALG9 R	TATGATTATCTGGCAGCAGGAAAGAACTTGGG
ATG1 5'-UTR F	TAGGCCGAGGTTAATTCTAGAACG
ATG1 5'-UTR R	ATAGTACTGTTCTCTGTTTCCCCAGA
ATG1 CDS F	GAGCTTCCAATCATTTGGAGTTATTC
ATG1 CDS R	CTATTCTTTGGGCTGGATCAAATGTC
ATG1 3'-UTR F	GAGGCAGAAGATGAACCACCAAA
ATG1 3'-UTR R	GTAAAGCATTTCGAGAGTAGCATAAC
PGK1 CDS	GAAGGACAAGCGTGTCTTCATCAG
PGK1 CDS	CGTACTTGATGGTTGGCAAAGCAG
hGAPDH F	GTCTCCTCTGACTTCAACAGCG
hGAPDH R	ACCACCCTGTTGCTGTAGCCAA
hULK1 F	GCAAGGACTCTTCCTGTGACAC
hULK1 R	CCACTGCACATCAGGCTGTCTG

Table 6 Primers for shRNA-mediated knockdown.

Name	Sequence (5'-3')
DDX3F	CCGGCGGAGTGATTACGATGGCATTCTCGAGAATGCCATCGTAATCACTC CGTTTTT
DDX3R	CCGGCGTAGAATAGTCGAACAAGATCTCGAGATCTTGTTCGACTATTCTA CGTTTTT

3.7 References

1. Gatica D, Lahiri V, Klionsky DJ. Cargo recognition and degradation by selective autophagy. Nat Cell Biol. 2018 Mar;20(3):233-242. doi: 10.1038/s41556-018-0037-z. PubMed PMID: 29476151; PubMed Central PMCID: PMCPMC6028034.

2. Chang C, Jensen LE, Hurley JH. Autophagosome biogenesis comes out of the black box. Nat Cell Biol. 2021 May;23(5):450-456. doi: 10.1038/s41556-021-00669-y. PubMed PMID: 33903736.

3. Melia TJ, Lystad AH, Simonsen A. Autophagosome biogenesis: From membrane growth to closure. J Cell Biol. 2020 Jun 1;219(6). doi: 10.1083/jcb.202002085. PubMed PMID: 32357219; PubMed Central PMCID: PMCPMC7265318.

4. Corona Velazquez AF, Jackson WT. So Many Roads: the Multifaceted Regulation of Autophagy Induction. Mol Cell Biol. 2018 Nov 1;38(21). doi: 10.1128/MCB.00303-18. PubMed PMID: 30126896; PubMed Central PMCID: PMCPMC6189458.

5. Nakatogawa H. Mechanisms governing autophagosome biogenesis. Nat Rev Mol Cell Biol. 2020 Aug;21(8):439-458. doi: 10.1038/s41580-020-0241-0. PubMed PMID: 32372019.

6. White E, Mehnert JM, Chan CS. Autophagy, Metabolism, and Cancer. Clin Cancer Res. 2015 Nov 15;21(22):5037-46. doi: 10.1158/1078-0432.CCR-15-0490. PubMed PMID: 26567363; PubMed Central PMCID: PMCPMC4646728.

7. Liu K, Sutter BM, Tu BP. Autophagy sustains glutamate and aspartate synthesis in Saccharomyces cerevisiae during nitrogen starvation. Nat Commun. 2021 Jan 4;12(1):57. doi: 10.1038/s41467-020-20253-6. PubMed PMID: 33397945; PubMed Central PMCID: PMCPMC7782722.

8. May AI, Prescott M, Ohsumi Y. Autophagy facilitates adaptation of budding yeast to respiratory growth by recycling serine for one-carbon metabolism. Nat Commun. 2020 Oct 7;11(1):5052. doi: 10.1038/s41467-020-18805-x. PubMed PMID: 33028817; PubMed Central PMCID: PMCPMC7542147.

9. Amaravadi R, Kimmelman AC, White E. Recent insights into the function of autophagy in cancer. Genes Dev. 2016 Sep 1;30(17):1913-30. doi: 10.1101/gad.287524.116. PubMed PMID: 27664235; PubMed Central PMCID: PMCPMC5066235.

10. White E. The role for autophagy in cancer. J Clin Invest. 2015 Jan;125(1):42-6. doi: 10.1172/JCI73941. PubMed PMID: 25654549; PubMed Central PMCID: PMCPMC4382247.

11. Lock R, Roy S, Kenific CM, et al. Autophagy facilitates glycolysis during Ras-mediated oncogenic transformation. Mol Biol Cell. 2011 Jan 15;22(2):165-78. doi:

10.1091/mbc.E10-06-0500. PubMed PMID: 21119005; PubMed Central PMCID: PMCPMC3020913.

12. Guo JY, Chen HY, Mathew R, et al. Activated Ras requires autophagy to maintain oxidative metabolism and tumorigenesis. Genes Dev. 2011 Mar 1;25(5):460-70. doi: 10.1101/gad.2016311. PubMed PMID: 21317241; PubMed Central PMCID: PMCPMC3049287.

13. Mulcahy Levy JM, Thorburn A. Autophagy in cancer: moving from understanding mechanism to improving therapy responses in patients. Cell Death Differ. 2020 Mar;27(3):843-857. doi: 10.1038/s41418-019-0474-7. PubMed PMID: 31836831; PubMed Central PMCID: PMCPMC7206017.

14. Fu Y, Liu S, Zeng S, et al. The critical roles of activated stellate cells-mediated paracrine signaling, metabolism and onco-immunology in pancreatic ductal adenocarcinoma. Mol Cancer. 2018 Feb 19;17(1):62. doi: 10.1186/s12943-018-0815-z. PubMed PMID: 29458370; PubMed Central PMCID: PMCPMC5817854.

15. Sousa CM, Biancur DE, Wang X, et al. Pancreatic stellate cells support tumour metabolism through autophagic alanine secretion. Nature. 2016 Aug 25;536(7617):479-83. doi: 10.1038/nature19084. PubMed PMID: 27509858; PubMed Central PMCID: PMCPMC5228623.

16. Amaravadi RK, Kimmelman AC, Debnath J. Targeting Autophagy in Cancer: Recent Advances and Future Directions. Cancer Discov. 2019 Sep;9(9):1167-1181. doi: 10.1158/2159-8290.CD-19-0292. PubMed PMID: 31434711; PubMed Central PMCID: PMCPMC7306856.

17. Karsli-Uzunbas G, Guo JY, Price S, et al. Autophagy is required for glucose homeostasis and lung tumor maintenance. Cancer Discov. 2014 Aug;4(8):914-27. doi: 10.1158/2159-8290.CD-14-0363. PubMed PMID: 24875857; PubMed Central PMCID: PMCPMC4125614.

18. Mizushima N, Levine B. Autophagy in Human Diseases. N Engl J Med. 2020 Oct 15;383(16):1564-1576. doi: 10.1056/NEJMra2022774. PubMed PMID: 33053285.

19. Yin Z, Pascual C, Klionsky DJ. Autophagy: machinery and regulation. Microb Cell. 2016 Dec 1;3(12):588-596. doi: 10.15698/mic2016.12.546. PubMed PMID: 28357331; PubMed Central PMCID: PMCPMC5348978.

20. Feng Y, He D, Yao Z, et al. The machinery of macroautophagy. Cell Res. 2014 Jan;24(1):24-41. doi: 10.1038/cr.2013.168. PubMed PMID: 24366339; PubMed Central PMCID: PMCPMC3879710.

21. Gross AS, Graef M. Mechanisms of Autophagy in Metabolic Stress Response. J Mol Biol. 2020 Jan 3;432(1):28-52. doi: 10.1016/j.jmb.2019.09.005. PubMed PMID: 31626805.

22. Russell RC, Yuan HX, Guan KL. Autophagy regulation by nutrient signaling. Cell Res. 2014 Jan;24(1):42-57. doi: 10.1038/cr.2013.166. PubMed PMID: 24343578; PubMed Central PMCID: PMCPMC3879708.

23. Kim J, Kundu M, Viollet B, et al. AMPK and mTOR regulate autophagy through direct phosphorylation of Ulk1. Nat Cell Biol. 2011 Feb;13(2):132-41. doi: 10.1038/ncb2152. PubMed PMID: 21258367; PubMed Central PMCID: PMCPMC3987946.

24. Abildgaard MH, Brynjolfsdottir SH, Frankel LB. The Autophagy-RNA Interplay: Degradation and Beyond. Trends Biochem Sci. 2020 Oct;45(10):845-857. doi: 10.1016/j.tibs.2020.07.007. PubMed PMID: 32828649.

25. Lahiri V, Hawkins WD, Klionsky DJ. Watch What You (Self-) Eat: Autophagic Mechanisms that Modulate Metabolism. Cell Metab. 2019 Apr 2;29(4):803-826. doi: 10.1016/j.cmet.2019.03.003. PubMed PMID: 30943392; PubMed Central PMCID: PMCPMC6450419.

26. Delorme-Axford E, Klionsky DJ. Transcriptional and post-transcriptional regulation of autophagy in the yeast Saccharomyces cerevisiae. J Biol Chem. 2018 Apr 13;293(15):5396-5403. doi: 10.1074/jbc.R117.804641. PubMed PMID: 29371397; PubMed Central PMCID: PMCPMC5900762.

27. Xie Y, Kang R, Sun X, et al. Posttranslational modification of autophagy-related proteins in macroautophagy. Autophagy. 2015;11(1):28-45. doi: 10.4161/15548627.2014.984267. PubMed PMID: 25484070; PubMed Central PMCID: PMCPMC4502723.

28. McEwan DG, Dikic I. The Three Musketeers of Autophagy: phosphorylation, ubiquitylation and acetylation. Trends Cell Biol. 2011 Apr;21(4):195-201. doi: 10.1016/j.tcb.2010.12.006. PubMed PMID: 21277210; PubMed Central PMCID: PMCPMC3714536.

29. Xie Z, Nair U, Klionsky DJ. Atg8 controls phagophore expansion during autophagosome formation. Mol Biol Cell. 2008 Aug;19(8):3290-8. doi: 10.1091/mbc.E07-12-1292. PubMed PMID: 18508918; PubMed Central PMCID: PMCPMC2488302.

30. Jin M, He D, Backues SK, et al. Transcriptional regulation by Pho23 modulates the frequency of autophagosome formation. Curr Biol. 2014 Jun 16;24(12):1314-1322. doi: 10.1016/j.cub.2014.04.048. PubMed PMID: 24881874; PubMed Central PMCID: PMCPMC4169046.

31. Sen ND, Zhou F, Ingolia NT, et al. Genome-wide analysis of translational efficiency reveals distinct but overlapping functions of yeast DEAD-box RNA helicases Ded1 and eIF4A. Genome Res. 2015 Aug;25(8):1196-205. doi: 10.1101/gr.191601.115. PubMed PMID: 26122911; PubMed Central PMCID: PMCPMC4510003.

32. Sen ND, Gupta N, S KA, et al. Functional interplay between DEAD-box RNA helicases Ded1 and Dbp1 in preinitiation complex attachment and scanning on structured mRNAs in vivo. Nucleic Acids Res. 2019 Sep 19;47(16):8785-8806. doi: 10.1093/nar/gkz595. PubMed PMID: 31299079; PubMed Central PMCID: PMCPMC7145680.

33. Wilky BA, Kim C, McCarty G, et al. RNA helicase DDX3: a novel therapeutic target in Ewing sarcoma. Oncogene. 2016 May 19;35(20):2574-83. doi: 10.1038/onc.2015.336. PubMed PMID: 26364611.

34. Botlagunta M, Vesuna F, Mironchik Y, et al. Oncogenic role of DDX3 in breast cancer biogenesis. Oncogene. 2008 Jun 26;27(28):3912-22. doi: 10.1038/onc.2008.33. PubMed PMID: 18264132; PubMed Central PMCID: PMCPMC5576029.

35. Chen HH, Yu HI, Cho WC, et al. DDX3 modulates cell adhesion and motility and cancer cell metastasis via Rac1-mediated signaling pathway. Oncogene. 2015 May 21;34(21):2790-800. doi: 10.1038/onc.2014.190. PubMed PMID: 25043297.

36. Cebollero E, Reggiori F. Regulation of autophagy in yeast Saccharomyces cerevisiae. Biochim Biophys Acta. 2009 Sep;1793(9):1413-21. doi: 10.1016/j.bbamcr.2009.01.008. PubMed PMID: 19344676.

37. Conrad M, Schothorst J, Kankipati HN, et al. Nutrient sensing and signaling in the yeast Saccharomyces cerevisiae. FEMS Microbiol Rev. 2014 Mar;38(2):254-99. doi: 10.1111/1574-6976.12065. PubMed PMID: 24483210; PubMed Central PMCID: PMCPMC4238866.

38. Ecker N, Mor A, Journo D, et al. Induction of autophagic flux by amino acid deprivation is distinct from nitrogen starvation-induced macroautophagy. Autophagy. 2010 Oct;6(7):879-90. doi: 10.4161/auto.6.7.12753. PubMed PMID: 20647741.

39. Natarajan K, Meyer MR, Jackson BM, et al. Transcriptional profiling shows that Gcn4p is a master regulator of gene expression during amino acid starvation in yeast. Mol Cell Biol. 2001 Jul;21(13):4347-68. doi: 10.1128/MCB.21.13.4347-4368.2001. PubMed PMID: 11390663; PubMed Central PMCID: PMCPMC87095.

40. Dever TE, Feng L, Wek RC, et al. Phosphorylation of initiation factor 2 alpha by protein kinase GCN2 mediates gene-specific translational control of GCN4 in yeast. Cell. 1992 Feb 7;68(3):585-96. doi: 10.1016/0092-8674(92)90193-g. PubMed PMID: 1739968.

41. Huang WP, Shintani T, Xie Z. Assays for autophagy I: the Cvt pathway and nonselective autophagy. Methods Mol Biol. 2014;1163:153-64. doi: 10.1007/978-1-4939-0799-1_10. PubMed PMID: 24841304.

42. Klionsky DJ. Monitoring autophagy in yeast: the Pho8Delta60 assay. Methods Mol Biol. 2007;390:363-71. doi: 10.1007/978-1-59745-466-7_24. PubMed PMID: 17951700.

43. Kummel A, Ewald JC, Fendt SM, et al. Differential glucose repression in common yeast strains in response to HXK2 deletion. FEMS Yeast Res. 2010 May;10(3):322-32. doi: 10.1111/j.1567-1364.2010.00609.x. PubMed PMID: 20199578.

44. Backues SK, Chen D, Ruan J, et al. Estimating the size and number of autophagic bodies by electron microscopy. Autophagy. 2014 Jan;10(1):155-64. doi: 10.4161/auto.26856. PubMed PMID: 24270884; PubMed Central PMCID: PMCPMC4389869.

45. Bernard A, Jin M, Xu Z, et al. A large-scale analysis of autophagy-related gene expression identifies new regulators of autophagy. Autophagy. 2015 Nov 2;11(11):2114-2122. doi: 10.1080/15548627.2015.1099796. PubMed PMID: 26649943; PubMed Central PMCID: PMCPMC4824583.

46. Backues SK, Lynch-Day MA, Klionsky DJ. The Ume6-Sin3-Rpd3 complex regulates ATG8 transcription to control autophagosome size. Autophagy. 2012 Dec;8(12):1835-6.

doi: 10.4161/auto.21845. PubMed PMID: 22960621; PubMed Central PMCID: PMCPMC3541296.

47. Jin M, Klionsky DJ. Regulation of autophagy: modulation of the size and number of autophagosomes. FEBS Lett. 2014 Aug 1;588(15):2457-63. doi: 10.1016/j.febslet.2014.06.015. PubMed PMID: 24928445; PubMed Central PMCID: PMCPMC4118767.

48. Kanki T, Wang K, Cao Y, et al. Atg32 is a mitochondrial protein that confers selectivity during mitophagy. Dev Cell. 2009 Jul;17(1):98-109. doi: 10.1016/j.devcel.2009.06.014. PubMed PMID: 19619495; PubMed Central PMCID: PMCPMC2746076.

49. Mochida K, Oikawa Y, Kimura Y, et al. Receptor-mediated selective autophagy degrades the endoplasmic reticulum and the nucleus. Nature. 2015 Jun 18;522(7556):359-62. doi: 10.1038/nature14506. PubMed PMID: 26040717.

50. Mizushima N. The role of the Atg1/ULK1 complex in autophagy regulation. Curr Opin Cell Biol. 2010 Apr;22(2):132-9. doi: 10.1016/j.ceb.2009.12.004. PubMed PMID: 20056399.

51. Noda T. Regulation of Autophagy through TORC1 and mTORC1. Biomolecules. 2017 Jul 7;7(3). doi: 10.3390/biom7030052. PubMed PMID: 28686223; PubMed Central PMCID: PMCPMC5618233.

52. Papinski D, Schuschnig M, Reiter W, et al. Early steps in autophagy depend on direct phosphorylation of Atg9 by the Atg1 kinase. Mol Cell. 2014 Feb 6;53(3):471-83. doi: 10.1016/j.molcel.2013.12.011. PubMed PMID: 24440502; PubMed Central PMCID: PMCPMC3978657.

53. Hu Z, Raucci S, Jaquenoud M, et al. Multilayered Control of Protein Turnover by TORC1 and Atg1. Cell Rep. 2019 Sep 24;28(13):3486-3496 e6. doi: 10.1016/j.celrep.2019.08.069. PubMed PMID: 31553916.

54. Matoba K, Kotani T, Tsutsumi A, et al. Atg9 is a lipid scramblase that mediates autophagosomal membrane expansion. Nat Struct Mol Biol. 2020 Dec;27(12):1185-1193. doi: 10.1038/s41594-020-00518-w. PubMed PMID: 33106658.

55. Yamamoto H, Kakuta S, Watanabe TM, et al. Atg9 vesicles are an important membrane source during early steps of autophagosome formation. J Cell Biol. 2012 Jul 23;198(2):219-33. doi: 10.1083/jcb.201202061. PubMed PMID: 22826123; PubMed Central PMCID: PMCPMC3410421.

56. Gomez-Sanchez R, Rose J, Guimaraes R, et al. Atg9 establishes Atg2-dependent contact sites between the endoplasmic reticulum and phagophores. J Cell Biol. 2018 Aug 6;217(8):2743-2763. doi: 10.1083/jcb.201710116. PubMed PMID: 29848619; PubMed Central PMCID: PMCPMC6080931.

57. Sawa-Makarska J, Baumann V, Coudevylle N, et al. Reconstitution of autophagosome nucleation defines Atg9 vesicles as seeds for membrane formation. Science. 2020 Sep 4;369(6508). doi: 10.1126/science.aaz7714. PubMed PMID: 32883836; PubMed Central PMCID: PMCPMC7610778.

58. Yin Z, Liu X, Ariosa A, et al. Psp2, a novel regulator of autophagy that promotes autophagy-related protein translation. Cell Res. 2019 Dec;29(12):994-1008. doi: 10.1038/s41422-019-0246-4. PubMed PMID: 31666677; PubMed Central PMCID: PMCPMC6951345.

59. Deng J, Erdjument-Bromage H, Neubert TA. Quantitative Comparison of Proteomes Using SILAC. Curr Protoc Protein Sci. 2019 Feb;95(1):e74. doi: 10.1002/cpps.74. PubMed PMID: 30238645; PubMed Central PMCID: PMCPMC6342620.

60. Lang MJ, Martinez-Marquez JY, Prosser DC, et al. Glucose starvation inhibits autophagy via vacuolar hydrolysis and induces plasma membrane internalization by down-regulating recycling. J Biol Chem. 2014 Jun 13;289(24):16736-47. doi: 10.1074/jbc.M113.525782. PubMed PMID: 24753258; PubMed Central PMCID: PMCPMC4059118.

61. Gatica D, Hu G, Liu X, et al. The Pat1-Lsm Complex Stabilizes ATG mRNA during Nitrogen Starvation-Induced Autophagy. Mol Cell. 2019 Jan 17;73(2):314-324 e4. doi: 10.1016/j.molcel.2018.11.002. PubMed PMID: 30527663; PubMed Central PMCID: PMCPMC6338489.

62. Licheva M, Raman B, Kraft C, et al. Phosphoregulation of the autophagy machinery by kinases and phosphatases. Autophagy. 2021 May 10:1-20. doi: 10.1080/15548627.2021.1909407. PubMed PMID: 33970777.

63. Sridharan S, Jain K, Basu A. Regulation of autophagy by kinases. Cancers (Basel). 2011 Jun 9;3(2):2630-54. doi: 10.3390/cancers3022630. PubMed PMID: 24212825; PubMed Central PMCID: PMCPMC3757434.

64. Steinfeld N, Lahiri V, Morrison A, et al. Elevating PI3P drives select downstream membrane trafficking pathways. Mol Biol Cell. 2021 Jan 15;32(2):143-156. doi: 10.1091/mbc.E20-03-0191. PubMed PMID: 33237833; PubMed Central PMCID: PMCPMC8120694.

65. Jung KW, Lee Y, Huh EY, et al. Rad53- and Chk1-Dependent DNA Damage Response Pathways Cooperatively Promote Fungal Pathogenesis and Modulate Antifungal Drug Susceptibility. mBio. 2019 Jan 2;10(1). doi: 10.1128/mBio.01726-18. PubMed PMID: 30602579; PubMed Central PMCID: PMCPMC6315099.

66. Szyjka SJ, Aparicio JG, Viggiani CJ, et al. Rad53 regulates replication fork restart after DNA damage in Saccharomyces cerevisiae. Genes Dev. 2008 Jul 15;22(14):1906-20. doi: 10.1101/gad.1660408. PubMed PMID: 18628397; PubMed Central PMCID: PMCPMC2492737.

67. Cartagena-Lirola H, Guerini I, Manfrini N, et al. Role of the Saccharomyces cerevisiae Rad53 checkpoint kinase in signaling double-strand breaks during the meiotic cell cycle. Mol Cell Biol. 2008 Jul;28(14):4480-93. doi: 10.1128/MCB.00375-08. PubMed PMID: 18505828; PubMed Central PMCID: PMCPMC2447123.

68. Eapen VV, Waterman DP, Bernard A, et al. A pathway of targeted autophagy is induced by DNA damage in budding yeast. Proc Natl Acad Sci U S A. 2017 Feb 14;114(7):E1158-E1167. doi: 10.1073/pnas.1614364114. PubMed PMID: 28154131; PubMed Central PMCID: PMCPMC5320992.

69. Liu X, Yao Z, Jin M, et al. Dhh1 promotes autophagy-related protein translation during nitrogen starvation. PLoS Biol. 2019 Apr;17(4):e3000219. doi: 10.1371/journal.pbio.3000219. PubMed PMID: 30973873; PubMed Central PMCID: PMCPMC6459490.

70. Holzen TM, Sclafani R. Genetic interaction of RAD53 protein kinase with histones is important for DNA replication. Cell Cycle. 2010 Dec 1;9(23):4735-47. doi: 10.4161/cc.9.23.14091. PubMed PMID: 21099362; PubMed Central PMCID: PMCPMC3048039.

71. Morawska M, Ulrich HD. An expanded tool kit for the auxin-inducible degron system in budding yeast. Yeast. 2013 Sep;30(9):341-51. doi: 10.1002/yea.2967. PubMed PMID: 23836714; PubMed Central PMCID: PMCPMC4171812.

72. Sweeney FD, Yang F, Chi A, et al. Saccharomyces cerevisiae Rad9 acts as a Mec1 adaptor to allow Rad53 activation. Curr Biol. 2005 Aug 9;15(15):1364-75. doi: 10.1016/j.cub.2005.06.063. PubMed PMID: 16085488.

73. Chen ES, Hoch NC, Wang SC, et al. Use of Quantitative Mass Spectrometric Analysis to Elucidate the Mechanisms of Phospho-priming and Auto-activation of the Checkpoint Kinase Rad53 in Vivo. Mol Cell Proteomics. 2014 Feb;13(2):551-565. doi: 10.1074/mcp.M113.034058. PubMed PMID: 33498138.

74. Albuquerque CP, Smolka MB, Payne SH, et al. A multidimensional chromatography technology for in-depth phosphoproteome analysis. Mol Cell Proteomics. 2008 Jul;7(7):1389-96. doi: 10.1074/mcp.M700468-MCP200. PubMed PMID: 18407956; PubMed Central PMCID: PMCPMC2493382.

75. Schleker T, Shimada K, Sack R, et al. Cell cycle-dependent phosphorylation of Rad53 kinase by Cdc5 and Cdc28 modulates checkpoint adaptation. Cell Cycle. 2010 Jan 15;9(2):350-63. doi: 10.4161/cc.9.2.10448. PubMed PMID: 20046099.

76. Lanz MC, Yugandhar K, Gupta S, et al. In-depth and 3-dimensional exploration of the budding yeast phosphoproteome. EMBO Rep. 2021 Feb 3;22(2):e51121. doi: 10.15252/embr.202051121. PubMed PMID: 33491328; PubMed Central PMCID: PMCPMC7857435.

77. Abreu CM, Kumar R, Hamilton D, et al. Site-specific phosphorylation of the DNA damage response mediator rad9 by cyclin-dependent kinases regulates activation of checkpoint kinase 1. PLoS Genet. 2013 Apr;9(4):e1003310. doi: 10.1371/journal.pgen.1003310. PubMed PMID: 23593009; PubMed Central PMCID: PMCPMC3616908.

78. de la Cruz J, Iost I, Kressler D, et al. The p20 and Ded1 proteins have antagonistic roles in eIF4E-dependent translation in Saccharomyces cerevisiae. Proc Natl Acad Sci U S A. 1997 May 13;94(10):5201-6. doi: 10.1073/pnas.94.10.5201. PubMed PMID: 9144215; PubMed Central PMCID: PMCPMC24656.

79. Lao JP, Ulrich KM, Johnson JR, et al. The Yeast DNA Damage Checkpoint Kinase Rad53 Targets the Exoribonuclease, Xrn1. G3 (Bethesda). 2018 Dec 10;8(12):3931-3944. doi: 10.1534/g3.118.200767. PubMed PMID: 30377154; PubMed Central PMCID: PMCPMC6288840.

80. Burckin T, Nagel R, Mandel-Gutfreund Y, et al. Exploring functional relationships between components of the gene expression machinery. Nat Struct Mol Biol. 2005 Feb;12(2):175-82. doi: 10.1038/nsmb891. PubMed PMID: 15702072.

81. Tarn WY, Chang TH. The current understanding of Ded1p/DDX3 homologs from yeast to human. RNA Biol. 2009 Jan-Mar;6(1):17-20. doi: 10.4161/rna.6.1.7440. PubMed PMID: 19106629.

82. Klionsky DJ, Abdel-Aziz AK, Abdelfatah S, et al. Guidelines for the use and interpretation of assays for monitoring autophagy (4th edition)(1). Autophagy. 2021 Jan;17(1):1-382. doi: 10.1080/15548627.2020.1797280. PubMed PMID: 33634751; PubMed Central PMCID: PMCPMC7996087.

83. Bjorkoy G, Lamark T, Pankiv S, et al. Monitoring autophagic degradation of p62/SQSTM1. Methods Enzymol. 2009;452:181-97. doi: 10.1016/S0076-6879(08)03612-4. PubMed PMID: 19200883.

84. Bernard A, Jin M, Gonzalez-Rodriguez P, et al. Rph1/KDM4 mediates nutrient-limitation signaling that leads to the transcriptional induction of autophagy. Curr Biol. 2015 Mar 2;25(5):546-55. doi: 10.1016/j.cub.2014.12.049. PubMed PMID: 25660547; PubMed Central PMCID: PMCPMC4348152.

85. Delorme-Axford E, Abernathy E, Lennemann NJ, et al. The exoribonuclease Xrn1 is a post-transcriptional negative regulator of autophagy. Autophagy. 2018;14(5):898-912. doi: 10.1080/15548627.2018.1441648. PubMed PMID: 29465287; PubMed Central PMCID: PMCPMC6070002.

86. Hu G, McQuiston T, Bernard A, et al. A conserved mechanism of TOR-dependent RCK-mediated mRNA degradation regulates autophagy. Nat Cell Biol. 2015 Jul;17(7):930-942. doi: 10.1038/ncb3189. PubMed PMID: 26098573; PubMed Central PMCID: PMCPMC4528364.

87. Downs JA, Lowndes NF, Jackson SP. A role for Saccharomyces cerevisiae histone H2A in DNA repair. Nature. 2000 Dec 21-28;408(6815):1001-4. doi: 10.1038/35050000. PubMed PMID: 11140636.

88. Javaheri A, Wysocki R, Jobin-Robitaille O, et al. Yeast G1 DNA damage checkpoint regulation by H2A phosphorylation is independent of chromatin remodeling. Proc Natl Acad Sci U S A. 2006 Sep 12;103(37):13771-6. doi: 10.1073/pnas.0511192103. PubMed PMID: 16940359; PubMed Central PMCID: PMCPMC1564209.

89. Redon C, Pilch DR, Rogakou EP, et al. Yeast histone 2A serine 129 is essential for the efficient repair of checkpoint-blind DNA damage. EMBO Rep. 2003 Jul;4(7):678-84. doi: 10.1038/sj.embor.embor871. PubMed PMID: 12792653; PubMed Central PMCID: PMCPMC1326317.

90. Redon C, Pilch DR, Bonner WM. Genetic analysis of Saccharomyces cerevisiae H2A serine 129 mutant suggests a functional relationship between H2A and the sister-chromatid cohesion partners Csm3-Tof1 for the repair of topoisomerase I-induced DNA damage. Genetics. 2006 Jan;172(1):67-76. doi: 10.1534/genetics.105.046128. PubMed PMID: 16219777; PubMed Central PMCID: PMCPMC1456192.

91. Tkach JM, Yimit A, Lee AY, et al. Dissecting DNA damage response pathways by analysing protein localization and abundance changes during DNA replication stress. Nat Cell Biol. 2012 Sep;14(9):966-76. doi: 10.1038/ncb2549. PubMed PMID: 22842922; PubMed Central PMCID: PMCPMC3434236.

92. Soto-Rifo R, Ohlmann T. The role of the DEAD-box RNA helicase DDX3 in mRNA metabolism. Wiley Interdiscip Rev RNA. 2013 Jul-Aug;4(4):369-85. doi: 10.1002/wrna.1165. PubMed PMID: 23606618.

93. Lai MC, Chang WC, Shieh SY, et al. DDX3 regulates cell growth through translational control of cyclin E1. Mol Cell Biol. 2010 Nov;30(22):5444-53. doi: 10.1128/MCB.00560-10. PubMed PMID: 20837705; PubMed Central PMCID: PMCPMC2976371.

94. Heerma van Voss MR, Kammers K, Vesuna F, et al. Global Effects of DDX3 Inhibition on Cell Cycle Regulation Identified by a Combined Phosphoproteomics and Single Cell Tracking Approach. Transl Oncol. 2018 Jun;11(3):755-763. doi: 10.1016/j.tranon.2018.04.001. PubMed PMID: 29684792; PubMed Central PMCID: PMCPMC6050443.

95. Zhao L, Mao Y, Zhou J, et al. Multifunctional DDX3: dual roles in various cancer development and its related signaling pathways. Am J Cancer Res. 2016;6(2):387-402. PubMed PMID: 27186411; PubMed Central PMCID: PMCPMC4859668.

96. Cruciat CM, Dolde C, de Groot RE, et al. RNA helicase DDX3 is a regulatory subunit of casein kinase 1 in Wnt-beta-catenin signaling. Science. 2013 Mar 22;339(6126):1436-41. doi: 10.1126/science.1231499. PubMed PMID: 23413191.

97. Heerma van Voss MR, Vesuna F, Trumpi K, et al. Identification of the DEAD box RNA helicase DDX3 as a therapeutic target in colorectal cancer. Oncotarget. 2015 Sep 29;6(29):28312-26. doi: 10.18632/oncotarget.4873. PubMed PMID: 26311743; PubMed Central PMCID: PMCPMC4695062.

98. Sun M, Zhou T, Jonasch E, et al. DDX3 regulates DNA damage-induced apoptosis and p53 stabilization. Biochim Biophys Acta. 2013 Jun;1833(6):1489-97. doi: 10.1016/j.bbamcr.2013.02.026. PubMed PMID: 23470959; PubMed Central PMCID: PMCPMC3638797.

99. Bol GM, Xie M, Raman V. DDX3, a potential target for cancer treatment. Mol Cancer. 2015 Nov 5;14:188. doi: 10.1186/s12943-015-0461-7. PubMed PMID: 26541825; PubMed Central PMCID: PMCPMC4636063.

100. Ariumi Y. Multiple functions of DDX3 RNA helicase in gene regulation, tumorigenesis, and viral infection. Front Genet. 2014;5:423. doi: 10.3389/fgene.2014.00423. PubMed PMID: 25538732; PubMed Central PMCID: PMCPMC4257086.

101. Egan DF, Chun MG, Vamos M, et al. Small Molecule Inhibition of the Autophagy Kinase ULK1 and Identification of ULK1 Substrates. Mol Cell. 2015 Jul 16;59(2):285-97. doi: 10.1016/j.molcel.2015.05.031. PubMed PMID: 26118643; PubMed Central PMCID: PMCPMC4530630.

102. Zheng Y, Liu L, Wang Y, et al. Glioblastoma stem cell (GSC)-derived PD-L1-containing exosomes activates AMPK/ULK1 pathway mediated autophagy to increase temozolomide-resistance in glioblastoma. Cell Biosci. 2021 Mar 31;11(1):63. doi: 10.1186/s13578-021-00575-8. PubMed PMID: 33789726; PubMed Central PMCID: PMCPMC8011168.

103. Tang F, Hu P, Yang Z, et al. SBI0206965, a novel inhibitor of Ulk1, suppresses non-small cell lung cancer cell growth by modulating both autophagy and apoptosis pathways. Oncol Rep. 2017 Jun;37(6):3449-3458. doi: 10.3892/or.2017.5635. PubMed PMID: 28498429.

104. Hu Z, Raucci S, Jaquenoud M, et al. Multilayered Control of Protein Turnover by TORC1 and Atg1. Cell Reports. 2019 2019/09/24/;28(13):3486-3496.e6. doi: https://doi.org/10.1016/j.celrep.2019.08.069.

105. Batth TS, Francavilla C, Olsen JV. Off-line high-pH reversed-phase fractionation for in-depth phosphoproteomics. J Proteome Res. 2014 Dec 5;13(12):6176-86. doi: 10.1021/pr500893m. PubMed PMID: 25338131.

106. Zarei M, Sprenger A, Rackiewicz M, et al. Fast and easy phosphopeptide fractionation by combinatorial ERLIC-SCX solid-phase extraction for in-depth phosphoproteome analysis. Nature Protocols. 2016 2016/01/01;11(1):37-45. doi: 10.1038/nprot.2015.134.

107. Post H, Penning R, Fitzpatrick MA, et al. Robust, Sensitive, and Automated Phosphopeptide Enrichment Optimized for Low Sample Amounts Applied to Primary Hippocampal Neurons. Journal of Proteome Research. 2017 2017/02/03;16(2):728-737. doi: 10.1021/acs.jproteome.6b00753.

108. Cox J, Mann M. MaxQuant enables high peptide identification rates, individualized p.p.b.-range mass accuracies and proteome-wide protein quantification. Nat Biotechnol. 2008 Dec;26(12):1367-72. doi: 10.1038/nbt.1511. PubMed PMID: 19029910.

109. Cox J, Mann M. MaxQuant enables high peptide identification rates, individualized p.p.b.-range mass accuracies and proteome-wide protein quantification. Nature Biotechnology. 2008 2008/12/01;26(12):1367-1372. doi: 10.1038/nbt.1511.

110. Tyanova S, Temu T, Cox J. The MaxQuant computational platform for mass spectrometry-based shotgun proteomics. Nature Protocols. 2016 2016/12/01;11(12):2301-2319. doi: 10.1038/nprot.2016.136.

111. Schneider CA, Rasband WS, Eliceiri KW. NIH Image to ImageJ: 25 years of image analysis. Nat Methods. 2012 Jul;9(7):671-5. doi: 10.1038/nmeth.2089. PubMed PMID: 22930834; PubMed Central PMCID: PMCPMC5554542.

112. Selth LA, Gilbert C, Svejstrup JQ. RNA immunoprecipitation to determine RNA-protein associations in vivo. Cold Spring Harb Protoc. 2009 Jun;2009(6):pdb prot5234. doi: 10.1101/pdb.prot5234. PubMed PMID: 20147192.

Chapter 4 Summary and Future Directions

Decades of autophagy research has been "protein centric". Therefore, I have extensive insight into the protein-protein interactions, post translational modifications and signaling cascades that regulate in the induction and execution of autophagy. As connections between RNA and autophagy emerge, and the focus shifts towards an "RNA centric" approach, I are now beginning to understand the transcriptional and post-transcriptional mechanisms that regulate autophagy. Therefore, the discovery and characterization of RNA-binding proteins that regulate autophagy will contribute a better understanding of the field and expand the scope of druggable therapeutic targets that modulate autophagy in diseases such as cancer and neurodegeneration.

4.1 Systematic workflow to identify RNA-binding proteins that regulate autophagy

Recent advancement in proteome-wide approaches have expanded the repertoire of RNA-binding proteins in the cells. These technologies help us identify new RNA-binding proteins and the target mRNAs. However, applying the RNA centric approach to study autophagy requires us to uncover regulators of ATG gene at the transcript levels. However, methods for identification of proteins that bind to specific mRNA are limited.

In Chapter 2, I set out to address this problem by utilizing labeled, invitro transcribed *ATG* RNA as bait to identify proteins that interact with it compared to a constitutive RNA such as *PGK1*. Using this approach, I identified RNA-binding proteins that interact with the 5' UTR and the 3' UTR of *ATG1* mRNA from lysates harvest following growth in either rich media or nitrogen starvation media. Further characterization of the binding interactors revealed an elegant

mechanism that controls the export and translation of *ATG1* mRNA in response to starvation conditions. Npl3 is an mRNA surveillance protein known for its roles in transcription and splicing. It has been shown to prime transcripts for export. My research reveals that Npl3 enables cells survival during nitrogen starvation by binding to *ATG1* 5' UTR in an RRM2-dependent manner. Npl3 co-transcriptionally imprint *ATG1* mRNA in the nucleus defines its cell fate in the cytoplasm by facilitating the interaction of *ATG1* mRNA with a stress granule protein, Pub1. Pub1 interacts with Npl3, and this interaction is required for the subsequent interaction with *ATG1* 3' UTR. Pub1 enhances the recruitment of polysome recruitment onto the Atg1 transcript by interacting with translation factors, other RNA-binding proteins that interact with translation factors and the large and small ribosomal subunits. Together, the Npl3-Pub1 axis provide a mechanism for export and protein synthesis, a fate sealed in the nucleus by Npl3. Furthermore, I found that the mammalian homolog of Pub1, TIA1 also binds *ULK1* and regulates ULK1 protein levels post-transcriptionally, suggesting the conserved nature of this pathway.

While I identified key molecular players in linking *ATG1* transcript imprinting and translational efficiency, several fascinating questions remain unexplored. I show that Pub1 and Npl3 interact in the presence of RNA. I speculate that interaction takes place in the nucleus given that the localization and function of Npl3 is in the nucleus. However, the exact localization of the Npl3-Pub1 complex needed to be elucidated. Furthermore, detailed structural studies to map the interaction sites between Npl3-Pub1-*ATG1* mRNA will enhance our understanding of how Npl3 relays *ATG1* to Pub1 for export. The interaction dynamics of Npl3-Pub1-*ATG1* were elucidated using biochemical approaches. However, it is worth noting the power of high-resolution microscopy to study the dynamics of *ATG1* localization and translation.

4.2 Differential translational regulation of *ATG1* dependent on external nutrient availability

In Chapter 3, utilizing the same approach, I identified the RNA helicase Ded1 as a regulator of Atg1 protein expression at the 5' UTR. Consistent with its role in promoting translation initiation, loss of Ded1 results in lowered Atg1 protein expression during nitrogen starvation but does not affect its transcription. Interestingly, Ded1 is responsive to external nutrient availability. The interaction of Ded1 and *ATG1* mRNA is significantly reduced in amino acid starvation compared to nitrogen starvation indicating that Ded1 differentially regulates Atg1 protein expression consistent with the cellular demand for autophagy.

In spite of these developments, several outstanding questions remain. Future work should focus more on the temporal and spatial interaction dynamics of *ATG1* mRNA proteome landscape. Several proteins have been shown to bind to *ATG1* mRNA, however, how these proteins coordinate with each other to co-transcriptionally imprint, export, and translated the mRNA during starvation needs to be further elucidated. Differential binding of the regulatory landscape in response to different starvation conditions also needs further investigation. Furthermore, master signaling regulates that unify the *ATG1* mRNA interactome to elicit a coordinated response will be an exciting question to tackle. A lot of attention has been given to *ATG1* transcript. Structural studies do suggest that *ATG1* mRNA has structured *5′ UTR* indicating the need for RNA-binding proteins to facilitate its translation. However, the *ATG13* 5' UTR also shows a similar pattern, making it an interesting target to identify RNA-binding proteins that regulate it. Therefore, identification and characterization of RNA-binding proteins that bind to other *ATG* transcripts, thus expanding the repertoire of autophagy regulators.

4.3 Stress granule formation and function

Spatial compartmentalization is an elegant way for cellular organization of various process that ensures precise control of biological reactions. Both membrane-bound cellular structures such as organelles and non-membrane bound structures provide this subcellular compartmentalization, facilitating the precise spatiotemporal regulation of numerous biological reactions (Decker & Parker, 2012). Stress granules and P-bodies are cytosolic membrane-less structures involved in post-transcriptional regulation. Upon translational inhibition, the mRNA-protein complexes including translation initiation proteins and small ribosomal subunits condense to form phase separated structures called Stress granules that facilitates storage of translationally inactive mRNA. During long periods of translation inactivity, stress granule components merge with P-body components that include mRNA decay factors, thus subjecting the inactive mRNAs to degradation (Haimovich et al., 2013; Youn et al., 2019). Interestingly, our studies into the role of RNA-binding proteins involved in regulating autophagy has uncovered several stress granule and P-body components. Pub1 and its mammalian homolog TIA1 have been shown to form stress granules during arsenite stress and glucose starvation (Buchan et al., 2008; Gilks et al., 2004). Interestingly, during nitrogen starvation, stress granules are not microscopically visible. Furthermore, TIA1 has been shown to translationally repress its target mRNAs while I show that during serum starvation, TIA1 is required for ULK1 protein expression through a post-transcriptional process, highlighting the differential regulation of RNA-binding proteins in exerting its influence on target transcripts. While Pub1 has been shown to enhance stability of its target transcripts for translation, here I show a post-transcriptional role of Pub1 in *ATG1* export and translation. Next, Ded1, another stress granule component shown to interact with Pub1 also regulates *ATG1* post-transcriptionally (Hilliker et al., 2011; Lahiri et al.,

2022). Both these proteins exert their influence at 3 h -6 h of nitrogen starvation. Interestingly, translation of *ATG1* mRNA under longer time points uncovers a role of P-body components such as Dhh1 and Psp2, suggesting the temporal dynamics of the *ATG1* proteome. Together, I have uncovered salient proteins involved in various stages of the *ATG1* life cycle. Immediately following transcription, Npl3 binds to *ATG1* co-transcriptionally in the nucleus where it imprints the transcript with Pub1. Pub1 facilitates export of *ATG1* mRNA to the cytosol, where I speculate it recruits known regulators such as Ded1, translation initiators and elongators, and the ribosome machinery to enhance the translation of *ATG1*. During long term starvation, this mRNP landscape is modulated to include Dhh1 and Psp2 that further ensure the expression of Atg1 protein to sustain autophagy.

These proteins condense during glucose starvation, a condition of lower autophagy and Atg1 protein expression. These findings raise the question of whether the translational and granule formation roles of RNA-binding proteins are decoupled from each other. I speculate that differential modification of RNA-binding proteins confers translational and condensation roles. Further investigation is needed to understand the temporal dynamics and regulatory mechanisms of these proteins in autophagy and stress response.

4.4 RNA-binding proteins as therapeutic targets to modulate autophagy

In humans, RNA-binding proteins comprise of 20% of expressed transcripts, highlighting its regulatory importance and ubiquitous nature. Mutational analysis of RNA-binding protein in human cancer revealed that 281 RBPs are enriched in mutations in at least one cancer type (Neelamraju et al., 2018). Furthermore, several RBPs have been implicated in neurodegeneration reflecting the increasingly compelling view that RNA-binding proteins are causative factors in

disease etiology (Conlon & Manley, 2017). Identifying RNA-binding proteins as regulators of autophagy get us closer to developing potential autophagy-targeting therapeutic approaches. A small class of chemical probes have been shown to target RNA-binding proteins implicated in autophagy such as ELAVL1/Hur, EIF4E, EIF4A, LIN28 and TARDBP/TDP-43 (Julio & Backus, 2021). However, the lack of small-molecule binding sites and the presence of long stretches of disordered regions hinder the development of drugs that target RNA-binding proteins. This perception is beginning to change with the advancement of small molecule screens, and the utilization of AI for drug discovery to tackle "undruggable" targets (El Hage et al., 2023). Therefore, exploring the role of RNA-binding proteins in regulating autophagy in disease contexts can provide valuable information on which proteins to target for its modulation.

4.5 References

1. Buchan, J. R., Muhlrad, D., & Parker, R. (2008). P bodies promote stress granule assembly in Saccharomyces cerevisiae. *J Cell Biol*, *183*(3), 441-455. https://doi.org/10.1083/jcb.200807043
2. Conlon, E. G., & Manley, J. L. (2017). RNA-binding proteins in neurodegeneration: mechanisms in aggregate. *Genes Dev*, *31*(15), 1509-1528. https://doi.org/10.1101/gad.304055.117
3. Decker, C. J., & Parker, R. (2012). P-bodies and stress granules: possible roles in the control of translation and mRNA degradation. *Cold Spring Harb Perspect Biol*, *4*(9), a012286. https://doi.org/10.1101/cshperspect.a012286
4. El Hage, K., Babault, N., Maciejak, O., Desforges, B., Craveur, P., Steiner, E., Rengifo-Gonzalez, J. C., Henrie, H., Clement, M. J., Joshi, V., Bouhss, A., Wang, L., Bauvais, C., & Pastre, D. (2023). Targeting RNA:protein interactions with an integrative approach leads to the identification of potent YBX1 inhibitors. *Elife*, *12*. https://doi.org/10.7554/eLife.80387
5. Gilks, N., Kedersha, N., Ayodele, M., Shen, L., Stoecklin, G., Dember, L. M., & Anderson, P. (2004). Stress granule assembly is mediated by prion-like aggregation of TIA-1. *Mol Biol Cell*, *15*(12), 5383-5398. https://doi.org/10.1091/mbc.e04-08-0715
6. Haimovich, G., Choder, M., Singer, R. H., & Trcek, T. (2013). The fate of the messenger is pre-determined: a new model for regulation of gene expression. *Biochim Biophys Acta*, *1829*(6-7), 643-653. https://doi.org/10.1016/j.bbagrm.2013.01.004
7. Hilliker, A., Gao, Z., Jankowsky, E., & Parker, R. (2011). The DEAD-box protein Ded1 modulates translation by the formation and resolution of an eIF4F-mRNA complex. *Mol Cell*, *43*(6), 962-972. https://doi.org/10.1016/j.molcel.2011.08.008
8. Julio, A. R., & Backus, K. M. (2021). New approaches to target RNA-binding proteins. *Curr Opin Chem Biol*, *62*, 13-23. https://doi.org/10.1016/j.cbpa.2020.12.006
9. Lahiri, V., Metur, S. P., Hu, Z., Song, X., Mari, M., Hawkins, W. D., Bhattarai, J., Delorme-Axford, E., Reggiori, F., Tang, D., Dengjel, J., & Klionsky, D. J. (2022). Post-transcriptional regulation of ATG1 is a critical node that modulates autophagy during distinct nutrient stresses. *Autophagy*, *18*(7), 1694-1714. https://doi.org/10.1080/15548627.2021.1997305
10. Neelamraju, Y., Gonzalez-Perez, A., Bhat-Nakshatri, P., Nakshatri, H., & Janga, S. C. (2018). Mutational landscape of RNA-binding proteins in human cancers. *RNA Biol*, *15*(1), 115-129. https://doi.org/10.1080/15476286.2017.1391436
11. Youn, J. Y., Dyakov, B. J. A., Zhang, J., Knight, J. D. R., Vernon, R. M., Forman-Kay, J. D., & Gingras, A. C. (2019). Properties of Stress Granule and P-Body Proteomes. *Mol Cell*, *76*(2), 286-294. https://doi.org/10.1016/j.molcel.2019.09.014